

CHEMISTRY AND STRUCTURE OF COALS: EVALUATION OF ORGANIC STRUCTURE
BY COMPUTER AIDED DIFFUSE REFLECTANCE INFRARED SPECTROSCOPY.{*}

E. L. Fuller, Jr., N. R. Smyrl, R. L. Howell, and C. S. Daw{**}

Plant Laboratory, Y-12 Plant, Box Y, Oak Ridge, TN 37830{***}

INTRODUCTION

Diffuse reflectance infrared Fourier transform (DRIFT) spectroscopy has become a very informative method of evaluating the chemistry and structure of coals, chars, and related materials {1,2,3}. Infrared spectroscopy has long been recognized as an informative means of studying the chemistry and physics of coals {4,5}. Recent advances in instrumentation, computer assistance, and techniques have appreciably enhanced the amount and caliber of the spectra and the scientific importance of the conclusions{6,7}. The enhanced sensitivity of these new instruments has permitted renewed interest in nondestructive spectroscopic studies by diffuse reflectance infrared spectroscopy{8,9}.

EXPERIMENTAL

The spectrometer, cell, and techniques for measuring the diffuse reflectance spectra of solid samples over a wide range of temperatures and pressures have been described previously {1,2,10,11}. A portion of this study is devoted to extending our capabilities to be able to study unperturbed solid surfaces of rather large pieces of coal and to directly monitor changes wrought in simulated chemical and physical processing. Grinding of coals is known to alter the chemical and physical structure of coals and although DRIFT studies require much less stringent treatment{9} there is most assuredly some modification due to the energy dissipation accompanying percussive grinding{12}. The coal sample for this study was a "run of the mine" aliquot taken from the -3/+4 mesh sieve fraction, sealed in a glass bottle and stored for approximately two months, free from thermal effects (drying) and extensive oxidation (weathering) which are known to markedly alter the morphology and chemistry of both the organic and the inorganic (mineral) constituents in coals{13}. This sample was provided by the Tennessee Valley Authority from the Paradise (Kentucky) Mine and is generally ranked as High Volatile C-Bituminous as representative of the feed stock for the fluidized bed combustion facility.

RESULTS AND DISCUSSION

Typically the cleaved surfaces (parallel to the bedding plane) vary in appearance due to the heterogeneous distribution of the macerals in the structure. The variation in reflection of visible light allowed us to focus on glossy or dull areas of the surface of the piece of coal and to note the variation in DRIFT response over distances greater than our beam size (ca. 2mm with our 6X condensing optics). Figure 1 shows the variation in DRIFT signal. Spectrum A was taken with the incident beam flooding a visibly homogenous region of high reflectivity and we note that there is appreciable specular reflection in the infrared with little or no spectral features indicative of diffuse reflection. The negative features (500 and 1100 cm^{-1}) are undoubtedly

due to anomalous dispersion or reststrahlen effects(14,15) which are regarded as detrimental to DRIFT analyses and allow us to deduce some information concerning the physical state (consolidation) of the coal structure in this region. In marked contrast we note appreciable difference when sampling and dull area of the same piece of coal. The DRIFT spectrum, spectrum B, is still of very poor quality due to the consolidated nature of the substrate. Very good DRIFT spectra can be obtained after gentle abrasion of the surface with fine grit "Emory Paper" and removal of the dislodged material as shown in Spectrum C of Figure 1. This mild abrasion forms a surface which is rough enough to reflect and absorb electromagnetic radiation much as a fine powder. This spectral response is virtually identical to that of powders of similar rank, given that the quantitative nature varies due to chemistry and structure of individual aliquots. These spectra in turn correlate quite well with their counterparts obtained in the transmission mode after encapsulation in KBr or some other support medium.

Figure 2 serves to show that one can use the DRIFT technique to monitor chemical and physical changes of a given sample of coal very well. Spectrum D shows the DRIFT response of the same area of the same sample in vacuum at 400 C after exposure to oxygen gas at 400 C long enough to attain the steady state conditions deduced by sensing no further change in spectral features (intensities, band shapes and intensities) with time. Visual observation allows one to semiquantitatively deduce some of the relevant steps associated with oxidation. Within the depth of DRIFT response the aromatic (e) and aliphatic (f,g,h) hydrogen content is essentially depleted and there is a marked increase in carbonyl content ranging from aldehydes/ketones (k) to the more oxygen rich acid anhydrides (i,j). These oxygen insertion precursors to gaseous carbon dioxide give rise to spectral intensities which actually exceed that of the omnipresent polynuclear aromatic (l) and methylene/ether (m,n,o) crosslinks. All of this is noted to have little effect on the oxy-hydrogen phenolic, alcoholic and acid entities that are present in various states of hydrogen bonding and gives rise to the broad absorption feature (3600 to 2000 cm^{-1}). A very rich and enticing potpourri of potentially valuable information to say the least.

One can note the limited penetration involved in DRIFT studies and also note that the oxygen attack involves a layer of material near the surface. Reabrasion of the same area of the same sample gives rise to DRIFT spectrum E of Figure 2 where we note the reversion to the spectral state so classically characteristic of the original coal. The hydrocarbon bands (e,f,g,h) are again prominent and the carbonyl bands (i,j,k) are greatly diminished indicating that there probably existed a gradient of oxygen density which "tailed" beyond the approximately 50 micrometers removed in the second abrasion. All of the spectral features of E are somewhat enhanced with respect to C due to an increase in DRIFT efficiency brought about by a more enhanced roughness and/or a modified refractive index due to loss of infrared inactive graphitic carbon during the combustion phase of this study. Future studies with thinner sectioning will allow us to obtain further details from a detailed and quantitative analysis of the chemical and structural profile of the steady state oxygen insertion/diffusion process.

To this end we have instigated a program to quantitatively analyze our DRIFT spectra. The problem is complex since virtually every band overlaps one or more adjacent bands. There is currently a strong international move to quantitatively analyze infrared spectra in general (16,17,18,19) and coal spectra in particular (6,7) using sophisticated and readily available computers (20). Figure 3 is our analysis of the data of DRIFT spectrum E, using the second derivative to rather accurately assess the frequencies of the individual contributing absorption bands in terms of the resultant inflection points in the summation composite. The results compare favorably with those of Painter et. al. (7). There has been a renewed interest in "resolution enhancement" of spectra by deconvolution (21) techniques now that fast Fourier transforms are available and the required algorithms have been developed. Griffiths et. al. (9) have been able to accurately position coal structure bands with Fourier self deconvolution of their spectra. Our results are given in Figure 4 for the hydrocarbon region of DRIFT spectrum E shown with the Fourier self-deconvolution. Comparison of Figures 3 and 4 merely point out the close relationship between deconvolution and derivatization in terms of the multiplicative operation that corresponds to each in the time domain (22,23). Both operations are mathematically classed as filter functions (albeit negative or "unsmoothing" filters in this instance) (24). The prime utility of both techniques is to accurately measure characteristic band frequencies without the human error associated with locating inflection points and "shoulders" reliably and reproducibly. That goal is achieved admirably in both cases. It is now such a simple task that we can turn it over to the simple "mind" of the computer where the maxima in both curves are evaluated without human intervention or bias. Table 1 tabulates the band position for our analyses compared to the results of others (25,26). These carbon-hydrogen stretching frequencies are ideally suited to test our program since they are relatively immune to substituent and environmental effects (25).

Quantitative analyses requires accurate evaluation of the intensity (height), integrated area and/or band width of the bands associated with the vibration of each entity. This can be done most reliably by iterative minimum least squares (16,17) or some related technique in which the summation of the composite peaks most closely matches the experimental spectrum. The band positions from the second derivative and/or Fourier self-deconvolution are used as first approximations and intensities are estimated ratiometrically (utilizing the area conservation inherent in deconvolution). Initial band widths are taken to be the optimum value (average) used in the Fourier self-deconvolution. Generally the iterations converge in 6 to 10 steps without divergence, which can occur if initial estimates are grossly disparate from the optimum value. Our results are given in Figure 5 where we note that the deviation (upper line) is at or near the signal/noise ratio of the experimental spectrum. When this case prevails (standard deviation approximately equals the signal/noise ratio) for the converged iterations there is no justification of further deconvolution and/or incorporation of additional bands in the envelope. Conversely, more stringent deconvolution is not warranted if the standard deviation is not appreciably diminished toward the signal/noise ratio. These

techniques are readily implemented with the aid of today's computers and we must be cautious that we do not abuse them by taking them beyond their limits.

The broad band due to the oxygen-hydrogen stretching vibrations is seen to be composed of 5 bands whose intensities and widths are given in Figure 6. The positions and widths of these bands closely match those of Solomon et. al.(6). Our spectrum is taken in vacuum (.00002 torr) and is a true vacuum spectrum as compared to the purge state that is approached when alkali halide pellets are allowed to equilibrate. It is readily noted that the five frequencies are associated with successively stronger hydrogen bonding (27,28,29). The relative strengths are due to higher degrees of coordination between that of a linear bond to that of the 5 fold interaction of cubic close packing of the acceptor ligands oriented somewhat symmetrically around the donor hydrogen of the covalent phenol, alcohol, or acidic entities. Intermediate states correspond to lesser interactions with hydrogen. Each band corresponds to increased O-H length, decreased O-H...O separation, increased bandwidth, and enhanced extinction coefficient in accordance with known behavior of similar hydrogen bonding(27-29). The importance in a good understanding of these hydrogen bonds is essential to understanding the structure and chemistry and structure of coals and related materials. More detail will be given in the oral presentation.

The utility of this computer aided analysis is quite evident when applied to the lower frequency range (Figure 8) where classical methods based on visual observation and operator judgement are far from quantitative. For example, the carbonyl bands at 1843, 1760 and 1720 cm^{-1} are readily resolved even in the presence of the very large aromatic peak at 1608 cm^{-1} (9). More details will be given in the oral presentation to note the quantitative aspects of analyzing successive spectra to elucidate the mechanism of oxidation of coals and chars.

CONCLUSIONS

Modern spectrometers with computer aided data acquisition and processing are very well suited to obtain diffuse reflectance infrared spectra of coals with a minimum time and effort for sample preparation. The spectra are of high caliber and are very comparable to the best transmission spectra. Quantitative data is obtained for the region penetrated by the incident beam. Depth profiling is possible utilizing this surface sensitivity of the DRIFT technique. Lateral scanning is also possible to allow one to evaluate the heterogeneity and specie distribution in the plane of the surface. The utility of DRIFT techniques, so well recognized for powdered coals, can be used on consolidated coals and thus measure and map chemistry and structure of the original coalified matrix. These studies are easily effected under controlled environments to maintain coal bed conditions (high relative humidity), generate inert atmospheres (nitrogen or argon gas), induce and monitor reactions (hydration/dehydration, oxidation, hydrogenation, carbonation ,etc.), or virtually any combination over a wide range of temperatures (77 K to 800 K) and pressures (.00002 torr to 2000 torr) with our present cell. All of the studies are easily made free of matrix and supports normally used for IR studies of

solids. The high quality of the spectra are well suited to quantitative analyses using modern computer aided deconvolution and related composite band evaluation techniques. We now can start to evaluate the complex chemistry and structure of coals and related materials and to follow the fate of each and every specie as we obtain spectra under realistic conditions of coalification and subsequent combustion or processing for fuels and feedstocks.

REFERENCES

1. N. R. Smyrl and E. L. Fuller, Jr., "Chemistry and Structure of Coals: Diffuse Reflectance Infrared Transform (DRIFT) Spectroscopy of Air Oxidation," in "Coal and Coal Products: Analytical Characterization Techniques" edited by E. L. Fuller, Jr., American Chemical Society, 1982.
2. E. L. Fuller, Jr., N. R. Smyrl, R. W. Smithwick, and C. S. Daw, "Chemistry and Structure of Coals: Air Oxidation Related to Fluidized Bed Combustion", Preprints, Div. Fuel Chem. A.C.S., 28, 44(1983).
3. M. P. Fuller and P. R. Griffiths, Anal. Chem. 50,1906 (1978).
4. D. W. van Krevelen, "Coal", Elsevier Publ., 1961.
5. Robert S. McDonald "Review: Infrared Spectrometry", Anal. Chem. 54, 1250, (1982).
6. P. R. Solomon, D. G. Hamblen and R. M. Carangelo, "Applications of Fourier Transform Spectroscopy Infrared Spectroscopy in Fuel Science", in "Coal and Coal Products: Analytical Characterization Techniques", edited by E. L. Fuller, Jr., American Chemical Society, 1982.
7. Paul C. Painter, Randy M. Snyder, Michael Starsinic, Michael Coleman, Deborah W. Kuehn, and Alan Davis, "Fourier Transform Infrared Spectroscopy: Application to the Quantitative Determination of Functional Groups in Coal", *ibid.*, 1982.
8. Peter R. Griffiths and Michael P. Fuller, "Mid-infrared Spectrometry of Powdered Samples" in "Advances in Infrared and Raman Spectroscopy" Vol. 9, p. 63, edited by R. J. H. Clark and R. E. Hester, Heyden and Sons, 1982.
9. Peter R. Griffiths, Shih-Hsien Wang, Issam M. Hamadeh, Paul W. Yang and David E. Henry, "Direct Investigation of Reacting Coals by Diffuse Reflectance Infrared Spectroscopy", Preprints, Division of Fuel Chemistry, A.C.S. 28, 27 (1983).
10. N. R. Smyrl, E. L. Fuller, Jr., and G. L. Powell, Applied Spectroscopy 37, 38 (1983).
11. E. L. Fuller, Jr., N. R. Smyrl, J. B. Condon and M. Eager, J. Nuclear Materials, IN PRESS(1983).
12. E. L. Fuller, Jr., J. Colloid and Interface Science 75, 577 (1980)
13. E. L. Fuller, Jr., J. Colloid and Interface Science 89, 309 (1982)
14. W. W. Wendtlandt and H. G. Hecht, "Reflectance Spectroscopy", Interscience Publ., 1966
15. F. A. Jenkins and H. E. White, "Fundamentals of Optics", McGraw-Hill, 1957.
16. R. D. B. Fraser and E. Suzuki, Anal. Chem.,38,1770 (1966)
17. R. D. B. Fraser and E. Suzuki, Anal. Chem.,39,37 (1969)
18. R. N. Jones and K. Shimokoshi, Applied Spectroscopy, 37, 59 (1983)
19. P. H. Von Cittert, Z. Phys., 69, 298 (1931).
20. R. Peter Young, "Computer Systems", in "Infrared and Raman Spectroscopy" edited by E. G. Brame, Jr., and J. G. Grasselli, Marcel Dekker, 1977.

21. W. E. Blass and G. W. Halsey, "Deconvolution of Absorption Spectra", Academic Press, 1981.
22. J. K. Kaupinen, D. J. Moffat, H. H. Mantsch and D. G. Cameron, Anal. Chem. 53, 1454 (1981)
23. R. E. Ziemer and W. H. Tranter, "Principles of Communications", Houghton Mifflin, 1976.
24. J. K. Kaupinen, D. J. Moffat, D/ G/ Cameron and H. H. Mantsch, Applied Optics 20, 1866 (1981).
25. Norman B. Colthup, Lawrence H. Daly, and Stephen E. Wiberley, "Introduction to Infrared and Raman Spectroscopy", Academic Press, 1964
26. Herman A. Szymanski, "IR: Theory and Practice of Infrared Spectroscopy", Plenum Press, 1964.
27. George C. McClellan and A. McClellan, "The Hydrogen Bond", W. H. Freeman, 1960.
28. Serge N. Vinogradov and Robert H. Linnell, "Hydrogen Bonding", Vand Nostrand Reinhold, 1971.
29. Walter C. Hamilton and James A. Ibers, "Hydrogen Bonding in Solids", W. A. Benjamin, 1968.

{*} This study was funded by the Tennessee Valley Authority through The Engineering Technology Division of The Oak Ridge National Laboratory.

{**} C. S. Daw is a member of The Engineering Technology Division, Oak Ridge National Laboratory, Oak Ridge, TN 37830

{***} Operated for The United States Department of Energy by Union Carbide Nuclear Division under U. S. Government Contract Number W-7405-eng-36.

TABLE 1. VIBRATIONAL FREQUENCIES EVALUATED FOR KENTUCKY #9(5B) COAL
(frequencies tabulated as wavenumbers, cm^{-1})

This work	Ref. 7	Ref 25-----Assignment
3051	-----	3050+/-50 Ar-H
3017	-----	3025+/-25 R2C=CHR & RCH=CHR
2958	2956	2962+/-10 RCH3
2925	2923	2925+/- 5 ArCH3 & R2CH2
2894	2891	2900+/- ? R3CH
2870	2864	2872+/-10 RCH3 & ArCH3
2854	2849	2855+/-10 R2CH2
2752	-----	2732+/-12 RCHO

DRIFT SPECTRA: MODIFIED KENTUCKY NUMBER NINE

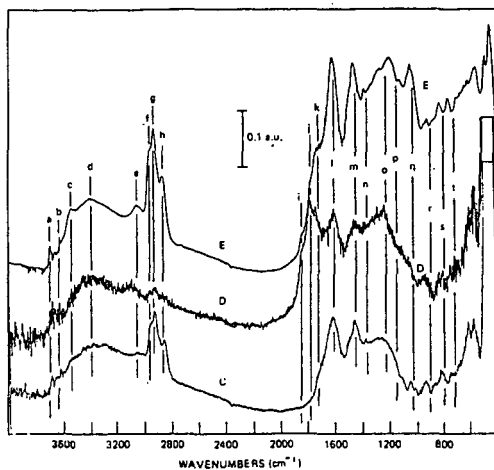


Figure 2. Effects of Chemical and Physical Treatment of Kentucky #9

REFLECTANCE SPECTRA: SOLID KENTUCKY NUMBER NINE

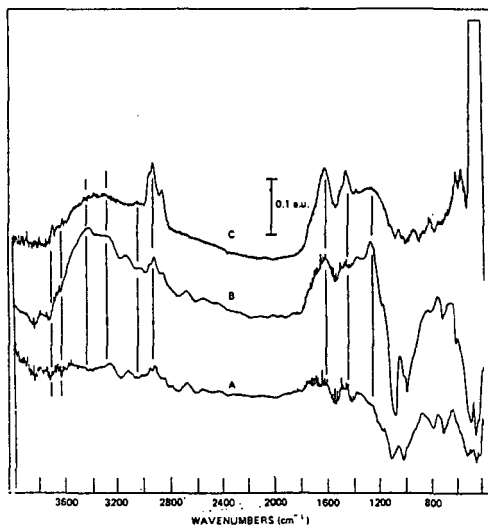


Figure 1. DRIFT Spectral Variation for Kentucky #9

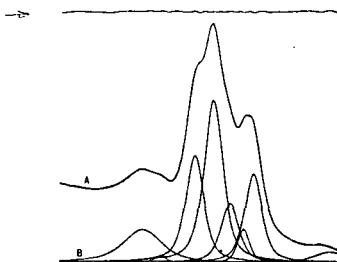


Figure 5. Least Squares Composite Sum for Hydrocarbon (K958)

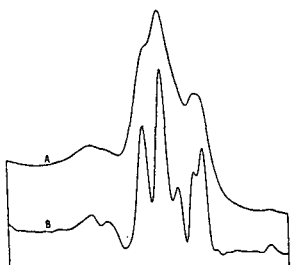


Figure 4. Fourier Self-deconvolution of Hydrocarbon Spectrum (K958)

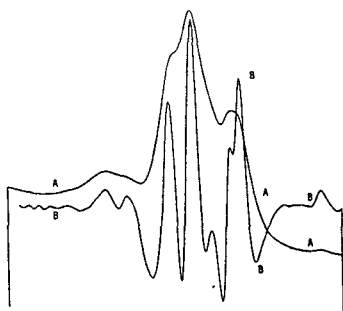


Figure 3. Second Derivative Analysis of Hydrocarbon Spectra (K958)

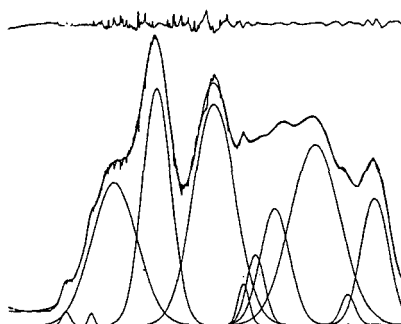


Figure 8. Least Squares Composite Sum for Low Frequency Bands (K958)

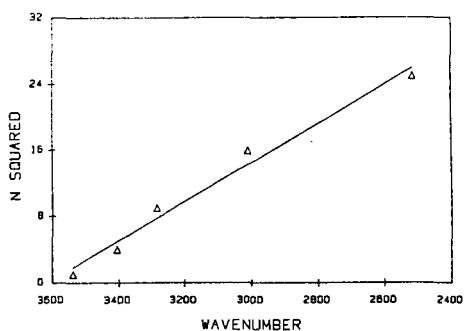


Figure 7. Hydrogen Bonded Hydroxyl Sequence Variation (K958)

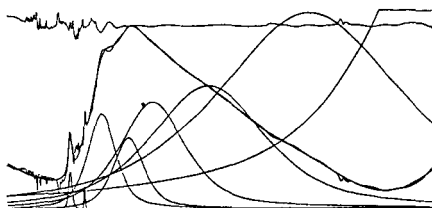


Figure 6. Least Squares Composite Sum for Hydroxyl Bands (K958)

RELATION BETWEEN HYDROCARBON STRUCTURE AND FRAGMENTS PRODUCED IN PYROLYSIS

Peter R. Solomon, Kevin R. Squire and Robert M. Carangelo

Advanced Fuel Research, Inc., 87 Church Street, East Hartford, CT 06108

Analysis of the heavy molecules which form tar in hydrocarbon pyrolysis can provide clues to the mechanisms of their release and to the structure of the parent molecule. This paper considers the relationship between the original hydrocarbon structure and the product tar. Pyrolysis experiments have been performed in a heated grid apparatus on several coals and lignins and on a polymer specifically synthesized to model features of natural hydrocarbons. Tars were collected and analyzed by Fourier Transform Infrared (FT-IR) Spectroscopy. The functional group composition of tars for a bituminous coal, a lignin and a polymer are all remarkably similar to the functional group composition of the parent material. It is believed that for these samples, the tar consists of minimally disturbed fragments of the original organic matrix. Molecular weights of tars were determined by Field Ionization Mass Spectrometry (FIMS) for tars collected from the heated grid apparatus and for samples pyrolyzed directly in the FIMS apparatus. The mass spectra all exhibit features reflecting structural aspects of the parent molecule and for the softening bituminous coals, the lignin and the polymer, the upper limit of molecular weight appears limited by vaporization. The process appears to be controlled by the combined effects of pyrolysis and vaporization, where bond breaking is required to produce fragments which are small enough to volatilize. The fragments are, therefore, similar in composition to the parent solid but lower in molecular weight.

A computer model for the coupled pyrolysis and vaporization of macromolecules has been used to interpret the results. The theory combines random cleavage of weak bonds in the polymer (to produce "metaplast") with transport of depolymerization fragments by vaporization and diffusion. The theory predicts product yields and molecular weight distributions in agreement with the observed results. An attempt has also been made to fit the regular structure in the FIMS spectra with an assumed distribution of likely homologous series. Although the assignments are highly speculative, it is possible to obtain a reasonable facsimile of the FIMS spectra with chemically reasonable choices.

EXPERIMENTAL

The pyrolysis experiments were performed in an apparatus which employs an electrically heated grid within an infrared cell to provide on-line, in-situ analysis of evolved products by Fourier Transform Infrared (FT-IR) Spectrometry. In the flash pyrolysis experiments, the cell was closed and the grid was heated to a final temperature at between 600 and 2000°C/sec. Char yield was obtained gravimetrically from the residue in the grid. Tar samples were obtained from the cold glass wall of the cell or from in-line filters and yields were obtained gravimetrically. Details of the experiment have been described previously (1,2).

The field ionization mass spectrometry (FIMS) experiments were performed at SRI International. The FIMS technique ionizes molecules with minimal fragmentation and so gives a direct molecular weight distribution (3).

The preparation of the polymer, poly(1,4-dimethylenenaphthalene), naphthalene rings linked by ethylene bridges, is described elsewhere (4).

RESULTS

In relating pyrolysis products to the parent hydrocarbon, one of the most striking observations is the similarity often seen for the functional group composition of the two materials. Figure 1 shows FT-IR spectra for the tars, parent hydrocarbons and their differences for the model polymer, a lignin, a lignite, and a bituminous coal. Except for the lignite, the pairs of spectra are quite similar.

An important difference in the bituminous coal spectrum is a higher methyl group concentration in the tar which appears to result from rupture of C(aliphatic)-C(aliphatic) bonds followed by radical stabilization. Similarly the loss of C(aliphatic)-O bonds in lignin tar is probably due to rupture of ether bonds and evolution of water.

Molecular weight distributions for the heavy products obtained for these 4 samples plus two additional coals are presented in Figs. 2 and 3. All samples except for the lignin (which was pyrolyzed in the heated grid apparatus) were directly pyrolyzed in the FIMS apparatus. These samples were heated at approximately 2-3°C/min to temperatures up to 460°C. The molecular weight distribution is for the sum of products obtained during pyrolysis. The darker spectra in Figs. 2b and 3 are the odd numbered masses for molecules which include nitrogens or C¹³. The simplest spectrum is that of the polymer. It consists of oligomers from monomers to heptamers. All the oligomers are released over a narrow temperature range between 400° and 425°C. This contrasts with the results obtained when the polymer tar is used as the sample in the FIMS. In this case, the sample distills with monomers and dimers coming off below 150°C, trimers and tetramers below 275°C and pentamers and hexamers near 400°C (4). This contrast suggests that the distribution of oligomers in Fig. 2a does not result from evaporation alone, but must be controlled by pyrolysis. The next simplest spectrum is that for lignin which appears to result from monomers, dimers and trimers. The large contribution of dimers in this spectrum is thought to be due to dilignols linked by thermally stable bonds.

The mass spectra of the coal pyrolysis products (Fig. 3) are the most difficult to interpret. The spectra consist of regularly spaced clusters of peaks on top of a smooth background. The height and width of the background increases with rank. Extensive studies of coal pyrolysis products have been performed by Meuzelaar and co-workers (5-7). Their results are obtained for electron impact ionization which produces fragmentation, while the FIMS spectra presented here have negligible fragmentation. Meuzelaar's results can, however, be used to guide our assignment of many of the FIMS peaks. For example, the following homologous series have been identified in Py-MS spectra: m/z- 110, 124, 138 (dihydroxy-benzenes); m/z-94, 108, 122, 136, 150 (phenols); m/z-142, 156, 170, 184 (naphthalenes); and m/z-96, 106, 120 (benzenes).

A number of observations can be made about the spectra: 1) The peaks are organized into peak clusters which have a long range periodicity of 12 1/2 mass units. For subbituminous and higher rank coals, the peaks clusters appear to be arranged in groups of 4 with the peak clusters at 160, 210, 260, 310, etc. being larger than the previous peak cluster. The interpretation is that each set of 4 peaks is a similar series differing by an additional fused aromatic ring. After the addition of a new ring, the next peak cluster is larger by 14, representing the addition of saturated carbons, but the spacing is gradually reduced as the number of extra carbons grow, reaching 12 1/2 mass units per cluster with the addition of the next ring. The change in spacing is thought to result from increasing unsaturations as the side chains grow and form rings. 2) There are relatively low intensities at mass numbers for unsubstituted aromatics such as naphthalene and anthracene; methyl or hydroxyl substituted aromatics have higher values but bi-substituted compounds appear to achieve a maximum. The interpretation is that fragments require the breaking of at least one and, more likely, two bonds, and therefore, are left with one or more substitutions. 3) There are a number of homologous series which are separated by saturated carbons. The relationship of these peaks can be seen by plotting their intensity as a function of the time (or temperature) at which they were evolved. Fig. 4 shows a series of peaks for a Pittsburgh Seam bituminous coal at 108, 122, and 136 compared to a series at 110, 124 and 138. The latter series evolves at a shorter time (lower temperature) than the former. The interpretation is that the 110 series is dihydroxy-benzene, while the former is a methyl hydroxy-benzene. The latter will likely require the breaking of C(aliphatic)-C(aliphatic) bonds which requires more energy and have higher temperatures than the breaking of C(aliphatic) bonds. 4) The relationship between the compound class and the temperature of evolution is further examined in Fig. 4b

which presents the time-dependent intensities of 5 masses associated with one cluster for a lignite. As can be seen, the temperature of evolution goes down with increasing molecular weight. The lignite peaks are more widely separated than for the bituminous coal. As can be seen, the highest molecular weight corresponds to oxygen substituted species, while the lowest corresponds to methyl. This reduction in pyrolysis temperature of oxygenated species is consistent with the rank dependence in pyrolysis products discussed in (8) presented at this symposium. The highest and broadest profile corresponds to a molecular weight having the widest variety of contributing compounds.

DISCUSSION OF TAR FORMATION IN COAL AND OTHER HYDROCARBONS

The mechanisms of tar evolution have been considered by a number of investigations (9-16). It is generally agreed that the process includes the following steps: 1) Formation of tar molecules, 2) transport and evaporation, and 3) possible repolymerization to form coke or char. The questions are: what is the source for tar, how are tar molecules formed, what are the transport bottlenecks and what is the relationship between the formation, transport and repolymerization of tar molecules? The following conclusions were reached in a recent review (17).

1. For bituminous coals, lignins, and some polymers, tar molecules appear to be minimally disturbed fragments of the coal's organic structure. The evidence for this is the striking similarity between the tar and parent material which has been observed in elemental composition, IR spectra (see Fig. 1) and NMR spectra.

2. The production of tar molecules involves bond breaking. The possibility that tar molecules exist in the parent material and are released through evaporation without any bond breaking can be ruled out on the basis of two observations. The first is that extractable molecules generally have a higher average molecular weight than tar molecules (18-20). The second observation is that the evaporation of previously formed tar has a much different temperature dependence than evolution of tar from coal, as discussed above.

3. The variation of yield and molecular weight distribution of tar with pressure suggest that the transport is controlled by gas phase diffusion. An example of the influence of pressure on the molecular weight distribution is illustrated in Fig. 5 which presents FIMS data for a Pittsburgh Seam coal tar produced at 4 atm., and a polymer tar produced at 5 atm. The reduction of the average molecular weight with increasing pressure is striking (see Figs. 2a and 7c). Unger and Suuberg have presented similar data (11-13) and have argued (14) that for softening coals this effect and the variation of yield with pressure can be explained by assuming that the limitation is the diffusion away from the liquid surface during the evaporation process. High pressures hinder the evolution of heavier molecules leading to cracking or repolymerization.

Considering the available evidence, tar formation in softening hydrocarbons may be viewed as a combined depolymerization and evaporation process in which the pyrolytic depolymerization continually reduces the weight of the molecular fragments through bond breaking and free radical stabilization until the fragments are small enough to be evaporated.

For non-softening coals, vaporization at the ambient pressure of the experiment does not appear to be the transport bottleneck. In Figs. 2 and 3, the very low molecular weight of the tars from non-softening lignite and subbituminous coal compared to that from the softening polymer, lignin and bituminous coal, suggests that some other mechanism for limiting the evolution of high molecular weight components must exist, possibly activated diffusion in the solid as suggested by Gavalas et al (15).

MODELING

A theory for the combined effects of bond breaking and vaporization has been developed. The theory combines random cleavage of weak bonds (similar to the concept used by Gavalas et al (15)) with transport of depolymerization fragments by vaporization and diffusion (like Unger and Suuberg (14)) to predict product yield

and composition. The assumptions in this theory include: (1) the bonds between the monomer units in the polymer molecules are the only weak bonds and are equally likely to be cleaved; and (2) repolymerization to form a different chemical structure is not included.

For any oligomer (1) with molecular weight M_1 the theory computes the rate of loss due to bond breaking to form smaller oligomers, the rate of increase due to formation of new oligomers from the breaking of higher molecular weight oligomers and the rate of loss due to evaporation. The process continues as long as hydrogen is available to stabilize the free radicals. Integrating the rate equations over time yields the amount and molecular weight distribution of the vaporized products which constitutes the tar. The computations for the polymer (which has only one monomer) are the numbers in parenthesis on Figs. 2 and 5. The predictions compare favorably with the second set of numbers which are the observed integrated intensities. The theory applied to lignin assuming 7 monomers was described in a recent publication (21). The theory gives reasonable results.

Coal is more difficult to model because of the variety of monomer types and bond energies. We have attempted to get a monomer distribution by fitting the clusters of peaks which show up consistently in the FIMS spectra. The scheme is outlined in Fig. 6. Starting with three basic single ring compounds with the probability for occurrence listed in column A, side chains (or 5 membered rings) are added with the probabilities in column B. Additional fused aromatic rings are added with the probabilities in column C and additional hydrogens to saturate the rings are added in column D. The probabilities shown are for the Pittsburgh Seam coal FIMS in Fig. 7c. The distribution of all possible combinations (the monomer distribution) is illustrated in Fig. 7a which compares reasonably well with the peak clusters in Fig. 7c. The dimer distribution is obtained by adding this distribution (minus 2 to account for the loss of hydrogen in the dimer bridge) to a second monomer distribution which includes molecular weights below 100 (introduced artificially by taking off one fused ring). The dimers were added to the monomers in a ratio of 3:1. This is a departure from the above theory which predicts that initially all oligomers are equally likely, but this compensates for the lack of trimers and tetramers. The resulting distribution is then convoluted with a vaporization probability to produce Fig. 7b which now has the peak clusters as well as the smooth background. The exercise shows that the assumed simple distribution is a possible choice. Other possibilities may also fit, but the choice must have sufficient regularities to produce the observed FIMS peaks.

The lignite molecular weight distribution is clearly controlled by processes other than vaporization as indicated by the lack of appreciable molecules above 200. Lignite is a non-softening solid. The rigid cross-linked nature of the molecular structure provides several possible explanations: (1) the cross-link density is so high and the available hydrogen for stabilization so low that there are very few dimers and trimers which can be released; (2) the rigid structure sterically hinders the escape of large molecules; (3) the rigid structure creates high pressures in the pores which hinders the escape of large molecules. These possibilities are currently under investigation.

CONCLUSIONS

1. Pyrolysis tars for a number of different hydrocarbons including softening coal, lignin and model polymers appear to be minimally disturbed fragments from the parent hydrocarbons. 2. FIMS spectra are useful in providing unfragmented molecular weight distributions for tar. The spectra for coals are remarkably regular. All spectra have the same series of peak clusters. Rank variations show up as variations in the intensity of the peak clusters and in the amount and width of a smooth background. 3. The spectra of the simplest compounds (lignin and a model polymer) can be modeled by a theory which combines random cleavage of weak bonds to form oligomers which are small enough to vaporize. The theory predicts the correct trends for softening coals but not for lignite and low rank coals. 4. A speculative scheme for matching FIMS spectra of coals with an assumed monomer distribution appears to give reasonable results.

ACKNOWLEDGEMENT

The authors wish to acknowledge the support of this program by the Gas Research Institute under contract #5083-260-0582 and the Morgantown Energy Technology Center of DOE under contract #DE-AC21-81FE01522. The authors are grateful to Sydney Buttrill of Stanford Research Institute for his efforts in providing the FIMS spectra and to Dr. Buttrill and Professor Henk Meuzelaar of the University of Utah for helping interpret the mass spectra.

REFERENCES

1. Solomon, P. R., Hamblen, D. G. and Carangelo, R. M., ACS Symposium Series, 205, Coal and Coal Products: Analytical Characterization Techniques, American Chem. Soc., Washington, DC, (1982) pg. 77.
2. Solomon, P.R., Hamblen, D.G. and Carangelo, R.M., Analytical Pyrolysis of Coal Using FT-IR, 5th International Symposium, on Analytical Pyrolysis, Colorado, (1982).
3. St. John, G.A., Buttrill, S.E., Jr. and Anbar, M., "Field Ionization and Field Desorption Mass Spectroscopy Applied to Coal Research", in Organic Chemistry of Coal, (Ed. J. Larsen), ACS Symposium Series, 71, 1978 p. 223.
4. Solomon, P.R., The Synthesis and Study of Polymer Models Representative of Coal Structure, Final Report for GRI, Contract #5081-260-0582, Phase I, (April, 1983).
5. Meuzelaar, H.L.C. and Harper, A.M., and Given, P.H., Utah Geological and Mineral Survey, Bulletin 118, 192, (1982).
6. Meuzelaar, H.L.C., Harper, A.M., Hill, G.R., and Given, P.H., Characterization and Classification of Rocky Mountain Coals by Curie-Point Pyrolysis Mass Spectrometry, Fuel, (in press), (1984).
7. Harper, A.M. and Meuzelaar, H.L.C., and Given, P.H., Correlations Between Mass Spectra of Rocky Mountain Coals and Conventional Coal Parameters, Fuel, (in press), (1984).
8. Solomon, P.R., Hamblen, D.G., Carangelo, R.M., Markham, J.R. and DiTaranto, M.B., The Variation of Coal Pyrolysis Behavior with Rank, ACS Division of Fuel Chemistry Preprints, 29 (1984).
9. Anthony, D.B., Howard, J.B., Hottel, H.C., and Meissner, H.P., "Fifteenth Symposium (International) on Combustion", The Combustion Institute, Pittsburgh, PA, 1974, 1303.
10. Suuberg, E.M., Peters, W.A. and Howard, J.B., "Seventeenth Symposium (Int.) on Combustion", The Combustion Institute, Leeds, England, 1978, 117.
11. Unger, P.E. and Suuberg, E.M., "International Conference on Coal Science", Pittsburgh, PA, 1983, 475.
12. Unger, P.E. and Suuberg, E.M., "Molecular Weight Distributions of Tars Produced by Flash Pyrolysis of Coals", Submitted to Fuel (Jan. 1983).
13. Unger, P.E. and Suuberg, E.M., ACS Division of Fuel Chemistry Preprints, 28, #4, 278, (1983).
14. Unger, P. E. and Suuberg, E. M. "Eighteenth Symposium (International) on Combustion", The Combustion Institute, Pittsburgh, PA, 1981, 1203.
15. Gavalas, G. R., Cheong, P. H. and Jain, R. Ind. Eng. Chem. Fundam., 1981, 20, 113 and 122.
16. Gavalas, G. R., and Wilks, K.A., AICHE Journal, 26, 201, (1980).
17. Solomon, P.R. and King, H.H. Tar Evolution from Coal and Model Polymers: Theory and Experiments, submitted to Fuel (1983).
18. Gavalas, G.B., and Oka, M., Fuel, 57, 285, (1978).
19. Lowry, H.H., "Chemistry of Coal Utilization", John Wiley & Sons, Pub., 1963.
20. Suuberg, E.M., (Private Communication).
21. King, H.H., Solomon, P.R., Avni, E. and Coughlin, R., ACS Division of Fuel Chemistry Preprints, 28, #5, 319 (1983).

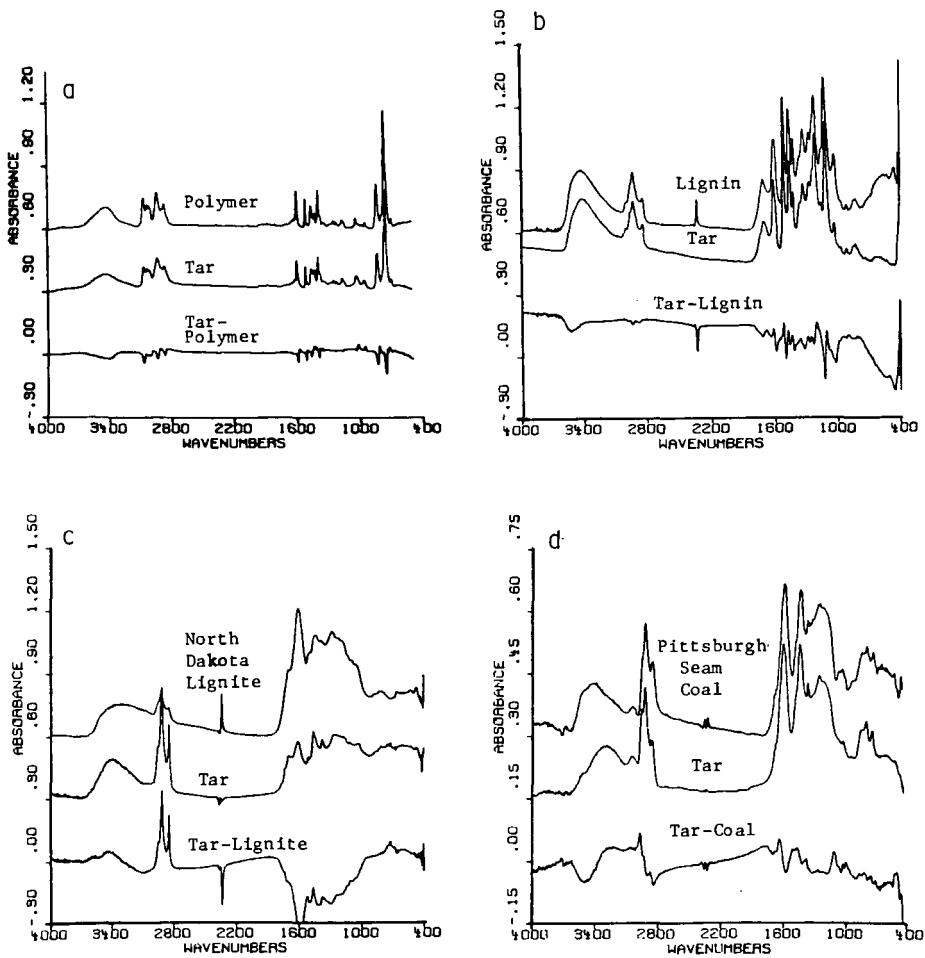
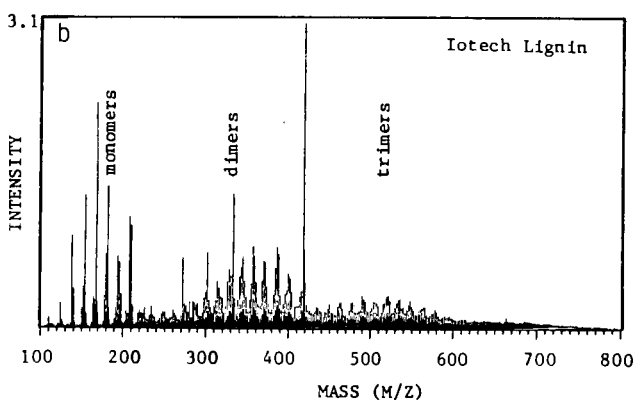


Figure 1. Comparison of FT-IR Spectra of Hydrocarbons and their Pyrolysis Tars.



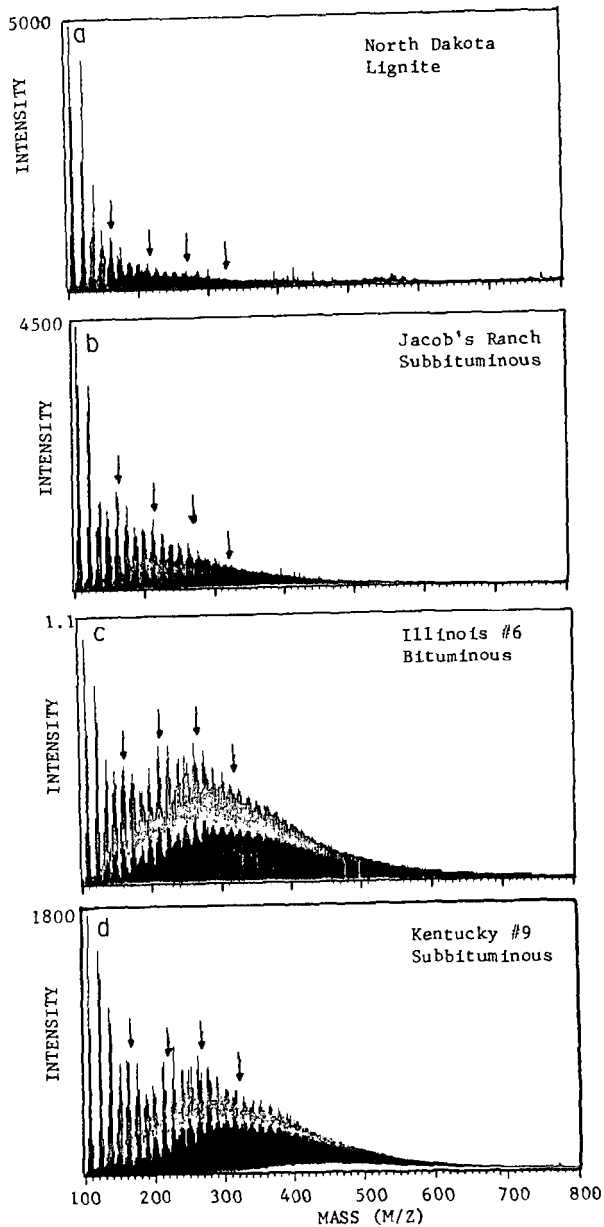


Figure 3. FIMS Spectra of a Lignite and 3 Coals. Arrows designate larger Peaks which begin Series of 4 Peak Clusters.

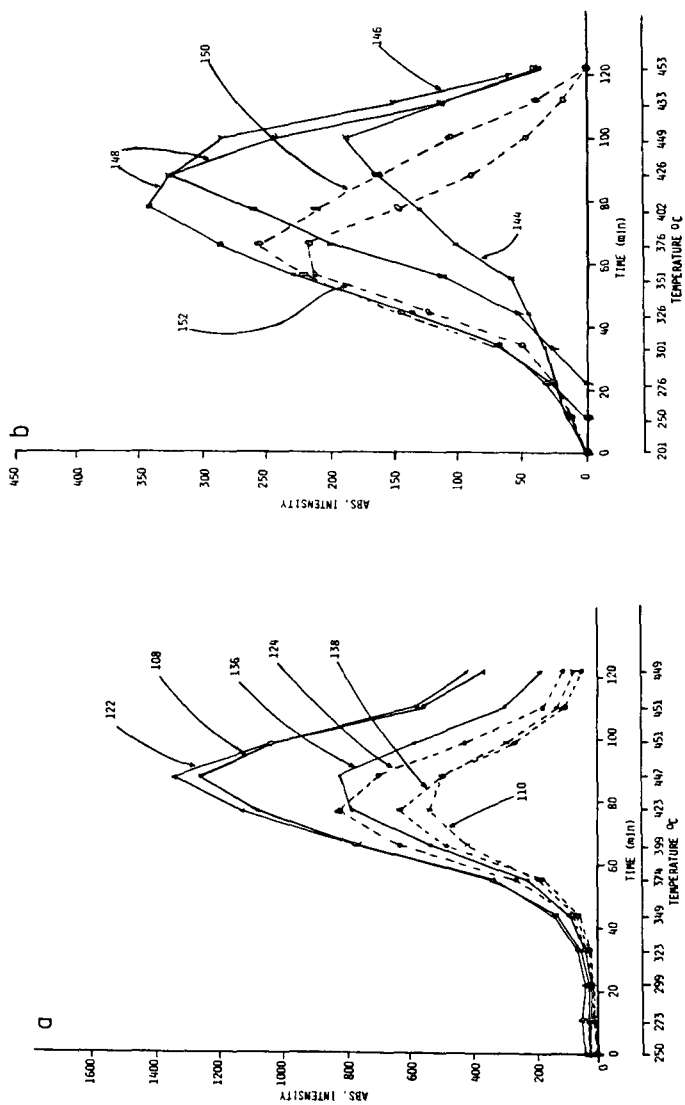


Figure 4. Intensity of Individual Mass Peaks as a Function of Pyrolysis Temperature.

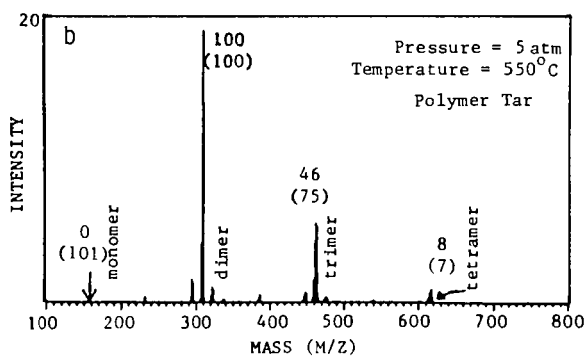
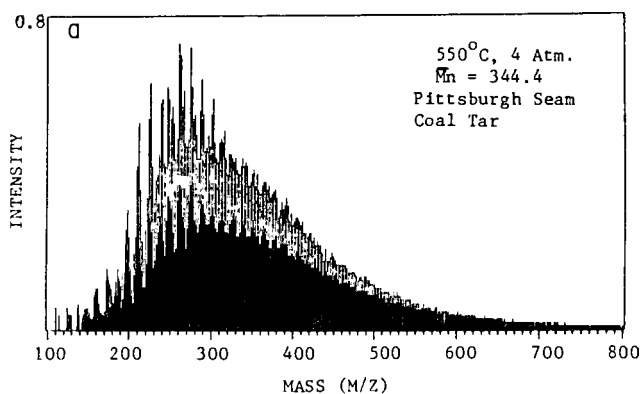


Figure 5. FIMS Spectra of two Hydrocarbon Tars Produced at Elevated Pressure. Spectra for Tars from the same Hydrocarbon produced in Vacuum are presented in Figs. 2a and 7c.

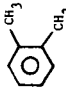
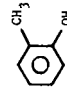
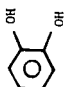
a			b			c			d		
BASIC COMPOUND			SIDE GROUPS			ADDITIONAL FUSED RINGS			RING SATURATION		
MW	Compound	Probability	MW	Group	Probability	MW	Number of Rings	Probability	MW	Number of Hydrogens	Probability
106		0.2	0	-	1.0	0	-	1.0	0	0	.25
			12	C	0.1	50	1	.6	2	2	.25
			14	CH ₂	1.0	100	2	.6	4	4	.5
108		1.0	24	C ₂	0.1	150	3	.6	6	6	.25
			26	C ₂ H ₂	0.2	200	4	.3	10	10	.25
			28	C ₂ H ₄	0.5	250	5	.2			
110		0.3	36-42	C-C ₂ H ₆	0.25	300	6	.1			
			48-56	C ₄ -C ₄ H ₈	0.15						
			60-70	C ₅ -C ₅ H ₁₀	0.07						

Figure 6. Compounds and Probabilities for Monomer Distribution in a Pittsburgh Seam Coal.

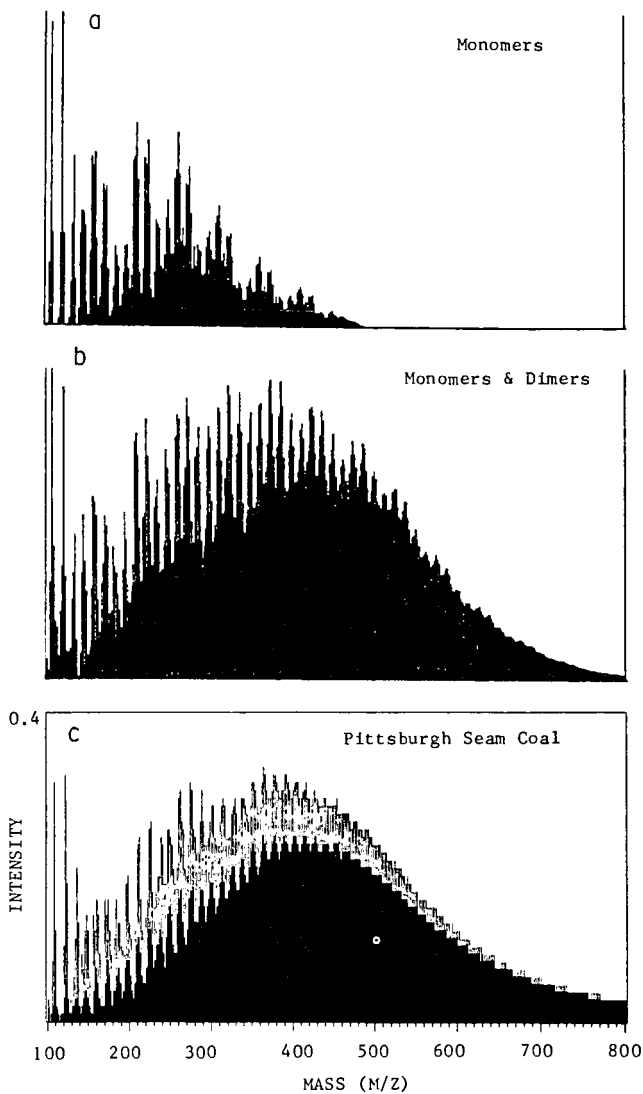


Figure 7. FIMS Spectra for a Pittsburgh Seam Coal (c) and Synthesized Spectra for Monomers and Monomers Plus Dimers.

INVESTIGATION OF ORGANIC STRUCTURAL CHARACTERISTICS OF LOW-RANK COAL LITHOTYPES

S.A. Benson, K.S. Groon, G.G. Montgomery, and H.H. Schobert

University of North Dakota
Energy Research Center
Box 8213, University Station
Grand Forks, North Dakota 58202

Introduction

The structural characteristics of low-rank coals and separated lithotypes were examined by several techniques. The bulk of the work was accomplished with pressure differential scanning calorimetry (PDSC). Supplemental information regarding functional groups was generated by electron spectroscopy for chemical analysis (ESCA) and infrared spectroscopy (IR). Aromaticities were calculated from the PDSC thermogram by a peak height ratio method which has been used in the past on whole coals, organic compounds, and polymers (1, 2). Aromaticities were determined for whole coals and separated lithotypes (fusain, durain, and vitrain). The fusain is the most aromatic of the lithotypes, with aromaticities ranging from 0.67 to 0.80. Calculations made using the proportions of each lithotype present in the coal determined a weighted aromaticity which corresponds very closely to aromaticity on the whole coal. ESCA was used to examine the carbon 1s peak for whole coal and lithotypes. Correlations were made between the relative abundances of C-C, C=O, and C-O bond types and coal lithotype. In nearly all cases, fusain had the largest ratio of C-C bonds. The spectral modes in the infrared which showed significant differences with lithotype include C=O and C-H stretching.

Methods and Procedures

Five low-rank coals and associated lithotypes listed in Table 1 were obtained from mines in the Fort Union and Powder River regions. The whole coals originated from channel samples representing one vertical section of the mine. Lithotypes were separated from samples taken near the location of the channel. The lithotypes were separated into three basic types based on megascopic differences. The vitrain is a very hard, vitreous lithotype. Durain has a dull, woody appearance and is soft compared to vitrain. The fusain is charcoal-like and very fragmental.

TABLE 1. COAL MINE LOCATION DESCRIPTION

Mine	Rank	County	State	Region	Seam
Beulah	Lignite	Mercer	North Dakota	Fort Union	Beulah-Zap
Indian Head	Lignite	Mercer	North Dakota	Fort Union	Beulah-Zap
Velva	Lignite	McHenry	North Dakota	Fort Union	Coteau
Glenharold	Lignite	Mercer	North Dakota	Fort Union	Scranton
Gascoyne	Lignite	Bowman	North Dakota	Fort Union	Harmon
Spring Creek	Subbituminous	Big Horn	Montana	Powder Creek	Dietz

A DuPont 1090 Thermal Analyzer system with a pressure DSC cell was used, to determine aromaticity. Details of this procedure have been published elsewhere (1, 2). Briefly, the procedure to determine the aromaticity involves hermetically sealing between 0.5 to 1.5 mg sample in an aluminum pan with a small hole punched in the

lid; the sample is then heated linearly from 150° to 600°C at 20°C/min under 500 psi oxygen to obtain the thermogram. The aromaticity is calculated from the thermogram as explained in the following section.

Samples were analyzed by transmission infrared spectrophotometry in an attempt to determine qualitative differences in functional groups among lithotypes. The dry coal spectra were obtained using KBr pellets. Appropriate amounts of coal and KBr were used to give a 0.4% or less coal to KBr mixture.

ESCA was used to determine the relative amounts of carbon as C-C, carbon bonded only to carbon or hydrogen; C-O, carbon in ether or phenol groups; and C=O, carbon in carboxyl or carbonyl groups. Samples used for ESCA analysis consisted both of ground samples and whole pieces of coal. The ground samples were pulverized to pass a 200 mesh sieve and pressed into 12.5 mm pellets using a standard laboratory press. The whole pieces of coal were attached to the sample holder with double stick tape and metal clips. Analysis was done using a Physical Electronics model 548 ESCA system. The sample bell jar was maintained at 10-100 nPa. Analysis time was approximately 30 minutes, using an analyzer pass energy of 25 eV. The x-ray beam was 5 mm in diameter to insure a large spectral area. The spectra were corrected for charging by assigning the hydrocarbon C-C peak to -284.6 eV. The spectra were resolved into components using a curve fitting routine employing a Gaussian-Lorentzian function to separate the carbon 1s peaks (3).

Results and Discussion

Aromaticities and temperatures of the peak maxima were determined for whole coals and lithotypes by the PDSC thermograms. The thermograms produced by the PDSC experiment of lithotypes from the Velva mine of North Dakota are shown in Figure 1. The apparent aromaticity, f' , of these samples was found by dividing the height of the high-temperature peak of the thermogram by the sum of the heights of both peaks. The corrected aromaticity, f_a , was then calculated by the empirical equation $f_a = 0.263 + 0.868 f'$ (1). (Preliminary work (1) suggests that different equations for calculating f_a from f' may be needed for different lithotypes; however, until further data is forthcoming, the equation given above will be used.) The results show that fusain is the most aromatic while durain and vitrain have lesser but similar aromaticities. The peak temperatures of the aromatic region of the PDSC thermogram were measured to determine the amount of ring condensation (1).

Five lignites and one subbituminous coal were examined by the PDSC method. The results indicate that the fusain was consistently the most aromatic of the lithotypes. The durain and vitrain of each coal were always lower, but similar to each other, in aromaticity. The peak temperatures and corrected aromaticities of all six coals and their lithotypes are summarized in Table 2.

The temperature of the aromatic peak (high-temperature peak) is important when determining the number or average number of aromatic clusters in coal. Figure 2 is a plot of the temperature of the aromatic peak versus the number of fused rings. This plot was prepared from thermograms of model compounds and polymers of known structure containing one to five fused rings. In general, most of the compounds lie within the band bounded by straight line rising at an angle of approximately 15 degrees. The temperature of the aromatic peak has been plotted for a series of run-of-the-mine coals as a function of rank, where P is peat, L is lignite, etc. Most of the coals fall within the band depicted by the dashed lines with a slow curve upward.

TABLE 2. PEAK TEMPERATURE AND AROMATICITIES OF COALS

Sample Description	Peak Temperatures, °C		Corrected Aromaticity, f _a
	Low	High	
Beulah (whole)	275	375	0.66
B-12 Fusain	290	390	0.88
B-12 Durain	280	365	0.66
B-12 Vitrain	295	375	0.65
Indian Head (whole)	275	360	0.68
IH-1 Fusain	280	390	0.77
IH-4 Durain	275	360	0.71
IH-4 Vitrain	280	380	0.71
Velva (whole)	285	350	0.70
V-5 Fusain	300	375	0.86
V-5 Durain	280	355	0.65
V-5 Vitrain	280	360	0.66
Glenharold (whole)	280	350	0.63
GH Fusain	270	350	0.67
GH Durain	275	345	0.62
GH Vitrain	275	345	0.63
Gascoyne Blue (whole)	380	380	0.57
GB Fusain	290	395	0.78
GB Durain	290	390	0.71
GB Vitrain	285	390	0.54
Spring Creek			
SP Fusain	297	400	0.77
SP Durain	285	400	0.69
SP Vitrain	285	400	0.74

The amount of ring condensation observed by the position of the aromatic peak in the thermograms can be determined by comparison to Figure 2. The extent of ring condensation was determined for lithotypes. The results suggest that fusain ranges from $2\frac{1}{2}$ to $3\frac{1}{2}$ ring clusters, durain ranges from 1 to $3\frac{1}{2}$ ring clusters, and vitrain ranges from 1 to $3\frac{1}{2}$. The average ring condensation for the composite samples ranges from $1\frac{1}{2}$ to $2\frac{1}{2}$. If vitrain and durain are considered to be derived from plant materials with little chemical alteration relative to fusain, it is reasonable to expect low values of ring condensation. Lignin would have a ring condensation number of 1, since the lignin structure is based on phenylpropane moieties. The more extreme thermal conditions which may have led to the formation of fusain would result in a greater aromatization, cross-linking, and condensation of rings.

The approximate amounts of lithotypes in the coals studied averaged 5% fusain, 40% durain, and 45% vitrain. The experimental aromaticities of the composite coals agree with values calculated from weighed aromaticities as shown in Table 3.

An example of an ESCA spectrum, for the carbon 1s region, is shown in Figure 3. The spectrum is resolved into separate peaks assigned to the C-O, C=O, and C-C bond types. The peak assignments are based on analogy to model polymers, particularly polyethylene terephthalate (3). The C-C peak was corrected to -284.6 eV to account

TABLE 3. CALCULATED VERSUS EXPERIMENTAL AROMATICITIES

Coal	Corrected Aromaticity of Lithotype			Calculated Aromaticity For Whole Coal	Calculated Aromaticity For Whole Coal
	Fusain	Durain	Vitrain		
Beulah	0.80	0.66	0.65	0.66	0.66
Indian Head	0.77	0.71	0.71	0.71	0.68
Velva	0.86	0.65	0.66	0.66	0.70
Glenharold	0.67	0.62	0.63	0.63	0.63
Gascoyne Blue	0.78	0.71	0.54	0.64	0.57

for the effects of sample charging. The ratios of individual peak intensities to the total intensity in the carbon is region are summarized in Table 4 for Beulah and Gascoyne lignites and their lithotypes. (The ratios of peak intensities to total intensities are shown because, for a series of experiments, the total intensity will vary from sample to sample depending on such factors as duration of the experiment and whether the sample is a chip or powder.) The relatively high concentration of C-C bonds in fusain as determined by ESCA is in agreement with the relatively high aromaticities of this lithotype determined by PDSC. The high aromaticity, reduced levels of oxygen functional groups, and the high proportion of oxidized (ie, C=O) functional groups among those remaining in fusain are all consistent with the concept that fusain has been exposed to severe thermal conditions at some point in the coalification process. The ratios of bond types for the composite sample of Beulah lignite are 0.37 for C=O/C-O and 0.09 for C=O/C-C; these agree fairly well with previously published values of 0.44 and 0.12 from ESCA examination of a different sample of Beulah lignite (3). However, as we have discussed elsewhere (3) it is desirable to incorporate data from several techniques or instruments before attempting to draw structural inferences.

TABLE 4. C=O, C-O, and C-C RATIOS DETERMINED FOR ESCA CARBON 1s SPECTRUM

Coal	C=O	C-O	C-C
Gascoyne (whole)	0.03	0.19	0.78
Fusain	0.07	0.03	0.90
Durain	0.04	0.15	0.81
Vitrain	0.04	0.10	0.86
Beulah (whole)	0.07	0.19	0.74
Fusain	0.09	0.05	0.86
Durain	0.05	0.16	0.79
Vitrain	0.0	0.21	0.88

The infrared spectra for the Beulah coal and lithotypes are shown in part in Figure 4. The intensity of the aliphatic C-H stretches for durain is much greater than that of fusain and the whole coal. The peak at 1700 cm^{-1} is most pronounced in the fusain spectra and appears as shoulders in the others. This peak may be assigned to carbonyl (C=O) stretching. The ESCA data indicates a higher concentration of C=O for fusain, providing qualitative agreement between the ESCA and IR data.

Conclusions

PDSC analysis of lithotype samples has shown that fusain is invariably the most aromatic of the lithotypes of these low-rank coals. Durain and vitrain have usually shown aromaticities similar to each other and significantly lower than fusain. It has been shown that experimental values obtained for the lithotypes could be weighted according to the approximate percentage of each lithotype in the coal, and a value for the whole coal could be calculated which compared quite well with the actual, experimental value. This correlation was especially significant when aromaticity values were used.

The correlations noted between the PDSC, ESCA, and IR include aromaticities and functional group analysis. The aromaticities determined by PDSC are supported by the ESCA C-C ratio, where in most cases fusain is the most aromatic. The unique features of the PDSC thermograms for vitrain are supported by ESCA data. For example, the shoulder peak at 400°C is an indication of increased aromatization. The C-C ratio from the ESCA spectra of vitrain is nearly as high as that of fusain but in the Beulah the vitrain C-C ratio was greater. The aliphatic nature of durain is shown by the aliphatic C-H stretching in the infrared spectra being relatively greater than in the spectra of the other lithotypes. High amounts of carboxyl content (C=O), supported by both ESCA and IR evidence, was characteristic of fusain.

The structural relationships of low-rank coals and associated lithotypes determined by ESCA, PDSC, and IR provides a means of examining coal aromaticities and functional groups. The techniques are relatively fast and help provide insight into the molecular "structure" of low-rank coals.

Acknowledgment

The authors would like to thank David Kleesattel for separating the lithotypes. Ms. Groon was supported by an Associated Western Universities summer research participation grant.

References

1. Benson, S.A. and H.H. Schobert. Structural Characteristics and Relationships in Low-Rank Coals. In Technology and Use of Lignite. U.S. Department of Energy Report GFETC/IC-82/1, p. 442-70, 1982.
2. Benson, S.A., K.S. Groon, and H.H. Schobert. Pressure Differential Scanning Calorimetry of Coals, Organic Compounds, and Polymers. Proceedings, 12th North American Thermal Analysis Society Conference, Williamsburg, Virginia, p. 22-36, September 1983.
3. Schobert, H.H., G.G. Montgomery, M.J. Mitchell, and S.A. Benson. Characterization of the Organic Structure of U.S. Lignites by Electron Spectroscopy and Thermal Analysis. Proceedings, 9th International Conference on Coal Science, Pittsburgh, Pennsylvania, p. 350-353, August 1983.

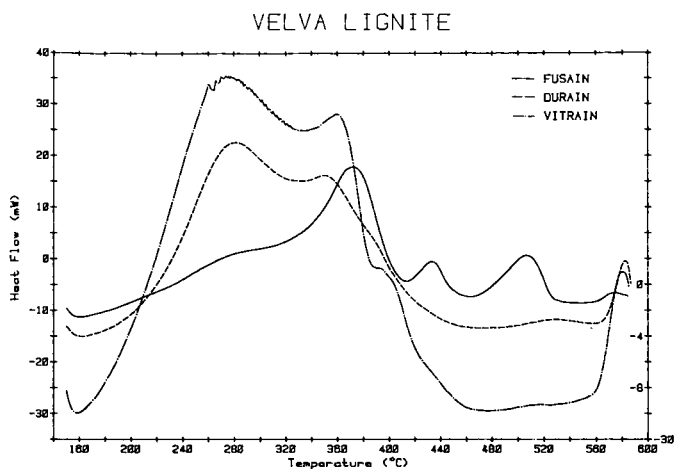


FIGURE 1. PDSC thermograms of lithotypes from the Velva, North Dakota mine.

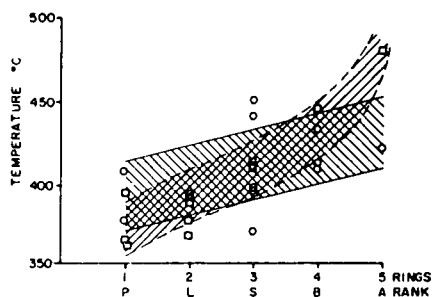


FIGURE 2. Temperature of aromatic peak as a function of number of fused rings for pure compounds (circular points; trend shown by band outlined with solid straight lines) or as a function of rank (square points; trend shown by band outlined with dashed curving lines) (1).

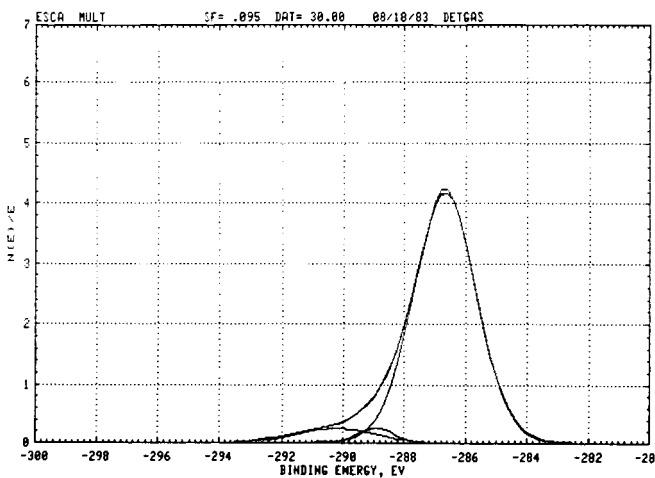


FIGURE 3. ESCA carbon 1s spectra of Gascoyne vitrain.

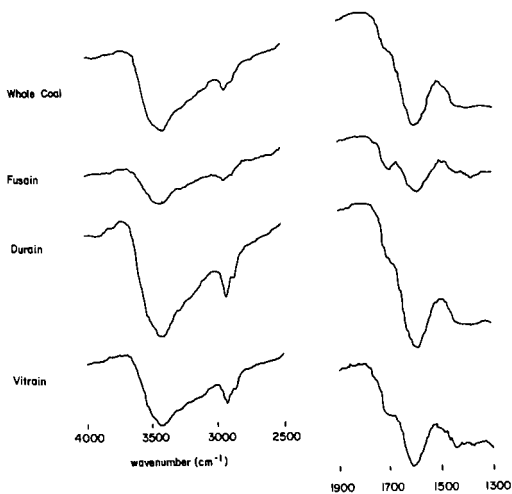


FIGURE 4. IR spectra of Beulah coal and lithotypes.

CONCERNING THE CALCULATION OF COAL
STRUCTURAL PARAMETERS FROM SPECTROSCOPIC DATA

P. Painter, M. Starsinic, E. Riesser, C. Rhoads and B. Bartges

Materials Science and Engineering Department
Steidle Building
The Pennsylvania State University
University Park, PA 16802

Because of the heterogeneous, multicomponent nature of coal, much structural analysis work has been channelled towards the determination of parameters that can be used to describe "average" structures. In principle, FT-ir measurements can be used to quantitatively determine the aliphatic CH, aromatic CH and OH content of coal (1-5), while solid state ^{13}C nmr spectroscopy can be used to determine the relative proportions of aromatic to aliphatic carbon (6-9). There is much active research aimed at extending the scope of these techniques to allow the measurement of additional functionalities. Nevertheless, with these measurements alone a number of fundamental structural parameters (H/C , $\text{H}_{\text{al}}/\text{C}_{\text{al}}$, $\text{H}_{\text{ar}}/\text{C}_{\text{ar}}$, etc.) can be calculated. Furthermore, with the measurement of one additional parameter, the number of methyl groups (as measured by the fraction of aliphatic carbon or hydrogen involved in such groups), it should be possible to determine the distribution of aliphatic carbon (ie. the relative proportions of CH , CH_2 , and CH_3 groups) and then describe a "mean structural unit" in terms of average aromatic ring size and the type and distribution of bridging units and substituents. This can be accomplished by using the equations originally described by van Krevelen and Schryver (10) and utilized by Dryden (11,12) for statistical structural analysis. Similar equations were also derived by Brown and Ladner (13) in order to utilize the data that was then becoming available from proton n.m.r. measurements. However, there were a number of uncertainties in applying these equations. Dryden used data from elemental analysis together with estimates of aromaticity and other parameters (eg. alicyclic hydrogen) that were to some degree uncertain. An iterative procedure was used to solve the equations. The application of the Brown-Ladner equation required assumptions concerning the aliphatic hydrogen-to-carbon atomic ratio. Quantities such as this can now be determined directly from combined FT-ir/ ^{13}C nmr measurements. We therefore considered that it might be a relatively straightforward task to calculate mean structural units for the coal samples for which we have accumulated spectroscopic data (4,9). And it is. Unfortunately, a major problem arises once we consider whether or not the numbers so derived mean anything. We will show that for an individual coal they do not. The form of the equations are such that errors accumulate dramatically and our spectroscopic measurements are insufficiently precise to obtain anything but a broad description of trends as a function of rank. We will first consider the data obtained for a set of vitrinite concentrates and specifically the problems with the FT-ir data. We will then demonstrate how even small errors in this data dramatically affect the calculation of structural parameters.

The fraction aromaticity, f_{ar} , can now be determined with what is considered to be reasonable precision by ^{13}C nmr using cross-polarization and magic angle spinning. It is probably more accurate to say that most fuel scientists are comfortable with the values of f_{ar} so derived, because there are a number of sources

of possible error and these are not easily quantified. For the sake of the arguments we wish to make here we will assume (optimistically) that the values of f_a are good to $\pm 5\%$. Values of f_a for a set of vitrinites reported previously (9) are combined with more recent measurements of additional samples by Martzel and Koenig (14) and Pugmire and Grant (15) in figure 1. There is some scatter, but a reasonably narrow band of values is apparent.

Unlike nmr measurements, where the ratio of peak areas is equal to the ratio of aromatic to aliphatic carbon, bands in the infrared spectrum require calibration. They are related to the concentration of the appropriate functional group through an absorption coefficient which is different for each band. This has led to all sorts of trouble and a variety of values of aromatic to aliphatic hydrogen ratio's can be found scattered throughout the literature. We will not discuss the various methods that can (and have) been used to calibrate infrared bands, this ground is covered elsewhere (5). In terms of the points we wish to make here, the actual values of H_{al} and H_{ar} are to some degree irrelevant, as we will be more concerned with the effects of errors in these values on subsequent calculations of structural parameters. Nevertheless, it is important and illuminating to consider one factor that is probably central to many of the discrepancies found in the literature. If we take a bituminous coal of, say 82% carbon content, we typically determine an aliphatic hydrogen content close to 4% and an aromatic hydrogen content of about 1%. There are numerous errors that can affect these measurements, but these are not simply cumulative. For example, if errors in sample preparation, band areas etc. were of the order of $\pm 10\%$, we might be able to quote values of 4-0.4% and 1-0.1% for aliphatic and aromatic CH content, respectively. However, the absorption coefficients for aliphatic and aromatic CH bands are presently being determined by equating band areas to hydrogen content determined from elemental analysis (1,5). If a sample has negligible COOH content we can write

$$H = H_{OH} + H_{ar} + H_{al} \quad (1)$$

where H is the hydrogen content determined by elemental analysis, and H_{OH} , H_{ar} and H_{al} is the hydrogen found as OH, aromatic CH and aliphatic CH, respectively. This can be rewritten as;

$$(H - H_{OH}) = I_{ar} \epsilon_{ar} + I_{al} \epsilon_{al} \quad (2)$$

where I is the intensity of the appropriate infrared band and ϵ is a conversion factor (equivalent to the reciprocal of the absorption coefficient in appropriate units) relating band area to corresponding hydrogen content. Theoretically, data from a set of coals can be used and ϵ_{ar} and ϵ_{al} determined graphically (1) or by obtaining numerical solutions to the resulting simultaneous equations (3,5). We have recently shown, however, that these equations are classically ill-conditioned (5). In other words, a range of solutions gives almost equally acceptable answers. We have spent a lot of time trying to pin down the "correct" answer, and the values we have recently come up with (5) are somewhat different to those originally reported (3). The key point here, however, is that the ill-conditioned nature of the equations means that the values of H_{ar} and H_{al} determined in this fashion are somewhat dependant. In other words, a 10% error in determining ϵ_{al} and hence H_{al} translates into a much larger error in H_{ar} . This is because the values of ϵ_{al} obtained from solutions to equation 2 will be adjusted to account for as much of the hydrogen as possible. Accordingly, if H_{al} is calculated to be 4-0.4%, H_{ar} will be calculated to be 1-0.4%. A 10% error in ϵ_{al} (hence A_{al}) translates into a 40% error in ϵ_{ar} (and H_{ar}). As a result, even

though the values of the absorption coefficients we have recently determined for the aliphatic CH stretching modes (5) are not far off the more recent values reported by Solomon (2), we still calculate vastly different values of H_{ar}/H_{al} .

Undaunted by these difficulties, we have reproduced our values of H_{ar}/H_{al} for a wide range of coals and vitrinite concentrates in figure 2. The knowledgeable reader will immediately recognize that for coals with a carbon content of 85% or higher these results are very similar to those reported by Brown (16) more than twenty five years ago. For lower rank coals Brown's results fall near the bottom of our band of values. The scatter in the data is not more than we would have intuitively estimated on the basis of coal heterogeneity. This is because these results are obtained by ratioing infrared bands and thus cancelling errors from a number of sources (eg. weighing, insufficient grinding, improper corrections for moisture and mineral contents of the coal). When we consider values of H_{ar} and H_{al} separately, however, these errors return with a bang, as can be seen in the plots shown in figure 3 for the vitrinite concentrates. This, unfortunately, has dire consequences for the calculation of structural parameters.

Before turning our attention to the calculation of these parameters, we will briefly mention measurements of methyl groups by FT-ir. The most easily recognized group frequencies for methyl groups are the stretching modes near 2960 and 2870 cm^{-1} and the symmetric bending mode near 1380 cm^{-1} . The overlap of these bands with other modes is severe and even sophisticated curve resolving procedures cannot entirely separate out the contributions of other functional groups. When methyl groups are attached to aromatic rings, however, a weak overtone band appears near 2730 cm^{-1} (17). This band is well separated from other modes and the precision of FT-ir measurements is such that its band area should be measurable with reasonable accuracy. The process is not entirely straightforward due to problems with establishing a baseline in this region of a typical coal spectrum (the position of the baseline can dramatically affect the measured area of an infrared band). This problem and its solution is discussed elsewhere (18). An absorption coefficient for this band was determined from model compounds. Unsurprisingly, this coefficient did not vary significantly amongst a variety of methyl substituted aromatic materials. This is because many of the methyl vibrational modes are not sensitive to the size and nature of the aromatic entity to which it is attached. We determined that for vitrinite concentrates obtained from bituminous coals the %C found as methyl groups attached to aromatic units varied between 3 and 5% (with one or two outside this range). These numbers agree very well with the total methyl content recently determined by ^{13}C nmr for some of the same vitrinites by Pugmire and Grant (15). Presumably, in vitrinites there are very few methyl groups present in ethyl, propyl or similar units. (This is not the case for exinites, which are much more aliphatic. We again determine that approximately 4%C is tied up in methyl groups attached to aromatic rings, but nmr analysis indicates a total methyl content of approximately 7%).

Given that we can determine reasonably accurate values for the relative proportions of aliphatic and aromatic carbon from ^{13}C nmr, aliphatic and aromatic hydrogen from FT-ir and methyl group concentration from either or both techniques, what can we calculate and to what extent does it mean anything? Space does not permit us to consider all the equations utilized by Dryden (11,12) and Brown and Ladner (13), but a relatively simple example indicates the problem. The following two equations can be used to describe the distribution of aliphatic groups;

$$H_{al} = H_{CH} + H_{CH_2} + H_{CH_3} \quad (3)$$

$$C_{al} = C_{CH} + C_{CH_2} + C_{CH_3} \quad (4)$$

The concentration of hydrogen and carbon present in aliphatic groups, H_{al} and C_{al} , can be determined from FT-ir and ^{13}C nmr, respectively. The % hydrogen and carbon present in methyl groups, H_{CH_3} and C_{CH_3} , can also be determined as discussed above. This leaves two equations in two unknowns. Consequently, we should be able to determine the distribution of aliphatic species in any particular coal. Consider, however, a typical example. A vitrinite concentrate (PSMC 71, 85.2%C) with $f = 0.73$, $H_{al} = 3.5\%$ and $C_{CH_3} = 3.6\%$. Solving equations (3) and (4) gives values of $C_{CH_2} = 11.8\%$ and $C_{CH} = 7.6\%$. Now consider the effects of relatively modest errors. For example, if we optimistically decide that f is equal to 0.73 ± 0.2 and H_{al} is equal to $3.5 \pm 0.2\%$, we can determine a range of values of C_{CH_2} and C_{CH} corresponding to the upper and lower limits of these values. The values of C_{CH} now fall in the range 15.1% to 2.2% while C_{CH_2} falls in the range 4.5% to 16.2%! Clearly for any single sample even small errors multiply to such an extent that it is not possible to define structural parameters with any degree of precision or confidence.

This situation is not confined to the simple example given above. For example, he previously (9) used the Brown-Ladner equation (13) to calculate the aliphatic hydrogen to carbon atomic ratio, H_{al}/C_{al} :

$$f_a = [C/H - H^*_{al}/(H_{al}/C_{al})]/C/H \quad (5)$$

where H^*_{al} is the fraction of total hydrogen present as aliphatic groups. Assuming errors of approximately $\pm 5\%$ in values of f , it was found that proportionally much larger errors were calculated in H_{al}/C_{al} , these errors increasing proportionally with rank. This is because H_{al}/C_{al} actually varies with the reciprocal of $(1-f)$, so that errors in f become increasingly significant. [For example, even small errors in f for a high rank coal, say $0.9 - 0.02$ or -2% results in much larger errors in $(1-f)$, $0.1 - 0.02$ or -20%].

Clearly, the accurate calculation of structural parameters for any specific coal is almost pointless, given the precision of the data presently available. Nevertheless, broad averages and trends as a function of rank can be determined. If we take the plots of f , H_{al} , H , etc. reproduced in figures 1 thru 3, then we can draw lines through the data. At any particular value of %C we can then read off these plots values that represent an "average" parameter value for coals of that rank. These average values can then be used to calculate structural parameters. This procedure is limited and unsatisfactory, but given the major effects experimental errors have on the data, it is the best we can do at this time. If nothing else they show trends as a function of rank. As an example a plot of the distribution of aliphatic CH groups is shown in figure 4. It can be seen that the proportion of CH_2 to CH groups increases as a function of rank, while the experimentally determined %C as CH_3 groups remains approximately constant.

References

1. Solomon, P. R. ACS Division of Fuel Chemistry Preprints, 24 #3, 184 (1979).
2. Solomon, P. R. Hamblen, D. G. and Carangelo, R. M. in "Coal and coal products. Analytical Characterization Techniques" E. L. Fuller, Ed. ACS Symposium Series #205, 77 (1982).

3. Kuehn, D. W., Snyder, R. W., Davis, A. and Painter, P. C. Fuel, 61, 682 (1982).
4. Snyder, R. W., Painter, P. C., Havens, J. R. and Koenig, J. L. Applied Spectroscopy (In press).
5. Riesser, E., Starsinic, M., Squires, E., Davis, A. and Painter, P. C. Fuel (In press).
6. Miknis, E. P., Maciel, G. E. and Bartuska, V. J. Org. Geochem. 1, 169 (1979).
7. Miknis, E. P., Sullivan, M. and Maciel, G. E. Org. Geochem. 3, 19 (1981).
8. Zill, K. W., Pugmire, R. J., Grant, D. M., Wood, R. E., Wiser, W. H. Fuel, 60, 717 (1981).
9. Painter, P. C., Kuehn, D. W., Starsinic, M., Davis, A., Havens, J. and Koenig, J. L. Fuel, 62, 103 (1983).
10. Van Krevelen, D. W. and Schuyer, J. "Coal Science" Elsevier (1957).
11. Dryden, I. G. C. Fuel, 37, 444 (1958).
12. Dryden, I. G. C. Fuel, 42, 55 (1962).
13. Brown, J. K. and Ladner, W. R. Fuel 39, 87 (1960).
14. Martzel, E. M. S. Thesis. Case Western Reserve University, Dept. of Macromolecular Science. (1983).
15. Pugmire, R. and Grant, D. Private communication, to be published.
16. Brown, J. K. J. Chem. Soc., 744 (1955).
17. Bellamy, L. J. The infrared spectra of complex molecules. Vol I, Third Edition Chapman and Hall, London (1975).
18. Starsinic, M. Ph.D. Thesis, The Pennsylvania State University (1984).

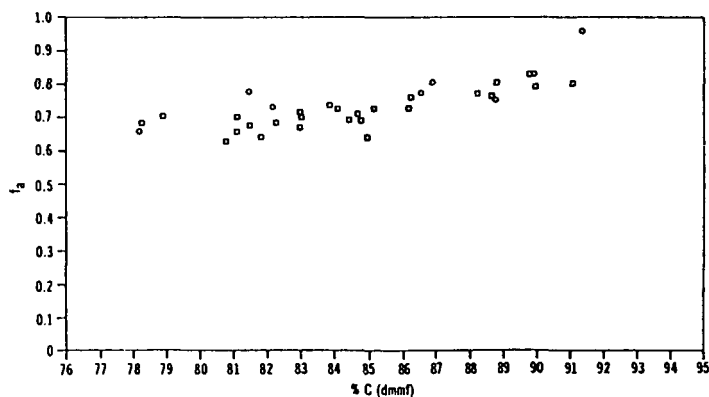


Figure 1. Plot of fraction aromaticity, f_a , vs %C dmmf for a set of vitrinite concentrates.

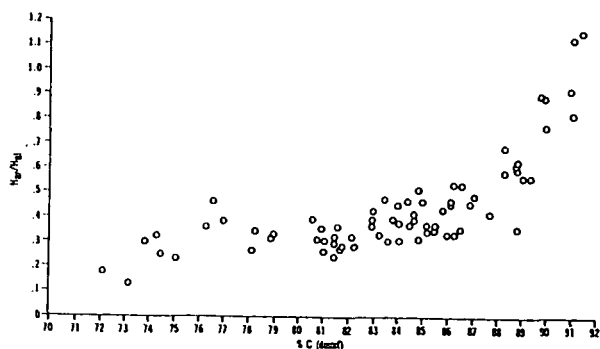


Figure 2. Plot of the ratio of aromatic to aliphatic hydrogen, H_{ar}/H_{al} , determined for a set of coals and vitrinite concentrates.

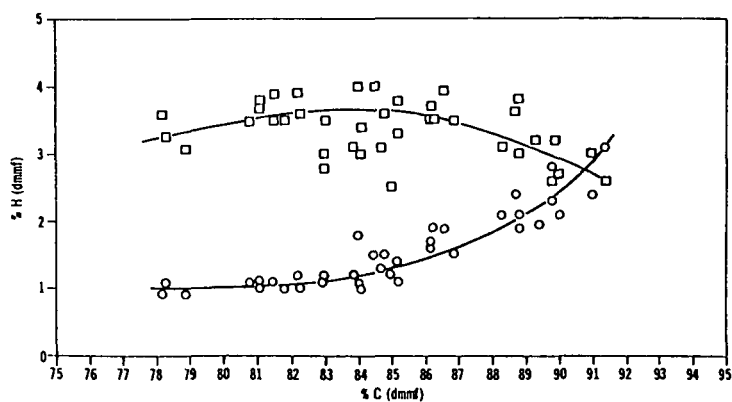


Figure 3. Plot of %H in aliphatic groups (top) and %H in aromatic groups (bottom) vs %C dmnf for a set of vitrinite concentrates.

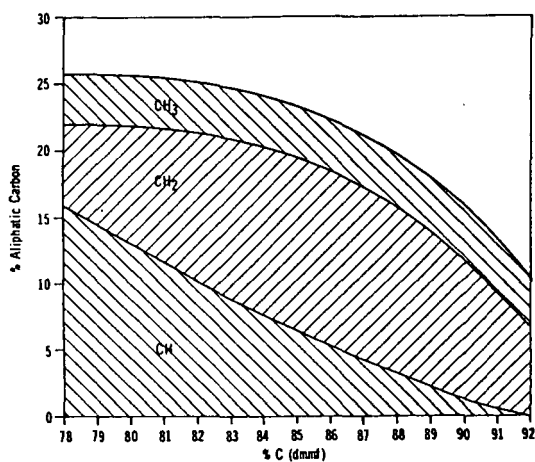


Figure 4. Plot of distribution of aliphatic groups as a function of rank of a set of vitrinite concentrates.

ASPHALTENE CHARACTERIZATION BY A NONSPECTROSCOPIC METHOD

Manuel A. Francisco
and
James G. Speight

Exxon Research and Engineering Co.
Clinton Township, Route 22 East
Annandale, New Jersey, U.S.A. 08801

INTRODUCTION

The emergence of the heavier crude oils as refinery feedstocks has become the accepted norm over the last decade (1). It is, however, a property of these feedstocks to be rich in asphaltenes (2,3,4) which are not very amenable to refinery processes and are usually responsible for coke lay-down and for catalyst deterioration (3,4).

The conventional definition of asphaltenes is based on the solution properties of petroleum residua in various solvents (5,6,7). This generalized concept has been extended to fractions derived from other carbonaceous sources, such as coal and oil shale. Thus, there are "petroleum asphaltenes", "coal liquid asphaltenes", "coal tar asphaltenes", "shale oil asphaltenes", "tar sand bitumen asphaltenes" and the like. With this extension, there has followed considerable scientific effort to further define asphaltenes in terms of molecular structures (9,10,11).

Nevertheless, it must always be recognized that asphaltenes (from whatever the source) are, in fact, a solubility class (Figure 1) and that the definition is, in fact, an operational one; that is, asphaltenes are soluble in benzene and insoluble in pentane. Usually, for virgin petroleum samples, the residuum is completely soluble in benzene. However, with heat-soaked samples or coal derived liquids, the benzene insolubles can be appreciable.

A more recent concept (14) extends the solubility classification of asphaltenes and involves, initially, a consideration of molecular weight vs. polarity for the molecular types found in petroleum residua and/or heavy oils (Figure 2). The polarity scale may be in definable arbitrary units, such as relative adsorptive strength on a solid, e.g. Attapulugus clay and/or silica gel (15), or by solubility in a variety of solvents of increasing polarity as practiced on separation of coal liquid fractions (13); this scale is thus a molecular weight-independent portion of the solubility parameter. For any particular

precipitating medium, say n-heptane, the precipitated asphaltenes will, therefore, consist of less polar materials of higher molecular weight and more polar materials of lower molecular weight; with n-pentane as the precipitating agent, both less polar and lower molecular weight materials are included in the precipitate and the total amount of precipitate increases (16,17). The concept also allows for a polarity range within the various asphaltenes where varying heteroatom (nitrogen, oxygen, and sulfur) contents of the petroleum asphaltenes or variations in the source (and method of preparation) that would be expected to influence polarity (18,19,20).

The present communication describes an extension to the concept of asphaltene polarity by the delineation of petroleum asphaltenes as a collage of functional types using ion-exchange chromatography.

EXPERIMENTAL

1. Feedstock

Arabian heavy crude oil vacuum (950°F+) residuum was used as the feedstock for all of these investigations.

2. Ion-exchange Fractionation

Separation of the feedstock by ion-exchange resins was carried out using a feedstock/solid ratio ~ 0.05* and the product fractions (Figure 3) were designated (a) bases; (b) acids; (c) neutral polars; and (d) neutral nonpolars.

3. Deasphalting

Separation into asphaltene and deasphalted oil fractions was achieved by mixing the fraction with n-heptane (1 gm. fraction:40 ml. n-heptane) at room temperature for 16 hr. with agitation. At the end of this time, the insoluble asphaltenes were separated by filtration and washed with fresh n-heptane (200 ml:1 gm. asphaltenes). The asphaltenes were "purified" from adsorbed material by dissolution in toluene (10 ml:1 gm. asphaltenes) and precipitated with n-heptane (80 ml:1 ml toluene); any soluble material was recovered and added to the deasphalted oil.

*The feedstock/resin ratio was computed on the basis of the number of active sites on the resin and is, therefore, subject to change and depends upon the nature of the resin.

4. General Techniques

Solvents were removed from the products by means of a Rotovap (60°C/40 mm Hg.) and final vestiges were removed by "drying" the products in vacuo (100°C/20 mm Hg.).

RESULTS AND DISCUSSION

The application of chromatographic adsorption techniques to investigate functional and/or structural types in asphaltenes is not new (21,22) but problems of precise identification may be limited by the incomplete recovery of the asphaltene from the adsorbent, particularly when the functionalized ion-exchange adsorbents are employed. However, ion-exchange fractionation of whole feedstocks has been cited to result in an overall more complete recovery of the asphaltenes (23).

In the present work, it has been found preferable to fractionate the whole residuum by ion-exchange chromatography not only to build up a picture of the asphaltenes in terms of functional types but also to note the overall distribution of functional types in the whole feedstock as well as the nuances of the deasphalting technique.

Thus, fractionation of Arabian heavy crude oil vacuum residuum by ion-exchange chromatography produced a series of fractions (Table 1) of varying functionality which could also be differentiated by infrared spectroscopy (Figure 4).

Subsequent heptane-deasphalting of these fractions not only allows cross-referencing of the two techniques but also allows the deasphalted oil and the asphaltenes to be represented on the basis of the different functionalities (Figures 5 and 6).

Obviously, the chemistry and structural features of petroleum asphaltenes will be dictated by the distribution of functional/structural types separated as an artifact of the deasphalting technique. This makes the representation of the structure/functionality of these carbonaceous constituents of petroleum by "average" structures very difficult to conceive (11,18).

Such carbonaceous materials are, therefore, best represented by a series of structural and/or functional types that are best fitted to describe their chemistry/reactivity.

LITERATURE CITED

1. "The Future of Heavy Crude Oil and Tar Sands", R. F. Meyer and C. T. Steele (editors), McGraw-Hill, New York, 1981.
2. J. G. Speight, "Asphaltenes as an Organic Natural Product and their Influence on Crude Oil Properties", presented at the Div. of Geochemistry, Am. Chem. Soc., New York, August 23-28, 1981.
3. J. G. Speight, "Th Desulfurization of Heavy Oils and Residua", Marcel Dekker Inc., New York, 1981.
4. M. L. Gorbaty and J. G. Speight, "The Characterization of Heavy Oils and Residua", paper presented at the 28th IUPAC Conference, Vancouver, B.C., Canada, August 16-21, 1981.
5. "Annual Book of ASTM Standards; American Society for Testing and Materials, Philadelphia, Part 24, Standard No. D-2006", 1975, withdrawn 1976.
6. "Annual Book of ASTM Standards; American Society for Testing and Materials, Part 15, Proposed Standard for Asphalt Composition".
7. "Standards for Petroleum and Its Products, Standard No. 1P 143/57", Institute of Petroleum, London.
8. J. G. Speight, R. B. Long and T. D. Trowbridge, Preprints, Am. Chem. Soc. Div. Fuel Chem., 1982, 27, (3/4), 268.
9. J. G. Speight, Applied Spectroscopy Reviews, 1972, 5, 211, and references cited therein.
10. T. F. Yen, PREPRINTS, American Chemical Society, Division of Petroleum Chemistry, 1972, 17(4), F102, and references cited therein.
11. J. G. Speight, Preprints, Am. Chem. Soc., Div. Petrol. Chem., 1979, 24(4), 910.
12. J. D. Brooks and G. H. Taylor, Chem. & Phys. of Carbon, Vol. 4, 243 (1968) Marcel Dekker, New York.
13. M. Farcasiu, T. O. Mitchell, D. D. Whitehurst, A.C.S. Div. Fuel Chemistry Preprints, Vol. 21, No. 7, 11, (1976).
14. R. B. Long, Preprints, Am. Chem. Soc., Div. Petrol. Chem., 1979, 24(4), 891.

15. L. W. Corbett, *Anal. Chem.* 41, 576 (1969).
16. D. L. Mitchell, J. G. Speight, *Fuel*, 1973, 52, 149.
17. L. W. Corbett, and U. Petrossi, *Ind. Eng. Chem. Prod. Res. Dev.* 17, 342 (1978).
18. J. G. Speight and R. B. Long in "Atomic and Nuclear Methods in Fossil Energy Research", R. H. Filby (editor), Plenum Press, New York, 1982, 295.
19. J. G. Speight and S. E. Moschopedis in "The Chemistry of Asphaltenes", J. W. Bunger and N. C. Li (editors), Am. Chem. Soc., Adv. in Chem. Series No. 195, Washington, DC, 1981, 1.
20. J. G. Speight, "The Structure of Petroleum Asphaltenes", Information Series No. 81, Alberta Research Council, 1978; and J. G. Speight, "Geochemical Influences on Petroleum Constitution and Asphaltene Structure" presented at the Div. of Geochem., American Chemical Society, Washington, DC, September, 1979.
21. M. L. Selucky, S. S. Kim, F. Skinner and O. P. Strausz in "The Chemistry of Asphaltenes", J. W. Bunger and N. C. Li (editors), Am. Chem. Soc., Adv. in Chem. Series No. 195, 1981, 83.
22. J. F. McKay, P. J. Amend, T. E. Cogswell, P. M. Harnsberg, R. B. Erickson and D. R. Latham in "Analytical Chemistry of Liquid Fuel Sources", Am. Chem. Soc., Adv. in Chem. Series No. 170, 1978, 128.
23. H. H. Oelert, *Z. Anal. Chem.*, 1969, 244, 91.

Table 1: Fraction yields from the ion-exchange chromatography of Arabian heavy crude oil vacuum (950°F+) residuum

<u>Fraction</u>	<u>Yield</u>	<u>Functionality type</u>
Bases	29.6	Quinoline nitrogen
Acids	3.2	Carboxylic acids and phenols
Neutral polar	19.4	Carbazole nitrogen
Neutral nonpolar	46.5	Saturate and aromatic hydrocarbons

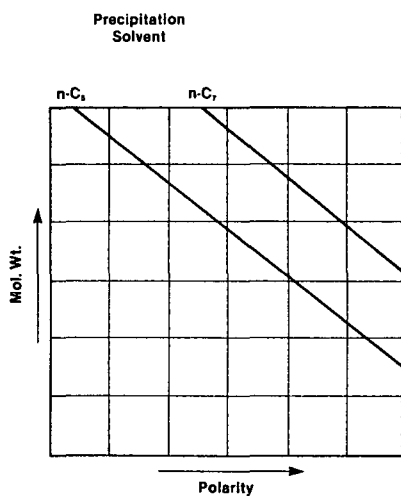


Figure 2: Schematic representation of asphaltene character

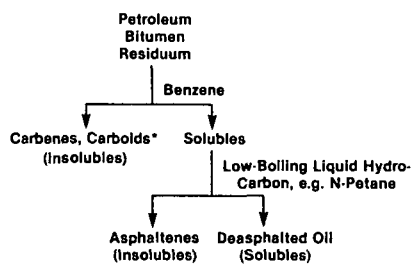


Figure 1: Schematic representation of asphaltene separation.

*In the case of coal liquids, these "insolubles" are often referred to as "preasphaltenes", "asphaltenes", etc. based on solubility in solvents such as pyridine and/or quinoline (12,13).

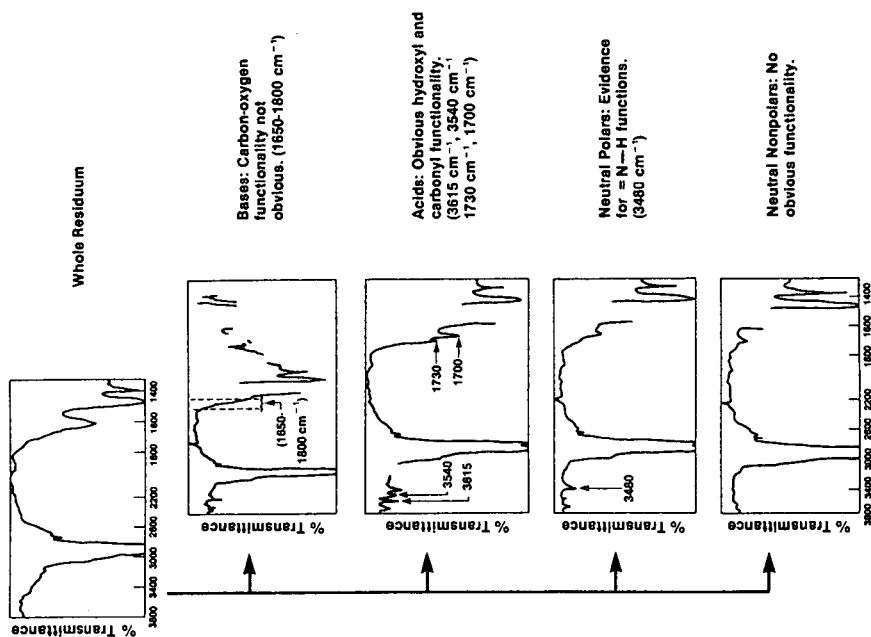


Figure 4: Infrared spectra of fractions separated by the ion-exchange technique

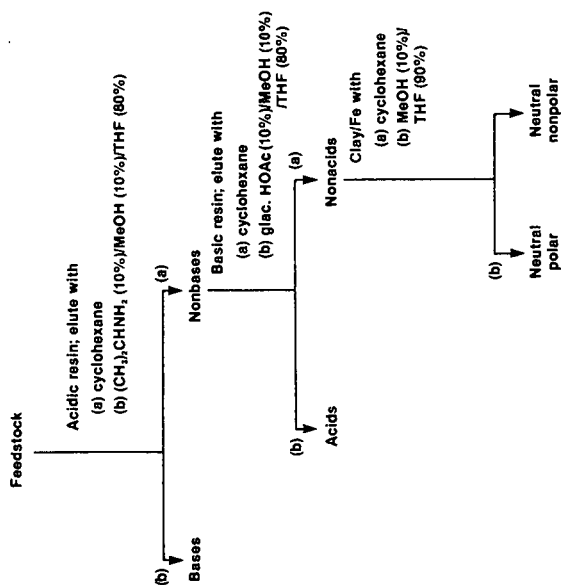


Figure 3: Schematic representation of the ion-exchange fractionation technique.

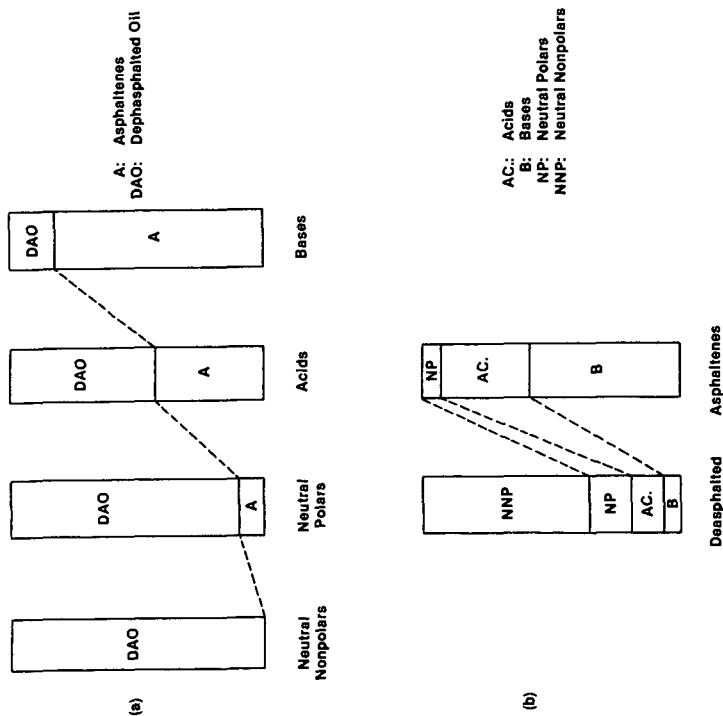


Figure 5: Schematic representation of (a) deasphalting the functionality fractions and (b) reconstruction of the deasphalted oil and asphaltenes on the bases of functional types.

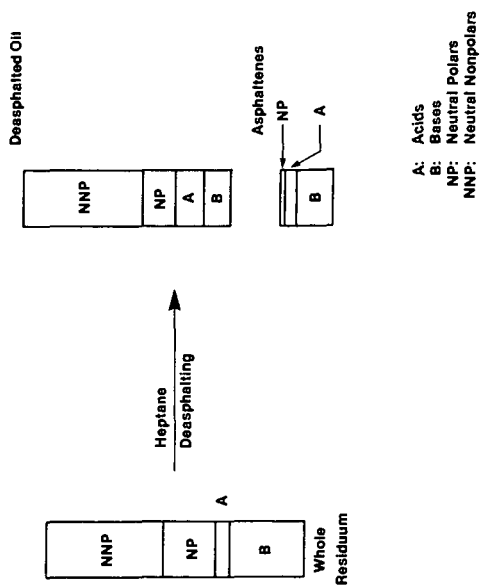


Figure 6: Schematic representation of the deasphalting technique in terms of functionality distribution/redistribution

APPLICATIONS OF X-RAY COMPUTED TOMOGRAPHY TO COAL STUDIES

D.H. Maylotte, P.G. Kosky, E.J. Lamby, C.L. Spiro

General Electric Corporate Research and Development
Schenectady, NY 12301

and

A. Davis, D.F. Bensley

Pennsylvania State University
University Park, PA 16802

X-ray computed tomography (CT) is a non-destructive, non-invasive technique which has been applied here to studies of the internal structures of coal and the penetration of tracer gas into those structures. The CT images are 2-D cross-sectional images of the coal rather than the shadowgraphs of traditional radiography. Compared to shadowgraphs, the CT images provide higher spatial and higher density resolution.

CT images are digital images of the effective x-ray attenuation coefficient for elementary volumes (voxels) within the sample. In these experiments a GE 8800 CT/T machine was used to take the image data, which were then reconstructed to product images with a voxel size of 0.3 mm x 0.3 mm x 1.5 mm. The CT number for each voxel is related to the experimental effective attenuation coefficient for that volume by the relationship:

$$\text{CT No.} = 1024 \times \left[1 + \frac{\mu(\text{material})_E - \mu(\text{water})_E}{\mu(\text{water})_{E_0}} \right]$$

where $\mu(\text{material})_E$ is the attenuation coefficient for the unknown material, $\mu(\text{water})_E$ is the attenuation coefficient of water taken under the same conditions, and $\mu(\text{water})_{E_0}$ is the attenuation coefficient of water taken under standard conditions. The CT images were displayed by assigning a grey scale to the CT numbers. The whiter the image the higher the CT number represented by it and the higher the electric density of the sectioned object. The data collection time for each image was nine seconds.

The x-ray tube for this work was operated at 120 Kev. The filtered emission is a continuum covering the range 20 Kev - 120 Kev, peaking at 35 Kev (Ref. 1). Over this energy range the three significant attenuation mechanisms are, (i) photoelectric absorption, (ii) Compton scattering, and (iii) coherent scattering. For carbonaceous materials the dominant mechanism in this energy range is Compton scattering; therefore, the CT images reflect the electron density distribution within the sample. For the low atomic number elements commonly found in coal the atomic weight is almost twice the atomic number (hydrogen contributes little to the total electron density) and therefore the images are approximately images of the mass density within the sample.

Figure 1 shows a CT image of a piece of Illinois #6 coal. The piece was cut from a larger block which, after mining, had been stored in a sealed vessel under deionized water. The dimensions of the piece were 2.5 cm x 2.5 cm x 10 cm long. The long axis was cut parallel to the bedding planes of the coal. This CT image was taken perpendicular to the

long axis of the coal piece. The coal was potted in a cylinder of epoxy which was then cut to expose the two smaller end faces of the coal and finally O-ring sealed in an acrylic plastic tube (5 cm I.D.).

A sample rectangle on the coal image has been displayed in Figure 1a, and a histogram of the CT values within that rectangle is shown in Figure 1b. Both the average and most probable CT number in the area was 1220. Subsequent to the CT experiments, this particular piece of coal has been sectioned along the plane whose structure was examined by the x-ray fan beam. A microlithotype examination of the exposed face showed that the predominant material in the region covered by the sample rectangle is vitrain. A number of bituminous coals have been examined by CT and, after sectioning, petrographically. CT numbers in the range 1210-1250 are the most commonly occurring numbers in these coals. This assignment of a CT number of circa 1210 to vitrain is also justified on theoretical grounds.

The CT number for a particular material can be calculated when the following system characteristics are known, (a) the emission spectra for the filtered source, (b) the elemental composition and number density of the material being examined, (c) the wavelength sensitivity and efficiency of the detection system. The results of such a calculation for a number of standard materials, minerals and for coal are given in Table 1.

Material	CT (Calc.)	CT (Obs.)
Coal ($C_{49}H_{43}O_7S_1N_1$)	1254	~ 1220
Kaolin ($Al_4Si_4O_{10}(OH)_8$)	3096	3078
Teflon C_2F_4	2106	2050
Calcite $CaCO_3$	4521	> 4096
Dolomite $CaMg(CO_3)_2$	3924	3900-4096
Water H_2O (standard)	1024	

TABLE 1: Calculated and Actual CT Numbers for Coal and Minerals

The calculation of the theoretical CT value for coal assumed the formula given in Table 1 and a density of 1.3 g.cm^{-3} . The calculated CT number is not significantly affected by the formula chosen to represent coal within the reasonable limits of the formulas for the three major maceral groups, i.e., vitrinite, exinite, and inertinite (2). However, the CT number is directly affected by the density chosen for the coal. This insensitivity of CT number to the formula of a hydrocarbonaceous material and its sensitivity to the density is demonstrated in Figure 2. In the density range around 1.3 g/cc the density sensitivity of the technique is 11 CT numbers for a 1% density change. For a uniform material the standard deviation of the CT numbers is ± 2 . The different maceral groups in coal have different densities in the range 1.1 to 1.6 g/cm^3 (2), and the CT image has enough density resolution to distinguish between them. However, the normal size range of many individual coal macerals is below the spatial resolution of the CT equipment being used in this work. In the present experiments, a CT voxel represents a volumetric average of the densities of the macerals contained within it.

In the case of kaolin the CT number for the bulk sample reflects the porosity of the kaolin as well as the CT number attributable to the mineral itself. The kaolin sample was therefore potted in a low viscosity epoxy resin which penetrated the outer layers of the sample (Figure 3). The CT number for the kaolin mineral and the void fraction within the kaolin can then be calculated from the relationships:

$$CT_{total}(1) = \epsilon \times CT_{epoxy} + (1 - \epsilon) CT_{kaolin} \quad 1)$$

$$CT_{total}(2) = \epsilon \times (CT \text{ \# of air} = 0) + (1 - \epsilon) CT_{kaolin} \quad 2)$$

where ϵ is the void fraction in the mineral. The Equation 1) was evaluated for a region where epoxy had penetrated the kaolin and Equation 2) was evaluated for a region inside the kaolin where the epoxy has not penetrated and air fills the spaces between the kaolin grains. The CT number for the cured epoxy was taken from the region outside of the mineral. The CT number for kaolin as obtained in this calculation is given in Table 1 and the void fraction in the bulk mineral was found to be 38%.

The results of Table 1 show that if a region of coal has a CT number above 1300 but less than 3100 then it is contaminated with a varying proportion of mineral matter, and if the CT number is greater than 3100 then it is contaminated with high atomic number minerals (e.g., calcite or pyrite). If the CT number is between 1100 and 1400 then the area is essentially organic, while if it is below 1000 then the area contains an unusually large component of voids.

The CT number for a particular volume of the imaging space is affected by the amount and density of the coal present, the minerals present, and the void space in that volume. Because of the large CT numbers associated with the mineral matter (Table 2), the mineral content of the CT volume would be expected to have a large effect upon the CT image.

Figure 4 shows the same CT image as in Figure 1a, but this time a reference line has been drawn over the image and the CT numbers plotted along that line. The white area at the bottom left of the image corresponds to the peak in CT number on the left-hand side of the graph.

After the CT experiments had been completed, and the coal sectioned along the CT image plane, automated x-ray microprobe measurements were made along the same region as the line in the CT image. The area of the microprobe beam was $50 \mu m \times 50 \mu m$ with an expected penetration of ca $1 \mu m$. The elements scanned in the microprobe were Si, Al, S, Fe, Mg, Na, K, Ca. The observed weight percents for the elements were totalled and plotted against distance (Figure 5). The automated microprobe measurements are in a finer grid than the CT data. If converted to the same grid size as the CT, then peaks in the microprobe spectra would appear shorter and broader. There does appear to be a first order correlation between the mineral matter in the coal and the variation in density of the CT image. CT images of raw coal can be regarded therefore as maps of the mineral distribution within the coal. A further distinction into minerals of elements with high atomic number (e.g., pyrite) and minerals with only low atomic number minerals (e.g., illite) may also be possible using images taken with different x-ray energies.

The porosity within this particular coal sample was examined by following the penetration of xenon gas into the sample at room temperature ($27^{\circ}C$). Xenon was chosen because of its relatively inert nature and because it has a strong x-ray K-absorption edge at 35 Kev, i.e., at the peak of the spectrum from the x-ray tube. The presence of xenon should therefore be detectable against the coal background. The penetration of xenon gas

into the coal was carried out by exposing one end face of the coal parallelepiped to a pressure of xenon (1130 torr) and monitoring the gas exiting the opposite face by following the pressure rise in a closed system of known volume. The penetration of gas within the coal was monitored, (a) with the coal containing its equilibrium moisture, (b) after the coal had been dried at 80°C for two weeks. The bulk gas flow through the coal was much faster in case (b) than in (a). After about 3.5 hours the pressure on both sides of the coal had equalized in case (b). Images from the second series of experiments are more indicative of the porosity within the coal and three images from these experiments are shown in Figure 6. These images were obtained by subtracting the digital image of the evacuated coal from the digital images taken while the xenon was penetrating into the coal. The resulting difference image is a map of xenon penetration. The images clearly show the non-uniform nature of the penetration of the xenon into the coal. The lighter areas in the image are the areas into which the xenon has preferentially penetrated. The plane of the CT image was situated about 15 mm in the coal block from the high pressure end. The presence of xenon in this plane was detected in the first image taken of this plane after the xenon had been introduced into the high pressure chamber (time elapsed was eight minutes). The major features of the pattern were streaks of xenon parallel to the bedding planes of the coal. Over the duration of the experiment these features grew in intensity and broadened out. This behavior suggested that the xenon penetrated into this plane by a network of fine cracks. The cracks that are interconnected and give access to the xenon reservoir appear to be primarily oriented parallel to the bedding planes of this piece of coal and many are associated with the mineral-rich regions of the coal. In these cracks, the xenon pressure rapidly reached the reservoir pressure, but because the cracks are very fine on the scale of the CT resolution, the actual amount of xenon introduced into a voxel even when the crack had reached reservoir pressure was still quite small and so the CT signal in the difference image was small. As the xenon diffused into the coal away from the crack more xenon was introduced into the voxel containing the crack, and into neighboring voxels and consequently, the numbers on the difference image increased.

Figure 7 shows a composite plot of the CT numbers along the line drawn on the difference images of Figure 6. For the data along each line, the curve has been normalized to its maximum value. The plot illustrates the spreading of the xenon into the neighboring coal from a source apparently situated ca 2.5 mm from the arbitrary origin. It may be possible to analyze these curves in terms of a diffusion parameter which depends upon the CT number of the original coal.

A calibration graph of CT number against xenon pressure is given in Figure 8. This shows that if the xenon pressure at the high pressure inlet was 1130 torr, then the maximum observable CT number increase within an image of the coal should be 263, provided that all the xenon remained in the gas phase within the coal. In fact, CT numbers much greater than the gas phase maximum are observed within the CT difference image (Figure 6). This is probably caused by the xenon being present within the coal both as a gas phase species and as adsorbed species.

In the final image used in Figure 6, the maximum CT value along the line had risen to 2171, or over eight times the maximum possible from solely gas phase absorption. On the assumptions that the occupied surface area for a xenon atom is 22 (\AA)^2 (3) and a coal material density of 1.3 g/cm^3 , then the apparent surface area in a region with a xenon difference CT number of 2171 is $51 \text{ m}^2/\text{g}$. Using a BET apparatus, a room temperature xenon absorption measurement on a micronized sample of coal from the same batch gave a surface area of $44 \text{ m}^2/\text{g}$. The final image of xenon penetration into the coal could therefore be regarded as a surface area image for the coal. This information should be useful in future studies on the reactivity of coal.

The primary interest in the CT technique is in making use of its non-invasive nature for in situ studies of coal combustion and gasification. The preliminary studies discussed here will provide a basis for understanding the images obtained from more complex experiments.

ACKNOWLEDGMENTS

We would like to express our appreciation to the U.S. Department of Energy for support of this work (Contract No. DE-AC21-82MC19210).

REFERENCES

1. Maylotte, D.H., Lamby, E.J., Kosky, P.G., St. Peters, R.L., "Proceedings fo the International Conference on Coal Science", Dusseldorf, 1981.
2. Stach, E., Mackowsky, M.-th., Teichmuller, M., Teichmuller, R., Taylor, G.H., Chandra, D., (Eds.), Coal Petrology, Gerbruder Borntraeger, Berlin, 1975.
3. McClellan, A.L., Harnsberger, H.L., "Cross-Sectional Areas of Molecules Adsorbed in Solid Surfaces", Coll and Interface Sci., 23, 577 (1967).

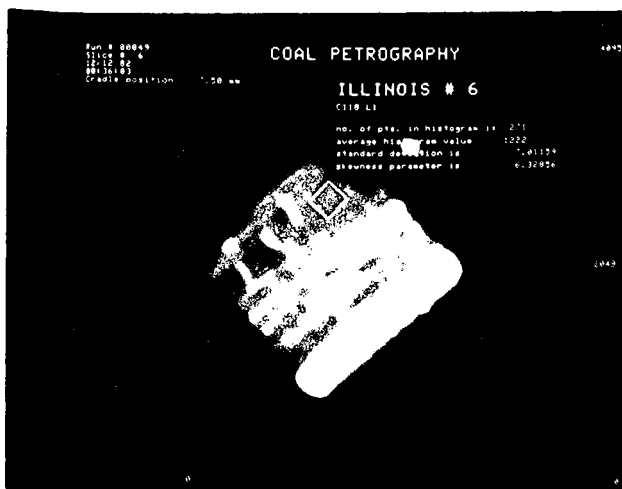


Figure 1a. CT Image of Encapsulated Illinois #6 Coal

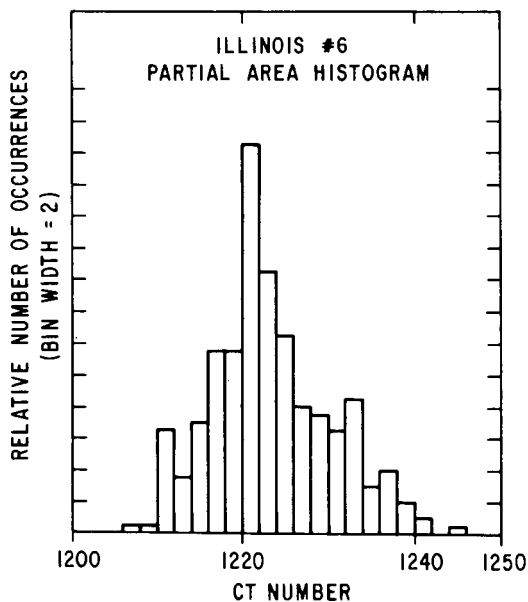


Figure 1b. Histogram of CT Values Within the Rectangular Outline of Figure 1a

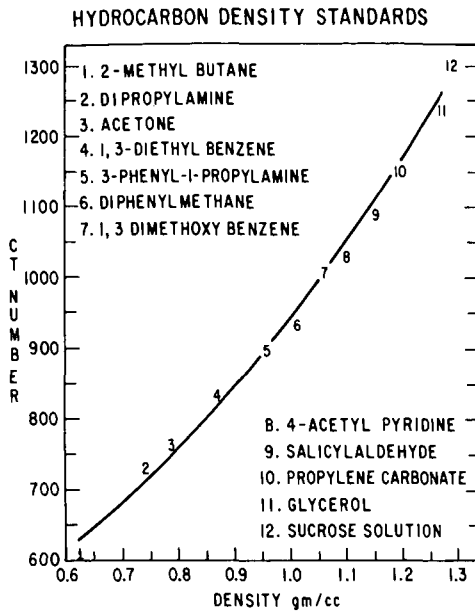


Figure 2. CT Number as a Function of Hydrocarbon Density

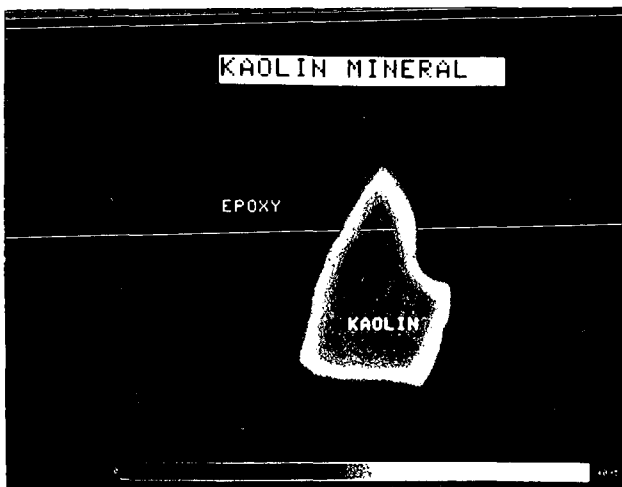
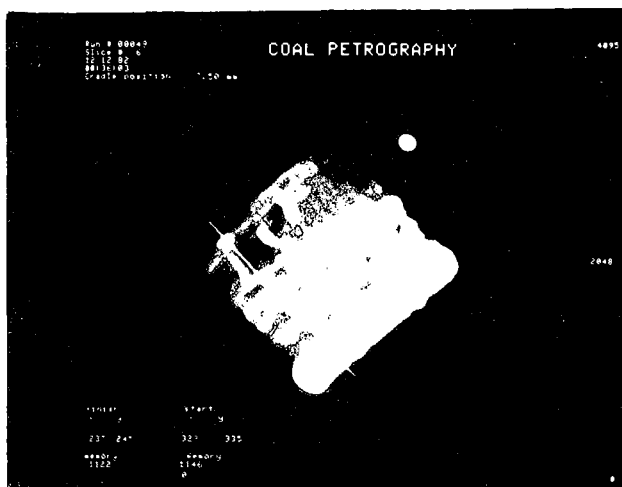
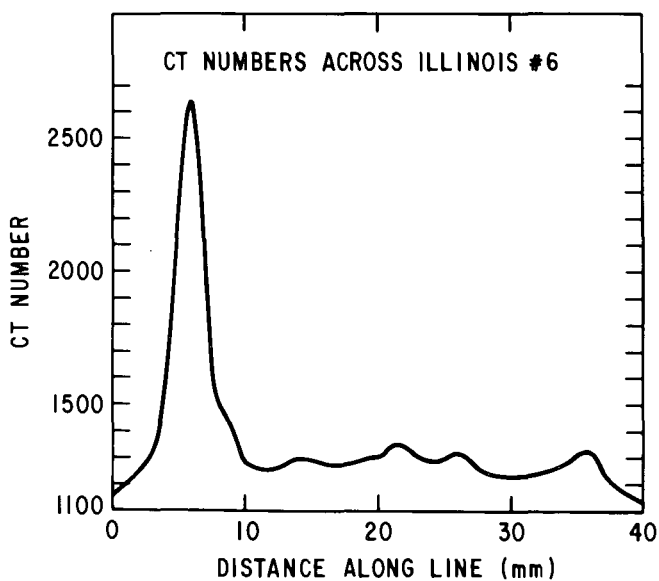


Figure 3. CT Image of Kaolin Sample Impregnated With Epoxy Around the Periphery



**Figure 4a. CT Image of Illinois #6 Coal
With a Line Drawn on the Image**



**Figure 4b. CT Numbers Along the Line
Drawn in Figure 4a**

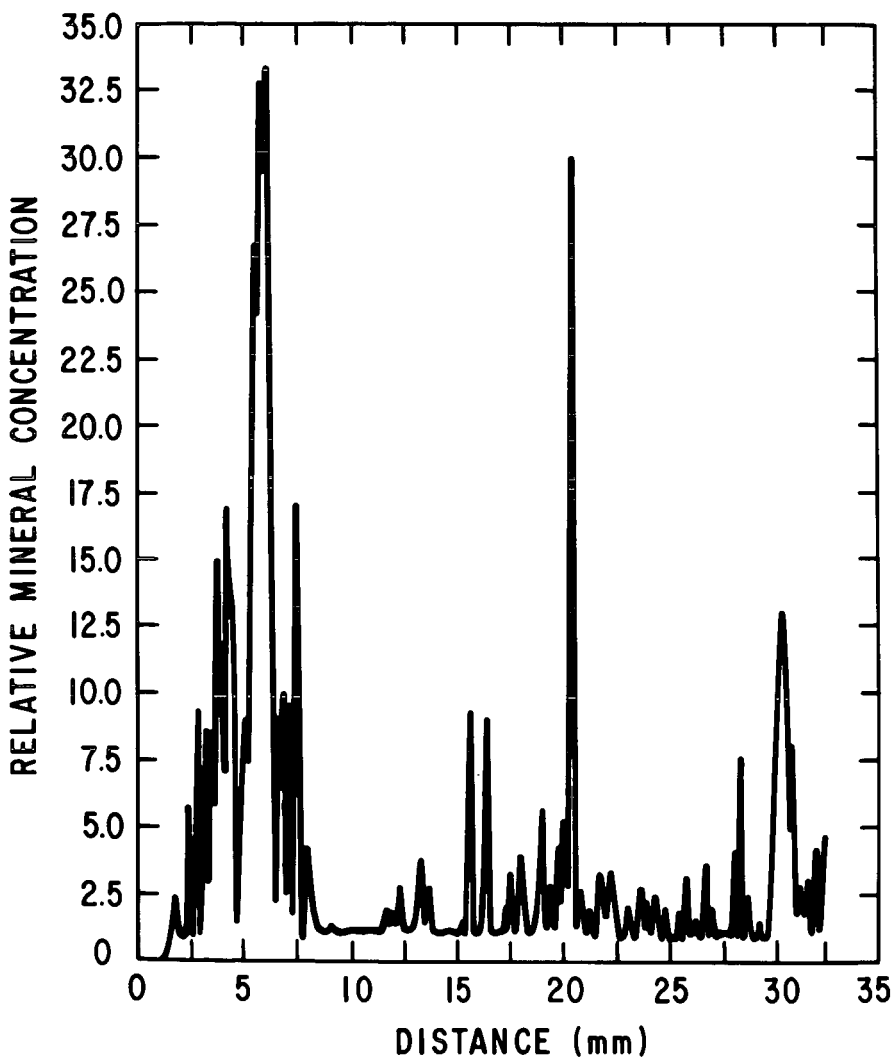


Figure 5. Relative Mineral Concentration Along the Line of Figure 4a.

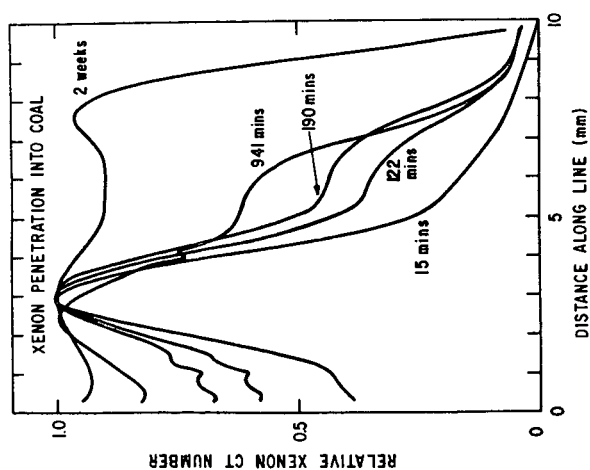


FIGURE 7. XENON PENETRATION INTO COAL ALONG THE LINE DRAWN IN FIGURE 6

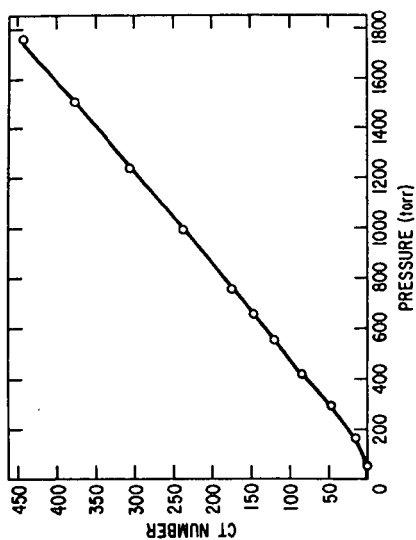


FIGURE 8. CT NUMBER AS A FUNCTION OF XENON GAS PRESSURE

EFFECTS OF COAL PREOXIDATION AND HEAT TREATMENT CONDITIONS ON RESULTING CHAR STRUCTURE OF CAKING COAL

D. J. Maloney* and R. G. Jenkins

Department of Materials Science and Engineering
The Pennsylvania State University, University Park, Pennsylvania, 16802

Introduction

When most bituminous coals are heated in the absence of air, they soften (i.e., become fluid), agglomerate, and, as gases and vapors are evolved, swell to form a coke. These properties can limit the utilization potential of certain coals because agglomerates can impede gas flow leading to poor mixing in reactors and, in the extreme case, eventual plugging. In addition, coals which pass through a plastic stage produce relatively unreactive chars (1,2). These factors can add substantially to the cost of a gasification process.

Coal agglomerating tendencies can be eliminated by mild oxidation of the raw coal prior to heat treatment. This method is very effective in removing the swelling and softening characteristics of caking coals (3). Also, under certain carbonization conditions, preoxidation can significantly enhance the subsequent reactivity of the resulting chars (2).

Recent studies at the Pennsylvania State University have been directed at understanding the effects of preoxidation on coal utilization potential under conditions of interest for entrained-flow gasification and pulverized coal combustion (rapid heating rate, short residence time). Studies were conducted on an eastern bituminous coal in an effort to evaluate the effects of preoxidation on devolatilization behavior (yield and kinetics), coal swelling and agglomerating tendencies, and resulting char structure and reactivity (4). This paper describes the changes in char structural features resulting from coal preoxidation and examines the relationship between char structure and subsequent gasification potential.

Experimental

The chars examined in this study were prepared from freshly mined and preoxidized samples of a strongly caking bituminous coal under widely varying pyrolysis conditions (heating rate and time). The parent sample was PSOC-1099, a HVA bituminous coal from the Pittsburgh No. 8 seam. All work described here was conducted on 200 x 270 mesh size fractions with mean particle diameters of 62 μm . Preoxidized coal samples were prepared by air oxidation of sized coal in a fluidized-bed furnace. Oxidation temperature, time, and weight gain were determined based upon complementary thermogravimetric studies of the air oxidation of each coal. Oxidation levels reported here are given as percent weight gain on oxidation (dry coal basis). The proximate analyses of the fresh and preoxidized coals used in this work are presented in Table 1.

Chars were prepared under rapid heating conditions ($\sim 10^4$ K/s) in an entrained-flow furnace at temperatures between 1073 and 1273K with residence times up to 0.27s. Slow pyrolysis (12 K/min) chars were prepared in a horizontal tube furnace at a temperature of 1273K with a soak time at final temperature of 1 h. Extensive analyses of the surface properties of the chars were performed. Char morphology was examined

* Present Address: U.S. DOE, Morgantown Energy Technology Center, P.O. Box 880, Collins Ferry Road, Morgantown, West Virginia, 26505.

TABLE 1
Proximate Analyses of Samples* Examined

Sample	Moisture Percent	Ash Percent	Volatile Matter Percent	Fixed Carbon Percent
PSOC-1099 (HVA bituminous coal)	1.3	10.6	34.0	54.1
PSOC-1099 (1 percent O ₂ added)	0.8	10.6	32.5	56.1
PSOC-1099 (2 percent O ₂ added)	1.0	10.5	31.6	56.9

* Proximate analyses were conducted on 200 x 270 mesh fractions of 62 μ m mean particle diameter.

using SEM. Total surface area was determined by CO₂ physisorption at 298K. Macro and transitional pore surface areas were determined by N₂ adsorption at 77K. Additional char structural information was obtained by ultimate analysis using a Perkin-Elmer Model 240 elemental analyzer. Char reactivities were determined in air at 668K using a thermogravimetric method described by Mahajan and co-workers (2,5). Complete details of all experimental procedures employed in this study are supplied in Reference 4.

Results

Figures 1 and 2 are scanning electron micrographs of chars prepared from fresh and pre-oxidized samples (2.5 percent oxygen added) of PSOC-1099 after heat treatment of 0.23 s at 1273K. Chars prepared from the fresh HVA coal, Figure 1, were thin-walled transparent structures commonly referred to as cenospheres (6-8), the mean diameters of which were more than twice that of the starting coal. This represents a ~10-fold increase in volume. During pyrolysis the sample shown lost 51 percent of its starting material (daf). Under the conditions employed in this work, cenospheres were fully developed during the first 0.1 s of heating time after which no observable changes in macroscopic properties were evident. When carbonized under slow heating conditions, this coal formed a fused swollen coke.

As illustrated in Figure 2, the preoxidized coal did not form the cenosphere structures observed in Figure 1. Preoxidized coal char particle sizes were similar with those observed for the parent sample prior to carbonization. Char particle shapes, however, were altered considerably. Particle surfaces were rounded with little evidence of the sharp, well-defined fracture surface characteristic of the starting coal. This indicates that the preoxidized coal passed through a fluid state during rapid heating. All pre-oxidized samples examined in the present study formed chars of similar size and shape during rapid pyrolysis. In contrast to this behavior, the preoxidized coal exhibited no signs of thermoplastic behavior when carbonized under slow heating conditions.

Figure 3 illustrates the development of char surface area (CO₂ area) as a function of heat treatment time at temperatures of 1073 and 1173K for chars produced from the fresh HVA coal. Char surface areas remained constant during the first 0.05 s of heat treatment after which surface areas increased with time. The CO₂ surface area for the parent coal was 170 m²/g. At each heat treatment temperature, a more than two-fold increase in surface area occurred during the pyrolysis process. At 1073K, the maximum char surface area obtained was 360 m²/g (daf char); while at 1173K, the maximum char surface area was 465 m²/g. The sigmoid-shaped curves shown in Figure 3 suggest that char surface areas were approaching maximum values. This observation is supported by the results of Radovic (9) and others (10-14).

The N_2 surface area determined for the fresh coal was $2.7 \text{ m}^2/\text{g}$. N_2 surface areas determined for the corresponding char samples were less than $2 \text{ m}^2/\text{g}$ for all the chars examined. These areas approximate the theoretical limits calculated for cenospheres of the size and weight produced in this study.

Generally, N_2 surface areas determined for coals or char samples are considerably lower than the corresponding CO_2 surface areas. N_2 adsorption kinetics (at 77K) on microporous materials are limited by activated diffusion and, therefore, N_2 adsorption gives an estimate of macro and meso porosity (15). CO_2 (at 298K), however, is accessible to surfaces present in macro, meso, and micro pores.

Figure 4 illustrates the development of char surface area as a function of weight loss during pyrolysis. Surface areas exhibited little change during the early stages of pyrolysis. After 25 percent weight loss, however, char areas increased rapidly up to a weight loss of approximately 45 percent. Subsequent weight loss, up to 50 percent, had little effect on resulting surface areas. It is of interest to note that the weight loss level at which surface areas began to increase coincided roughly with the initiation of cenosphere growth (4).

CO_2 surface areas determined for the untreated and preoxidized coal samples and selected chars generated from these samples are presented in Table 2.

TABLE 2
Comparison of CO_2 Surface Areas
Determined for Fresh and Preoxidized
Coals and Their Corresponding Chars

Carbonization Temperature (K)	Raw Coal	Surface Areas m^2/g (daf basis)			
		1073	1173	1273	1273
Carbonization Time (s)	Coal	0.27	0.25	0.23	3600*
Sample					
PSOC-1099 (untreated)	170	360	465	465	88
1.2 percent oxygen added	160	290	480	475	
2.5 percent oxygen added	150	320	500	522	188

* Slow heating conditions (12 K/min) followed by 1 h soak time at 1273K.

Preoxidation had little effect on the surface area of the coal sample prior to carbonization. During pyrolysis, preoxidation had a mild effect on resulting char surface area, however, no specific pattern was evident. After heat treatment at 1073K, surface areas of chars prepared from preoxidized coals were less than that observed for the corresponding unoxidized coal char. At carbonization temperatures of 1173 and 1273K, preoxidized coal formed chars with slightly higher surface areas than the corresponding chars prepared from the unoxidized coal. When slow heating conditions and extended heat treatment times were employed, preoxidation led to a significant increase in resulting char surface area. Following extended hold times at elevated temperatures, char surface areas were greatly reduced when compared with char surface areas observed for the rapidly heated (short time) samples.

The carbon and hydrogen percentages obtained from ultimate analysis provide some useful information concerning changes in char composition as a function of carbonization

conditions. The C/H ratios presented in Figures 5 and 6 show that as carbonization temperatures and times were increased, hydrogen was preferentially removed from the char samples. As the temperature of carbonization was increased, the rate of hydrogen evolution relative to carbon evolution increased significantly. The preoxidized coal behavior was similar to that of the fresh coal. Under comparable carbonization conditions, no significant differences were observed in the C/H ratios determined for chars derived from the fresh and preoxidized coal samples.

Preoxidation effects on char composition are illustrated more clearly in Figure 7. Over 80 percent of the hydrogen present in the fresh HVA coal sample was removed during 0.23 s of heat treatment at 1273K. Less than 50 percent of the original carbon was removed in the same time interval. Preoxidation reduced the quantities of both hydrogen and carbon liberated during comparable heat treatments.

The relative gasification potential of the chars produced in this study were evaluated by examining the reactivities of selected samples during gasification in one atmosphere of air (20 kPa O₂). The reactivity parameter reported here is $\tau_{0.5}$, which, at a given reaction temperature, is the time corresponding to a fractional burn-off of one-half. Mahajan, Yarzab, and Walker (5) demonstrated the utility of this parameter for correlating char reactivity data for gasification in air, steam, and CO₂.

Table 3 shows the reactivity parameters, $\tau_{0.5}$, determined for chars generated from PSOC-1099 as a function of carbonization temperature and preoxidation level. The carbonization times employed were the maximum residence times attainable at each furnace operating temperature. These were 0.27 s at 1073K, 0.25 s at 1173K, and 0.23 s at 1273K. The reactivity parameters reported are the mean values determined from three replicate reactivity tests. Typically the standard deviation from the mean was less than ± 10 percent.

TABLE 3
Comparison of Air Reactivities at 668K
for Chars Prepared from PSOC-1099 as a Function of
Carbonization Temperature and Preoxidation Level

Furnace Temperature (K)	Reactivity Parameter $\tau_{0.5}$ min		
	No Oxygen Added	1.2% Oxygen Added	2.5% Oxygen Added
1073	33	32	36
1173	46	46	46
1273	69	64	66

As carbonization temperature was increased from 1073K to 1273K, the subsequent char reactivity decreased by a factor of two. This was true for chars prepared from both the unoxidized and preoxidized parent samples. Preoxidation had no apparent effect on subsequent char reactivity. Values of $\tau_{0.5}$ determined for chars prepared from unoxidized and preoxidized coals were equivalent within the limits of reproducibility of the reactivity measurement.

Discussion

Nsakala and co-workers (16,17) and Radovic (9, 18) examined lignite coal chars generated under rapid heating, short residence time conditions. Each of these investigators reported increases in char surface areas, determined by CO_2 adsorption, of 200 to $300 \text{ m}^2/\text{g}$. The results presented here concur with these findings. Nsakala, et al. (16, 17), also reported significant increases in N_2 surface area during pyrolysis of a lignite. Similar increases in N_2 area were not observed for the bituminous coal examined in the present study.

Mahajan, et al. (2), reported that surface areas of chars produced from preoxidized coals were several times larger than those prepared from fresh coal samples. These investigators examined coals of similar rank and employed preoxidation conditions comparable with those used in the present study. They employed slow heating conditions (10 K/min) and extended soak times (1 h) at final temperature (1273K) during the carbonization process. When slow heating conditions (12 K/min to 1273K, followed by 1 h soak time at 1273K) were employed in the present study, chars produced from the unoxidized coal had CO_2 surface areas significantly lower than the chars produced from the preoxidized coal (Table 2). However, under rapid heating conditions, preoxidation had only a slight effect on resulting char surface area. It is apparent from the results shown here that preoxidation effects on resulting char area were greatly diminished when employing rapid heating conditions and short carbonization times.

Decreases in char reactivity with increasing heat treatment temperature were reported previously for coal chars (1,9,18) and other disordered carbonaceous solids (19). Jenkins and co-workers (1) examined chars prepared under slow heating conditions (10 K/min heating rate, 2 h soak time at final temperature). They reported that char reactivities during air gasification decreased by as much as 10 times when carbonization temperature was increased from 873K to 1273K. Radovic (9,18) examined reactivities of chars prepared from a lignite under rapid heating, short contact time carbonization conditions similar to those employed in the present study. He observed a decrease by a factor of 10 when carbonization temperature was increased from 975K to 1275K.

Jenkins, et al. (1), suggested that the effect of temperature on subsequent char reactivity could be explained on the basis of the concentration and accessibility of active sites. Firstly, they observed that the lower temperature chars had a significantly higher level of macro and transitional porosity (estimated from N_2 adsorption) and, thus, a more open or accessible pore structure than did the higher temperature chars. Secondly, they noted that the chemical nature of the char surface changed with changing carbonization temperature. Lower temperature chars had a higher hydrogen content than did the higher temperature chars. They suggested that hydrogen was preferentially removed during air gasification leaving behind nascent carbon active sites which are more reactive to oxygen. The chars generated in this study were essentially void of surface area associates with macro and transitional pores. Char reactivities exhibited no correlation with the micropore areas determined for these chars. Considering these results, it is probable that char reactivities were more strongly influenced by the amount of hydrogen remaining in the char. This suggestion is supported by the elemental composition data presented in Figures 5 through 7.

Mahajan and co-workers (2) observed that under slow heating conditions (10 K/min, 1 h soak at 1273K) preoxidation markedly enhanced subsequent char reactivity (by a factor of up to 40). The results of this study suggest that preoxidation effects on resulting char surface area and reactivity are greatly diminished when rapid heating conditions and short carbonization times are employed. In support of this observation, selected coal and char samples were carbonized under conditions comparable with those used by Mahajan and co-workers (2). Chars were prepared from the fresh HVA coal and

preoxidized (2.5 percent oxygen added) coal. In addition, the 1273K chars (0.23 s carbonization time) prepared by rapid heating of these samples were recarbonized under slow heating conditions. The reactivity parameters determined for these chars are presented in Table 4. Increasing hold times at the final carbonization temperature (1273K) from 0.23 s to 3600 s led to a seven-fold decrease in reactivity for the chars prepared from the unoxidized coal. When comparable hold times were employed, heating rate had little effect on subsequent char reactivity. Chars prepared from preoxidized coals were about a factor of two more reactive than the corresponding chars prepared from the unoxidized coal. The important factor in determining the subsequent char reactivity was the hold time at final temperature and not the heating rate.

TABLE 4

Effect of Carbonization Conditions on Subsequent Reactivity
of Chars Prepared from Raw and Preoxidized Samples of PSOC-1099

Char Preparation Method	Heating rate	Reactivity Parameter t0.5 min		
		30,000 K/s	0.2 K/s	30,000 K/s*
	Hold Time at 1273K	0.23 s	3600 s	3600 s
Parent Sample				
Raw (unoxidized)		69	450	490
2.5 percent oxygen added		66	300	260

* Chars were prepared in the entrained-flow furnace under rapid heating conditions and were recarbonized by heating at 0.2 K/s and holding for 3600 s at 1273K.

Mahajan and co-workers (2) attributed the enhancement of char reactivity as a result of preoxidation to the large increases in micropore surface areas they observed for these chars. Under rapid heating, short contact time, carbonization conditions similar increases in surface area and char reactivity were not observed. However, when carbonization times were extended, preoxidation effects became evident. These results provide some insight concerning the role which oxygen plays in the carbonization process. From the work of Jenkins, et al. (1), and others (10-14), it is known that increasing the severity (time, temperature) of carbonization conditions results in a sealing up or closing of char porosity. This annealing process reduces the accessibility and quantity of active gasification sites present in the char. The results of this study and the work of Mahajan, et al. (2), suggest that preoxidation inhibits the annealing process and, thereby, leads to the production of more reactive coal chars. This inhibition does not become manifest in the initial stages of the carbonization process.

Acknowledgments

Funding for this work was provided by the Cooperative Program in Coal Research at the Pennsylvania State University and by the U.S. Department of Energy under Contract No. DE-AC01-79ET14882. Additional support was supplied by a Mining and Mineral and Mineral Fuels Conservation Fellowship. Elemental analyses were generously supplied by the United Technologies Research Center under the direction of Dr. James D. Friehaut.

References

1. Jenkins, R. G., S. P. Nandi, and P. L. Walker, Jr., Fuel, 52, 288, 1973.
2. Mahajan, O. P., M. Komatsu, and P. L. Walker, Jr., Fuel, 59, 3, 1980.
3. Maloney, D. J., R. G. Jenkins, and P. L. Walker, Jr., Fuel, 61, 175, 1982.
4. Maloney, D. J., Ph.D. Thesis, The Pennsylvania State University, 1983.
5. Mahajan, O. P., R. Yarzab, and P. L. Walker, Jr., Fuel, 57, 643, 1978.
6. Newall, H. E., and F. S. Sinnatt, Fuel, 3, 424, 1924.
7. Newall, H. E., and F. S. Sinnatt, Fuel, 5, 335, 1926.
8. Newall, H. E., and F. S. Sinnatt, Fuel, 6, 118, 1927.
9. Radovic, L. R., Ph.D. Thesis, The Pennsylvania State University, 1982.
10. Chiche, P., S. Durif, and S. Pregermain, Fuel, 44, 5, 1965.
11. Miura, S., and P. L. Silveston, Carbon, 18, 93, 1980.
12. Razouk, R. I., F. Z. Saleeb, and A. M. Youssef, Carbon, 6, 325, 1968.
13. Toda, Y., Fuel, 52, 94, 1973.
14. Toda, Y., Fuel, 52, 99, 1973.
15. Walker, P. L., Jr., Phil. Trans. R. Soc. Lond., A300, 65, 1981.
16. Nsakala, N., R. H. Essenhig, and P. L. Walker Jr., Fuel, 57, 605, 1978.
17. Nsakala, N., Ph.D. Thesis, The Pennsylvania State University, 1977.
18. Radović, L. R., P. L. Walker, Jr., and R. G. Jenkins, Fuel, 62, 849, 1983.
19. Blake, J. H., G. R. Bopp, J. F. Jones, M. G. Miller, and W. Tambo, Fuel, 46, 115, 1967.

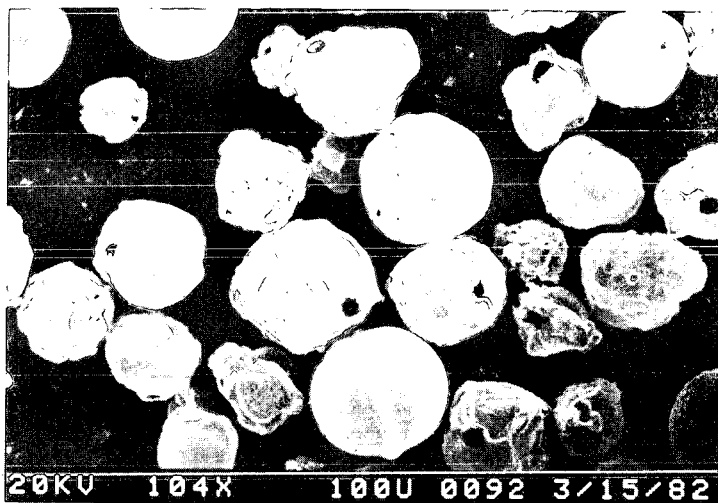


FIGURE 1. SCANNING ELECTRON MICROGRAPH OF THE CHAR PRODUCED FROM PSOC-1099 FOLLOWING HEAT TREATMENT AT 1273 K FOR 0.23 s

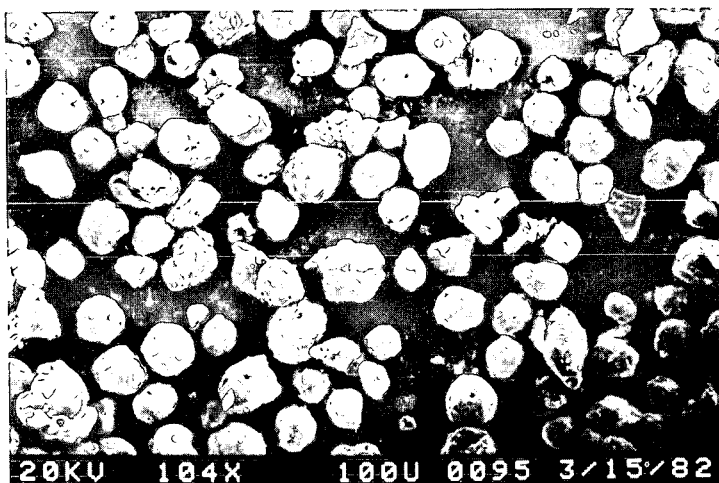


FIGURE 2. SCANNING ELECTRON MICROGRAPH OF THE CHAR PRODUCED FROM PREOXIDIZED PSOC-1099 (2.5% OXYGEN ADDED) FOLLOWING HEAT TREATMENT AT 1273 K FOR 0.23 s

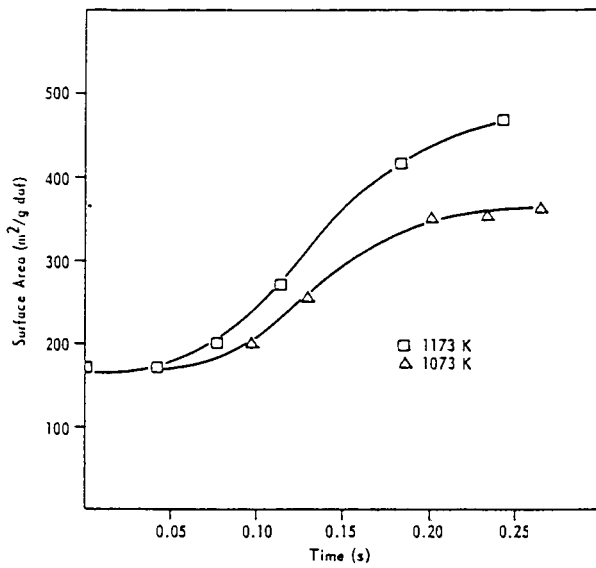


Figure 3. EFFECTS OF CARBONIZATION TIME AND TEMPERATURE ON RESULTING CO₂ SURFACE AREA FOR CHARS PREPARED FROM PSQC-1099

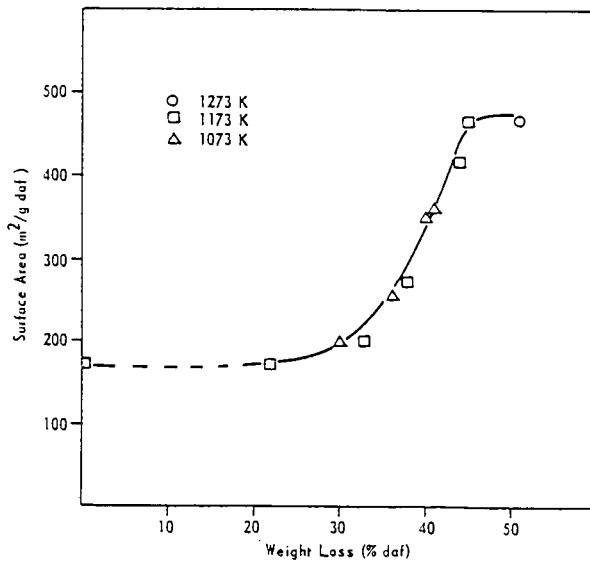


Figure 4. EFFECT OF PYROLYSIS YIELD ON RESULTING CO₂ SURFACE AREA FOR CHARS PREPARED FROM PSQC-1099

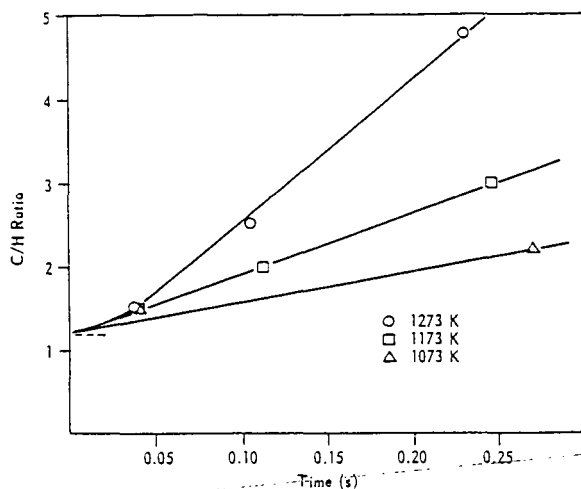


Figure 5. EFFECTS OF CARBONIZATION TIME AND TEMPERATURE ON RESULTING ATOMIC C/H RATIOS FOR CHARS PREPARED FROM PSOC-1099

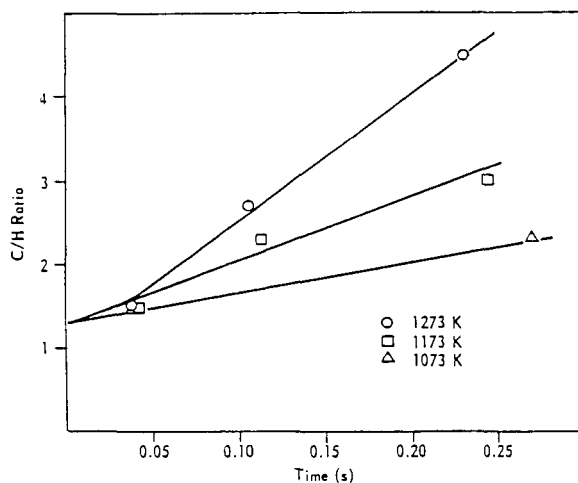


Figure 6. EFFECTS OF CARBONIZATION TIME AND TEMPERATURE ON RESULTING ATOMIC C/H RATIOS FOR CHARS PREPARED FROM PREOXIDIZED PSOC-1099 (2.5% Oxygen Added)

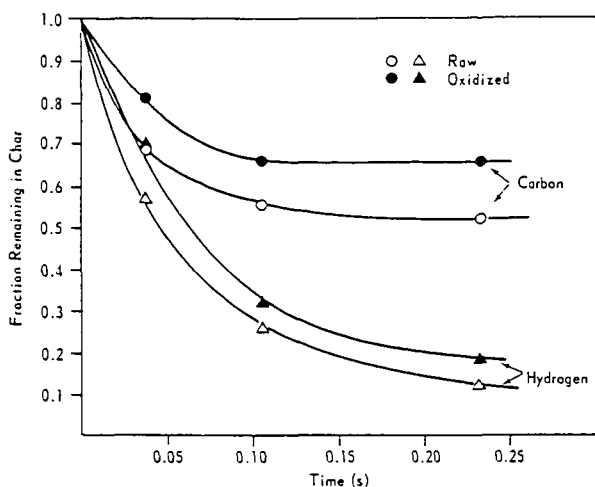


Figure 7. WEIGHT FRACTIONS OF CARBON AND HYDROGEN REMAINING IN CHARS AS A FUNCTION OF TIME AT 1273 K FOR RAW AND PREOXIDIZED (2.5% Oxygen Added) SAMPLES OF PSOC-1099

High Temperature Transformations of Minerals in Coal and the Relationship to the Organic Structure

P.A. Montano and A.S. Bonmannavar

Department of Physics, West Virginia University
Morgantown, WV 26506

I. Introduction

The major use of coal is in direct combustion for the generation of electricity. Because of the environmental hazards involved in its use, considerable research has become necessary to fully understand the behavior of the different compounds appearing in coal and the ways in which they transform throughout the course of processing.

Of all the minerals present in coal, iron disulfides (pyrite and marcasite) are the most deleterious. They are one of the major sources of SO_2 pollution. Clay minerals represent a large percentage of the inorganic matter in coal. These minerals are transformed at high-temperature to ferrous and ferric glass phases. Mössbauer spectroscopy can be very helpful in understanding the transformation of iron-bearing minerals during combustion. Such a technique was used to study the oxidation of pyrite at moderate temperatures (maximum 400°C). The oxidation of pyrite in an IL#6 coal occurs in three steps: a) to iron sulfates between 25°C to 310°C, b) to $\gamma\text{-Fe}_2\text{O}_3$ between 310°C and 325°C, and c) to $\alpha\text{-Fe}_2\text{O}_3$ above 325°C. (1,2) was also observed that the rate of oxidation is strongly particle size dependent. Wendeborn enumerates no less than sixteen concurrent reactions for the oxidation of pyrite. Schwab and Philinis observed that in the range of 400-500°C, the oxidation of pyrite proceeds mainly through the formation of oxides. Sulfate formation amounted to only 12% of the oxide formation at the lower temperature and decreased with increasing temperature. From thermodynamics and kinetics of the reaction of sulfur in coal, Attar suggested that the final products of the reaction depend on temperature, pyrite particle size and oxygen partial pressure.

The Mössbauer effect has also been used by Huffman and Huggins (5) to study the residual ashes in coal. They observed the transformation of pyrite to hematite, siderite to hematite, and of ankerite and Fe^{2+} in clays to ferric ions in glassy materials. The composition of the ashes was strongly dependent on the original minerals and the cooling conditions.

In this work we report a series of in situ Mössbauer measurements in four well-characterized bituminous coals. We intend to study the sequence of chemical reactions taking place during the transformation of the iron-bearing minerals. Special emphasis is placed upon the valence state of the iron and the identification of the intermediate states.

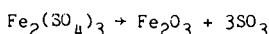
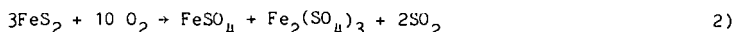
II. Experimental Description

The coals used in this study were: Blacksville #2, Powhatan #5, Ky 9/14 and IL #6 obtained from St. Clair County, Illinois. Table I gives the ultimate analysis of these four coals. The oxidation process was carried out in a specially built reactor. The reactor chamber consists of a quartz cylinder with an outer diameter of 2.5 cm. The sample was mounted in the center of the cylinder allowing the flow of air through it. The quartz tube was placed inside a horizontal furnace capable of reaching 1200°C. A chromel-alumel thermocouple was inserted into the middle of the reactor near the sample to detect the temperature. The reactor was held

horizontally. The sample, a coal pellet, was mounted between two graphite holders in the center of the reactor. For the process of oxidation, air was allowed to flow through the sample at a constant rate. A computerized Mössbauer spectrometer was used in this study to accumulate, record and fit the data. The fitting is based on a non-linear least-square procedure assuming Lorentzian-like shapes. The source used was a $-100 \text{ mCi } ^{57}\text{Co}$ in a rhodium matrix. A krypton ($3\frac{1}{2} \text{ CH}_4$) proportional counter was used as a detector (care was taken to cool the windows of the detector during the measurements). In situ ^{57}Fe Mössbauer spectra of all the samples were recorded during oxidation at various temperatures between 22°C and 710°C . All the isomer shifts are given in reference to $\alpha\text{-Fe}$ (the zero velocity standard). The reduction measurements were performed under hydrogen flow as well as under a nitrogen atmosphere.

III. Experimental Results and Discussion

The Mössbauer spectra of all the coals at room temperature show the presence of FeS_2 (pyrite) in various amounts. The spectrum of pyrite is known to give a characteristic quadrupole split doublet, isomer shift (IS) = 0.31 mm/sec and quadrupole splitting (QS) = 0.61 mm/sec . In all the coals depending on the degree of weathering (room temperature oxidation), the presence of $\text{FeSO}_4 \cdot \text{H}_2\text{O}$ (szomolnokite) was observed, IS = 1.18 mm/sec and QS = 2.69 mm/sec . In some samples minor amounts of jarosite and coquimbite (ferric sulfates) were also observed. The major iron-bearing clay minerals detected in the present experiments were illite and mixed clays (as detected by x-ray diffraction). The amount of iron in such minerals is very small and detection becomes easier after analyzing the high temperature ashes. On heating the coal in air, FeS_2 will be oxidized to a mixture of sulfates and oxides, and we would expect the Mössbauer spectrum to consist of a superposition of a magnetically split six-line pattern due to the iron oxides and doublets resulting from unreacted FeS_2 and iron sulfates. The above reactions could be summarized as:



In Figures 1 and 2 the in situ Mössbauer spectra for the Blacksville #2 and IL#6 coal are shown. On heating the coals through the various temperatures it was observed 1) for FeS_2 , the QS remains almost unchanged but its isomer shift decreases rapidly. The decrease in the IS is attributed mainly to the second order Doppler shift. 2) For $\text{FeSO}_4 \cdot \text{H}_2\text{O}$, the QS is observed to decrease at high temperatures. This decrease is mainly due to the temperature dependence of the electric field gradient (through population of excited electronic states). The area fraction of iron sulfates increased with temperature; this is due to the formation of sulfates through reactions (1) and (2). On increasing the temperature above 300°C and for short periods of time, the formation of ferrimagnetic $\gamma\text{-Fe}_2\text{O}_3$ is observed (see reference 1). The formation of $\gamma\text{-Fe}_2\text{O}_3$ has also been reported by other authors.⁽⁶⁾ On further heating the coal to 350°C , the conversion of $\gamma\text{-Fe}_2\text{O}_3$ to $\alpha\text{-Fe}_2\text{O}_3$ is observed (easily detected by the difference in magnetic hyperfine fields). The conversion of $\gamma\text{-Fe}_2\text{O}_3$ to $\alpha\text{-Fe}_2\text{O}_3$ is complete at 400°C , and a characteristic six-line pattern due to $\alpha\text{-Fe}_2\text{O}_3$ is observed. The presence of $\gamma\text{-Fe}_2\text{O}_3$ as an intermediate state depends on the coal as well as oxidation time. The longer the time, the more $\gamma\text{-Fe}_2\text{O}_3$ to $\alpha\text{-Fe}_2\text{O}_3$ conversion is observed. Of course at higher temperatures only $\alpha\text{-Fe}_2\text{O}_3$ is stable. How the coal composition affects the amount of $\gamma\text{-Fe}_2\text{O}_3$ formed is not well understood, although one is inclined to believe that particle size and impurities in the pyrite (or marcasite) would be important factors in this process. The above was also observed in all the coals studied. Two typical room temperature spectra for the Blacksville #2 and IL#6 coals are shown in Figures 3 and 4. The six-line spectrum characteristic of $\alpha\text{-Fe}_2\text{O}_3$ is easily observed as the dominant feature in the figures. Noted is the presence of

two extra doublets containing Fe^{3+} , attributed to decomposition of the clays and formation of amorphous materials with Fe^{3+} as an impurity. The doublets are not identical in both spectra indicating that the environment of Fe^{3+} is different. This is indicative of a variation in clay composition between the two coals. Because of the small amounts of iron in such phases, their clear identification is rather difficult and still remains a challenging problem for the spectroscopist. Similar spectra were also observed for the other two coals.

The Mössbauer spectral area of each species was used to determine the relative amounts of FeS_2 , Fe^{2+} , Fe^{3+} (not as oxide) and Fe_2O_3 . In this analysis we will neglect any variation in Debye-Waller (D-W) factors between the different species. Consequently the relative amounts will indicate the qualitative variation in sample composition at the different temperatures. The absolute amounts vary depending on their respective D-W factors. Since such a correction is very difficult, we limit ourselves to the assumption that all the species show a similar temperature dependence for the D-W factors. Figure 5 shows the decomposition of FeS_2 as a function of temperature for all the coals under study. Figure 6 shows the amount of Fe^{2+} as a function of temperature for all the coals; the divalent ion contribution is mainly from the ferrous sulfates. In Figure 7 the variation in Fe^{3+} and iron oxides (both γ and α) are shown as a function of temperature. It is evident that for the most weathered coals, there is more ferric sulfate present (e.g. IL#6). For the fresher coal (BL#2), the amount of ferric sulfate is smaller and the transformation from iron sulfides to sulfates to oxides is rapid. At 710°C the ferric ion is present mainly as $\alpha\text{-Fe}_2\text{O}_3$. At this temperature we are above the antiferromagnetic to paramagnetic transition temperature of $\alpha\text{-Fe}_2\text{O}_3$ and no magnetic splitting is observed. The $\alpha\text{-Fe}_2\text{O}_3$ particle sizes seem to be very similar in all the coals studied. This is evident from Figure 8 where the normalized magnetic hyperfine field at the ^{57}Fe nucleus is plotted versus temperature. The temperature dependence is very similar for all the samples (only $\alpha\text{-Fe}_2\text{O}_3$ plotted) indicating similar particle sizes. Most likely sintering has occurred during combustion. Weathering of the coal seems to be one of the major factors hindering the rapid conversion of FeS_2 to oxides at low temperatures. Eventually at higher temperatures the ferric sulfate particles are converted to oxides. It appears that the presence of particles of ferrous and ferric sulfates slows down the rapid oxidation of FeS_2 . There is also a physical factor present. It is highly probable that the smaller sulfide particles were oxidized at room temperature in a weathered coal and the remaining particles are larger and more difficult to oxidize.^(1,2) It is evident that the fresher coal oxidized faster than the others (see Figure 7).

Under reduction conditions and below 450°C , all the iron sulfides are transformed into pyrrhotites. The degree of transformation depends on time as well as the type of coal. The major factor affecting the Fe/S ratio in the pyrrhotites is the total amount of sulfur available as H_2S . Partial H_2S pressure is the crucial quantity controlling the stoichiometry of the pyrrhotites. A high percentage of H_2S in the reactor at high temperatures assures the formation of pyrrhotites with a high number of metal vacancies. The pyrrhotite surface interacts with CO and CO_2 in the presence of hydrogen. The products are removed from the surface and the pyrrhotites retain a metal character. At temperatures higher than 450°C the pyrrhotites start to transform into troilite and eventually into iron metal. The formation of troilite (FeS) is also possible at lower temperatures if H_2S is continually removed from the reactor by flowing hydrogen. The clay minerals are also transformed during reduction with the iron ion preferring to retain a divalent state. The degree of transformation is strongly coal dependent.

The authors acknowledge the support of the Energy Research Center of West Virginia University.

REFERENCES

1. Shyu, H.J., Vaishnava, P.P., and Montano, P.A., Fuel 60, 1023 (1981).
2. Attar, A., Fuel 57, 201 (1978).
3. Wendeborn, H., "Der Chemie-Ingenieur," Vol.III, 5, edited by A. Eucker and M. Jacob, 334.
4. Schwab, G.M. and Philinis, J., J. Amer. Chem. Soc. 69, 2588 (1947).
5. Huffman, G.P. and Huggins, F.E. in "Recent Chemical Applications of Mossbauer Spectroscopy," eds. J. Stevens and G.K. Shenoy, ACS, Advances in Chemistry, 194 (1980).
6. Marusak, L.A., Walker, Jr., P.L. and Mulay, L.N., IEEE Trans. Mag. MAG-12(6), 889 (1976).
7. Bommanavar, A.S. and Montano, P.A., Fuel 61, 523 (1982).

TABLE I Ultimate Analysis (WT%, dry basis)

Coal	H	C	N	S	O	HTA
IL#6	4.7	67.6	1.2	4.0	8.0	13.96
Powhatan #5	4.9	71.1	1.1	3.5	7.5	11.8
Ky 9/14	4.9	71.3	1.5	3.4	9.7	9.3
Blacksville #2	5.2	75.83	1.4	3.4	3.5	10.1

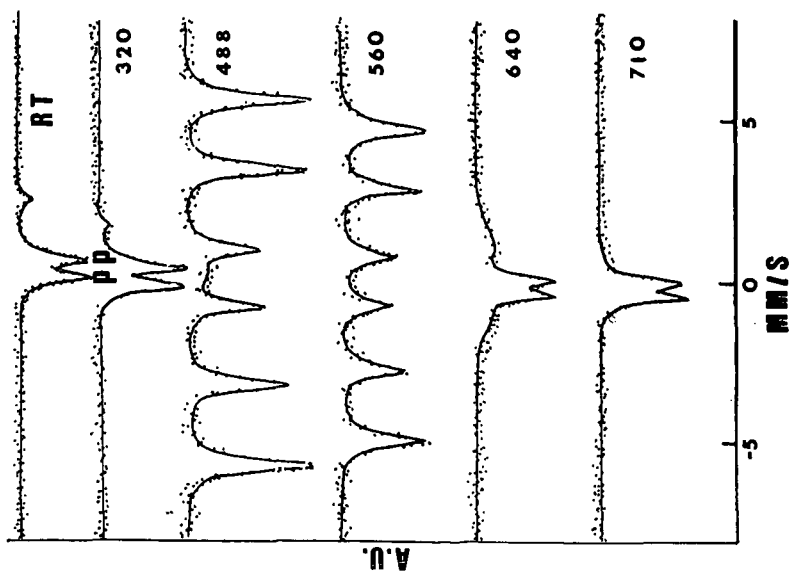


FIGURE 1 Mossbauer spectra of the Blacksville #2 coal as a function of temperature: pp indicates the position of pyrite.

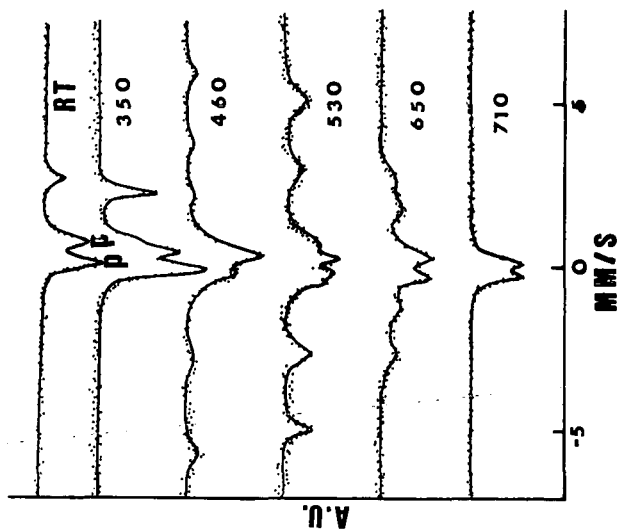


FIGURE 2 Mossbauer spectra of the IL #6 coal as a function of temperature.

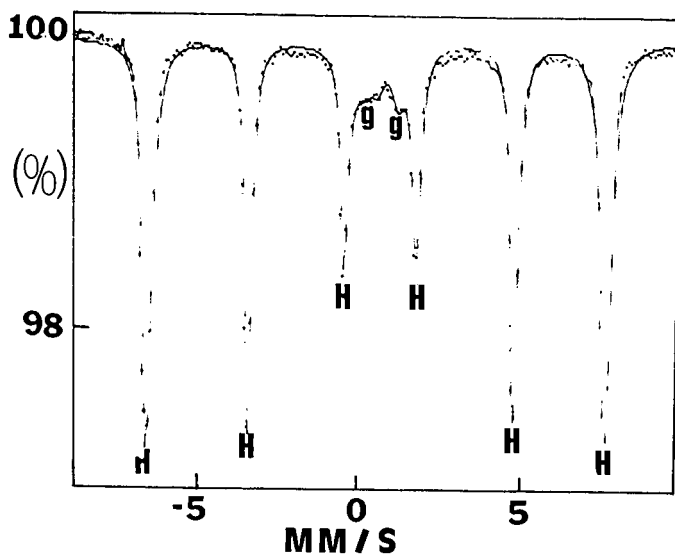


FIGURE 3 Mössbauer spectrum at room temperature after oxidation at 710°C of the Blacksville #2 coal. H: $\alpha\text{-Fe}_2\text{O}_3$
g: Fe^{3+} in amorphous clay (two doublet)

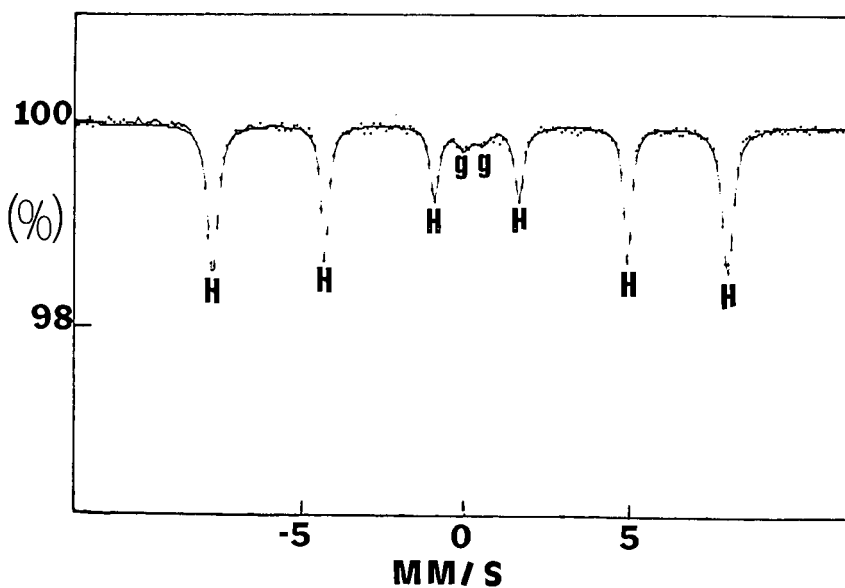


FIGURE 4. The same as above but IL #6 instead of Blacksville #2.

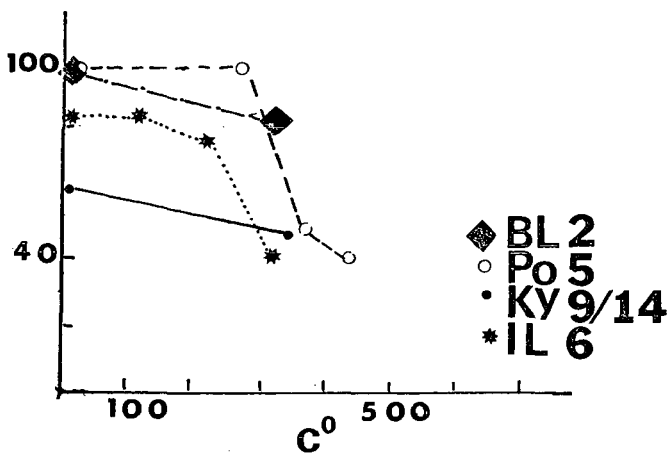


FIGURE 5 Decomposition of FeS_2 in percent as a function of temperature. BL2: Blacksville #2; Po5: Powhatan #5; Ky 9/14; and IL6: IL #6.

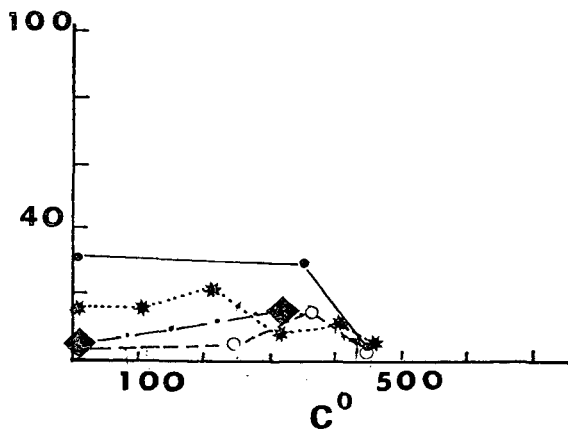


FIGURE 6 Transformation of Fe^{2+} in percentage vs. temperature. Key to the figure is found in Figure 5.

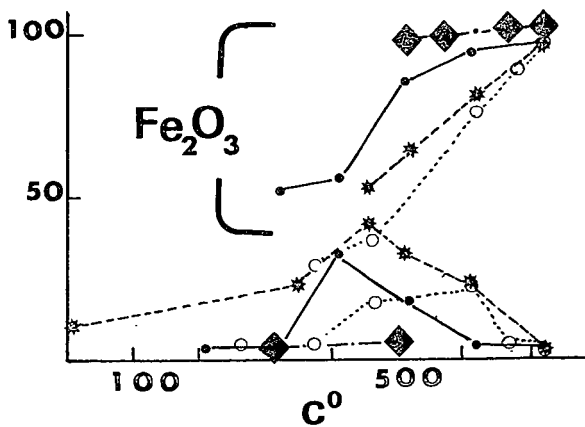


FIGURE 7 Conversion to Fe_2O_3 and Fe^{3+} (not oxides) as a function of temperature. See Figure 5 for the key to the symbols.

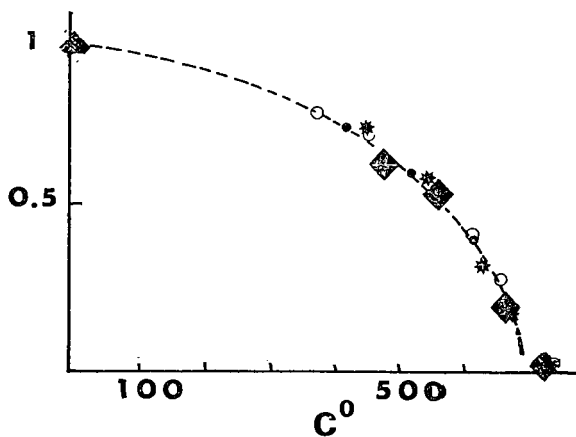


FIGURE 8 Magnetic hyperfine field normalized to room temperature for all the samples vs. temperature.

Enumeration of Graphite Carbon-Bond-Network Defects Having Ring Sizes Ranging from 2 to 9.

Jerry Ray Dias

Department of Chemistry
University of Missouri
Kansas City, Missouri 64110

Graphite-like Structures

A covering of the plane by congruent regular n -gons (all vertex angles and edge lengths are equal) is called a *regular* tessellation of the plane (1). The graphite σ -bond structure is a regular tessellation of the plane by hexagons. The only regular tessellations of the plane by n -gons are for $n = 3, 4$, and 6 ; no other regular tessellations of the plane exist. If m denotes the number of regular n -gons at every vertex, then $m(1-2/n)\pi = 2\pi$ which simplifies to $1/n + 1/m = 1/2$. *Homogeneous* tessellations (all edge lengths are equal) occur when different polygons are used with the same set of polygons at each vertex. Since the number of n -gons at every vertex is three for the graphite σ -bond structure, the various isomeric graphite tessellations in a plane must be given by $(1-2/n_1) + (1-2/n_2) + (1-2/n_3) = 2$ which simplifies to $1/n_1 + 1/n_2 + 1/n_3 = 1/2$. The only acceptable solutions to the latter equation for n_1, n_2, n_3 are $6, 6, 6$ or $3, 12, 12$ or $4, 6, 12$ or $4, 8, 8$. These translate to the tessellated structures shown in Figure 1. Note that these tessellated graphite related structures are listed in decreasing order of their aromatic or π -bond energy stability associated with polycyclic conjugated hydrocarbons where the hexagonal web ($n_1 = 6, n_2 = 6, n_3 = 6$) is totally aromatic, the middle structures are either less aromatic ($n_1 = 3, n_2 = 12, n_3 = 12$) or have aromatic and antiaromatic components ($n_1 = 4, n_2 = 6, n_3 = 12$), and the latter structure is almost totally antiaromatic ($n_1 = 4, n_2 = 8, n_3 = 8$). The homogeneous tessellated structures (Figure 1) have only angle distortions from the ideal angle of 120° for the graphite structure. If bond (edge) distortions are permitted then other planar lattice structures become possible (2). They include plane nets composed of an equal number of pentagonal and heptagonal rings or trigonal and nonagonal rings and twice the number of pentagonal rings to octagonal rings or twice the number of heptagonal rings to tetragonal rings in compliance with the equation $3r_3 + 2r_4 + r_5 - r_7 - 2r_8 - 3r_9 - 4r_{10} - 5r_{11} - 6r_{12} - \dots = 0$ (*vide infra*) where r_n is the number of rings of size n .

These other graphite lattices are unknown but can possibly exist as island defects in graphite or amorphous carbon (carbon-bond-network defects). Twinning of graphite crystals result in the formation of 4- and 8-membered rings along the twinning line. Similarly, a partial lateral dislocation leads to a similar 4-8 boundary. A single carbon-atom-lattice-vacancy forms a hole shaped like perinaphthenyl radical and a two-carbon-atom-lattice-vacancy forms a hole shaped like pyrene (3). A partial line dislocation can produce a sp^3 -hybridization-buckled-network defect (4). Other types of graphite defect structures involve layer stacking and foreign atom incorporation. The 419 other isomers of pyrene enumerated in a previous paper also represent other possible carbon-bond-network defect structural units that may possibly exist as localized islands in graphite and amorphous carbon (5).

Diamond-like Structures

There are two basic three-dimensional 4-connected nets or lattices that can be constructed with equal links and regular tetrahedral bond angles (6). The most stable is the (cubic) diamond-like lattice which is made up of the totally staggered arrangement of links where each and every two-tetrahedral-atom unit resembles the staggered conformation of ethane and every six-tetrahedral-atom ring system resembles the chair conformation of cyclohexane. The less stable wurtzite-like (hexagonal diamond) lattice is composed of 1/4 eclipsing links and 3/4 staggered links and has (normal) layers of made up of fused polycyclic hexagonal rings in chair conformational-like arrangements which are mutually joined in such a way that boat conformational-like hexagonal rings are formed between these layers. A lattice which alternates in a regular or periodic manner between the cubic and hexagonal diamond structures could lead to the SiC polytypes. Two other lattices possible for 4-connected tetrahedral atoms are worthy of note (6). One is based on the cyclopentagon which has an internal angle of 108° that is close to the regular tetrahedral angle value of 109.5° . A net which radiates out from a central pentagonal dodecahedron can be constructed. The other is based on the planar (and angle strained) cyclohexagon. An infinite net which radiates from a column of planar cyclohexagons leads to a structure that can be described as a 6-fold rotation twin of cubic diamond.

Isomer Enumeration of Polycyclic Conjugated Hydrocarbons

Consider the σ -bond graphs of three of the 420 possible polycyclic conjugated hydrocarbon isomers of pyrene shown in Figure 2 (5). Pyrene (1) has $N_{PC}=4$, peripheral third degree carbon vertices (numbered 1 to 4), isomer 2 has $N_{PC}=5$, and isomer 3 has $N_{PC}=6$; all pyrene polycyclic conjugated isomers have $N_H=10$ second degree vertices on the periphery of their σ -bond graphs. Note that the previously derived equation of $N_{PC} - N_H + 6 = 3r_3 + 2r_4 + r_5 - r_7 - 2r_8 - 3r_9 \dots$ correctly enumerates the relative number of ring sizes different from the hexagonal ring in these three pyrene isomers (1 to 3).

Carbon-Bond-Network Defects in Graphite

The principle assumption in this treatment of carbon-bond-network defects is that this kind of defect is formed in an initially ideal graphite lattice in such a manner that the initial number of carbon atoms are conserved (i.e., Frenkel-like defects). Also, the graphite crystal is regarded basically as a super-large polycyclic aromatic hydrocarbon and that these carbon-bond-network defects occur remote to the crystal edge; under these conditions $N_{PC} - N_H + 6 = q - 2N_4 + 3r_3 + 2r_4 + r_5 - r_7 - 2r_8 - 3r_9 = 0$ since $N_{PC} - N_H + 6 = 0$ for benzenoid PAHs. A two-dimensional projection on the (110) plane of the diamond lattice gives a 6-gon tessellated structure with hexagonal rings possessing two shortened parallel edges. Dislocations in the diamond lattice of silicon parallel to this (110) plane result in ring size combinations which obey the above general equation as a consequence of avoiding energetically unfavorable dangling bonds (7). A (110) projection of the diamond-cubic lattice of germanium containing an intrinsic Z-shaped faulted dipole was shown to exhibit a combination of pentagonal and heptagonal rings ($r_5 - r_7 = 0$) which complies with the above equation (8). A study of $\langle 011 \rangle$ tilt boundaries in the diamond-cubic lattice gave a two-dimensional projection showing ring size combinations consistent with this equation (9).

Naphthalene has only four polycyclic conjugated hydrocarbon isomers as enumerated in Figure 3. If one takes an ideal graphite lattice, excises out a naphthalene substructure, and replaces it with a substructure corresponding to the other three naphthalene isomers, one obtains the three carbon-bond-network defects enumerated in Figure 4; the graphite partial structure shown in Figure 4 will be

referred to as the ovalene graphite cell. Similarly, if one excises out a pyrene substructure from an ideal graphite lattice and replaces it with another substructure corresponding to one of the other 419 isomers of pyrene, one obtains other carbon-bond-network defects. Note that for all the defect graphite cell structures shown in Figure 4, the combination of ring sizes is predicted by $3r_3+2r_4+r_5-r_7-2r_8-3r_9=0$. If one distinguishes between rings of the naphthalene the outer rings formed upon their insertion into the ovalene graphite cells, then the equation $3r_3+4r_4+5r_5+6r_6+7r_7+8r_8+9r_9 = q_p + 2q_i$ can be partitioned into the two following equations where the superscript "i" designates "inner" and the superscript "o" designates "outer" ring system:

$$3r_3+4r_4+5r_5+6r_6+7r_7+8r_8+9r_9 = q_p^i + 2q_i^i$$

$$5r_5+6r_6+7r_7+8r_8 = q_p^o + 2q_i^o$$

These equations with specific values for q_i^i , q_p^i , q_i^o , q_p^o , and N_{IC} are given in Figure 4. If one excises the pyrene structural unit from the circumpyrene ideal graphite cell, rotates the pyrene structural unit, and reinserts it, then one obtains another carbon-bond-network defect. Thus there are probably more than 419 different elementary carbon-bond-network defects since each of the different 420 structural isomeric units of pyrene can be inserted with different orientations into the empty circumpyrene graphite cell. The simplest carbon-bond-network defect is that graphite cell corresponding to azupyrene since the surrounding graphite hexagonal units would be nearly normal. Carbon-bond-network defects having ring sizes 3 to 9 are shown to be most probable within the constraints of this model.

A recent example of thermal (500°C) isomerization of azupyrene to pyrene has been published (10). This example (Figure 5) is probably mechanistically the simplest type of isomerization possible for pyrene isomers since a pairwise detachment and reattachment exchange of *syn* internal bonds to the internal third degree carbon atom vertices would convert azupyrene to pyrene. Annealing graphite with analogous defects can cause their migration to the surface or annihilate them as shown in Figure 5.

Although large vacancy defects no doubt exist in graphite, one or two carbon-atom-lattice-vacancies most likely do not exist. Point defects have excess energy due to strain and dangling bonds. Each dangling bond amount to ~2.5eV, and thus there will be a tendency to form point defects which minimize the number of dangling bonds. Consider a two carbon-atom-lattice-vacancy which forms a hole which is shaped like pyrene (3); the four dangling bonds in this defect could form two bridging bonds if some lattice distortion and associated strain energy is permitted. Since it is likely that this strain energy is less than 10 eV, the equilibrium in Figure 6 probably lies to the right side of the equation; note that the equation $3r_3+2r_4+r_5-r_7-2r_8-3r_9=0$ is again obeyed (i.e., $r_5-2r_8=2-2 \times 1=0$).

These examples demonstrate the broad applicability of the general equation $3r_3+2r_4+r_5-r_7-2r_8-3r_9 \dots = 0$ for predicting the relative number of nonhexagonal ring sizes in planar graphs of molecular carbon systems where minimization of dangling bonds is a dominant energetic factor. Amorphous carbon can be regarded as a mix of graphite and diamond lattice types and carbon-bond-network defects (11). These structural concepts should be useful in study of the mechanism of carbonization by which pitch is thermally converted to coke and coke to graphite (12).

References

1. Berman, G., Fryer, K. "Introduction to Combinatorics;" Academic Press New York, NY, 1972.
2. Balaban, A. T., Rentia, C. C., Ciupitu, E. *Rev. Roum. Chim.* 1968, 13, 231.
3. Kelly, B. T. "Physics of Graphite;" Applied Sci. Pub.: NJ, 1981.
4. Ubbelohde, A. R., Lewis, F. A. "Graphite and its Crystal Compounds;" Oxford Univ. Press: London, England, 1960.
5. Dias, J. R. *Match (Math. Chem.)* 1983, 14, 83.
6. Wells, A. F. "Three-Dimensional Nets and Polyhedra;" John Wiley & Sons, Inc.: NY, 1977, Chapter 9.
7. Tan, T. Y. *Phil. Mag. A* 1981, 44 (1), 101-140.
8. Chiang, S.-W., Carter, C. B., Kohlstedt, D. L. *Phil. Mag. A* 1980, 42 (1) 103-121.
9. Moller, H.-J. *Phil. Mag. A* 1981, 43 (4), 1045-1055
10. Anderson, A. G., Kao, L. G. *J. Org. Chem.* 1982, 47, 3589.
11. Dias, J. R. *Carbon*, in press.
12. Lewis, I. C. *Carbon* 1982, 20, 519.

APPENDIX: Glossary of Terms

N_C - total number of carbon atoms in a PAH

N_H - total number of hydrogen atoms in a PAH

N_{Ic} - number of internal carbon atoms in a PAH having a degree of 3

N_{Pc} - number of peripheral carbon atoms in a PAH having a degree of 3

PAH6 - polycyclic aromatic hydrocarbon containing exclusively fused hexagonal rings

$|P|=p=N_C$ - total number of graph points

p_3 - number of graph points (vertices) having a degree of 3

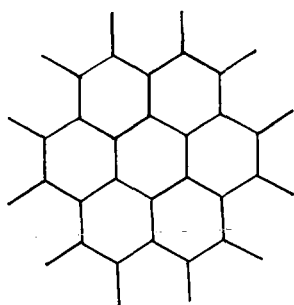
$|Q|=q$ - number of graph edges (lines or C-C bonds)

q_I - number of internal graph edges

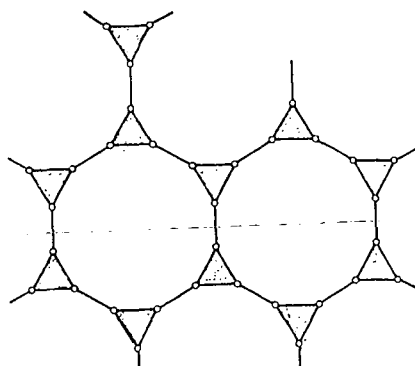
q_P - number of peripheral graph edges

q_b - number of graph edges connecting to phenyl-like ring substituents

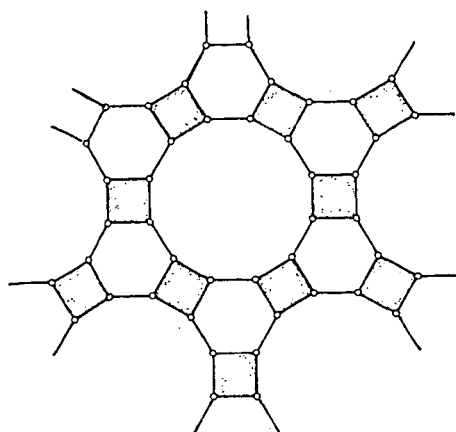
r - number of rings



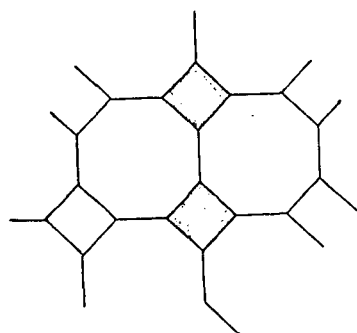
$$n_1 = 6, n_2 = 6, n_3 = 6$$



$$n_1 = 3, n_2 = 12, n_3 = 12$$



$$n_1 = 4, n_2 = 6, n_3 = 12$$



$$n_1 = 4, n_2 = 8, n_3 = 8$$

Figure 1 . Graphite related tessellated structures.

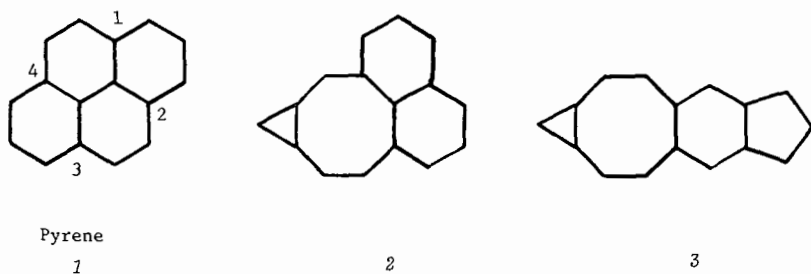


Figure 2. Three of the 420 possible polycyclic conjugated hydrocarbon isomers of pyrene.

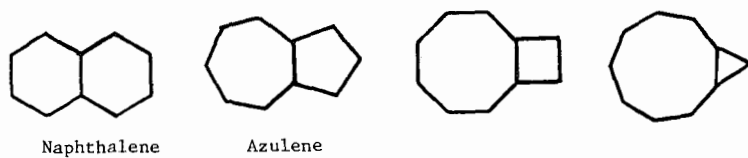


Figure 3. Polycyclic conjugated isomers of naphthalene.

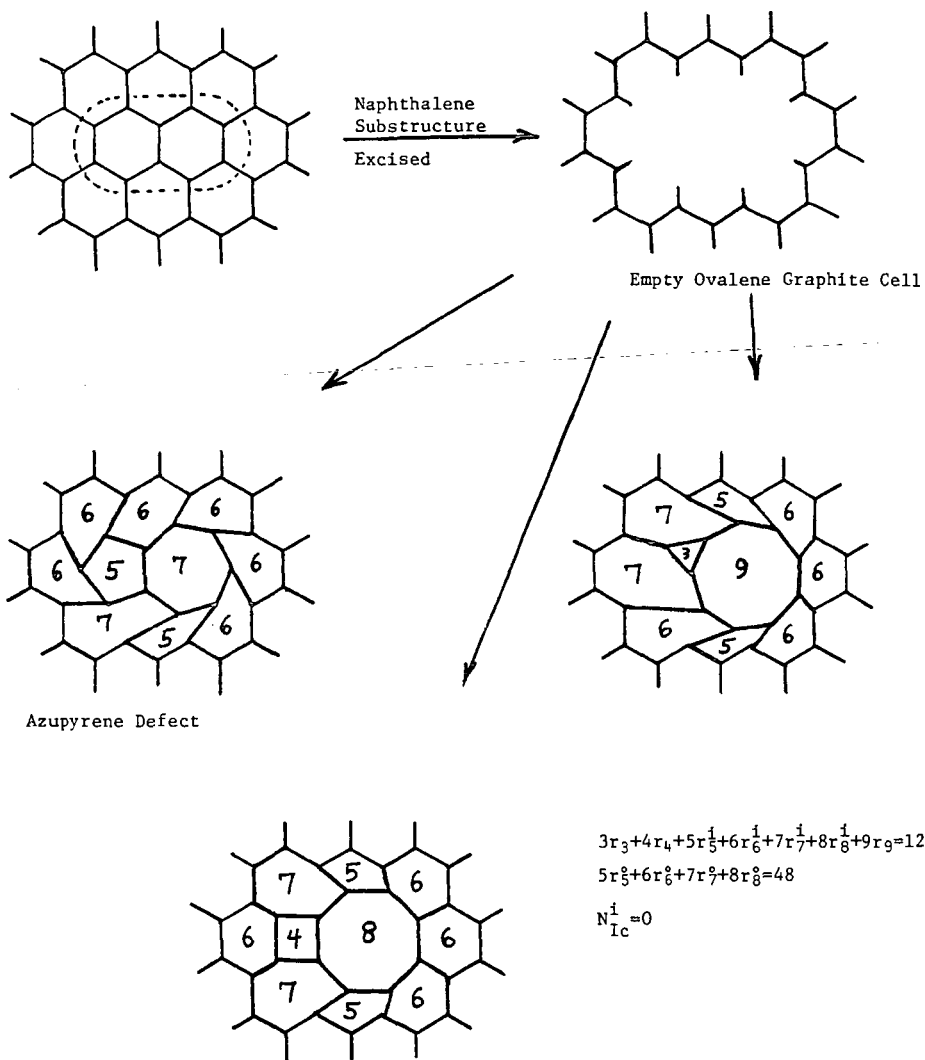


Figure 4. Carbon-bond-network defects in ovalene graphite cells.

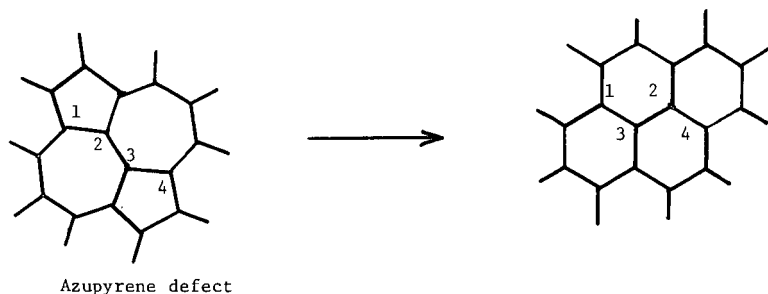


Figure 5. Thermal isomerization of azupyrene to pyrene.

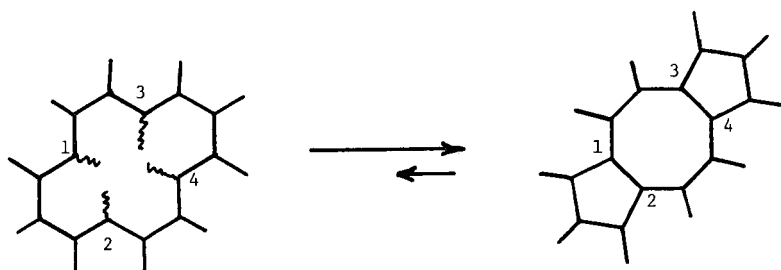


Figure 6. Example of minimization of dangling bonds.

INFLUENCE OF PARTICLE STRUCTURE ON THE RATE OF GAS-SOLID GASIFICATION REACTIONS

K. A. Debelak, J. T. Malito and R. M. Patrick

Department of Chemical Engineering
Vanderbilt University
Nashville, TN 37235

Introduction

Changes in structural parameters, such as surface area available for reaction, porosity, and pore size distribution, will markedly affect the rate of gas-solid reactions. Accompanying these changes in structural parameters are changes in the resistance to diffusion of gaseous products and reactants through the pores of the solid. Understanding the nature of this diffusion, therefore is important in predicting simultaneous diffusion and reaction rates. A quantitative measure of pore diffusion for first-order reactions is given by the effectiveness factor which is a unique function of the effective diffusivity. For microporous solids such as coal, there have been few measurements of effective diffusivity. Furthermore, the effective diffusivity changes as a function of coal conversion as pore walls are gasified. The objective of this work is to determine the changes in the particle structure of coal as it undergoes the reaction, $C + CO_2 \rightarrow 2CO$ and to include the effect of these changes in surface area and effective diffusivity on the overall reaction rate.

A number of workers (1-6) have made measurements of changes in surface area as a function of conversion. Most report that surface area increases during reaction. Only Turkdogan et al (1) and Patel et al (7) have made any measurements of effective diffusivity as a function of conversion. The changes in effective diffusivity, D_e , and total surface area, S , may be expressed as functions of conversion. Once these functions are established, they can be included in an overall rate expression. Recently Bhatia and Perlmutter (8) and Gavali (9) have developed random pore models for gas-solid reactions at chemically controlled rates. These models can be shown to be essentially identical (10). In both cases expressions have been derived which relate surface area to conversion. Bhatia and Perlmutter (11) have extended their model to include diffusion and transport effects where they assume that effective diffusivity will vary with the structural parameters of the solid in the form $D_e = D/\gamma(\epsilon)$ where $\gamma(\epsilon)$ is the tortuosity which varies as reaction proceeds. The random pore models provide a way to interpret rate data in terms of the measurable parameters of surface area and effective diffusivity.

Experimental

The experimental equipment to determine surface and effective diffusivity is the same as used previously (12). The surface area device is a flow-type adsorption apparatus. Surface area measurements were made by adsorbing CO_2 at $0^\circ C$ for 1 hour. The adsorbed CO_2 was then desorbed by heating the sample at $120^\circ C$. This process was repeated at several relative CO_2 pressures to obtain an adsorption isotherm. The surface area was calculated using the Dubinin-Polanyi theory (13) with modifications by Medek (14). Effective diffusivity determinations were made by pulsed chromatography employing the method of moments. The theoretical model used to describe the mass transfer in the chromatographic bed was the same as used previously (12). Axial dispersion and external mass transfer coefficients

were determined from correlations in Shah and Ruthven (15) and Bird (16), respectively. From the two moment equations the adsorption constant K_a and the diffusion parameter D_e/r_c^2 where D_e is effective diffusivity and r_c is diffusion length were calculated. These diffusion studies were made on CO_2 , CO , CH_4 , and N_2 over a temperature range of 50°C to 250°C . To produce char, a sample of raw coal was heated at $25^\circ\text{C}/\text{min}$ to the reaction temperature in a helium gas stream and held at reaction temperature for 1 hour. The sample was cooled and surface area and effective diffusivity measurements were made again. The chars produced were reheated to reaction temperature and reacted with CO_2 . A known volume of CO_2 was injected and the outlet gas was collected and analyzed to determine the extent of the reaction. The sample was then cooled and surface area and effective diffusivity measurements were made. The sample was then reheated and reacted again. This procedure was repeated until there was no further appreciable carbon conversion. Measurements of reaction rates for the char/ CO_2 reaction were made using a thermal gravimetric balance. Devolatilization temperatures and reaction temperatures ranged from 1073K to 1373K.

Results and Discussion

There are significant changes in the surface area and diffusion parameter as a result of devolatilization. Table 1 gives these changes at different devolatilization temperatures. The char surface areas are from 1.5 to 2.0 times as great as the raw coal. The ratio of char/coal surface area increases as devolatilization temperatures increases and reaches a maximum at 1273K and then decreases. The increase in surface area represents the opening of pores inaccessible before devolatilization. Walls closing off pores are devolatilized and small pores inaccessible to initial CO_2 adsorption are exposed. As the devolatilization temperature increases to 1373K the amount of new pores structure begins to decrease as more material is devolatilized. The ratios of the char/coal diffusion parameters for N_2 are less than one indicating that the new pore structure has a greater resistance to diffusion. The ratio of char/coal diffusion parameter increases as devolatilization temperature increases but is still less than one. The devolatilization process produces an increase in surface area and a decrease in diffusion parameter.

The CO_2 /char gasification reaction causes continuous changes in the pore structure of the char. Specific surface area initially increases, passes through a maximum and then decreases as a function of conversion. The specific surface area was correlated with conversion using Bhatia and Perlmutter's expression for surface area as a function of conversion. Figures 1-4 are plots of surface areas versus conversion using the Bhatia and Perlmutter model at each reaction temperature. From the slope and intercept of the least squared line an initial surface area S_0 , and a structural parameter, ψ were calculated. These values along with the measured initial surface areas are given on Figures 1-4. The calculated and measured initial surface areas disagree by as low as 2.5% and as high as 33%. Bhatia and Perlmutter's model indicates that when the structural parameter ψ is greater than 2 that there is a maximum in surface area as a function of conversion. All the values of ψ determined are greater than 2 and the values of ψ increase as a function of reaction temperature up to 1273K and then decrease at a reaction temperature of 1373K. Bhatia and Perlmutter's model has not been widely tested, and the range of conversion over which it applies has not been established. The data of Hashimoto et. al (6) correlated to a conversion of 0.75 for one char and to a conversion of 0.3 for another char. These data correlate from conversion of 0.40 at 1373K to 0.75 at 1173K.

The calculated diffusion parameter, D_e/r_c^2 , and the adsorption equilibrium constant, K_a for the diffusion of carbon dioxide in helium as a function of conversion are displayed in Table 3. The diffusion parameters and equilibrium constants for carbon monoxide, nitrogen and methane as a function of conversion and at different reaction temperature also were calculated but are given elsewhere (17). There is an increase in diffusion parameter with conversion. There appears to be an inverse relationship between the adsorption constant and the diffusion parameter. Intuitively, as the pore structure becomes more open, or as the reactive core decreases in diameter, the resistance of mass transfer decreases.

Walker, et al studied the diffusion of methane in coals and determined that diffusion is activated (18,19). An Arrhenious relationship was proposed to explain the influence of temperature on the diffusion parameter. Activation energies, ΔH_0^\ddagger , and pre-exponential factors, $(D_e/r_c^2)_0$ parameters were calculated from diffusion data obtained at 100°C or greater. The results are listed in Table 6 for char reacted at 1073K. For all gases the activation energy generally decreases with conversion, as expected, since higher energies are associated with smaller pores and pore entrances and with smaller reactive core radii. Patel, et al (7) also observed a decrease in the diffusion of methane through various activated anthracite coals. Activation energies and pre-exponential factors as a function of conversion at the other reaction temperatures are available elsewhere (17). Using calculated activation energies and pre-exponential factors, diffusion parameters were estimated at reaction temperatures. These parameters vary non-linearly with conversion and follow the order $N_2 > CO > CH_4 > CO_2$.

Reaction rate data for char/ CO_2 reaction obtained using the TGA exhibited maxima at intermediate conversions. The Bhatia and Perlmutter model assuming a kinetically controlled reaction and rearranged in linear form was used to interpret the rate data. Values of ψ and S_0 determined from the surface area studies were used in the model. These data are plotted in Figures 5-8. Reaction rate constants were calculated from the slopes of these plots. An Arrhenious plot for the reaction rate constants is given in Figure 9. An activation energy of 150 KJ/mole was calculated from the slope of this plot. The assumption of a kinetically controlled reaction appears to be correct since the reaction rate data in Figures 5-8 are linear as the Bhatia/Perlmutter model suggests and the Arrhenious plot is linear. However, effectiveness factors still need to be calculated and this is currently being done using the Bhatia/Perlmutter model which includes transport effects.

Conclusions

Devolatilization results in an increase in surface area and a decrease in diffusion parameter. A maximum increase in surface area occurs at a devolatilization temperature of 1273K whereas the diffusion parameters increases as devolatilization temperature increases. Specific surface area exhibits a maximum at a conversion of approximately 0.35. The Bhatia/Perlmutter is able to correlate the data to a conversion of at least 0.4. The structural parameter ψ has a maximum at reaction temperature of 1273K. The diffusion parameters, D_e/r_c^2 , are conveniently estimated using the model of Shah and Ruthven (15) and method of moments. The diffusion parameter varies non-linearly with conversion and follows the order $N_2 > CO > CH_4 > CO_2$. The reaction of CO_2 with Wyodak char at temperatures between 1073K and 1373K can be modeled by the Bhatia/Perlmutter model assuming kinetic control. The activation energy is 150 KJ/mole. To confirm this, however, effectiveness factors need to be determined from the simultaneous solution of the equations describing diffusion and reaction including the functions accounting for changes in diffusivity and surface area as a function of conversion.

Acknowledgements

This work was supported by the U.S. Department of Energy Contract # DE-AC-21-81MC16053.

References

1. Turkdogan, E.T., Olsson, R.G., and Vinters, J.V., Carbon, 8, 545, (1970).
2. Kawahta, M., Walker, P.L., "Proceedings of the Fifth Carbon Conference, Vol. 2, 251, Pergamon Press, London, (1962).
3. Kalbach, W.M., Brown, L.F., West, R.E., Carbon, 9, 117, (1970).
4. Marsh, H., Rand, B., Carbon, 47, 79, (1971).
5. Berger, J., Siemieniewski, J., Tomkov, Fuel, 55, 9, (1976).
6. Hashimoto, K., et al., Ind. Eng. Chem. Process Des. Dev., 18, 72, (1979).
7. Patel, R.L., Nandi, S.P., and Walker, P.L., Jr., Fuel, 51, 47, (1972).
8. Bhatia, S.K., and Perlmutter, D.D., AIChE J., 26, 379, (1980).
9. Gavalas, G.R., AIChE J., 26, 577, (1980).
10. Scott, P.E., M.S. Thesis, Vanderbilt University, (1983).
11. Bhatia, S.K., and Perlmutter, D.D., AIChE. J., 27, 247, (1981).
12. Debelak, K.A., Clark, M.A., and Malito, J.T., ASC Div. of Fuel Preprints, No. 1, 31, (1982).
13. Gregg, S.J., and Sing, K.S.W., Adsorption Surface Area and Porosity, New York, Academic Press, 223, (1967).
14. Medek, J., Fuel, 56, 131, (1977).
15. Shah, D.B., and Ruthven, D.M., AIChE. J., 23, 804, (1977).
16. Bird, R.B., Stewart, W.E., Lightfoot, E.N., Transport Phenomena, New York, John Wiley and Sons, Inc., (1960).
17. Patrick, R.M., M.S. Thesis, Vanderbilt University, (1983).
18. Walker, P.L., Jr., and Kini, D.A., Fuel, 44, 453, (1965).
19. Nandi, S.P., and Walker, P.L., Jr., Fuel, 49, 309, (1970).

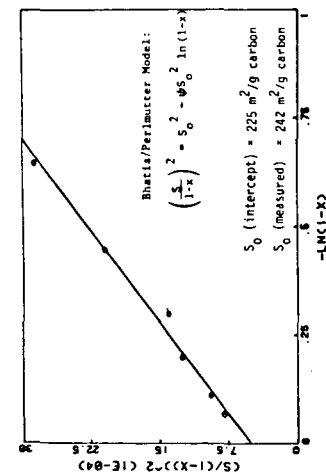


Figure 1. Plot of Bhatia/Perlmutter Model for Surface Area for Wyodak Char Reacted at 800°C $\psi = 7$.

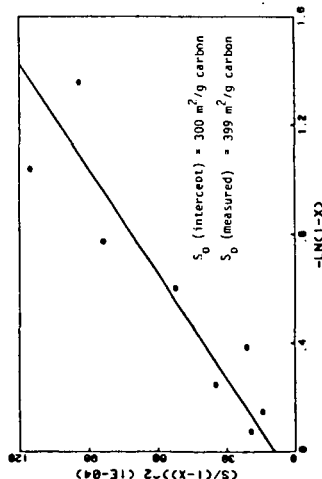


Figure 2. Plot of Bhatia/Perlmutter Model for Surface Area for Wyodak Char Reacted at 900°C $\psi = 8.7$.

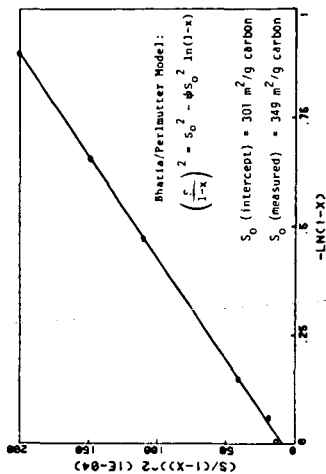


Figure 3. Plot of Bhatia/Perlmutter Model for Surface Area for Wyodak Char Reacted at 1000°C $\psi = 23.6$.

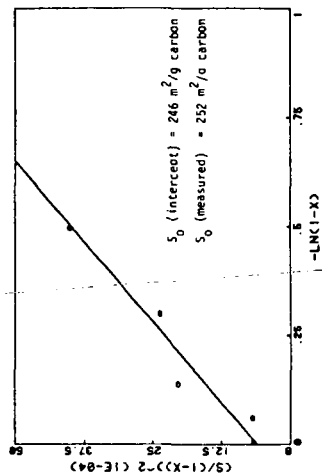


Figure 4. Plot of Bhatia/Perlmutter Model for Surface Area for Wyodak Char Reacted at 1100°C $\psi = 31.2$.

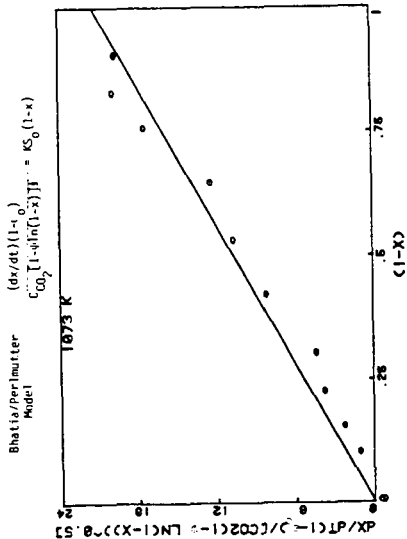


Figure 5. Reaction of Coal Char with Carbon Dioxide at 1073°K. Data fitted to B/P model.

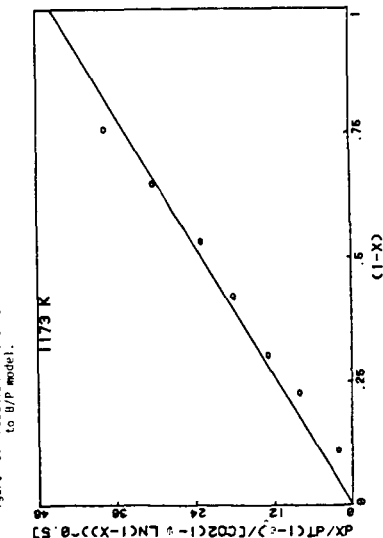


Figure 6. Reaction of Coal Char with Carbon Dioxide at 1173°K. Data fitted to B/P model.

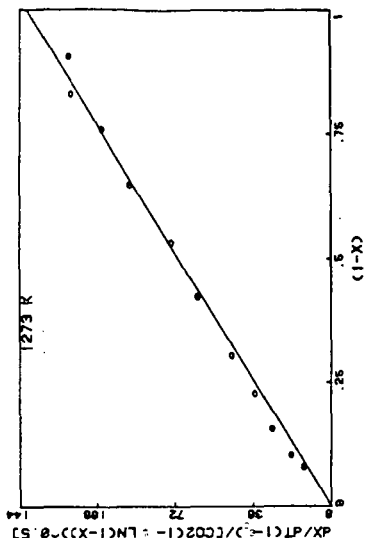


Figure 7. Reaction of Coal Char with Carbon Dioxide at 1273°K. Data fitted to B/P model.

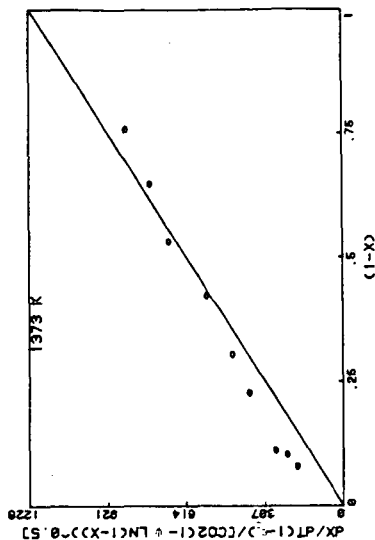


Figure 8. Reaction of Coal Char with Carbon Dioxide at 1373°K. Data fitted to B/P model.

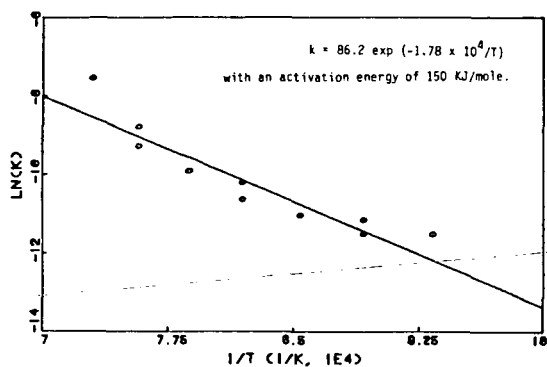


Figure 9. Arrhenius Plot for the Rates Constants.

TABLE 1
EFFECTS OF PYROLYSIS ON WYOMING SUBBITUMINOUS COAL

Pyrolysis Temperature (*K)	Weight (Char/Coal)	Ratio of Specific Area (Char/Coal)	Ratio of H ₂ Diffusion Measured at 323*K (Char/Coal)
1073	.5605	1.81	.234
1173	.5855	1.90	.422
1273	.5749	2.03	.658
1373	.5527	1.47	.708

TABLE 2

WYODAK COAL CHAR REACTED AT 1073°K DIFFUSION PARAMETERS
AND ADSORPTION EQUILIBRIUM CONSTANTS FOR
CARBON DIOXIDE IN HELIUM

Conversion	Adsorption Constant, K_a					Diffusion Parameter, $10^3 D_e/r_c^2$ (s ⁻¹)				
	323°K	373°K	423°K	473°K	523°K	323°K	373°K	423°K	473°K	523°K
0	244	36.7	17.3	11.8	9.79	1.21	5.16	8.36	11.1	12.8
0.061	190	-	19.5	13.1	10.1	1.65	-	5.53	7.79	10.1
0.100	102	-	34.5	11.7	9.74	2.44	-	4.37	7.82	8.57
0.176	94.1	29.3	16.7	10.7	9.11	2.30	5.05	6.02	9.57	10.3
0.247	71.8	23.7	14.4	9.87	8.82	2.73	6.83	6.51	10.6	9.51
0.357	56.7	20.5	11.9	8.88	7.99	3.48	6.08	11.8	13.0	12.4
0.473	41.9	17.8	11.4	8.08	7.36	4.12	6.55	8.53	14.9	15.1
0.583	31.4	15.2	11.0	8.95	7.77	7.64	11.3	12.6	17.3	21.4
0.701	26.1	13.6	-	8.60	-	9.01	13.7	-	21.5	-
0.778	24.1	12.8	8.22	8.71	7.94	11.5	32.0	55.9	48.4	48.1
0.849	34.4	24.3	19.9	11.6	10.4	13.9	54.7	56.5	71.2	64.3
0.865	27.2	25.7	16.2	12.5	11.2	20.4	79.4	74.2	70.3	78.2
0.902	30.3	31.4	17.9	16.0	14.8	25.3	103	80.6	79.0	99.3
0.926	46.9	27.6	19.2	17.1	15.2	52.6	99.3	92.4	105	129

TABLE 3

WYODAK COAL CHAR REACTED AT 1073°K ARRHENIUS PARAMETERS
FOR DIFFUSION OF CARBON DIOXIDE, CARBON
MONOXIDE, NITROGEN, AND METHANE

Conversion	CO ₂		CO		N ₂		CH ₄	
	ΔH_a^\ddagger (KJ/mol)	$(D_e/r_c^2)_0$ (s ⁻¹)	ΔH_a^\ddagger (KJ/mol)	$(D_e/r_c^2)_0$ (s ⁻¹)	ΔH_a^\ddagger (KJ/mol)	$(D_e/r_c^2)_0$ (s ⁻¹)	ΔH_a^\ddagger (KJ/mol)	$(D_e/r_c^2)_0$ (s ⁻¹)
0.0	9.94	0.13	11.0	1.46	9.68	1.09	19.6	8.26
0.061	12.9	0.20	6.18	0.42	5.36	0.35	10.7	1.00
0.100	9.16	0.070	11.2	1.79	6.89	0.57	13.8	2.46
0.176	10.5	0.13	9.84	1.27	6.08	0.48	11.1	1.35
0.247	8.64	0.082	7.29	0.59	5.40	0.36	11.8	1.64
0.357	9.78	0.14	7.15	0.60	5.03	0.34	8.54	0.72
0.473	9.70	0.15	9.88	0.40	4.87	0.32	6.95	0.48
0.583	6.97	0.10	3.34	0.22	4.25	0.28	5.29	0.33
0.701	7.33	0.13	4.69	0.33	4.13	0.29	5.13	0.33
0.778	3.93	0.13	3.32	0.20	2.66	0.18	3.97	0.23
0.849	2.40	0.12	2.84	0.22	3.82	0.28	3.85	0.27
0.865	-	-	3.58	0.26	-	-	6.00	0.45
0.902	3.83	0.24	4.15	0.33	-	-	4.93	0.36
0.926	6.14	0.52	5.15	0.47	5.19	0.48	5.03	0.42

THE REACTION OF CO₂ WITH COKE ON SPENT CATALYSTS

W. P. Hettinger, Jr., J. F. Hoffman and S. M. Kovach

Ashland Petroleum Company
Research and Development Department
Ashland, Kentucky 41114

Introduction

The processing of residuum from the bottom of the crude oil barrel into transportation fuels has become both economically attractive and necessary as crude oil has become heavier and more expensive. In processing these heavier feedstocks, as with Ashland Oil's RCCSM heavy oil conversion process, more coke is produced than in conventional FCC operations. Tremendous amounts of heat are produced during the regeneration of coked catalysts. Conventional methods to moderate the temperature in the regenerator of a circulating fluidized bed include controlling operational parameter-(eg. cat/oil, feed preheat, and reactor temperature), direct addition of steam and/or water to the riser or regenerator (U.S. Patent 4,405,444), the use of multi-bed regenerators (CAN Patent 1,137,455), the use of steam coils in the regenerator, and the incomplete combustion of coke (U.S. Patent 4,354,923). Because of economic constraints on varying the operational parameters and metallurgical limitations, and temperature stability of catalysts, especially when loaded with Ni and V,⁽¹⁾ a practical limit to the regenerator temperature exists. In a further effort to lower the amount of heat produced in the regenerator, other solutions to the problem were sought.

Program

One new approach not mentioned above was to employ the Boudouard Reaction, one of the principle reactions studied for many years in the steel industry as related to iron production. This paper reports the results of a study of the partial regeneration of spent (coked) cracking catalysts with CO₂ (Boudouard Reaction). It also reports a second and equally interesting reaction which was uncovered in the course of this work. The second reaction is called the H-reaction, which is the reaction of the hydrogen associated with the carbon in the "catalytic coke" with CO₂ to produce CO and water. Catalytic coke on spent catalyst is a species which is 92-97%C and 3-8%H and contains minor amounts of sulfur and nitrogen.

The reaction of carbon with CO₂ to produce carbon monoxide (Boudouard Reaction)^(2,3,4) is endothermic as is well known. The H-reaction also appears to be slightly endothermic. The H-reaction would lower the amount of heat produced in the regenerator if it could be achieved at the exit temperature of the reactor (1000°F) or at a slightly higher temperature in the spent catalyst stripper section by removing hydrogen before it can undergo combustion. Carbon dioxide in the flue gas from an FCC or RCC unit is available for these reactions.

The pertinent thermodynamics parameters for the coke-O₂ and coke-CO₂ reactions are presented in Table 1.⁽⁵⁾ The equilibrium constant of the Boudouard Reaction does not favor the formation of CO at temperatures below 1300°F. In order to obtain significant amounts of CO, temperatures above 1800°F are required.⁽⁶⁾ By use of a promoter, substantial

amounts of CO can be produced at 1350-1400°F. The most active promoters of the Boudouard Reaction are salts of the alkali metals and the metals of Group VIII in the periodic table⁽⁶⁾. The H-reaction was found to proceed at a much lower temperature than the Boudouard Reaction, hence, it is of greater interest because of the lower temperature at which it can be initiated.

In past investigations of the Boudouard Reaction, the fate of the hydrogen present in very small quantities in coke has not apparently been of interest. In this investigation, an attempt has been made to confirm the production of the H₂O formed by the reaction of the hydrogen-associated coke with CO₂, and to determine the lower temperature limit where this reaction can be utilized.

The objectives of this work were to determine:

- 1) The metals which would promote the Boudouard Reaction, but do not adversely affect the activity and selectivity of the cracking catalyst.
- 3) The effect of nickel and vanadium, which are deposited on the catalyst during the cracking reaction, as promoters of the Boudouard Reaction.
- 3) The fate of hydrogen during the reaction of coke with CO₂.
- 4) The temperature at which the H-reaction initiates.

Experimental

Catalyst samples which had been coked in a commercial circulating fluidized bed unit were impregnated with aqueous solutions of a metal salt (chloride or nitrate) by the incipient wetness technique. The solutions were prepared with the appropriate metal salt to give 1.0 wt% as the element on the catalyst after impregnation. The impregnated catalysts were then dried at 300°F for at least three hours before testing. The activity of the impregnated catalyst to promote the Boudouard Reaction was determined by measuring the amount of carbon which had reacted during a 30 minute test. The reaction was performed at 1400°F in a 1" ID Vycor reactor with a thermocouple well in the dense phase of the fluidized bed. Twenty grams of the coked metal impregnated catalyst was heated to the reaction temperature and equilibrated in a stream of helium. Carbon dioxide was then introduced at a constant rate of 1.7 scfh. The CO concentration in the product gases was monitored at regular intervals by gas chromatography. After each test, the catalyst was cooled in helium and the %C left on the catalyst was determined.

In order to study the H-reaction, the catalyst was heated to 600°F for one hour in helium to remove physically adsorbed water. After cooling to 100°F in helium, the catalyst was heated in CO₂ to the desired temperature, 900-1400°F, over a 30 minute period, and then held at this temperature for an additional 30 minutes. The moisture content of the gas stream was measured over the entire 60 minute test with a Shaw hygrometer (Model SH), which was equipped with a gold spot sensor. This sensor was capable of measuring dew points between -58°F and +68°F. The amount of H₂O produced during the H-reaction was calculated by integrating the plot of dew point vs. time.

Results and Discussion

A. Metal Promoters for the Boudouard Reaction

A wide variety of metal salts have been tested as possible promoters for the Boudouard Reaction. The results of the screening tests showed that the most active promoters were the alkali metals and the metals of Group VIII, which agreed with earlier literature reports(6). The screening tests consisted of impregnating each metal onto the coked catalyst and then determining its activity by measuring the %C on the catalyst after contact with CO₂ for 30 minutes. Each promoter was tested on the same spent catalyst (Ni+V = 5900 ppm). The metals were divided into three classes (Table 2) based on their activity to promote the Boudouard Reaction.

An important requirement of this investigation was that the cracking activity and selectivity of the catalyst should not be affected by the promoter. The cracking activity and selectivity were measured by a standard micro-activity test (MAT)(7). The catalyst was calcined at 1100°F for 2 hours to remove all of the coke before running the MAT. The highest activity promoters in Table 2 were evaluated by the MAT. The results of the MAT evaluation are given in Table 3. Catalyst cracking activity is related to the MAT conversion, and selectivity is related to the coke producing factor (CPF) and hydrogen producing factor (HPF). The CPF or HPF is defined as the ratio of the amount of coke or hydrogen produced during the test to the amount produced with a standard catalyst at the same conversion.

A comparison of Table 2 and 3 showed that while the lithium promoted catalyst exhibited the highest activity for the Boudouard Reaction, the cracking activity, as expected, had been drastically reduced by the addition of lithium. Of the other promoters in the highest activity group of Table 2, copper and strontium were selected for further study based on the MAT results. Barium was also selected for further study even though on the standard catalyst the activity was in the lowest class. At Ni+V concentrations greater than 8000 ppm, barium did exhibit substantial activity for the Boudouard Reaction.

Lithium because of its deleterious effect on cracking activity, and rhodium, because of its cost, were not considered possible promoters at the 1.0 wt% and 0.5 wt% levels, respectively. In an attempt to use these high activity promoters, the effect of promoter concentration on activity was examined (Table 4). At feasible concentrations of the promoters (0.1% Li and 5 ppm Rh), their activity had decreased to a level comparable to the unpromoted reaction.

The effect of the contaminant metals (Ni and V), which were deposited on the catalyst during the cracking reaction, on the activity of the various promoters was investigated. Each promoter was impregnated on various spent equilibrium catalyst samples. The results of these tests were plotted as %C on catalyst after the 30 minute test (normalized to 1.0 wt% C initially on the catalyst) versus Ni+V (Figures 1-3 for copper, strontium and barium promoted catalysts, respectively). Each metal promoted the Boudouard Reaction to a greater extent as the concentration of Ni+V increased. The promoter and the contaminant metals exhibited a synergistic effect on increasing the rate of the Boudouard Reaction. The circled data points in Figures 1-3 supported the idea of synergism. These data points were the results of experiments in which the Ni/V ratio on the catalyst was equal to one. The

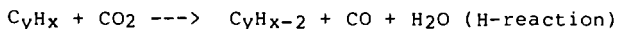
remaining data points, those that fall on the curves, were the results of experiments in which the promoters were impregnated on catalysts with Ni/V ratios equal to 1/3. The circled data points showed, at comparable metals levels, that less coke had undergone reaction with CO₂ in the catalysts with lower vanadium concentrations. Vanadium, when impregnated on spent catalyst, exhibited moderate activity (35% carbon removal on a catalyst containing 5900 ppm Ni+V). Nickel and vanadium, deposited on the catalyst during the cracking reaction, promoted the Boudouard Reaction only when the total concentration of these metals was greater than 8000 ppm. At Ni+V concentrations, above 15,000 ppm, these metals promote the Boudouard Reaction to the same extent as the highest activity metals (see Figure 4).

In the previous experiments, the catalyst samples were impregnated with the promoter after the catalyst was deactivated with coke. However, in a commercial process, the promoter could be deposited on the catalyst during manufacture or during the process. A series of experiments were performed to compare the activity of barium impregnated on the catalyst before coking and after coking. The conclusion was that barium exhibited a higher activity when the metal was impregnated before the catalyst was deactivated (see Table 5).

A series of experiments were performed to test the ability of a barium promoted catalyst (Ni+V = 12,600 ppm) to maintain activity over ten coking-regeneration cycles. Each cycle consisted of, first, coking the regenerated catalyst with a vacuum gas oil at 900°F, then allowing the spent catalyst to react with CO₂ for 30 minutes at 1400°F, and finally, regenerating the catalyst with air at 1200°F. In Figure 5, the peak height of CO in the GC analysis of the product gas stream plotted against the number of coking-regeneration cycles. The amount of CO in the gas stream was determined 5 times (at 2, 9, 16, 23 and 30 minutes) during coke-CO₂ reaction. The activity of the promoter decreased slightly over the ten cycles.

B. H-Reaction Studies

Coke has a composition in the range of 92-97% C and 3-8% H⁽⁸⁾ with trace amounts of nitrogen and sulfur. In previous reports^(9,10) on promoting the Boudouard Reaction, the hydrogen in coke has either been assumed not to react with CO₂ or not mentioned. Hydrogen in the coke on spent catalyst was calculated to be responsible for 15-25% of the heat generated during the regeneration of catalyst spent. In this investigation, the hydrogen in coke was found to react with CO₂ to produce water according to the reaction sequence:



While the enthalpy change for this reaction has not been determined, it is believed to be considerably more endothermic than for the combustion reaction. By allowing the H-reaction to occur, the amount of hydrogen which must undergo combustion in the regenerator section of a fluidized reactor system would be decreased, thus, less heat would then be produced in the regenerator.

With a hygrometer inserted into the product gas stream line, the amount of water in the product gas stream, as measured by the dew point (in

°C), was determined. The concentration of water in the gas stream was determined by the equation:

$$\log (\text{H}_2\text{O in ppm}) = 13.33 - 261.3/\text{Dew Point } (^\circ\text{K})$$

A comparison of the amount of H_2O produced during the reaction of CO_2 with a coked and a regenerated catalyst is given in Figure 6. The difference in the two plots is a measure of the amount of water produced by the H-reaction. The water observed in the dew point plot of the regenerated catalyst is attributed to catalyst dehydroxylation at 1400°F . With this technique, the amount of hydrogen in coke on a catalyst is found to be between 3-10%. The range in this value is the result of uncertainty in the amount of hydrogen in the coke which did not react during the 30 minute test.

C. Initiation Temperature of the H-Reaction

One of the potentially useful aspects of the H-reaction is that it could be made to occur in the reactor (spent catalyst) stripper of the RCC^{SM} process unit. The temperature of the catalyst in the stripper is usually between 900 - 1050°F . The thermodynamics of the H-reaction as compared to the water gas shift reaction indicates that hydrogen in coke will react at temperatures within this range. Carbon dioxide could easily be used either in place of or in conjunction with steam as a stripper gas. The advantage of reacting hydrogen in the stripper in the RCC^{SM} process unit is apparent from the data in Figure 7. This figure shows the relationship for a particular set of unit operating conditions between Conradson carbon in the feed, the water addition to the riser, and the hydrogen content in the coke in order to maintain the RCC^{SM} process unit in heat balance at a CO_2/CO ratio in the flue gas equal to one. By lowering the hydrogen content in coke, feedstocks with higher Conradson carbon values can be processed with the heat balance being maintained in the RCC unit.

The temperature at which a measurable amount of water is produced by the H-reaction has been determined. The initiation temperature was determined by a series of temperatures in which the catalyst was heated to a predetermined temperature (eg., 900° , 1000° , 1400°F) in CO_2 and the amount of water produced during the CO_2 reaction was measured. Before each test, the catalyst was heated to 600°F in an attempt to remove physically adsorbed water. The results of these experiments are shown in Figure 8. The set of dew point plots show that substantially more water is produced at 1000°F and 1400°F than at 900°F . Temperatures between 800° - 900°F give identical dew point plots to the one at 900°F . These data indicate that the rate of the H-reaction becomes measurable between 900° and 1400°F . The source of the water in the dew point plots obtained at reaction temperature below 900°F is believed to be adsorbed water.

A series of experiments in a product distribution unit (PDU) were performed to quantify the amount of water produced by the H-reaction. The PDU is a homogeneous fluid bed reactor which uses a liter of catalyst. The larger volume of catalyst allows for a more accurate determination of the water produced by the hydrogen reaction. The catalyst was heated in the reactor at 1250°F in dry O_2 free N_2 overnight to remove all adsorbed and chemical water. The catalyst was then coked with a reduced crude oil and the entrained hydrocarbons were stripped from the catalyst with N_2 . At this point, CO_2 was introduced into the reactor, at either 1000° or 1100°F . The product gases from the H-reaction were

monitored for their water content continuously. After two hours, the CO₂ was stopped and air was introduced into the reactor to burn the remaining hydrogen off the catalyst. The amount of hydrogen which had reacted with CO₂ was calculated by comparing the water produced by the H-reaction to the water produced by the combustion reaction. From these calculations, it was found that 4% of the hydrogen in the coke on the catalyst reacts at 1000°F, while at 1100°F, 10% of the hydrogen in the coke on the catalyst has reacted.

Conclusions

This report describes an investigation into a novel method to lower the amount of heat produced in the regenerator of an RCCSM process unit. Three metal promoters (Cu, Sr and Ba) were found for the Boudouard Reaction which allowed the reaction to occur at 1400°F without severely affecting the cracking activity of the catalyst. Another promising result of this investigation was that a fraction of the hydrogen in coke reacts with CO₂ at 1000°F. At this temperature, a portion of hydrogen could be removed from the catalyst in the reactor stripper, thereby lowering the amount of hydrogen in coke which must be burned off the catalyst. This would allow for the processing of heavier feedstocks in an RCCSM process unit, while maintaining moderate temperatures in the regenerator.

References

1. Zandona, O. J., Busch, L. E., and Hettinger, Jr., W. P., NPRA 80th Annual Meeting, Paper AM-82-61, March 21-23, 1982
2. Boudouard, Ann Chim. Phys., 24 5 (1901).
3. Holstein, W. L., Bodart, M., J. Catal. 75 337 (1982)
4. Jalan, B. P., Rao, Y. K., Carbon 16 175 (1978)
5. Stull, D. R., Westrum, Jr., E. F., and Sinke, G. C., "The Chemical Thermodynamics of Organic Compounds", John Wiley and Sons, Inc., New York, 1969
6. McKee, D. W., General Electric Technical Information Series, Report No. 78CRD076, Schenectady, NY, April, 1978
7. Hettinger, Jr. W. P., Beck, H. W., Cornelius, E. B., Doolin, P. K., Kmecak, R. A. and Kovach, S. M., Div. Petrol. Chem. Preprints, ACS 28 (4) 920 (1983)
8. Sotirchos, S. V., Mon, E., and Amundson, N. R., Chem. Eng. Sci. 38 55 (1983)
9. Marsh, H. and Rand, B., Carbon 9 63 (1971)
10. Hippo, E., and Walker, Jr., P. L. Fuel 54 245 (1975)

Table 1
Thermodynamic Parameters

Reaction	H (kcal/mole)		G (kcal/mole) at 1000°K
	at 298°K	at 1000°K	
$C + 1/2 O_2 \rightleftharpoons CO$	-26.42	-26.77	-47.95
$C + O_2 \rightleftharpoons CO_2$	-94.05	-94.32	-94.61
$H_2 + 1/2 O_2 \rightleftharpoons H_2O$	-57.80	-59.24	-46.04
$C + CO_2 \rightleftharpoons 2CO$	+41.21	+40.78	- 1.29
$H_2 + CO_2 \rightleftharpoons H_2O + CO$	+ 9.83	+ 8.31	+ 0.62

Table 2
Classes of Boudouard Reaction Promoters

<u>High Activity</u>	<u>% Coke Reacted</u>	<u>Low Activity</u>	<u>% Coke Reacted</u>
Li	69	Mo	29
Co	55	Sn	28
CuCl ₂	55	Ca	27
Ni	53	Ti	25
Rh (0.5 wt%)	53	Cr	25
Fe	52	La	25
Na	52	Y	25
Ru (0.5 wt%)	52	Zn	24
Sr	46	Zr	24
Cu(NO ₃) ₂	42	U	23
		B	22
Moderate Activity		Ba	22
		Cs	22
V	35	K	20
Ag	31	In	20
Bi	30	Mn	20
		Cd	16
		None	15
		W	15
		Sb	9

Catalyst - Super DX w/1.10% C

Temperature - 760°C

Reaction Time - 30 minutes

Promoter Concentration - 1.0 wt% except where noted

Table 3

MAT Results of Promoted Catalysts

<u>Promoter</u>	<u>Concentration (wt%)</u>	<u>Conversion (vol)(%)</u>	<u>CPF</u>	<u>HPF</u>
None	0	61	1.2	13
Li	1.0	10	3.9	10
CuCl ₂	1.0	65	1.5	17
Cu(NO ₃) ₂	1.0	62	1.6	18
Sr	1.0	50	1.2	10
Ba	1.0	56	1.1	9
Fe	1.0	52	2.3	22
Ni	1.0	53	3.2	33
Li	0.5	16	3.7	11

Table 4

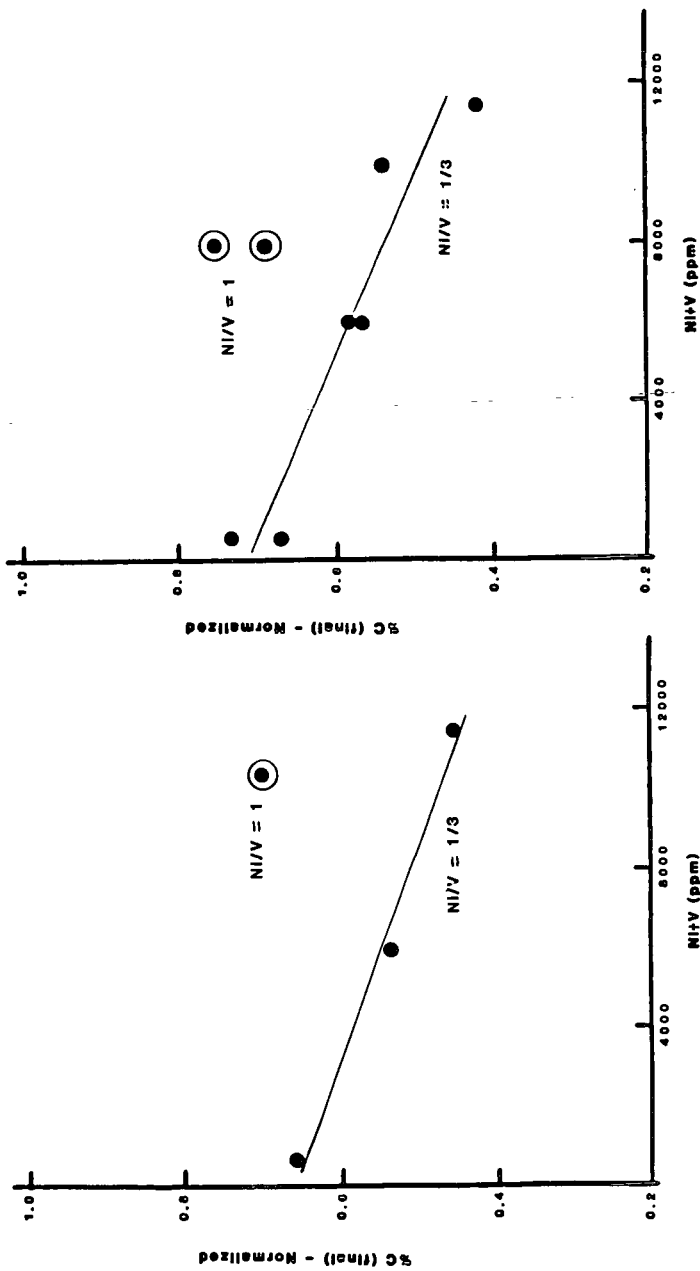
The Effect of Promoter Concentration on the Boudouard Reaction

<u>Li Conc. (wt%)</u>	<u>% Coke Reacted</u>
1.0	69
0.5	44
0.33	35
0.1	25
<u>Rh Conc. (ppm)</u>	
5000	53
500	44
50	26
5	17

Table 5

Sequence of Promoter Addition

<u>Catalyst</u>	<u>%C Reacted</u>	<u>Sequence</u>
1.0 wt% Ba on Catalyst X	.64	Coke over Ba
1.0 wt% Ba on Catalyst X	.71	Ba over Coke
1.0 wt% Ba on Catalyst G	.74	Coke over Ba
1.0 wt% Ba on Catalyst G	.84	Ba over Coke



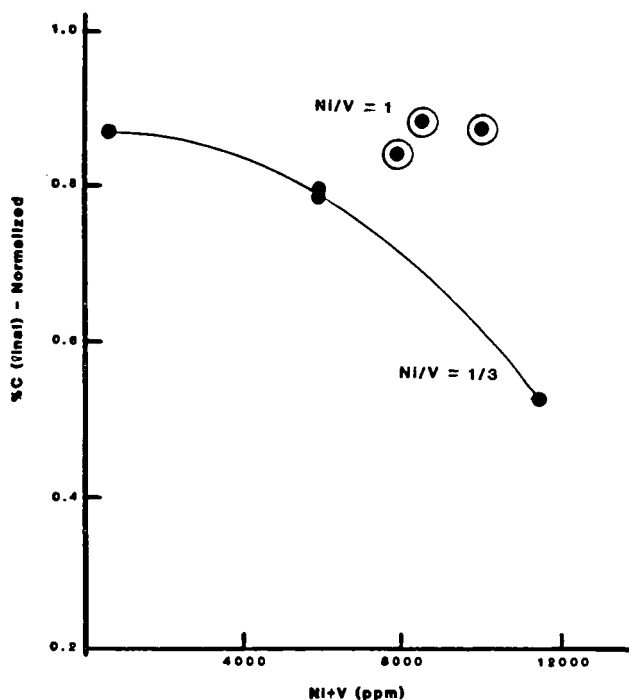


Figure 3. The Effect of Metals on Promoter Activity - Barium

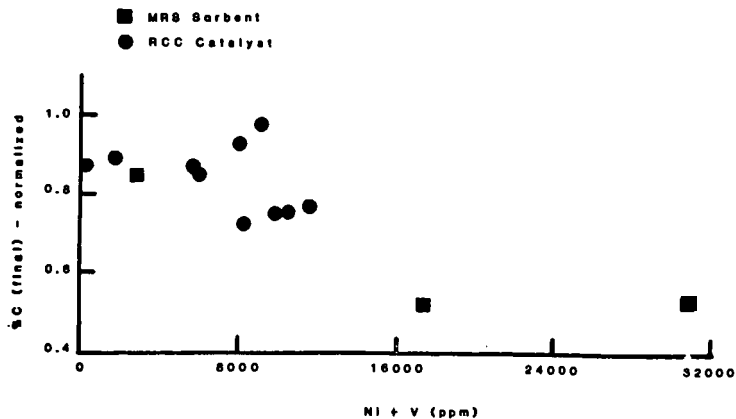


Figure 4. The Effect of Metals on the Rate of the Unpromoted Boudouard Reaction

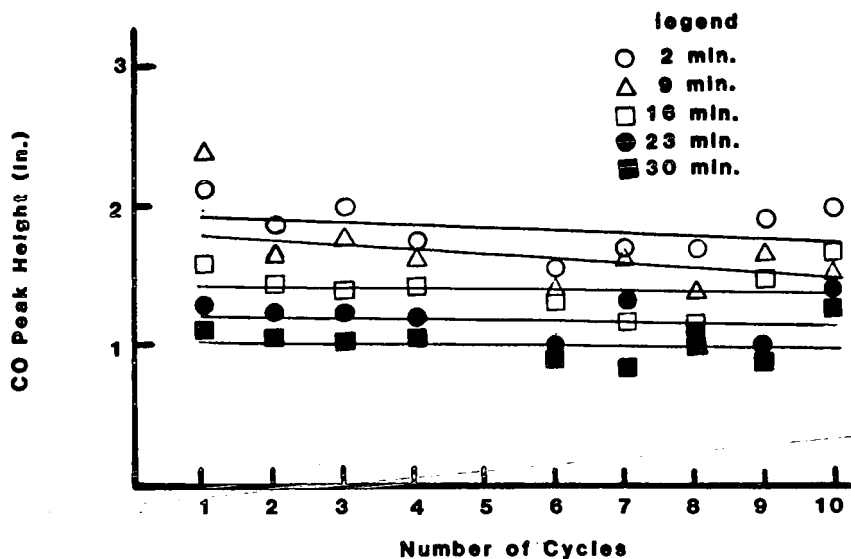


Figure 5. The Effect of Repeated Coking-Regeneration Cycles on the Activity of the Boudouard Reaction Promoter

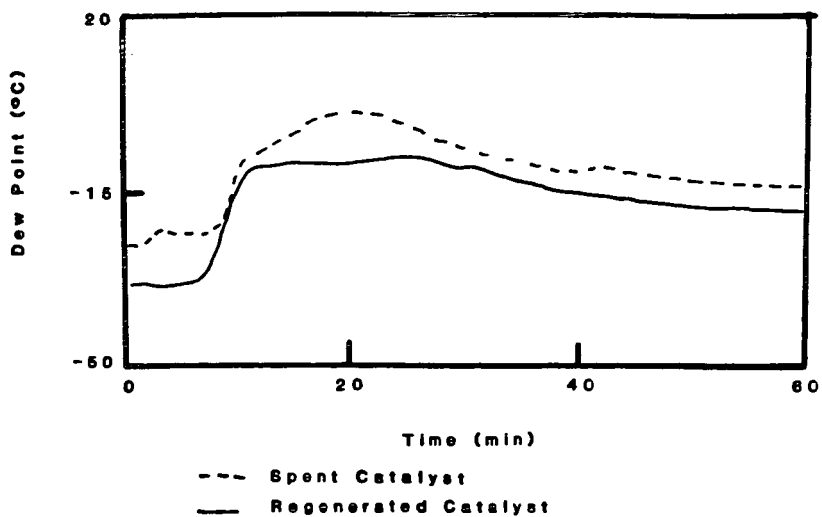


Figure 6. H-Reaction Comparison of Spent and Regenerated Catalysts

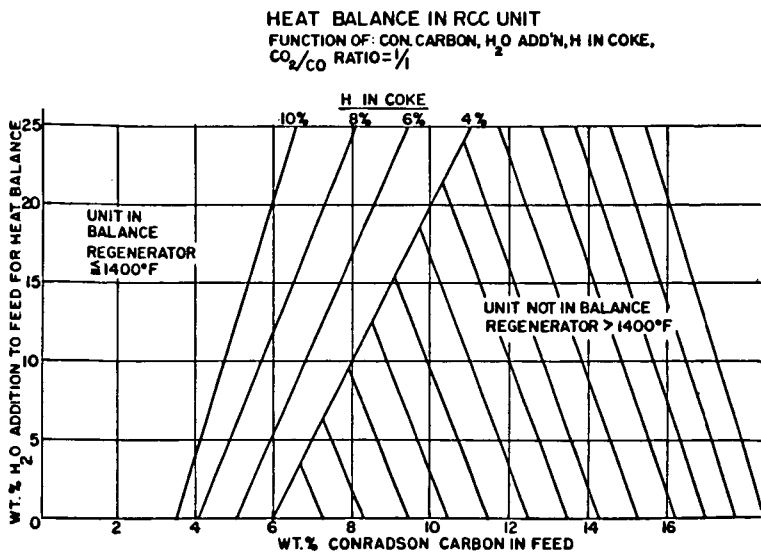


Figure 7. Heat Balance in RCC Unit

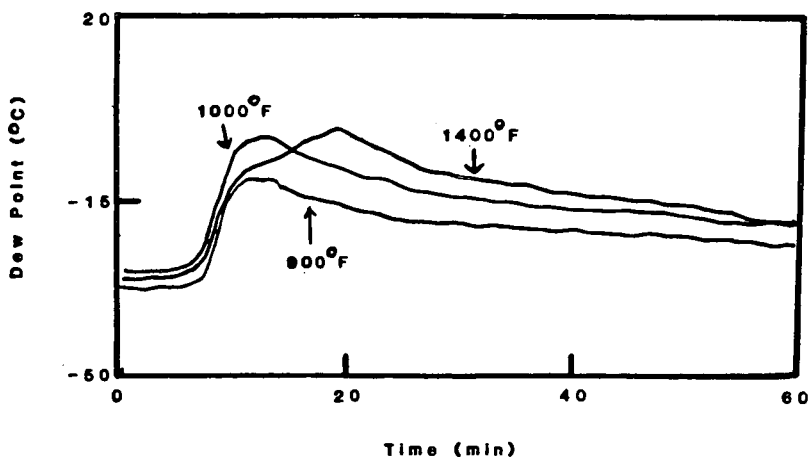


Figure 8. Initiation Temperature of the H-Reaction

COAL WEATHERING: CAUSES, EFFECTS AND IMPLICATIONS

John L. Cox and Charles R. Nelson

Gas Research Institute
8600 West Bryn Mawr Avenue
Chicago, Illinois 60631

INTRODUCTION

If it is meaningful to single out one characteristic of coal as having unique importance, that designation would have to go to the dynamic nature of coal's chemical and physical properties. The chemical and physical properties of coal can and often do undergo substantial changes after removal of the coal from its natural environment. This phenomenon is known as weathering and can alter the coal's calorific value, beneficiation, coking, liquefaction, and gasification characteristics. Weathering also influences standard tests and other experimental results, and thus has important implications with respect to fundamental research on the structure and properties of coal. This short review focuses on the incomplete state of our knowledge of the causes, effects and implications of coal weathering.

CAUSES AND EFFECTS OF COAL WEATHERING

Weathering commences once the coal is unearthed and/or removed from the coal seam unless precautions are taken to prevent its exposure to oxygen (air) and changes in temperature and humidity. The exposure of coal to and its subsequent reaction with the oxygen in air is recognized as the most important contributor to weathering. The reaction of the coal with oxygen occurs readily at ambient temperature, results primarily in oxidation of the coal's organic constituents, and leads to an increase in the oxygen content and a decrease in the atomic hydrogen-to-carbon ratio of the coal (1-5).

The general outlines of the oxidation of coal's organic constituents by oxygen have been well characterized. Peroxides have been detected as transient intermediates in the early stages of coal oxidation (3,6,7), and it is generally thought that decomposition of the peroxides leads to creation of the new oxygen-containing functional groups (3,6-13). The formation of hydroxyl, carbonyl and carboxyl groups, and ether linkages have been detected or inferred from wet chemical and spectroscopic data (4,7,12-21). In general, the chemical structural changes that accompany coal's oxidation at low temperatures (from ambient to 200°C) by molecular oxygen are strongly dependent upon coal rank, particle size, oxygen partial pressure, moisture content, and temperature (1-5,17,22,23). Considerable uncertainty still exists, however, concerning the mechanisms whereby the peroxides are formed and subsequently decompose.

Perhaps the most elusive aspect of the reaction of coal with oxygen has been identification of the initiation reaction, the step by which the oxidation reaction gets started. Although the oxygen molecule has two unpaired electrons, one on each oxygen atom, and behaves as a diradical ($\cdot O-O\cdot$) it is too unreactive to be the species which actually oxidizes the coal. However, the fact that coal already contains substantial concentrations of carbon radicals (12,24-26) suggests the possibility that initiation may occur by reaction between molecular oxygen and a carbon radical in the coal to form a peroxy radical (Coal-OO \cdot). The peroxy radical could then serve as the initiator for free radical chain reactions which lead to peroxides and their decomposition products. The evidence for free-radical chain processes for the decomposition of the peroxides, however, is not unequivocal. Since water, a protic solvent, is invariably present in coal and has been observed to facilitate the oxidation of coal by oxygen (2,3,5,22,23) the decomposition of the intermediate peroxides might also occur, at least in part, via ionic reaction mechanisms (27). Clearly, many of the mechanistic aspects of the oxidation of coal by oxygen remain unresolved and present challenging problems for further exploration.

The reaction of coal with oxygen is also notorious for its idiosyncrasies. One of these is that the thermoplastic properties of bituminous and subbituminous coals are often extensively altered long before changes can be detected in the coal's chemical composition (1,2,5,28,29). In general, exposure of the coal to oxygen at ambient temperature can result in a very rapid reduction in the fluidity that it exhibits when heated and a significant narrowing of its plastic temperature range (5,10,28-30). The loss of the coal's thermoplastic properties suggests that a more highly cross-linked macromolecular structure has been formed which will not easily melt and flow when heated. However, the exact nature of the changes that occur in the coal's macromolecular structure which adversely affect its thermoplastic properties remain points of considerable uncertainty and interest.

The weathering of coal's inorganic constituents, in sharp contrast to the situation with coal's organic constituents, is quite well understood. Except for the iron bearing mineral pyrite which is readily air-oxidized, the coal's inorganic constituents apparently remain unchanged by weathering (31-33). The pyrite in coal is oxidized initially to iron sulfates, which are then transformed to iron oxyhydroxide (33). Pyrite oxidation, as expected, is accelerated by increasing humidity, temperature, and oxygen partial pressure. Although oxidation of the coal's organic and inorganic constituents occur simultaneously, they are generally regarded as quite separate processes.

Another contributor to weathering is the stresses caused by cyclic sorption and desorption of moisture which produce fissures and cracks that mechanically weaken the coal (2,5,34). This decrepitation phenomenon is referred to as slackening. The thermal cycling of coal also contributes to slackening. Slackening is much more rapid and extensive for lignites and subbituminous coals than for higher rank coals (5,34). Slackening can also accelerate oxidation by increasing the exposed surface area of the coal to air. Although oxidation can be accelerated by slackening, its possible participation in and importance to slackening has not been stressed or studied. The oxidation of coal's organic constituents could participate in slackening through the creation of new hydrophilic sites which would promote moisture sorption.

TECHNOLOGICAL ASPECTS OF COAL WEATHERING

The changes in coal's chemical and physical properties produced by weathering may affect the suitability of the coal for existing and future technological uses. Coal's major domestic uses include: direct combustion for electricity generation and for industrial process heat, steam and power generation; and conversion to coke for steel production (35). Coal-based synthetic fuel (gas and liquid) and chemical technologies are currently under development. Coal-water and coal-oil slurries are also being investigated as potentially economical means of converting solid coal into a form suitable for transport through pipelines and use as a liquid-like fuel.

Oxidation reduces the calorific value of coal. Low rank coals will lose about 190 Btu-per-pound for each 1% increase in oxygen content while high rank coals will lose about 240 Btu-per-pound for each 1% increase in oxygen content (34). The oxygen content of freshly mined and crushed lignite coals can increase several percent in a matter of weeks when the coal is stored in air at ambient temperature. Such rapid oxidation can lead to spontaneous combustion of the coal under certain storage conditions (34,36).

Oxidation also converts coal to a more hydrophilic material which makes beneficiation more difficult. The purpose of beneficiation is to upgrade the quality of the coal so that it can meet specific end-use requirements. Beneficiation is primarily carried out to reduce the mineral matter (including pyrite) and clay content of the coal. Oxidation reduces the hydrophobicity-hydrophilicity differences between coal's organic constituents and mineral matter which, in turn, makes it more difficult to selectively separate mineral matter particles on the basis of their hydrophilic surface properties (37-39). This results in a reduction in the efficiency of beneficiation by flotation, agglomeration and flocculation processes.

The new oxygen-containing functional groups that are created when the coal is oxidized also increase its adsorptive affinity for polar molecules such as water as well as its water solubility (40-42). Hence, the dewatering and drying of coal becomes more energy intensive and less efficient as the coal's degree of oxidation increases. The stability and viscosity of coal-water and coal-oil slurries would also be affected by the more polar surface properties of particles of oxidized coal. Additionally, the peroxides produced during coal oxidation could potentially have a detrimental affect on the stability and viscosity of coal-oil slurries.

The detrimental effects of oxidation on a coal's suitability for producing high-quality metallurgical coke have been extensively studied (1,2,5,16,28,43) and are well understood from a practical viewpoint. The adverse effects include reduction in coke strength, coal bulk-density-control problems, overheated charges, carbon deposits leading to oven damage, coke handling problems, and reduced coke yields as a result of increased coke breeze, increased coke reactivity and decreased coking rate (1,2,5,16,43). One important effect of oxidation is to destroy the coal's thermoplastic properties which, in turn, prevents its organic components from adequately fusing and binding together during the coking process. This results in a reduction in coke strength and yield.

The effects of oxidation on coal's behavior during thermal processing can be predicted to be profound but have not been extensively investigated. The new oxygen-containing functional groups that are created when the coal is oxidized will lead to increased yields of carbon monoxide and carbon dioxide at the expense of tar and/or liquid yields during gasification, liquefaction, pyrolysis, and thermal depolymerization in non-hydrogen-donating solvents (1,2,4,43-47). The increased cross-linking of coal's macromolecular structure that accompanies oxidation will also reduce its swelling during heating, extractability by organic solvents, and tend to increase the molecular weight distribution of the extractable material and low-temperature pyrolysis tars (1,2,46,47). An enhancement of char surface area (by a factor of up to 10) and gasification reactivity (by a factor of up to 40) has also been observed as a consequence of the preoxidation of bituminous coals (48).

CONCLUSIONS

The changes brought about by weathering that affect the suitability of coal for existing and future technological uses have a very definite molecular basis. At a molecular level, however, we are for the most part at a very primitive level of understanding of the weathering process. In spite of the recent research interest that has been shown in this important phenomenon, insufficient definitive experimental data exist to permit a detailed mechanistic description to be written which accounts for this phenomenon's complexities and idiosyncrasies. The complexity of the coal itself contributes significantly to the experimental difficulties. Hence, progress in elucidating the mechanistic details of weathering will require a more aggressive approach and help from many disciplines.

REFERENCES

1. L. D. Schmidt, J. L. Elder, and J. D. Davis, Ind. & Eng. Chem., **32**, 548 (1940).
2. L. D. Schmidt, in Chemistry of Coal Utilization, vol. 1, H. H. Lowry, ed., John Wiley & Sons, Inc., 627 (1945).
3. R. E. Jones and D.T.A. Townend, J. Soc. Chem. Ind., **68**, 197 (1949).
4. J. D. Brooks and T. P. Maher, Fuel, **36**, 51 (1957).
5. R. J. Gray, A. H. Rhoades, and D. T. King, Trans. ASME, AIME, **260**, 334 (1976).
6. R. E. Jones and D.T.A. Townend, Nature, **155**, 424 (1945).
7. R. Liotta, G. Brons, and J. Isaacs, Fuel, **62**, 781 (1983).
8. H.A.W. Van deVries, C. Bokhoven, and K.N.M. Dormans, Brennstoff-Chemie, **50**, 289 (1969).
9. G. Albers, L. Lenart, and H. Oelert, Fuel, **53**, 47 (1974).

10. H. M. Wachowska, B. N. Nandi, and D. S. Montgomery, Fuel, 53, 212 (1974).
11. E.A.C. Chamberlain, G. Barrass, and J. T. Therlaway, Fuel, 55, 217 (1976).
12. T. Yokono, K. Miyazawa, Y. Sanada, and H. Marsh, Fuel, 60, 598 (1981).
13. J. C. Donini, S. A. LaCour, B. M. Lynch, and A. Simon, Proc. 64th CIC Coal Symp., 132 (1982).
14. M. G. Rockley and J. P. Devlin, Appl. Spectrosc., 34, 407 (1980).
15. P. C. Painter, M. M. Coleman, R. W. Snyder, O. Mahajan, M. Komatsu, and P. L. Walker, Jr., Appl. Spectrosc., 35, 106 (1981).
16. D. E. Lowenhaupt, P. R. Griffiths, M. P. Fuller, I. M. Hamadeh, Proc. Ironmaking Conf., 41, 39 (1982).
17. D. C. Cronauer, R. G. Ruberto, R. G. Jenkins, A. Davis, P. C. Painter, D. S. Hoover, M. E. Starsinic, and D. Schlyer, Fuel, 62, 1124 (1983).
18. P. B. Tooke and A. Grint, Fuel, 62, 1003 (1983).
19. J. R. Havens, J. L. Koenig, D. Kuehn, C. Rhoads, A. Davis, and P. C. Painter, Fuel, 62, 936 (1983).
20. D. L. Perry and A. Grint, Fuel, 62, 1024 (1983).
21. A. Grint and D. L. Perry, Proc. Intl. Conf. Coal Sci., 655 (1983).
22. D. C. Cronauer, R. G. Ruberto, R. S. Silver, R. G. Jenkins, I.M.K. Ismail, and D. Schlyer, Fuel, 62, 1116 (1983).
23. E. Beier, Proc. Intl. Conf. Coal Sci., 735 (1983).
24. H. Ohuchi, M. Shiotani, and J. Sohma, Fuel, 48, 187 (1969).
25. J. W. Larsen, J. Clardy, A. Davis, R. C. Neavel, H. L. Retcofsky, and H. W. Sternberg, in Scientific Problems in Coal Utilization, B. R. Cooper, ed., U.S. DOE Technical Information Center, 93 (1978).
26. A. G. Sharkey, Jr. and J. T. McCartney, in Chemistry of Coal Utilization, 2nd Supplemental Volume, M. A. Elliott, ed., Wiley-Interscience, 241 (1981).
27. R. Curci and J. O. Edwards, in Organic Peroxides, D. Swern, ed., Wiley-Interscience, 199 (1970).
28. B. S. Ignasiak, B. N. Nandi, and D. S. Montgomery, Fuel, 49, 214 (1970).
29. D. L. Marchioni, Intl., J. Coal Geol., 2, 231 (1983).
30. D. J. Maloney, R. G. Jenkins, and P. L. Walker, Jr., Fuel, 61, 175 (1982).

31. F. E. Huggins, G. P. Huffman, D. A. Kosmack, and D. E. Lowenhaupt, Intl. J. Coal Geol., 1, 75 (1980).
32. F. E. Huggins, G. P. Huffman, and R. J. Lee, Coal and Coal Products: Analytical Characterization Techniques, E. L. Fuller, Jr., ed., ACS Symp. Series No. 205, 239 (1982).
33. F. E. Huggins, G. P. Huffman, and M. C. Lin, Intl. J. Coal Geol., 3, 157 (1983).
34. J. F. Fryer and A. J. Szladow, in Storage of Coal Samples, Info. Series No. 66, Alberta Research Council, 1 (1973).
35. H. Perry, Science, 222, 377 (1983).
36. J. R. Herring and R. J. Rich, Intl. Conf. Coal Sci., 753 (1983).
37. H. A. Hamza, K. H. Michaelian, and N. E. Andersen, Intl. Conf. Coal Sci., 248 (1983).
38. H. B. Gala, S. H. Chiang, G. E. Klinzing, J. W. Tierney, and W. W. Wen, Intl. Conf. Coal Sci., 260 (1983).
39. B. C. J. Labuschagne and J. G. Van der Watt, Intl. Conf. Coal Sci., 264 (1983).
40. S. Kelekek, T. Salman, and G. W. Smith, Proc. 64th CIC Coal Symp., 145 (1982).
41. A. Taweel, A.M.H.A. Farag, J. Kwak, H. A. Hamza, and M. Falk, Proc. 64th CIC Coal Symp., 125 (1982).
42. T. Murata, Fuel, 60, 744 (1981).
43. J. C. Crelling, R. H. Schrader, and L. G. Benedict, Fuel, 58, 542 (1979).
44. R. C. Neavel, in Coal Science, vol. 1, M. L. Gorbaty, J. W. Larsen, and I. Wender, eds., Academic Press, 1 (1982).
45. E. Furimsky, J. A. MacPhee, L. Vancea, L. A. Ciavaglia, and B. N. Nandi, Fuel, 62, 395 (1983).
46. B. S. Ignasiak, D. M. Clugston, and D. S. Montgomery, Fuel, 51, 76 (1972).
47. H. Wachowska and W. Pawlak, Fuel, 56, 342 (1977).
48. O. P. Mahajan, M. Komatsu, and P. L. Walker, Jr., Fuel, 59, 3 (1980).

SELECTION AND CHARACTERIZATION OF LOW-RANK COAL SAMPLES

S.A. Benson, D.R. Kleesattel, and H.H. Schobert

University of North Dakota
Energy Research Center
Box 8213, University Station
Grand Forks, North Dakota 58202

INTRODUCTION

The collection of low-rank coal samples at the University of North Dakota Energy Research Center (UNDERC) includes coals from the major lignite and sub-bituminous coal regions of the United States. Primarily, the coals were collected to provide fresh, homogeneous, and well characterized samples for projects in coal science research at UNDERC. In the past, research has been performed on coal in which no information was reported or available on how the samples were prepared and stored, or on the geography and geology of the coal seam. Richard Neavel (1) pointed out that work on "poorly selected, poorly collected, poorly prepared, poorly preserved and poorly characterized coal samples will only lead us into further confusion." It is important that coal science research be performed with carefully collected, prepared, and documented samples so that the resulting data on coal properties, composition, and reactivity will be meaningful to other researchers.

In the past several years a great deal of interest has surfaced dealing with sample banks. The American Physical Society (2) identified the need for a sample bank of well-selected, characterized and preserved coal samples the lack of which has been a major obstruction in the past to advancement of coal research. A Coal Sample Bank Workshop was held in March 1981 sponsored by the Gas Research Institute and the U.S. Department of Energy to identify the need and problems associated with setting up a National Coal Sample Bank (3). It is our hope that the information presented in this paper will be of use to researchers interested in establishing a sample bank or interested in incorporating low-rank coal samples in existing sample banks. The motivation for such work at UNDERC is the need for this type of research to be accomplished for low-rank coals.

Channel samples of low-rank coals have been collected from various mines in North Dakota, Montana, Colorado, New Mexico, and Texas. The samples were carefully collected, homogenized, and stored in an inert atmosphere. The coals were prepared in several different sizes from -1/2 inch to -60 mesh and quantities from 15 kilograms to 250 grams. At UNDERC the coals will be used to study various coal features such as the distribution of inorganics, organic structure, ash and slag chemistry, physical and mechanical properties, and pyrolysis and extraction behavior. In addition, trace element analysis, proximate, ultimate, heat content, ash fusion, and ash analysis will be performed.

SAMPLE SELECTION AND COLLECTION PROCEDURES

The selection of coals was based either on some desired unique characteristics such as sodium content, or slag viscosity, or on production tonnage. The goal is eventually to have a set of coals available which represent a wide range of coal properties characteristic of low-rank coals. The selection and preparation of coals will be an ongoing project at UNDERC for at least two more years and the total suite of samples will extend beyond the coals collected to date. The coal ranks to be included range from low-grade lignite to high-rank subbituminous.

When a mine has been chosen for sampling, a pit within the surface mine is selected, based either on some unique characteristic or on ready accessibility to the pit. A "typical section" is selected for sampling which is free of faults, slumping, or evidence of groundwater flow. The face of the seam or seams to be sampled is cleaned to expose fresh nonweathered coal free from extraneous mineral matter which may have fallen from the overburden. The coal seam is measured and a megascopic description is made of the coal and associated sediments. A channel sample is collected to provide approximately 100 kilograms of coal. In some cases, one-kilogram samples are also collected at various intervals throughout the seam, including overburden, interburden (if two seams are sampled) and underclay, to study the within-seam variability. All samples are sealed in plastic bags and transported to UNDERC for preparation. A list of samples collected through November 1983 is in Table 1.

TABLE 1
LOW-RANK COALS COLLECTED

<u>Mine</u>	<u>Rank</u>	<u>State</u>	<u>Region</u>
Abasloka (Sarpy Creek)	Subbituminous	Montana	Powder River
Indian Head	Lignite	North Dakota	Fort Union
Beulah (High-Na)	Lignite	North Dakota	Fort Union
Beulah (Low-Na)	Lignite	North Dakota	Fort Union
Gascoyne (Red Pit)	Lignite	North Dakota	Fort Union
Gascoyne (Blue Pit)	Lignite	North Dakota	Fort Union
Velva	Lignite	North Dakota	Fort Union
Spring Creek	Subbituminous	Montana	Powder River
Falkirk	Lignite	North Dakota	Fort Union
Glenharold	Lignite	North Dakota	Fort Union
Colorado Coal Co.	Subbituminous	Colorado	Green River
Navajo	Subbituminous	New Mexico	San Juan
San Miguel	Lignite	Texas	Gulf Coast
Martin Lake	Lignite	Texas	Gulf Coast
Savage	Lignite	Montana	Fort Union
Center	Lignite	North Dakota	Fort Union

The channel sample is crushed, split, and stored in plastic or glass containers under an argon atmosphere. The crushing is done using a hammer mill. A diagram which illustrates the procedure used for preparing the coals is shown in Figure 1. The final splitting of the -60 mesh coal is done by a rotary riffle in an argon-purged glove box. These samples are stored in plastic or glass containers which are in turn sealed in a plastic pouch. The -8 mesh coals are stored in plastic containers and purged with argon.

The samples collected at various locations within the seam are prepared for selected characterization techniques, such as petrography of separated lithotypes; x-ray diffraction of the overburden; interburden; underclay; and trace element analysis. This type of work is being done to examine the variability of organic and inorganic constituents within the seam and to understand interrelationships between coal properties.

RESULTS AND DISCUSSION

The geologic and geographic description of the sampling area along with the analytical determinations will be available for all samples. The types of analytical results being obtained include proximate, ultimate, heat content, ash fusion, ash analysis, and trace element analysis. As an example, the results obtained for Indian Head lignite will be summarized here. Table 2 summarizes the geographic and geologic description of the Indian Head Mine. The results of the analytical determinations for the traditional ultimate, proximate, heat content and ash analysis are summarized in Table 3. The trace element determinations performed by neutron activation analysis (NAA) are listed in Table 4. The NAA analyses were made by North Carolina State University (4).

TABLE 2
GEOGRAPHIC AND GEOLOGIC DESCRIPTION
OF INDIAN HEAD MINE

County	Mercer
State	North Dakota
Town	Zap
Basin	Williston
Group	Fort Union
Formation	Sentinel Butte
Bed	Beulah-Zap
Age	Paleocene
Grand Forks Number	83-0008
Sampling Date	11/83

The information shown in Tables 2-4 is steadily supplemented by characterization data from several research groups within the UNDERC Coal Science Division, which include Ash and Slag Chemistry, Organic Chemistry, Distribution of Inorganics and Geochemistry, Physical Properties and Moisture, and Coal Reactivity. Samples of lithotypes have been separated for characterization by many of the above techniques to supplement the "whole coal" data. Petrography is also being performed on the homogenized channel sample and the separated lithotypes.

SUMMARY AND CONCLUSIONS

The low-rank coals have been collected to obtain coals which represent a broad range of low-rank coal characteristics. These coals are carefully collected, prepared, and stored under an argon atmosphere. These samples are not comparable to those in a premium sample bank, because they are stored at room temperature and are not collected in large reserve quantities. All the data generated will be entered in a computer system and can be readily accessed. The results of studies on these coals will provide insight into the interrelationships of various coal properties, both with each other and with coal-specific process responses.

TABLE 3
RESULTS OF ANALYSES FOR INDIAN HEAD LIGNITE

<u>Ultimate Analysis</u>	<u>Wt % (as received)</u>
C	44.08
H	6.36
N	0.64
S	0.38
<u>Proximate</u>	
Moisture	34.0
Volatile Matter	27.4
Fixed Carbon	33.8
Ash	4.8
<u>Heat Content</u>	7329 Btu/lb
<u>Ash Analysis</u>	<u>Wt % of ash</u>
SiO ₂	21.1
Al ₂ O ₃	11.9
Fe ₂ O ₃	8.5
TiO ₂	1.0
P ₂ O ₅	0.5
CaO	20.9
MgO	6.5
Na ₂ O	11.9
K ₂ O	0.1
SO ₃	15.6
TOTAL	98.1

Mineralogy of coal by x-ray diffraction of low-temperature ash -
quartz
kaolinite
pyrite

Carboxylic acid group content 2.48 meq/gram.

ACKNOWLEDGMENTS

This work is funded by the U.S. Department of Energy, Office of Fossil Energy, under Cooperative Agreement DE-FC01-83FE60181.

TABLE 4

NEUTRON ACTIVATION ANALYSIS OF INDIAN HEAD LIGNITE FROM NORTH DAKOTA

Element	Concentration, ppm
Titanium	110 \pm 20%
Iodine	<3.0
Manganese	4.6 \pm 5%
Magnesium	410 \pm 15%
Copper	<25.0
Vanadium	3.00 \pm 2%
Chlorine	16 \pm 20%
Aluminum	3020 \pm 1%
Samarium	0.4 \pm 2%
Uranium	0.3 \pm 10%
Lanthanum	4.7 \pm 1%
Cadmium	<1.0
Gold	<0.001
Arsenic	5 \pm 1%
Antimony	0.2 \pm 1%
Bromine	1.1 \pm 1%
Sodium	6220 \pm 1%
Potassium	<500.0
Cerium	7.80 \pm 10%
Calcium	3760 \pm 10%
Selenium	0.50 \pm 10%
Thorium	1 \pm 1%
Chromium	2 \pm 15%
Europium	0.09 \pm 10%
Ytterbium	0.4 \pm 20%
Barium	520 \pm 5%
Cesium	0.1 \pm 10%
Silver	<0.08
Nickel	<25.0
Scandium	1.3 \pm 1%
Rubidium	<5.0
Iron	3570 \pm 3%
Zinc	6.4 \pm 20%
Cobalt	1.60 \pm 1%
Silicon	<35,000.0
Molybdenum	<10.0

REFERENCES

1. Neavel, R.C. "Coal Structure and Coal Science: Overviews and Recommendations", 178th National Meeting of the ACS, Honolulu, Hawaii, Fuel Division, Preprints, Vol. 24, No. 1, p. 73, 1979.
2. Reviews of Modern Physics, Vol. 53, No.4, Part II, October 1981.
3. Coal Sample Bank Workshop, Atlanta, Georgia, March 1981, sponsored by GRI/DOE.
4. Weaver, J.N. "Analytical Methods for Coal and Coal Products," Karr, C., Ed., Academic Press: New York, Vol. 1, pp. 377-401, 1978.

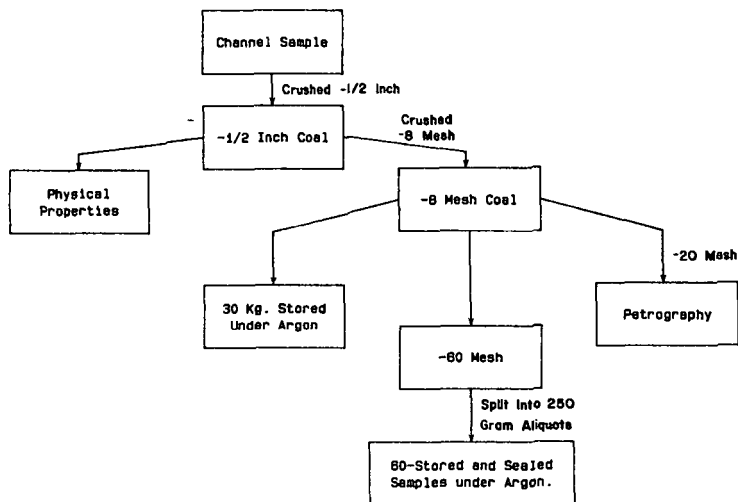


FIGURE 1. Schematic of sample preparation procedure for channel sample.

PROCESS FOR PRODUCING LOW-ASH, LOW-SULFUR COAL

C. W. Fan, R. Markuszewski, and T. D. Wheelock

Chemical Engineering Department and
Energy and Mineral Resources Research Institute
Iowa State University
Ames, Iowa 50011

Introduction

Previous work has shown that ash-forming mineral matter, including iron pyrites, can be removed from coal by leaching fine-size coal with a hot caustic solution under pressure followed by washing with a dilute mineral acid (1-4). Recently, similar results have been achieved by leaching fine-size coal with hot sodium carbonate solutions. In both cases much of the mineral matter reacts with alkali to form acid-soluble compounds. Since sodium carbonate is readily available, low in cost, and much less corrosive than sodium hydroxide, it could be used advantageously. Unfortunately, iron pyrites are not leached as readily by sodium carbonate solutions as by caustic solutions. However, this difficulty can be circumvented by employing a multistep process in which the coal is first leached under oxydesulfurization conditions at 120-150°C to extract pyritic sulfur and then leached at higher temperature in the same alkaline solution but under non-oxidizing conditions to convert other minerals to acid-soluble materials. Pyrites readily react with oxygen dissolved in hot alkaline solutions to form water-soluble sulfur species (5,6). But if oxydesulfurization is conducted at the higher temperatures (250°C and above) required for the reaction of other minerals with alkali, coal losses will be excessive because of oxidation. Therefore a two-step leaching process is needed. The results of applying such a process to several bituminous coals are presented below.

Experimental Methods

Bituminous coals from several sources were used for the leaching experiments (Table 1). These coals were first ground to pass either a 200 or 400 mesh screen (U.S. standard). For some leaching experiments the coals were precleaned by a physical separation process which reduced both the ash and total sulfur contents. Precleaning involved mixing the ground coal with perchloroethylene and water, allowing the suspension to settle, and separating the two liquid layers as prescribed by Vivian (7). The coal macerals tended to concentrate in the

Table 1. Bituminous coals used in leaching experiments

Coal Seam	Location	Coal Form	Size, mesh	Ash ^a , wt. %	Tot. S ^b , wt. %
Illinois No. 6	Trivoli, IL	Raw	-200	12.75	3.71
Illinois No. 6	Trivoli, IL	Precleaned	-200	4.92	2.83
Pittsburgh No. 8	Moundsville, PA	Raw	-400	37.11	6.55
Pittsburgh No. 8	Moundsville, PA	Precleaned	-400	6.20	3.67
Lower Kittanning	Armstrong Co., PA	Raw	-200	17.87	10.61

^aDry basis

^bDry, ash-free basis

perchloroethylene layer whereas the minerals tended to concentrate in the water layer. This procedure was repeated five times with each coal which was precleaned. Approximately 87% of the Illinois No. 6 coal and 78% of the Pittsburgh No. 8 coal were recovered during precleaning. These values are expressed on an ash-free basis.

For most leaching experiments, 15g. of coal and 120 ml. of a 1.0 M sodium carbonate solution were placed in a 300-ml. stirred reactor made of type 316 stainless steel. The first leaching step involved reaction with oxygen dissolved in the solution under a partial pressure of 13.6 atm. at 150°C for 1 hr. (5, 8). During this step gas was bled from the reactor to avoid any build-up of gaseous reaction products in the system. Following the first step, the system was purged with nitrogen and the temperature of the system was raised to 250°C, whereupon the second leaching step was conducted for an additional 1 hr. under an inert atmosphere. After this treatment, the reactor was cooled quickly and the coal recovered by filtration. The filter cake was washed with water, dried for 4 hr. in an oven at 95°C, weighed, and sampled for chemical analysis. A portion of the leached coal was washed with a mineral acid (2M) by stirring the mixture in a flask for 30 min. After the acid treatment, the coal was recovered by filtration and the cake was washed with water, dried, weighed, and sampled for chemical analysis. These washing steps were conducted at either room temperature (25°C) or at the boiling point (100°C). In some cases, the regular washing step was extended by mixing the acid-treated coal with boiling water for 30 min., filtering, and then washing with more boiling water. Ash and total sulfur contents of the coal were determined by standard ASTM procedures (9).

Experimental Results

An initial set of experiments was conducted to see how effective the second leaching step was by itself when not preceded by the oxydesulfurization step. For this set of experiments raw coals were leached with a 1.0 M sodium carbonate solution at 250°C and then washed with 2M hydrochloric acid or sulfuric acid. When hydrochloric acid was employed, the acid washing step was always conducted at the boiling point and the final water washing step at room temperature. However, when sulfuric acid was used, the washing steps were conducted at various temperatures to see whether the temperature of the acid or the water had any effect.

The results of the first set of experiments presented in Table 2 indicate that the ash and total sulfur contents of the coals were reduced substantially by the treatment while the product recovery or yield was high. The results seemed to be affected by the source of the coal and the washing temperature, but it was not clear whether they were affected by the type of acid. The largest percentage reduction in either ash content or total sulfur content was achieved with Illinois No. 6 coal. In run 3 the ash content of Illinois No. 6 coal was reduced by 83% and the total sulfur content by 39%. The leached coal was washed with hot sulfuric acid in this run. Somewhat poorer results were realized when cold sulfuric acid was used. Also, extended washing with hot water had little effect when cold acid was employed.

The raw Pittsburgh No. 8 coal had a very high ash content which was reduced about one-third by the single-step leaching and washing treatment (Table 2). The total sulfur content was reduced 18-23% by this treatment. It seemed to make little difference which acid was applied to the leached coal.

The results achieved with Lower Kittanning coal were intermediate between those achieved with the other coals. Thus, the ash content was reduced 44-47% and the total sulfur content 25-27% when this coal was leached with an alkaline solution and washed with either of the hot acids. When the leached coal was

Table 2. Results of leaching raw coals with a hot alkaline solution followed by washing.

Run No.	Coal Seam	Acid Washing		Water Washing		Product %		
		Acid	Temp., °C	Type	Temp., °C	Yield ^a	Ash ^b	Tot. S ^a
1	Ill. 6	HCL	100	Regular	25	94	2.61	2.40
2	Ill. 6	H ₂ SO ₄	25	Regular	25	94	3.40	2.72
3	Ill. 6	H ₂ SO ₄	100	Regular	100	94	2.21	2.25
4	Ill. 6	H ₂ SO ₄	25	Extended	100	94	3.97	2.67
5	Pitts. 8	HCL	100	Regular	25	96	24.8	5.03
6	Pitts. 8	H ₂ SO ₄	25	Regular	25	96	24.5	5.34
7	Low Kit.	HCL	100	Regular	25	89	9.44	7.70
8	Low Kit.	H ₂ SO ₄	25	Regular	25	89	13.34	7.73
9	Low Kit.	H ₂ SO ₄	100	Regular	100	89	10.05	8.01

^aDry, ash-free basis

^bDry basis

washed with cold sulfuric acid, the ash content was reduced slightly less.

A second set of experiments was conducted in which the raw coals were leached first under oxydesulfurization conditions and then under nonoxidizing conditions at higher temperature (250°C). As the results shown in Table 3 indicate, this approach resulted in significantly greater sulfur removal. Under the best conditions, the total sulfur content of Illinois No. 6 coal was reduced 56%, Pittsburgh No. 8 coal 63%, and Lower Kittanning coal 86%. The total sulfur content seemed to be reduced by about the amount of inorganic sulfur present in the raw coal.

In most cases the two-step leaching method produced a lower ash content than the single-step leaching method. This result was probably due to the more complete removal of iron pyrites by the two-step approach. Also when two leaching steps were used, a cleaner product was obtained by washing with hydrochloric acid than by washing with sulfuric acid. However, when washing with hot sulfuric acid was followed by extended washing with hot water, the results approached those achieved by washing with hydrochloric acid. This effect can be seen in the case of Illinois No. 6 coal by comparing the results of run 14 with those of run 10 and in the case of Lower Kittanning coal by comparing the results of run 20 with those of run 16.

The coal recovery on a dry, ash-free basis was slightly lower for two leaching steps than for one leaching step. It seems likely that the lower recovery was due to coal oxidation in the first step. Although the coal loss was small, previous work (8) suggests that the loss could be reduced to an even lower level by decreasing the temperature in the first step.

In the final set of experiments, precleaned coals were leached by the one-step and two-step methods utilized before with the raw coals. The leached coals

Table 3. Results of two-step leaching of raw coals followed by washing.

Run No.	Coal Seam	Acid Washing		Water Washing		Product %		
		Acid	Temp., °C	Type	Temp., °C	Yield ^a	Ash ^b	Tot. S ^a
10	Ill. 6	HCL	100	Regular	25	91	1.82	1.63
11	Ill. 6	H ₂ SO ₄	25	Regular	25	91	4.07	1.81
12	Ill. 6	H ₂ SO ₄	100	Regular	100	91	2.97	1.84
13	Ill. 6	H ₂ SO ₄	25	Extended	100	91	3.31	1.65
14	Ill. 6	H ₂ SO ₄	100	Extended	100	91	2.43	1.62
15	Pitts. 8	HCL	100	Regular	25	92	17.3	2.41
16	Low Kit.	HCL	100	Regular	25	85	2.38	1.49
17	Low Kit.	H ₂ SO ₄	25	Regular	25	85	5.69	1.93
18	Low Kit.	H ₂ SO ₄	100	Regular	100	85	3.21	1.96
19	Low Kit.	H ₂ SO ₄	25	Extended	100	85	5.20	1.60
20	Low Kit.	H ₂ SO ₄	100	Extended	100	85	2.74	1.55

^a Dry, ash-free basis^b Dry basis

were washed with hot hydrochloric acid, followed by water washing at room temperature. By using precleaned coals, very low ash contents were achieved with either the one-step or two-step leaching methods. As Table 4 indicates, the ash content of Illinois No. 6 coal was reduced to less than 0.5% and that of Pittsburgh No. 8 coal to less than 0.9% by either method. Thus by using a combination of physical and chemical cleaning the ash content of Illinois No. 6 coal was reduced 96% and the ash content at Pittsburgh No. 8 coal 98%. The combination of physical and chemical cleaning was particularly effective in the case of Pittsburgh No. 8 coal, since even the two-step leaching process by itself reduced the ash content of this coal only by one-half.

Combined physical and chemical cleaning also achieved lower total sulfur contents than was achieved by either method alone (Table 4). Physical precleaning made more of a difference when it was followed by the one-step leaching process than by the two-step process. However, the lowest sulfur contents were achieved when the two-step leaching process was applied to precleaned coals. Application of this combination reduced the total sulfur content by more than 60% in the case of either Illinois No. 6 coal or Pittsburgh No. 8 coal.

Conclusions

A coal leaching process for removing ash-forming mineral matter has been demonstrated. This process involves leaching fine-size coal with a hot, dilute sodium carbonate solution followed by washing with a dilute mineral acid and water. While much of the mineral matter reacts with the alkali at 250°C to form acid-soluble compounds, iron pyrites are incompletely reacted by the hot alkali alone. This difficulty can be overcome by using a two-step leaching process in which oxygen is introduced under pressure in the first step to convert the pyritic sulfur to water-soluble species. The temperature of the first step should be limited to 150°C

Table 4. Effect of coal precleaning on results of leaching experiments.

Run No.	Coal Seam	Coal Form	Leaching Steps ^a	Washed Product, %		
				Yield ^b	Ash ^c	Tot. S ^b
21 1	Ill. 6	Precleaned	II only	95	0.49	1.81
	Ill. 6	Raw	II only	94	2.61	2.40
22 10	Ill. 6	Precleaned	I & II	92	0.41	1.35
	Ill. 6	Raw	I & II	91	1.82	1.63
23 5	Pitts. 8	Precleaned	II only	95	0.88	2.55
	Pitts. 8	Raw	II only	96	24.8	5.03
24 15	Pitts. 8	Precleaned	I & II	93	0.76	1.92
	Pitts. 8	Raw	I & II	92	17.3	2.41

^aStep I: 150°C, 13.6 atm. O₂ pressure.

Step II: 250°C, inert atmosphere

^bDry, ash-free basis

^cDry basis

to minimize coal oxidation. The leaching process can be combined advantageously with physical precleaning in produce coal with less than 1% ash and markedly reduced sulfur content.

Literature Cited

1. Crawford, A., The de-ashing of coal by combined jig washing, froth flotation, and extraction with caustic soda, BLOS Final Report No. 522, Item No. 30, Feb. 19, 1946, British Intelligence Objectives Sub-Committee, London, (A.T.I.-118668, Central Air Documents Office, Wright-Patterson Air Force Base, Dayton, Ohio).
2. Reggel, L., Raymond, R., Wender, I., and Blaustein, B.D., Preparation of ash-free, pyrite-free coal by mild chemical treatment, Am. Chem. Soc. Div. of Fuel Chem. Preprints 17 (1):44-48 (1972).
3. Stambaugh, E.P., Hydrothermal coal process, in: Coal Desulfurization: Chemical and Physical Methods (T. D. Wheelock, ed.), ACS Symposium Series 64, Am. Chem. Soc., Washington, D. C., 1977, pp. 198-205.
4. Das, S. K., and Yang, R. T., Coal cleaning using sodium hydroxide and acid solutions, presented at 109th AIME meeting, Las Vegas, NV, Feb. 26, 1980.
5. Chuang, K.-C., Chen, M.-C., Greer, R. T., Markuszewski, R., Sun, Y., and Wheelock, T. D., Pyrite desulfurization by wet oxidation in alkaline solutions, Chem. Eng. Commun. 7 (1-3):79-94 (1980).
6. Stephenson, M. D., Wheelock, T. D., and Markuszewski, R., Sulfur species leached from pyrite during oxidative desulfurization of coal in alkaline solutions, Proceedings 1983 International Conference on Coal Science, Pittsburgh, PA, Aug. 15-19, 1983, pp. 252-255.

7. Vivian, T. A., presented at Chemical Engineering Department Seminar, Iowa State University. Ames, IA, April 9, 1980.
8. Wheelock, T. D., Oxydesulfurization of coal in alkaline solutions, Chem. Eng. Commun. 12(1-3): 137-160 (1981).
9. American Society for Testing and Materials, Annual Book of ASTM Standards, Part 26 (Methods D 3174 and D 3177), Philadelphia, PA, 1975.

OXYDESULFURIZATION OF COAL. FURTHER STUDIES OF OXY-ALKALINOLYSIS

Clifford G. Venier, Mono. M. Singh, Tetsuo Aida,
and Thomas G. Squires

Applied Organic Chemistry, Ames Laboratory-DOE*,
Iowa State University, Ames, IA 50011

Although it is clear that increasing amounts of coal will be burned each year for decades, no satisfactory technology for the chemical "deep cleaning" of coal has been developed. This situation arises from the fact that the forms of organic sulfur in coals are chemically reduced, and therefore, relatively unreactive under most desulfurization conditions. Early attempts to develop "oxy-desulfurization" processes failed to take into account that organic sulfur is no more susceptible to free radical oxidation than are carbon and hydrogen; and thus, even though pyritic sulfur is removed by these processes no selective removal of organic sulfur can be accomplished.

The use of more sulfur-selective electrophilic oxidants to chemically clean coal was introduced by the Jet Propulsion Laboratory's development of a chlorine based process (1-3). Unfortunately, this powerful oxidant also chlorinates coal, replacing some of the carbon-hydrogen bonds with carbon-chlorine bonds; and as many as 20 chlorines per 100 carbons are introduced (1, 3). Removal of this inadvertently introduced chlorine became a new problem which has proved very difficult to solve. JPL has attempted to dechlorinate the intermediate product using a variety of conditions including hydrogenation at temperatures up to 700°C (2).

In the meantime, TRW, Inc. had shown that substantial amounts of organic sulfur are apparently removed from coal by heating it with molten caustic (4-6). Since the replacement of oxidized sulfur functions as well as chlorine by hydroxide ions are common reactions in both aliphatic and aromatic chemistries, we reasoned that electrophilic oxidation followed by treatment with strong base would be superior to either treatment alone.

On this basis, we developed a two-step process for the desulfurization of coal in which the coal is first mildly oxidized and then heated with alkaline materials. In our first report (7), oxy-alkalinolysis was demonstrated to be more effective than either chlorination or alkali fusion. We now wish to present results using bromine as the first stage oxidant and add a few model studies which shed additional light on the chemistry underlying the processes.

EXPERIMENTAL

General

Western Kentucky No. 9 coal from the Ames Lab coal library, which had been prepared and stored under O₂-free conditions, was used. Bromination of the coal and the alkali fusion of the brominated samples were carried out under N₂ atmosphere. Before use, the coal was sized to pass through a 200 US mesh screen. Methylene

*Operated for the U.S. Department of Energy by Iowa State University under Contract No. W-7405-Eng-82.

chloride, potassium hydroxide pellets (85%), potassium iodide, sodium thiosulfate, potassium dichromate, and soluble starch, all certified ACS grade, were used as obtained from commercial sources. AR grade bromine was used in the bromination of coal. The analysis of the samples were carried out by the Ames Lab Analytical Services.

Bromination of Coal

A typical procedure for the bromination of coal samples is described below:

To a well stirred mixture of 70 ml of CH_2Cl_2 and 50 ml of water was added an accurately weighed (about 2.50 g) sample of coal. While stirring the mixture vigorously, 3 ml (58.6 mmol) of bromine was introduced in three equal portions. Stirring was effected by ultrasonic irradiation. After a total of 60 min., the mixture was filtered through a previously weighed fluoropore filter (3 m, Millipore). The coal residue was thoroughly washed 8-10 times using 20-25 ml of water each time. The brominated coal was then dried under vacuum in an oven at 110°C . After drying, the gain in weight of coal was recorded.

Estimation of Bromine

In a separate series of experiments, the bromine left unreacted after the bromination of coal was estimated by adding excess of KI to the filtrate and titrating the liberated I_2 with $\text{Na}_2\text{S}_2\text{O}_3$ previously standardized with $\text{K}_2\text{Cr}_2\text{O}_7$ using starch. This enabled us to determine the amount of Br_2 consumed by coal (0.5 g) during oxidation. The incorporated Br_2 was estimated from the elemental analyses.

Alkali Fusion

In a typical experiment 15-10 g KOH was at first fused at 380° in a steel reactor placed in a salt ($\text{NaNO}_3 + \text{NaNO}_2 + \text{KNO}_3$) bath and fitted with a N_2 inlet-outlet device, paddle stirrer and a port for loading coal. The molten mass of KOH was held at 380° until no more water was expelled. About 0.5 g of coal was then introduced and the molten mass was stirred at 380° - 390° for 30 min. After cooling, the contents of the reactor vessel were mixed with water and the resulting slurry was acidified with 1:1 HCl. The mixture was then kept over a steam bath for 30 min. and finally filtered through fluoropore (3 m, Millipore), washed very thoroughly with warm water, dried in an oven under vacuum at 110° overnight.

RESULTS

In order to understand the data, we will express changes in the coal on oxidation and KOH fusion in terms of atom ratios, most usually atoms per one hundred carbon atoms, $\text{xx}/100\text{C}$. This is equivalent to gram-atoms of X per 100 gram-atoms of carbon. This approach allows careful focus on changes in the organic fraction of the coal without regard to changes in the mineral matter.

The results of coal bromination are given in Tables 1 and 2 and a number of aspects of the reaction of bituminous coal with bromine are illustrated in Figure 1. Up to a ratio of more than 10 mmol of bromine per 100 g-atom of carbon, all of the bromine is consumed within the 60 minute reaction time. The weight of product increases markedly during the early stages of bromination, increasing by about one-third when 15 moles of bromine per 100 gram-atoms of carbon is

used. Increasing the ratio beyond 15 gives no further weight increase. As seen in Table 2, about one-fourth of the hydrogen in the coal is lost (see Figure 2a), even in the most lightly brominated samples, and sulfur falls off slowly and steadily with increased bromine consumption (See Figure 3a).

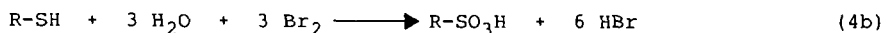
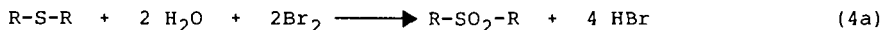
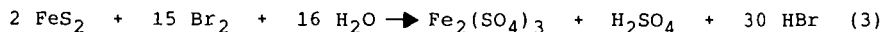
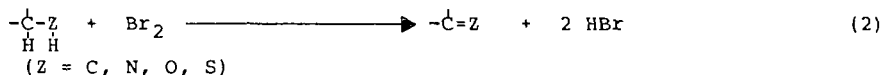
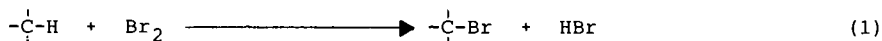
Table 3 shows the results of subjecting the preoxidized samples to fusion with KOH for 30 minutes at 380°C. Note that under these conditions, the sulfur level of the raw W. Kentucky #9 coal treated with KOH alone is reduced from 1.9S/100C to 0.7S/100C. There is a small increase in the sulfur level after fusion when insufficient bromine is used, but in general, the sulfur levels attainable in 30 minute KOH fusions for preoxidized samples decreases with increasing bromine consumption (See Figure 3b). Under the best condition a level of 0.1S/100C (94% desulfurization) is achieved. Bromine levels after fusion are uniformly low, confirming that organic halogen is removable by KOH fusion.

DISCUSSION

The Oxidation Step

Our previous paper established that chlorine is an effective oxidant (7); however, gaseous chlorine is not as easy to study in detail as is bromine because chlorine cannot be introduced as accurately nor kept in solution as easily. Therefore, we have determined the stoichiometry of the oxidation of coal with bromine, assuming that the result can be generalized to the other halogens.

Bromine is consumed in four phenomenologically identifiable processes: (1) substitution for hydrogen; (2) dehydrogenation of the coal; (3) oxidation of iron pyrite to sulfate and ferric iron; and (4) oxidation of divalent sulfur compounds to the tetravalent state, equations 1-4 respectively.



Given the following data: (1) the total bromine consumed, (2) the amount of bromine incorporated into the coal, and (3) the loss of hydrogen from the coal; one can calculate the amount of bromine consumed by processes 1 and 2, and then by difference, the amount of bromine consumed in oxidizing sulfur.

Table 4 shows that even at a bromine consumption level of 14 Br₂/100C, virtually all of the consumed bromine is accounted for without sulfur oxidation. The conclusion that some non-sulfur-oxidizing processes are very fast is also borne out by careful comparison of hydrogen loss versus sulfur reduction. Fifty-seven percent of the sulfur is removed under the most severe bromination conditions; roughly one-third of this sulfur is removed at a bromine-to-carbon ratio of 0.12. On the other hand, three-fourths of the

hydrogen consumed under the severest conditions has been removed at a ratio of 0.12.

Bromine in carbon tetrachloride or in water is used in most qualitative organic analysis schemes to diagnose the presence of (1) carbon-carbon unsaturation, (2) phenols, (3) compounds with relatively stable enol forms, (4) many amines, most notably anilines, and (5) other easily oxidized functional groups (8). Divalent organic sulfur compounds fall in this latter category along with hydroquinones and a few compounds possessing a very activated carbon-hydrogen bond. Thus, the concomitant consumption by coal of bromine in processes which do not oxidize sulfur is not surprising, and has been suggested before (9, 10); however, the extent to which it occurs is disconcerting.

The Alkali Fusion Step

The ratio of sulfur to carbon in the brominated coals drops modestly (from 1.5S/100C to 0.8S/100C) when the bromine to carbon ratio increases from 0.12 to 0.40 (See Figure 3a). However, over the same range, the susceptibility of the product to subsequent sulfur removal by KOH fusion is markedly enhanced. Fusion of the aforementioned samples with KOH leads to final sulfur values of 0.8S/100C and 0.1S/100C respectively (See Figure 3b). The organic sulfur in the sample treated with 40 Br₂/100C is clearly different from that in the sample treated with 12 Br₂/100C. On the basis of model compound studies reported previously (7), we are confident that it is the oxidation state of sulfur which has changed.

CONCLUSIONS

This study shows that preoxidation of coal samples by bromine markedly increases the efficiency of sulfur removal by molten caustic treatment. Under conditions which give a 65% sulfur reduction with KOH fusion alone, a preoxidized sample can be 94% desulfurized. That some hydrogen substitution and dehydrogenation processes are faster than sulfur oxidation has been demonstrated. The substitution reactions are probably phenol brominations and the replacement of active aliphatic hydrogen by bromine. The dehydrogenation reactions probably involve oxidation of easily oxidized carbon-carbon and carbon-oxygen bond systems.

**Table 1. Bromine consumed by
W. Ky. #9 Coal.***

$\left(\frac{\text{mol Br}_2}{\text{g-atom C}}\right) \times 100$ used	$\left(\frac{\text{mol Br}_2}{\text{g-atom C}}\right) \times 100$ cons'd
0	0
13.3	12.2
16.5	13.0
26.2	18.5
33.0	21.6
39.1	23.3

*One gram of W. Ky #9 coal contains .7086g (0.059g-atom) of carbon.

**Table 2. Product Analytical Data for
Brominated W. Ky. #9 Coal.**

Run No.	$\left(\frac{\text{mol Br}_2}{\text{g-atom C}}\right) \times 100$ used	$\left(\frac{\text{g-atom}}{\text{g-atom C}}\right) \times 100$		
		Br	H	S
1	0	0	86.0	1.9
2	11.9	7.1	68.3	1.5
3	15.9	8.3	68.5	1.2
4	23.8	8.6	65.6	1.1
5	31.8	9.4	62.2	0.8
6	39.7	9.8	61.9	0.9

**Table 3. Product Analytical Data
for KOH Fused Samples.**

Run No.	$\left(\frac{\text{g-atom}}{\text{g-atom C}}\right) \times 100$		
	S	Br	H
1	0.7	0.0	45.4
2	0.8	0.1	41.2
3	0.6	0.2	46.9
4	0.3	0.3	43.0
6	0.1	0.1	45.1

Table 4. Relative Stoichiometries of Bromine Consumption.

Run No.	$\left(\frac{\text{mol Br}_2}{100 \text{ g-atom C}}\right) \text{ consumed}$				
	Substitu- tion for H Process 1	Dehydro- genation Process 2	Sum of processes 1 and 2	Obs.	Obs.- (1+2)*
6	9.8	7.2	17.0	23.2	6.6
5	9.4	7.2	16.6	20.2	3.4
4	8.6	5.9	14.5	17.0	2.7
3	8.3	4.6	12.9	13.8	0.5
2	7.1	5.3	12.4	11.9	-0.5

*FeS₂ requires 3.4 Br₂/100 C; depending on functional group distribution, organic S requires 1.9-2.8 Br₂/100 C; total required for S oxidation is 5.3-6.2 Br₂/100 C.

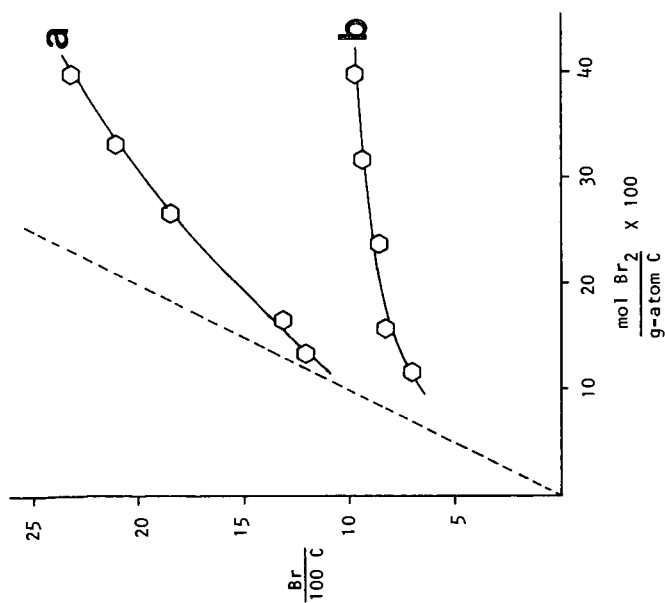


Figure 1. Reaction of Bromine with W. Ky. #9 Coal: (a) Consumption of Bromine and (b) Incorporation of Bromine as Functions of the Bromine to Coal Ratio (60 Minute Reaction).

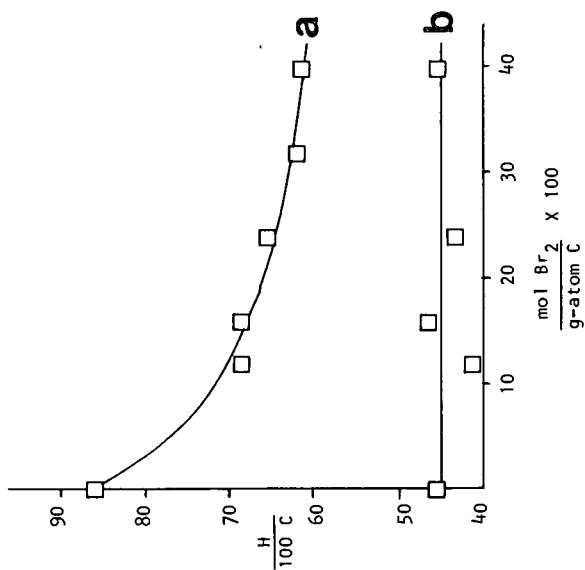
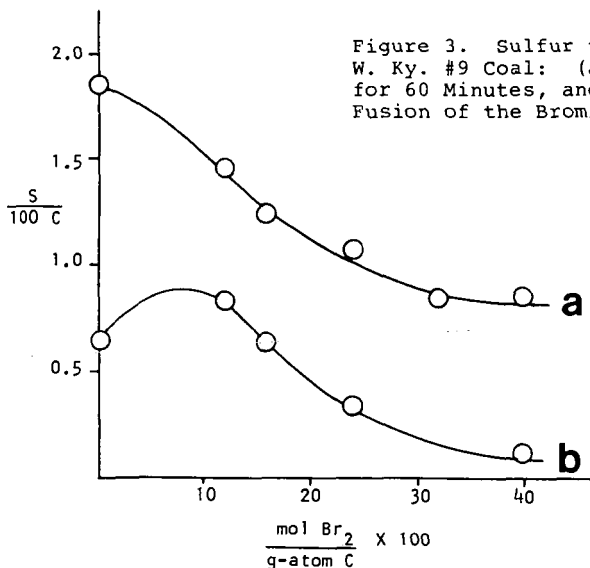


Figure 2. Hydrogen to Carbon Ratio in W. Ky. #9 Coal: (a) after Bromination for 60 Minutes, and (b) after KOH Fusion of the Brominated Samples.



REFERENCES

1. Vasilakos, N. P.; Corcoran, W. H. Fuel 1983, 62, 1111 and references therein.
2. Hsu, G. C.; Kalvinskas, J. J.; Ganguli, P. S.; Gavalas, G. R. Am. Chem. Soc. Symp. Ser. 1977, 64, 206; and personal communications.
3. Vasilakos, N. P.; Corcoran, W. H. Fuel 1983, 62, 795.
4. Masciantonio, P. X. Fuel 1965, 44, 169.
5. Meyers, R. A.; Hart, W.D.; McClanathan, L.C.; paper presented to the 17th Intersociety Energy Conversion and Engineering Conference, Los Angeles, CA, August, 1982. We wish to thank Dr. Meyers for kindly supplying us with a preprint of his paper.
6. Meyers, R. A.; Final Report, U. S. Department of Energy Contract No. DE-AC22-80PC30141, TRW, Inc., Redondo Beach, CA.
7. Aida, T.; Venier, C. G.; Squires, T. G. Prepr. Pap. - Am. Chem. Soc., Div. Fuel Chem. 1982, 27(3-4), 328.
8. Shriner, R. L.; Fuson, R. C.; Curtin, D. Y. "The Systematic Identification of Organic Compounds"; Fifth Ed., Wiley, New York, NY, 1964, pp. 121-124.
9. Cunningham, A. C.; Ladner, W. R.; Wheatley, R.; Wyss, W. F. Fuel 1966, 45, 61.
10. Weiler, J. F. Fuel 1935, 14, 190.

VOLATILITIES OF INORGANIC ELEMENTS IN COALS DURING ASHING

K. J. Doolan, K. E. Turner, J. C. Mills, A. C. Knott, and R. R. Ruch*

BHP Central Research Laboratories
Shortland, Australia 2307

*Illinois State Geological Survey
Champaign, IL 61820

INTRODUCTION

There are several reasons for requiring volatility information in coal:

a) Environmental

The flame temperature within the boiler furnace of a pulverized fuel power station may reach well above 1600°C when burning a bituminous coal. The higher the volatility of an element at temperatures of this magnitude then the higher will be the proportion of the element which will eventually escape to atmosphere, either in vapor form or in condensed form on unprecipitated fly ash particles. Elements which display some toxicity towards human, animal or plant life will therefore tend to impose a degree of detrimental impact on the environment.

b) Engineering design

The achievement of a satisfactory mass balance study of a coal combustion system must accommodate elements reporting to the primary bottom ash, precipitated and unprecipitated fly ash, and gaseous discharge components. Foreknowledge of volatility information can assist in the interpretation of data.

c) Analysis

Coal is a very complex heterogeneous matrix. Some techniques are suitable for the direct determination of many elements in whole coal samples while other techniques require an ashed sample.

d) Data base information

Many reports of elemental volatilities at various ranges of ashing temperatures and atmospheres have been published. An investigation covering a large number of elements, coal types, and ashing temperatures, would contribute significantly to an understanding of what could be expected under a given set of circumstances.

The literature on element volatility in coal is extensive. A summary has been compiled and discussed in the detailed NERDDP Report covering this work (1). When different reports are compared inconsistencies occur for many elements as ashing temperatures are raised from 370° to 2200°C. Several reports detailing ash derived from radiofrequency oxygen plasma ashing (RFA) at 150°C indicate quantitative retention of most elements studied making it a very suitable material for the analysis of inorganic elements in coal.

This investigation was designed to study the losses of 58 inorganic elements present at trace to minor concentrations in six coal samples.

EXPERIMENTAL

A set of six coals (four representative Australian bituminous coals and two US NBS standards, 1632A and 1635) were chosen to form the primary samples for this effort. Several other coals were selected to provide further information on specific elements.

Each of the coals was milled to less than 76 μm particle size in a slow speed Siebtechnik mill. The procedures for the preparation of the ash residues were as follows:

- 150°C(RFA) - multiple 0.6 g samples were processed in refractory boats with a layer loading of 1.5 mg/mm² in an LFE-504 Low Temperature Plasma Asher (150W power, 150 ml/min oxygen flow rate) until constant weight was achieved. The samples were removed from the asher three times daily and raked with a stainless steel spatula to present a fresh surface for oxidation. Total ashing time for each sample was approximately three days, except NBS1635 which required seven days.
- 370°C - samples were placed directly into a laboratory air oven maintained at the required temperature, and remained until constant weight was achieved (approx. 14 days).
- 815°C - samples were placed in a furnace at 200°C, and brought to 500°C over 30 min, transferred to a second muffle at 500°C and brought to 815°C over 30 min, then held at 815°C for 30 min.
- 1500°C - samples of 815°C ash were placed in a 10 ml platinum crucible (specially altered by the attachment of fine platinum wires to allow manipulation from above), lowered into the hot zone of a vertical tube furnace, and held at this temperature for 30 min. All of the residues from this procedure had fused, and were pulverized in a Siebtechnik mill.

The analytical methods employed for determining the 58 elements in this study were X-ray spectroscopy (XRF), instrumental neutron activation analysis (NAA), atomic absorption spectroscopy (AAS), inductively coupled plasma spectroscopy (ICP), specific ion electrode potentiometry (ISE), and optical emission spectroscopy (OES). The specific details for these procedures have been previously published (1-6). The elements determined by each technique are summarized in Table 1. In many cases, where possible, elements were determined by several methods.

RESULTS AND DISCUSSION

An element was considered volatile if the difference between its concentration in the starting coal and in the ash, on a normalized basis, was greater than the experimental uncertainty for a particular element. A greater than 20 percent change in concentration was usually required for the change to be considered significant. The volatility of an element was designated inconclusive when it was very near the experimental uncertainty or if different analytical techniques indicated conflicting results.

The results of this study are summarized in Table 2. Only six of the 58 elements investigated undergo some degree of volatilization at temperatures up to 815°C. This group of elements--boron, bromine, cadmium, fluorine, mercury, and selenium--was augmented at higher temperature, 1500°C, by a further ten--arsenic, gallium, germanium, manganese, potassium, sodium, strontium, thallium, yttrium, and zinc--which were each volatilized from at least one of the coals. Note in Table 2 that Bi, Gd, Ho, and Te were below the limits of detection for all the six coals

investigated, eliminating the evaluation of volatility trends. Other elements (In, Dy, and P) were below detection in four of the coals. Results for NBS1635 indicated seventeen elements were below limits of detection. Thus, under the oxidizing conditions prevalent during the preparation of the various coal ashes, there were 38 elements which at no stage were observed to undergo significant volatilization.

RFA Volatilization

Mercury was consistently retained in the RFA residue of each of the six coals studied in this project. Conversely, the literature has reported the consistent and unambiguous loss of mercury. Attention to details of RF ashing, which influence the actual temperature of the oxidation, possibly explains this discrepancy. For example, the sample layer loading within each sample container inside the RF ashing instrument, the particle size, the mineral matter content, and the chemical composition, could all play a part in influencing the localized temperature.

The implication of the literature was that bromine is volatilized. The 'difference' between the literature and the present work derives from there being a variable loss observed herein, with four coals showing definite volatilization, one (SC143B) showing retention, and one (NBS1635) being inconclusive.

Selenium is generally regarded as a relatively volatile trace element though consistently is retained under the conditions of RFA preparation. There was, however, the single incidence with SC146 in the present work for which this element was considered to have been volatilized.

Only fluorine was found to be volatilized significantly during the oxidation of each of the coals.

Low temperature ashing, although a time consuming procedure, is highly recommended for preparing coal samples for analyses where the analytical method to be used requires the carbonaceous material to be removed. Of all the elements surveyed in this study only a few (F, Br, B, and Se) indicated significant volatility. It is recommended that laboratories check their ashing procedures critically (especially for Hg) before attempting this approach however.

370°C Volatilization

At a temperature of 370°C selenium was significantly volatilized from four of the six coals. In contrast the literature implies that selenium is consistently lost under these ashing conditions.

Boron occupies a curious and special position, with regard to the volatility data in this work as well as to those literature reports which have addressed the lower temperature volatilization behavior of this element. Boron volatilization data implied that there were occasionally substantial losses at 370°C. However, the 815°C ash data for the above-mentioned coals indicated a retention of boron. The results of the present study may be interpreted in terms of respective kinetics for low temperature volatilization and higher temperature oxidative retention. Boron is well known to be predominantly associated with organic matter in coals, an affiliation which has been proposed to explain the high emissions of this otherwise refractory element in the stack gases from coal fired power stations (7). The competing reactions of organo-boron volatilization and oxidation must be considered to favor the former at low temperatures and the latter at higher temperatures. The absence of 370°C loss for all coals, plus the variable behavior with the NBS1635 ashes, implies a probable strong dependence of boron volatility upon the chemical forms of the element present in individual coals, and possibly localized oxidative conditions during the preparation of the ash residues.

815°C Volatilization

The 500°-900°C temperature range ashes have been the most extensively investigated in the literature, with 15 separate works being available for comparisons with the results of the present study. Fourteen elements listed as "inconclusive" retention from literature reports were found to be essentially retained in the 815°C ash in this study. This included Sb, As, B, Cr, Co, Cu, Ga, Pb, Mn, Mo, Sn, Ti, V and Zn. Cadmium was found to be volatilized in several coals at 815°C in contrast to literature reports where retention was claimed. All coals studied showed some significant loss of Se at this temperature. Sodium was found to be essentially retained in the six coals tested.

1500°C Volatilization

The very high temperature to which these ashes were heated yielded an increase in elemental volatilities from all coals. However, there was no element which was lost from every one of the six primary coals. Thallium was lost from five coals, arsenic from four, gallium and yttrium from two each, and germanium from one bituminous coal, with manganese, potassium, sodium, strontium, and zinc from NBS1635 only. In the literature, one report indicated consistent and complete volatilization of arsenic by 1400°C, while the alkalis, sodium and potassium, as well as strontium, were considered involatile. Cobalt and vanadium were not observed to have been volatilized from any of the coals of this study.

Environmental Considerations

The volatilities of the inorganic elements studied in this project are of considerable interest in relation to the classifications of potential environmental concern as assigned in a National Research Council Panel Report to trace elements in reference to impact on environmental quality and health (8). The exact reasoning behind one or other designation for a particular element is quite complex, taking into consideration such aspects as toxicity to human, animal and plant life, chemical reactivity following release into the environment, leachability by groundwaters, amongst others. These elements are categorized in Table 3 and listed also according to the following volatility designations as observed in this study:

high (volatilization generally observed in coals below 815°C)

moderate (volatilization observed for coals below 1500°C)

Low (volatilization negligible at 1500°C)

Table 3 indicates that B, Cd, Hg, Se, and F are classified as moderate or greatest environmental concern and also high volatility. Both B and F have relatively large concentrations in most coals (>50 ppm), Se is generally ~1 ppm or higher, and Hg and Cd tend to be lower than 1 ppm. This combination of toxicity, concentration, and volatility gives some qualitative emphasis to an elements possible environmental impact.

CONCLUSION

The investigation of the volatility behavior of 58 elements in coals, from analyses of the whole coals and their ashes prepared under static oxidizing conditions at temperatures up to 1500°C, showed that only very few elements are lost up to 815°C. This gives further support for utilization of low-temperature plasma ashing to prepare coal samples for analysis. By 1500°C, volatilization losses of nearly one-third of the inorganic elements studied became appreciable.

The most probable factors affecting the volatility of an element are the ambient chemical and physical states. Volatilization will depend upon the distribution of the element between various mineral phases or organically associated

species in the coal, and upon the prevailing temperature and oxidizing or reducing conditions during combustion. Observations of boron and mercury volatilities under various conditions support this conclusion. Time effects may also be important, as completion of ashing under RFA and 370°C conditions takes many days. The present study could not, nor did it seek to, achieve a thorough assessment of these factors.

ACKNOWLEDGMENT

Support for this work came from Australia NERDDP Project Grant Number 80/0220. The assistance of Richard Cahill (ISGS) for performing the neutron activation analyses is gratefully acknowledged.

REFERENCES

1. Doolan, K. J., K. E. Turner, J. C. Mills, A. C. Knott, and R. R. Ruch, 1983, Final Report - Part 6, Volatilities of Inorganic Elements in Coal During Ashing, NERDDP Project Grant No. 80/0220.
2. Mills, J. C., K. E. Turner, P. W. Roller, and C. B. Belcher, 1981, Direct Determination of Trace Elements in Coal: Wavelength Dispersive X-ray Fluorescence Spectrometry with Matrix Correction Using Compton Scattered Radiation, X-ray Spectrometry, Vol. 10, p. 131.
3. Knott, A. C., K. E. Turner, and K. J. Doolan, 1981, Final Report - Part 1, Wavelength Dispersive X-ray Fluorescence Spectrometry, NERDDP Project Grant No. 78/3031.
4. Mills, J. C., K. J. Doolan, and A. C. Knott, 1983, Final Report - Part 4, Method for the Determination of Fluorine, Beryllium, Boron, and Lithium, NERDDP Project Grant No. 80/0220.
5. Doolan, K. J., 1982, The Determination of Mercury in Solid Fuels by High Temperature Combustion - Cold Vapor Atomic Absorption Spectrometry, Anal. Chim. Acta, Vol. 140, p. 187.
6. Harvey, R. D., R. A. Cahill, C.-L. Chou, and J. D. Steele, 1983, Mineral Matter and Trace Elements in the Herrin and Springfield Coals, Illinois Basin Coal Field, ISGS Contract/Grant Report 1983-4.
7. Gladney, E. S., L. E. Wangen, D. B. Curtis, and E. T. Jurney, 1978, Observations on Boron Release from Coal Fired Power Stations, Environ. Sci. Technol., Vol. 12, p. 1084.
8. National Research Council, 1980, Trace Element Geochemistry of Coal Resource Development Related to Environmental Quality and Health, PECH Report, National Academy Press.

Table 1. Methods Utilized for the Analyses of Coal and Coal Ash.

	NAA	XRF	OES	ICP	AAS	ISE		NAA	XRF	OES	ICP	AAS
Ag	X				X		Lu	X	X			
Al			X	X			Mg			X	X	
As	X	X					Mn	X	X	X	X	
B			X	X			Mo	X	X			
Ba	X	X	X	X			Na	X		X	X	X
Be			X				Ni	X	X	X	X	
Bi		X					P			X	X	
Br	X	X					Pb		X			
Ca			X	X			Rb	X	X	X		
Cd					X		Sb	X	X			
Ce	X	X					Sc	X	X			
Co	X	X	X				Se	X	X			
Cr	X		X	X			Si			X	X	
Cs	X	X					Sm	X				
Cu		X	X	X			Sn		X			
Dy	X	X					Sr		X	X	X	
Eu	X						Ta	X	X			
F						X	Tb	X				
Fe			X	X			Te		X			
Ga	X	X					Th	X	X			
Gd		X					Ti		X	X	X	
Ge		X					Tl		X			X
Hf	X	X					W	X				
Hg					X		U	X	X			
Ho		X					V		X	X	X	
In	X	X					Y		X			
K	X		X	X	X		Yb	X	X			
La	X						Zn	X	X	X	X	
Li				X			Zr		X	X	X	

Table 2. Elements with significant volatilization observed initially at indicated temperatures.

Coal Number (Rank Classification)	RFA, ~150°C	370°C	815°C	1500°C
SC143B (Bituminous)	fluorine	boron mercury	cadmium selenium	arsenic gallium thallium yttrium
SC146 (Bituminous)	bromine fluorine selenium	boron mercury	cadmium	-
SC147 (Bituminous)	bromine fluorine	boron mercury	selenium	arsenic cadmium thallium
SC151 (Bituminous)	bromine fluorine	boron mercury selenium	-	arsenic cadmium germanium thallium
NBS1632a (Bituminous)	bromine fluorine	boron mercury selenium	-	arsenic cadmium gallium thallium yttrium
NBS1635 (Subbituminous)	boron fluorine	mercury selenium	-	manganese potassium sodium strontium thallium zinc

Note 1. The following elements may be volatilized at 1500°C in the indicated coals, however the data is either not sufficiently accurate for a firm conclusion to be drawn or there is unresolved conflict between data from different analysis techniques:

Ce (NBS1635) Pb (SC147)
Ga (SC146) K (NBS1632)

Note 2. Boron was lost only at 370°C from SC146, SC147, SC151 and NBS1632a, but from the RFA, 370°C and 1500°C residues from NBS1635. No B was lost from any 815°C ash preparation.

Note 3. Those elements which were below the limits of detection are summarized as follows:

All coals	Bi, Gd, Ho, Te	NBS1632A	Dy, In
SC143B	Dy, In, P	NBS1635	As, Br, Cd, Cs, Co, Dy
SC146	In		Ge, Hf, In, Lu, Rb, Sb,
SC147	In, P		Sb, Sn, Ta, Th, U, Yb

Table 3. Volatility classifications of 'elements of concern'

NRC PECH Panel Classification (8)	element	volatility
greatest concern	arsenic	moderate
	boron	high
	cadmium	high
	lead	low
	mercury	high
	molybdenum	low
	selenium	high
moderate concern	chromium	low
	copper	low
	fluorine	high
	nickel	low
	vanadium	low
	zinc	moderate
minor concern	antimony	low
	barium	low
	bromine	high
	chlorine	-
	cobalt	low
	germanium	moderate
	lithium	low
	manganese	moderate
	sodium	moderate
	strontium	moderate
radioactive	thorium	low
	uranium	low
elements of concern but with negligible concentrations	beryllium	low
	tellurium	-
	thallium	moderate
	tin	low

Refer to text for volatility classification bases.

DESCRIPTIVE OXIDATIVE PROFILES FOR PYRITE
IN THE LOW TEMPERATURE ASH COMPONENT OF COALS
BY DIFFERENTIAL THERMAL ANALYSIS

C.M. EARNEST

Perkin-Elmer Corporation
Main Avenue - M/S 131
Norwalk, CT 06856

INTRODUCTION

There are two forms of FeS_2 which may be present in coals. Pyrite is the cubic modification and marcasite is an orthorhombic form. Marcasite is referred to as the low temperature form. Of the two, pyrite is by far the most abundant in the mineral matter of coals. These sulfur-containing minerals are of special interest from an environmental standpoint since their combustion produces sulfur dioxide gas. The $\text{Fe}_2\text{O}_3(\text{s})$ product of oxidation contributes to the ash material of coals along with combined $\text{SO}_x(\text{g})$ with any existing $\text{CaO}(\text{s})$ in the ash. The amount of iron and its oxidation state influence the ash fusion temperature.

The mechanism of oxidation of pyrite and marcasite in air has been the subject of much study and speculation (1-13). The techniques of differential thermal analysis (DTA), thermogravimetry (TG), and derivative thermogravimetry (DTG) offer direct methods for studying the oxidative behavior of these minerals. Thermal analysis data on the oxidation of sulfides, in general, are somewhat inconsistent. It has already been pointed out by several workers (8,11,13), the factors which seem to be important in such thermal analysis studies are good air circulation in the analyzer, constant experimental conditions, and small sample sizes. Kopp and Kerr (11) have reported that the oxidative peak temperature is lowered with decreasing particle size.

In the course of a detailed thermal analysis study dealing with low temperature ash (LTA) components of several pyrite containing coals from southwestern Illinois and eastern Kentucky, it was observed that the thermal analysis peaks obtained by DTA, TG, and DTG were, in many cases, either altered or shifted when compared to those exhibited by the individual minerals themselves. In the following study, some sample handling techniques, synthetic mineral mixtures, and low temperature ash materials are investigated in an attempt to explain some of these phenomena as observed in dynamic air atmospheres.

EXPERIMENTAL

The pyrite ore used in this study was obtained from Dr. O. Katkins, Department of Geology, University of Pittsburgh at Johnstown (UPJ), Johnstown, PA. A second pyrite specimen was purchased from Wards Natural Science Establishment, Inc. (Rochester, NY). Both the UPJ and Wards specimen were subjected to careful mechanical grinding prior to use. The thermal curve shown for pyrite in Figure 1 of this paper is that of the UPJ specimen.

The high purity marcasite specimen (Iowa, USA) was obtained from F.I. Fiene, Institute for Mining and Mineral Resources (IMMR), University of Kentucky, Lexington, KY. All low temperature ash specimens of this study were also obtained from IMMR. All pyrite estimates given for the LTA specimens were made

using a Phillips Model 3100 X-Ray Diffractometer located at IMMR. The sulfur analysis values for these LTA specimens were obtained using a Perkin-Elmer Model 240C Elemental Analyzer with the Sulfur Analysis Kit. A Perkin-Elmer Model 240DS microcomputer data station was used with the elemental analyzer. These values represent all of the sulfur contained in the LTA specimen except for the small quantity which may be present as calcium sulfate or gypsum.

All DTA thermal curves reported in this work were obtained using a Perkin-Elmer microcomputer-based DTA 1700 High Temperature Differential Thermal Analysis System. Only the DTA mode of operation of this instrument was used in the studies presented here. Ceramic liners (60 mm³) were used in the DTA sample holder cup. However, it was found that platinum liners could also be used with small pyrite samples and with all LTA specimens of this study in dynamic air purge. In these cases, the pyrite oxidation is complete prior to the decomposition temperature for pyrite.

RESULTS AND DISCUSSION

Pyrite and Marcasite Specimens

In this study, both pyrite and marcasite specimens exhibited broad multi-step DTA oxidative profiles when DTA samples of approximately 21 milligrams were studied in an undiluted fashion. The temperature of initiation of the exothermic activity was ca. 360°C when the specimens were heated at 10°C per minute. The temperature range of the exothermic oxidative profile was found to be highly dependent upon sample size and heating rate. Smaller sample sizes and slower heating rates gave oxidative profiles which were more singular in nature for these undiluted samples.

Dilution of the pyrite or marcasite with alumina or inert material allows a better oxidant availability to the sample material and more closely simulates the distribution of pyrite in natural specimens such as the LTA component of coals. Figures 1 and 2 give the DTA oxidative thermal curves for diluted samples of pyrite and marcasite, respectively. As one can see, very similar oxidative profiles are obtained for these diluted specimens. The major difference which was observed in these studies is that the sharp exothermic peak maximum for the FeS₂/Al₂O₃ mixture was, on the average, 25°C lower in temperature for the marcasite specimens than the pyrite specimens of this study. No such difference was observed for the broad exothermic profiles associated with the larger undiluted samples.

Herrin 6 LTA Specimen

The oxidative profiles for the pyrite component of low temperature ash materials from coals are somewhat different from those given for pyrite and marcasite in Figures 1 and 2. The DTA thermal curve, shown in Figure 3, is that which was obtained for a LTA specimen of the Herrin 6 seam (southwestern Illinois). As one can see, a multi-step exothermic oxidative region with peak maxima at 407°C, 464°C, and 508°C is obtained. This LTA specimen was analyzed to contain 9.9% sulfur and the pyrite and marcasite content was estimated by XRD to be 19% and 2%, respectively. Since this coal was subjected to low temperature ashing in an oxygen plasma where temperatures near 100°C are reached, the presence of considerable iron sulfates is likely. This turns out to be the case as is described in a paper (17) which follows this writing. Rao and Gluskoter (14) found the iron sulfates content in 44 specimens of the Herrin 6 seam to vary from 0 to 32 percent. In general, however, the iron sulfate minerals rarely comprised more than 7 percent of the LTA matter for the Herrin 6 seam.

Pyrite/Iron Sulfate/ Al_2O_3 Synthetic Mixture

Since ferrous sulfate is known to be the intermediate step in the total oxidation of pyrite (4), a study was performed to determine the effect of the presence of iron (II) sulfates on the oxidative profile of pyrite. Figure 4 shows the resulting DTA, TG, and DTG oxidative thermal curves obtained from a synthetic mixture containing 23.1% pyrite, 13.76% $\text{FeSO}_4 \cdot \text{H}_2\text{O}$, and 63.1% Al_2O_3 diluent were heated at 10°C per minute in dynamic air atmosphere. Although not labeled in the DTA thermal curve, the exothermic region gives peak maxima at 465°C and 520°C with a relative minimum separating these at 478°C . The endothermic event beginning near 600°C is the normal ferrous sulfate decomposition as observed in dynamic air atmosphere (16). When this DTA pattern is compared with that observed in Figure 1 for the pyrite/ Al_2O_3 mixture, one will note that the presence of iron sulfates lowers the temperature of the major peak maximum by 27°C and also converts the oxidative profile to a clearly defined two stage event. One will note that the peak maximum at 465°C is in common with that in the LTA material for the Herrin 6 seam which gives a maximum at 464°C . The TG and DTG thermal curves in Figure 4 show that the exothermic peak at 465°C is associated with a weight gain and the one at 520°C is associated with a weight loss event. It should be pointed out that the pyrite/iron sulfate synthetic mixture exhibits an iron sulfate decomposition above 600°C while the thermal curves for pyrite/ Al_2O_3 mixture did not.

Variation of the Pyrite Exothermic Response with Pyrite Level in LTA Specimens

A study was performed to see how the oxidative profile varied with the pyrite level in a series of LTA ash specimens. For this study, LTA specimens from the Herrin 6 seam (southwestern Illinois), Hazard 8 seam (eastern Kentucky), and two specimens of the Hazard seam from two different locations in eastern Kentucky. Table I gives the estimated pyrite levels for three of the four LTA specimens as obtained by XRD techniques. The total sulfur, as assigned by the Perkin-Elmer 240C Elemental Analyzer, is also given for the LTA specimens. As one can see, the pyrite level varies from as high as 19% in the Herrin 6 specimen to a low of 2% in the Hazard 7 LTA specimen.

Figure 5 shows the DTA oxidative thermal curves obtained for these LTA specimens in a dynamic air purge of 50 cc/min. The sample weights used were 23.1 mg for the Herrin 6, 35.0 mg in the Hazard 8, 29.5 mg in the Hazard 7, and 28.7 mg of the Hazard 7A LTA specimen. One will immediately note that the middle exothermic event ($T_{\text{max}} = 464^\circ\text{C}$) in the Herrin 6 specimen is in common with the other 3 specimens. This event is observed at 464°C in the Hazard 8 LTA specimen and at 459°C in the Hazard 7A specimen. One will recall that this peak was also observed at 465°C in the synthetic pyrite/ FeSO_4 mixture. The temperature of this peak maxima decreases as the amount of pyrite decreases and thus occurs at 438°C for the Hazard 7 specimen which was estimated to contain only 2% pyrite.

From these thermal curves one might predict that the exothermic oxidative profiles become multi-peaked and show activity at higher temperatures as the pyrite level increases. This is in agreement with our previous experiments given earlier in this work. The temperature of onset of oxidation is very similar in all four of the LTA specimens even though the mineral content of the Illinois coal is quite different from the three Kentucky coal LTA specimens. All four LTA specimens contained significant iron sulfate component. This iron sulfate level being less as the pyrite level decreases. This may be seen by the

decrease in magnitude and temperature of the decomposition peak observed at 667°C in the Herrin 6, 662°C in the Hazard 8, etc. This endothermic peak, in some cases, overlaps and predominates over less intense illite-smectite or smectite clay mineral dehydroxylation in these low temperature ash specimens.

The clay mineralogy was noticeably different in the four LTA specimens. For example, all three of the Kentucky coals contained detectable levels of kaolinite, as is evidenced by the exothermic ordering peak (spinel formation) at 968°C, 976°C, and 984°C in the Hazard 8, Hazard 7, and Hazard 7A, respectively. The Herrin 6 seam showed no evidence of kaolinite at the level of detectability of DTA. The double endothermic peak at 108°C and 150°C in the Herrin 6 specimen is due to the loss of interlayer water from both illite and illite-smectite mixed layer clay minerals. The lower temperature event (108°C) may also be due, in part, to the dehydration of iron sulfate species such as the $\text{FeSO}_4 \cdot 7\text{H}_2\text{O}$ (melanterite), $\text{FeSO}_4 \cdot 4\text{H}_2\text{O}$ (rozenite), and $\text{Fe}_2(\text{SO}_4)_3 \cdot 9\text{H}_2\text{O}$ (coquimbite). Likewise, the endothermic peaks in the Hazard 8 (113°C), Hazard 7 (111°C) and Hazard 7A (113°C) specimens are due to the same water loss phenomena. Because of the fact that the Hazard 7 specimen contains very little iron sulfate component, the thermal curves for the three Kentucky specimens indicate that these endothermic events are mostly due to the presence of illite and mixed layer clays containing illite clay mineral.

The Herrin 6 contained a measurable calcite component while the three Kentucky specimens did not. The endothermic peak at 890°C in the DTA thermal curve for the Herrin 6 seam is associated with the decomposition of calcite although it is sharpened by its association with the oxidation products of the pyrite. This will be discussed in detail in a paper which follows (17). One will also note that the clay mineral dehydroxylation endotherm (ca. 540°C) which is observed immediately after the pyrite oxidation is more distinguishable in the Hazard 7 and 7A specimens than in the Hazard 8 specimen. This is primarily due to the lower kaolinite and higher pyrite level in this specimen than is present in the two Hazard 7 specimens.

CONCLUSION

The temperature range as well as the nature of the exothermic oxidative profile for pyrite was found to be highly dependent upon sample size and heating rate. Smaller sample sizes and slower heating rates favor a more singular oxidative profile. Dilution of the pyrite or marcasite specimen with alumina or inert material allows a better oxidant availability to the sample material and more closely simulates the distribution of pyrite in natural specimens such as LTA specimens from coals.

The presence of iron sulfates lowers the peak temperature and converts the oxidative profile for pyrite specimens to a two stage event. Furthermore, pyrite specimens, as well as LTA specimens from coals, containing significant levels of iron sulfates were observed to exhibit a DTA endothermic event between 630°C and 670°C which is characteristic for the decomposition/oxidation of the iron sulfates component. This thermal event was absent from the DTA oxidative thermal curves for pyrite samples which initially contained no iron sulfates.

The DTA oxidative profiles for LTA specimens containing varying amounts of pyrite and iron sulfates showed that the exothermic oxidation of the pyrite component becomes more multistep in nature as the pyrite level increases. The iron sulfate content of the LTA material was observed to increase with the pyrite in the same specimen. This was reflected in the DTA thermal curves by the magnitude of the endothermic thermal event near 660°C. In the LTA specimens of this study, this iron sulfate decomposition/oxidation endotherm near 660°C in the DTA thermal

curve was observed to overlap and, in some cases, mask the less intense endothermic dehydroxylation peak of mixed layer clays which contain smectite clay mineral components.

ACKNOWLEDGMENTS

The author would like to express his sincere appreciation to F.I. Fiene for both the low temperature ash specimens and supporting XRD results. He would also like to thank R.F. Culmo and Kathy Weisgale for performing the sulfur analyses which were presented in this work.

REFERENCES

1. R.C. MacKenzie, "The Differential Thermal Investigation of Clays", Mineralogical Society, London, 1957, p. 366.
2. J.R. Blachere, J. Am. Ceram. Soc., 49 (1966) 590-593.
3. L.G. Berg and E.N. Shlyapkina, J. Thermal Anal., 8 (1975) 329-337.
4. A.C. Banerjee, in Thermal Analysis ICTA 80 Vol. 2 (W. Hemminger, Editor), Birkhaeuser Verlag, Basel, 1980, pp. 241-246.
5. Nandita Chakrabarti, D.R. Glasson, and S.A.A. Jayaweera, Thermochim. Acta, 51 (1981) 77-84.
6. R. Dimitrov and B. Boyanov, Thermochim. Acta, 64 (1983) 27-37.
7. D.N. Todor, Thermal Analysis of Minerals, Abacus Press, Kent, 1976, 116-117.
8. E.M. Bollin, in Differential Thermal Analysis, Vol 1 (R.C. MacKenzie, Editor), Academic Press, London, 1970, p. 193.
9. Haw-Jye Shyu, P.O. Vaishnava, and P.A. Montano, Fuel, 60 (1981) 1022-1026.
10. G.M. Schwab and J. Philinis, J. Am. Chem. Soc., 769 (1947) 2588.
11. O.C. Kopp and P.F. Kerr, Am. Miner., 43 (1958) 1079.
12. R.A. Schloenlaub, J. Am. Cer. Soc., 52 (1969) 40.
13. T. Kennedy and B.T. Sturman, J. Thermal. Anal., 8 (1975) 329-337.
14. C.P. Rao and H.J. Gluskoter, "Occurrence and Distribution of Minerals in Illinois Coals", Illinois Geological Survey Circular 476, Urbana, Illinois, 1973.
15. F.W. Frazier and C.B. Belcher, Fuel, 52 (1973) 41.
16. P.K. Gallagher, D.W. Johnson, and F. Schrey, J. Amer. Ceram. Soc., 53 (1970) 666.
17. C.M. Earnest, in preparation.

Table I

Pyrite and Total Sulfur Content
For The
Four LTA Specimens Of This Study

<u>LTA Specimen</u>	<u>Pyrite (XRD Estimate)</u>	<u>% Total Sulfur</u>
Herrin 6	19%	9.9
Hazard 7	2%	1.7
Hazard 7A	5%	3.8
Hazard 8	NA	6.5

NA = Not Analyzed

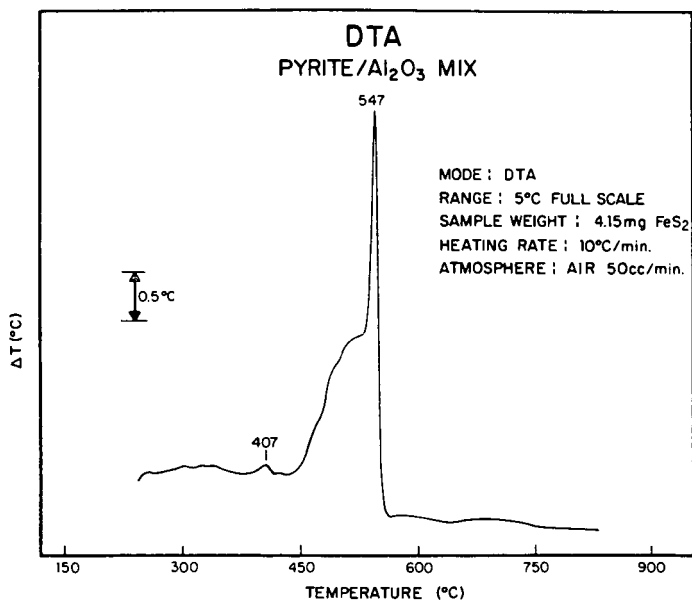


Figure 1. DTA Oxidative Thermal Curve for Pyrite/Al₂O₃ Mixture
Containing 4.15 mg of Pyrite

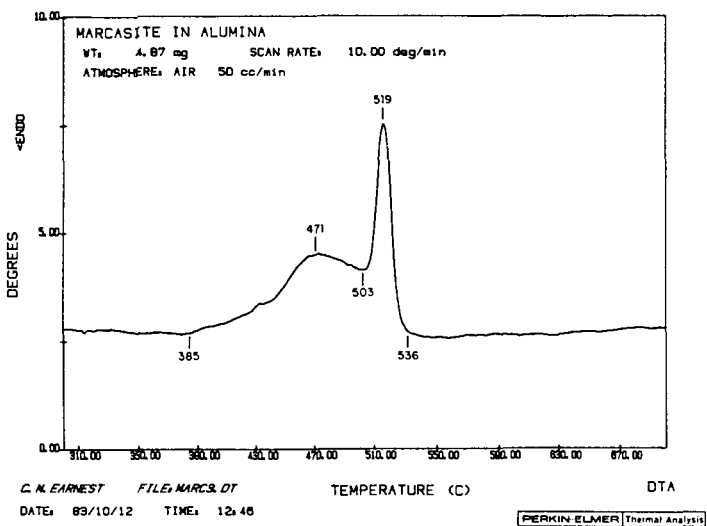


Figure 2. DTA Oxidative Thermal Curve for a Marcasite/ Al_2O_3 Mixture Containing 4.87 mg of Marcasite

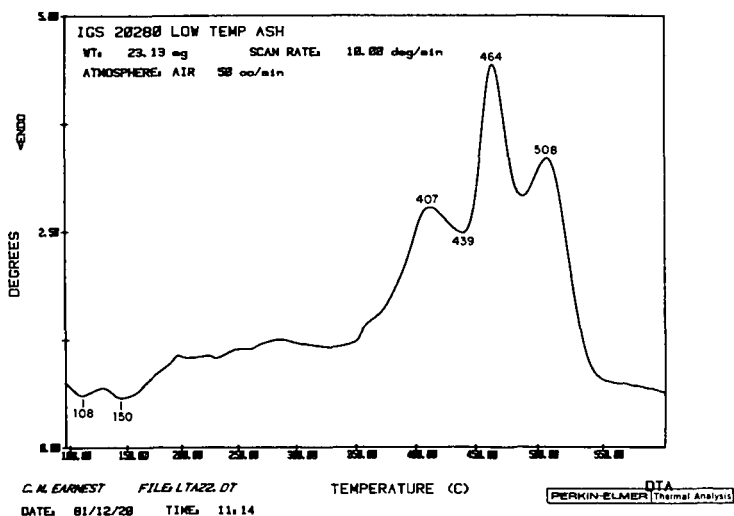


Figure 3. DTA Thermal Curve for Low Temperature Ash Component of the Herrin 6 Seam in Dynamic Air Atmosphere

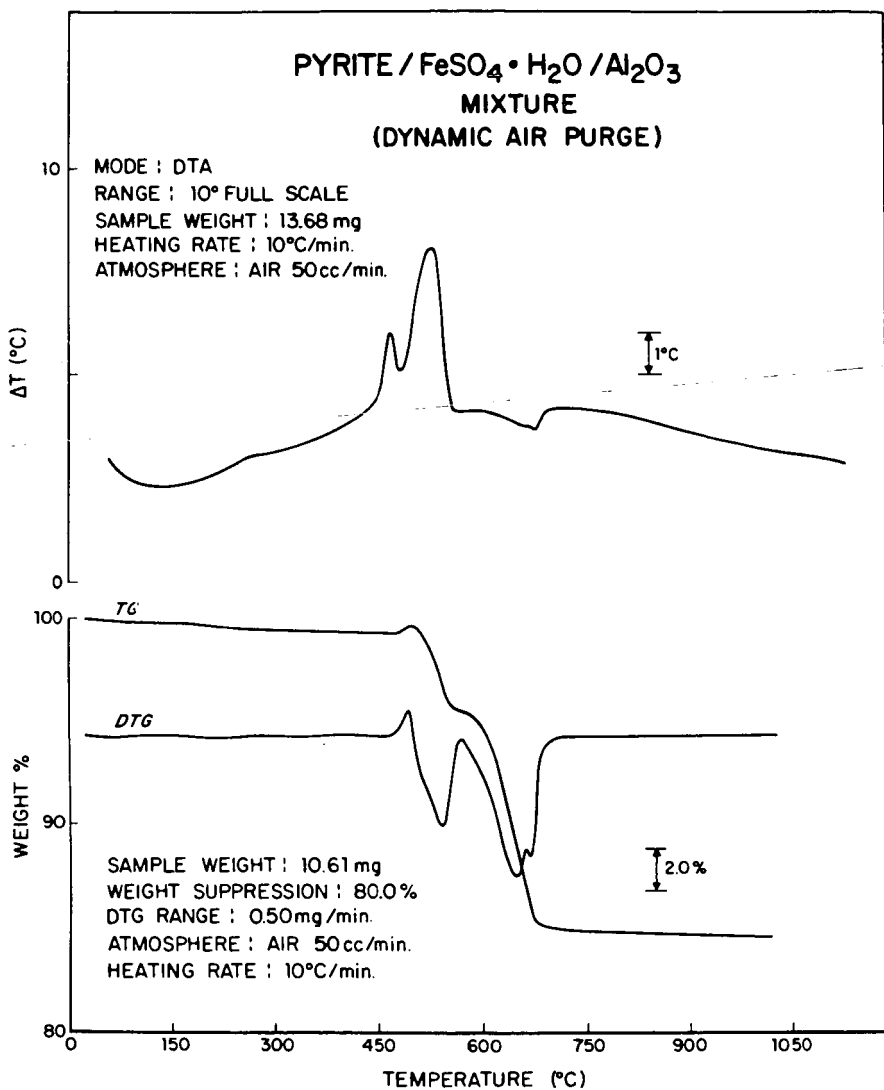


Figure 4.

DTA, TG, and DTG Thermal Curves for Pyrite/
 $\text{FeSO}_4 \cdot \text{H}_2\text{O}$ / Al_2O_3 Synthetic Mixture

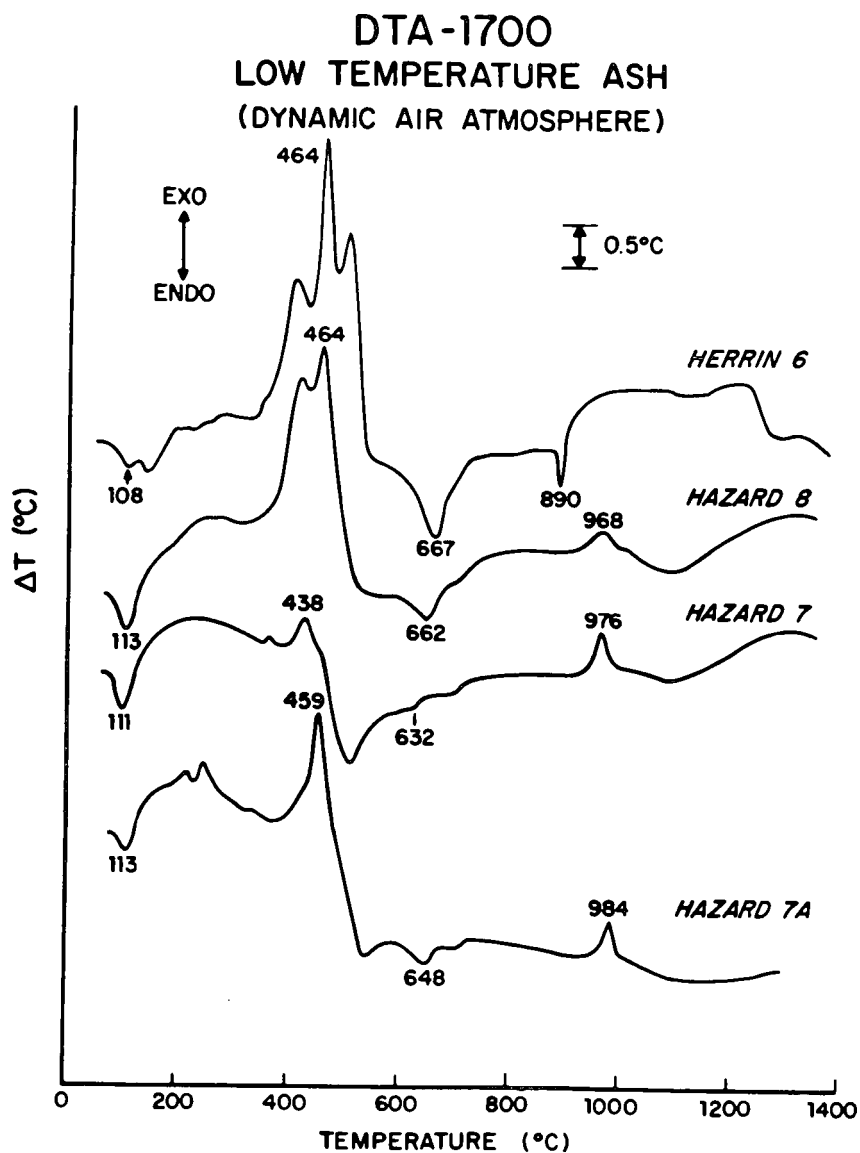


Figure 5

LOW-RANK COAL LIQUEFACTION
H-DONOR STUDIES USING ^2H NMR

S.A. Farnum, B.W. Farnum, J.R. Rindt,
D.J. Miller, and A.C. Wolfson

University of North Dakota
Energy Research Center
Box 8213, University Station
Grand Forks, North Dakota 58202

Several batch autoclave experiments were carried out using natural abundance 30.7 MHz ^2H NMR spectroscopy of product fractions to assess H-donor activity during lignite liquefaction. ^2H NMR observations of deuterium enrichments and measurement of ^2H NMR distributions have been used to investigate liquefaction reactions (1-3).

The development of high field superconducting magnets that operate in the Fourier transform mode with high sensitivity probes has made it possible to monitor liquefaction reactions by natural abundance ^2H NMR (0.0156% natural abundance). It is, therefore, no longer necessary to add large amounts of deuterated solvents or even large amounts of deuterated H-donors which swamp out critical aspects of the liquefaction reaction. The use of natural abundance ^2H NMR allows the investigator to examine typical liquefaction reactions without disturbing the system by the addition of large amounts of extraneous materials.

Martin et al. demonstrated recently that very important and often very spectacular variations may be found in the internal distribution of deuterium within molecules (4, 5). Measurement of the naturally abundant ^2H NMR distribution may be used to provide valuable information on the selectivity of ^2H repartition. Martin et al. applied measurements of this type to determine the origin of natural products such as alcohols in which samples from various sources with different histories had different ^2H NMR distributions (4).

It may be inferred from the work of Cronauer et al (6) and of Brower (7), that the method of Martin may be applied to the investigation of the reactions of H-donors during coal liquefaction. Brower (7) reported that the H/D kinetic isotope effect for the reaction of coal with tetralin containing deuterium at the alpha positions is 2.1 ± 0.1 at 335°C. The reaction mixture was 1 g of deuterated or undeuterated tetralin with 1 g of subbituminous coal in glass ampules. Rates of reaction were compared by monitoring the naphthalene/tetralin ratios.

When Cronauer (6) carried out liquefaction of Powhatan No. 5 coal in 100% 1,2,3,4- d_4 -tetralin solvent and in 100% d_{12} -tetralin, he also showed clearly that the abstraction of ^1H from a hydroaromatic carbon having one ^2H and one ^1H substituent is greatly preferred. Since the natural abundance of ^2H is only 0.015%, the probability that a carbon would have two ^2H substituents is very, very small. It is therefore possible to use the natural system as an in situ probe for comparing reactivities of H-donors under actual liquefaction conditions.

If reactions occur which involve a hydroaromatic carbon, and ^1H is preferentially abstracted each time, the ^2H distribution will show an increase in that spectral region. If a large amount of H-donor activity in the regions α and β to aromatic rings (H_α and H_β) occurs during liquefaction, the ^2H distribution should reflect this by showing a corresponding increase in the 5.0 - 1.8 ppm region of the natural abundance ^2H NMR spectrum.

Since the natural abundance ^2H NMR spectrum reflects the reactive history of the sample, adequate blank experiments must be performed to determine original or non-affected ^2H distributions. They always differ from the proton NMR distributions

when the sample has reactive history that involved H-transfer reactions. Since we used a process coal-derived liquid as our solvent, the blank autoclave run was essential.

Another aspect of liquefaction involves the interaction of processing gases with the solvent or directly with the coal or coal fragments. This question has been addressed by several investigators (1, 3, 8, 9, 10). The types of molecules that are active during liquefaction either through exchange reactions, through hydrogenation, hydrogen transfer, or through direct reaction with H_2 gas may be inferred by substituting deuterium gas 2H_2 for the H_2 in the reactive gas mixture. The reactive sites are then located by 2H NMR of the enriched reaction mixture.

Experimental

Autoclave experiments were designed to simulate processing conditions in our continuous process bottoms recycle liquefaction unit.

The experiments were carried out in a 1-liter hot-charged autoclave (11). The coal (65 g maf) solvent (120 g) slurry was hot-charged into the preheated autoclave, reaching the operating temperature of $450^\circ C$ in less than two minutes. The reactant gas (40 g, unlabeled) was 50/50 H_2/CO or $^2H_2/CO$ at a pressure of 3700 psig under reaction conditions. Residence time was 20 minutes after which the entire contents of the autoclave were transferred into a quench vessel, cooled and depressurized at room temperature. Gases were analyzed and the product slurry was distilled (ASTM D-1160). The trap contents (mainly water), the ASTM D-1160 distillate, and vacuum bottoms were subjected to separations and NMR analyses.

Mass balances were obtained using a different portion of the slurry and analyzing it for water, ash, tetrahydrofuran (THF) solubility, and vacuum distillate at 5 torr. The additive, when used, was 1,2,3,4-tetrahydrophenanthrene (THPhen) (0.33 g). The run matrix is shown in Table I.

TABLE I
AUTOCLAVE TESTS WITH BIG BROWN LIGNITE, RECYCLE
SLURRY DISTILLATE, $450^\circ C$ and 3400-3700 PSI TOTAL PRESSURE

<u>Run No.</u>	<u>Processing Gas</u>	<u>Additive</u>
3	H_2/CO	None
4	H_2/CO	THPhen
5	$^2H_2/CO$	THPhen

The coal and solvent chosen for these tests were a Texas lignite from the Big Brown mine and a recycle slurry ASTM D-1160 distillate from a continuous processing unit (CPU) run carried out at UNDERC using the same coal. The solvent was distilled from slurry collected on the thirteenth bottoms recycle pass. A cold trap was used during distillation to assure the collection of all volatile oils and water.

The ASTM D-1160 distillate of the autoclave product was further separated into alkanes, aromatics, and polars by open column chromatography on neutral silica gel with pentane, methylene chloride, and methanol as elution solvents. The fractions were cleanly separated as shown by examination of their 200 MHz 1H NMR spectra. The vacuum bottoms (10 g) were Soxhlet extracted with refluxing $CHCl_3$ (500 ml) for 20 hours, followed by THF (500 ml) for 20 hours. The residue consisting of inorganic

material, insoluble organic matter and unreacted coal amounted to 65-70% of the vacuum bottoms. Chloroform extracted 25-30% while the remainder of 3-4% was extracted with THF.

NMR spectra were obtained at 200 MHz in CD_2Cl_2 for protons and at 50.3 MHz in CDCl_3 for ^{13}C using pulsing conditions appropriate to the sample. ^2H NMR spectra were pulsed at 30.7 MHz 1-30,000 times depending on the sample. A 45° flip angle was used with an acquisition time of 4 seconds and a delay of 4 seconds. The solvent used was methylene chloride, CH_2Cl_2 .

^2H enrichments of the fractions from Experiment 5 were determined by standard addition of CD_2Cl_2 to a preweighed oil sample. The standard addition line gave a linear regression value of $r = 0.993$. The sample was weighed tightly covered and diluted immediately with CH_2Cl_2 . The enrichment of the water samples from the distillation trap was determined directly against a standard D_2O in H_2O curve whose linear regression value of r was 0.9999.

RESULTS AND DISCUSSION

Effect of Added H-Donor

Test numbers 3 and 4 were identical except that a small amount of an H-donor, THPhen, was added to Test 4 (Table I). Total percent conversion was essentially the same for Runs 3 and 4 (72%, 70%). Conversions to THF solubles were 56% and 60%, respectively.

The 50 MHz ^{13}C spectra for the light oils, the distillable oils, and their fractions and the CHCl_3 soluble vacuum bottoms were very similar for Runs 3 and 4. The 200 MHz ^1H NMR spectra of the products were likewise indistinguishable from run to run with corresponding fractions showing the same spectral features.

The natural abundance 30.7 MHz ^2H NMR distributions are, however, quite different from each other for the autoclave tests with and without the addition of small amounts of the H-donor, THPhen (Table II). These differences are mainly seen in the alpha + beta and in the aromatic regions of the spectrum (Figure 1). The change in the alpha + beta region gave a run 4/run 3 ratio of 1.25, clearly indicating increased H-transfer activity during Run 4.

TABLE II
 ^2H NMR AREA DISTRIBUTIONS FOR AUTOCLAVE TEST
WITH BIG BROWN TEXAS LIGNITE, H_2/CO , 450°C, MPa (3700 PSI)

	Run 3 (Area %)	Run 4 (Area %)	Run 4/3 (Area %)
Aromatic (9.6 - 5.8 ppm)	39.7	45.9	1.16
Alpha + Beta (5-1.8 ppm)	28.6	35.7	1.25
Other (1.8-0.1 ppm)	31.6	19.4	0.61

To test the effect of H-donor addition without liquefaction reaction, two portions of liquefaction recycle solvent distillate were equilibrated for three weeks at room temperature with and without the addition of the same amount of H-donor. When compared by ^2H NMR spectroscopy, there was no change in ^2H distribution.

The change in the ^2H distribution under liquefaction conditions therefore may be attributed to an increased cumulative isotope effect during liquefaction with small amounts of added H-donor. The small increase in THF soluble product, 60% as compared with 56% may be related to the H-donor activity increase but is not as notable during autoclave testing as it would be in CPU recycle operation.

Processing with $^2\text{H}_2/\text{CO}$

Autoclave Test 5 was conducted with deuterium-labeled 50/50 $^2\text{H}_2/\text{CO}$ and added THPhen. A deuterium-enriched product was obtained. Total conversion was 67% and conversion to THF solubles was 50%. The 50% conversion of lignite to THF solubles in Run 5 processed with $^2\text{H}_2/\text{CO}$ is significantly lower than the 60% conversion in Run 4 processed with $^1\text{H}_2/\text{CO}$. The deuterium isotope effect resulting from the use of $^2\text{H}_2$ rather than $^1\text{H}_2$, in the gas mixture would be expected to lower the yield of THF solubles since the rate of reaction of $^2\text{H}_2$ is expected to be slower than the rate of reaction of $^1\text{H}_2$ (7).

Examination of the product by ^2H NMR using the methods described in the Experimental section showed that ^2H entered every fraction of the product, including the H_2O , the ASTM distillate, and the soluble vacuum bottoms (Table III). The water was the most highly enriched fraction, probably due to the easy exchange of water hydrogens with the $^2\text{H}_2$ gas. Other hydrogens expected to exchange rapidly with $^2\text{H}_2$ gas are those *ortho* and *para* to phenolic OH groups and methylene hydrogens *alpha* and *beta* to aromatic rings. The fractions (polars, aromatics, ASTM D-1160 dist.) containing these types of bonds show appreciable enrichment (Table III). In the case of the aromatic fraction (Figure 2), it is even possible to assign some of the most exchangeable hydrogens to specific compounds. For example, the peaks at 3.9 ppm and 3.6 ppm in the proton NMR spectrum (Figure 2, top) can be plainly seen as enriched peaks in the deuterium NMR spectrum (bottom). These peaks are assigned to the methylene hydrogens of fluorene and acenaphthene respectively. It is notable that very little enrichment or exchange occurs on terminal methyl carbons of alkyl chains (0.9 ppm); however, the methylene region (~ 1.2 ppm) is enriched.

TABLE III

PRODUCTS FROM AUTOCLAVE TEST 5 (BIG BROWN TEXAS LIGNITE,
 $^2\text{H}_2/\text{CO}$, 450°C, 3400 PSIG), DETERMINED BY ^2H NMR

<u>Product</u>	<u>No. Grams in Product</u>	<u>Wt % ^2H</u>	<u>Wt % H in Sample</u>	<u>*Enrichment Factor</u>
Water	29.31	2.62	11.11	760
ASTM D-1160 Distillate	109.4	0.606	7.17	270
<u>Fraction of Distillate:</u>				
Alkanes	11.4	0.58 (by diff.)	14.88	120
Aromatics	44.9	0.542	7.20	240
Polars	30.9	0.967	7.81	400
ASTM D-1160 CHCl_3 Soluble Bottoms	25.74	0.605	5.84	330

* $\frac{\text{atom \% } ^2\text{H}}{0.0156\% \text{ (Natural Abundance)}}$

Figure 3 shows the comparison of the ASTM D-1160 distillate polar fraction 200 MHz ^1H NMR spectrum (top) and the 30.7 MHz ^2H NMR spectrum (bottom). The aromatic region of the ^2H spectrum was more enriched than the rest of the spectrum.

Since considerable amounts of ^2H (about 35 wt. % of the $^2\text{H}_2$ added) entered the product, it is impossible to assign any of the incorporated ^2H to reaction product rather than exchange product. However, it is possible to note that some portions of the product that were enriched are materials that do not undergo exchange easily. The ^2H NMR spectrum of the alkanes separated from the ASTM D-1160 distillate shows incorporation of deuterium into both methylene and methyl regions of the spectrum and the overall enrichment of the alkane fraction is $\sim 120 \times$ natural abundance.

The most actively enriched portions of the alkanes, aromatics, and polars may be seen by comparing Autoclave Run 4 (H_2/CO) with Run 5 ($^2\text{H}_2/\text{CO}$), Table IV and to compare ASTM D-1160 distillate oils, Table V.

Summary

1. Differences in natural abundance ^2H NMR distributions resulted from differences in the processing history of the samples.
2. The addition of small amounts of H-donor to a liquefaction reaction changed the natural abundance ^2H NMR distribution with respect to an identical run without added donor. The ^1H distribution and ^{13}C distribution were unchanged. Changes were probably the result of increased hydrogen transfer activity and the cumulative deuterium isotope effects.
3. Tests made using $^2\text{H}_2/\text{CO}$ showed product incorporation of ^2H to >270 times the natural abundance as determined by standard addition ^2H NMR. The ^2H distribution was not the same as in the unlabeled test.
4. ^2H entered all fractions of the product during the test with $^2\text{H}_2/\text{CO}$, including ASTM distillate alkanes, phenols and polars, H_2O and soluble vacuum bottoms. Polars and H_2O were the most enriched fractions, probably due to easy H-exchange.
5. Processing with $^2\text{H}_2/\text{CO}$ resulted in decreased conversion to THF solubles when compared with an identical run with $^1\text{H}_2/\text{CO}$.

Acknowledgments

UNDERC carried out this work for the U.S. Department of Energy under Cooperative Agreement No. DE-FC21-83FE-60181.

TABLE IV

^2H NMR AREA PERCENTAGES OF SEPARATED FRACTIONS
OF RUN 4 AND RUN 5 PRODUCT ASTM-1160 DISTILLATE

<u>Integrated Area %, Column Fractions, ASTM Distillate</u>		<u>Run 4</u>	<u>Run 5</u>	<u>Run 5/4</u>
Alkanes	$^2\text{H}_\text{O}$	100.0	100.0	N/A
Aromatics	$^2\text{H}_\text{ar}$	50.0	35.8	0.72
	$^2\text{H}_{\alpha+\beta}$	39.3	51.1	1.31
	$^2\text{H}_\text{O}$	10.7	13.1	1.19
Polars	$^2\text{H}_\text{ar}$	33.8	43.2	1.28
	$^2\text{H}_{\alpha+\beta}$	50.2	42.9	0.85
	$^2\text{H}_\text{O}$	16.0	13.9	0.87

TABLE V

COMPARISON OF RESULTS WITH LABELED AND UNLABELED SYNGAS
($\text{CO}/^2\text{H}_2$), (CO/H_2), ^1H NMR AREA PERCENTAGES, ^2H NMR AREA PERCENTAGES

<u>Integrated Area, % ASTM D-1160 Distillate</u>	<u>Run 4 (unlabeled)</u>	<u>Run 5 (labeled)</u>	<u>Run 5/Run 4</u>
$^1\text{H}_\text{ar}$	37.7	35.0	0.93
$^1\text{H}_{\alpha+\beta}$	31.4	34.3	1.09
$^1\text{H}_\text{O}$	30.9	29.9	0.97
$^2\text{H}_\text{ar}$	45.9	43.7	0.95
$^2\text{H}_{\alpha+\beta}$	35.7	43.1	1.21
$^2\text{H}_\text{O}$	19.4	13.2	0.68

REFERENCES

1. Frantz, J.A. and D.M. Camaioni. Amer. Chem. Soc., Div. Fuel Chem. Preprints, 1981, 26 (1), 105-113.
2. Ratto, J.J., L.A. Heredy, and R.P. Skowronski. Amer. Chem. Soc., Div. Fuel Chem. Preprints, 1979, 24 (2), 155-165.
3. Heredy, L.A., R.P. Skowronski, J.J. Ratto, and I.B. Goldberg. Amer. Chem. Soc., Div. Fuel Chem. Preprints, 1981, 26 (1), 114-122.
4. Martin, G.J., M.L. Martin, F. Mabon, M.J. Michon. Anal. Chem., 1982, 54, 2380-2382.
5. Martin, G.J., M.L. Martin, F. Mabon, and J. Bricout. J. Am. Chem. Soc., 1982, 104, 2658-2659.
6. Cronauer, D.C., R.I. McNeil, D.C. Young, and R.G. Ruberto. Fuel, 1982, 61, 610-619.
7. Brower, K.R. J. Org. Chem., 1982, 47, 1889-1893.
8. Schweighardt, F.K., B.C. Bockrath, R.A. Friedel, and H.L. Retcofsky. Fuel, 1976, 1254-1255.
9. Skowronski, R.L., L.A. Heredy, and J.J. Ratto. Amer. Chem. Soc., Div. Fuel Chem. Preprints, 1978, 23 (4), 155-160.
10. Wilson, M.A., P.J. Collin, P.F. Barron, and A.M. Vassallo. Fuel Proc. Technol., 1982, 5, 281-298.
11. Rindt, J.R., D.E. Severson, and A.M. Souby. "UND Hot-Charged Time-Sampled Batch Autoclave System," presented April 1980, AIChE Conf., Philadelphia, PA.

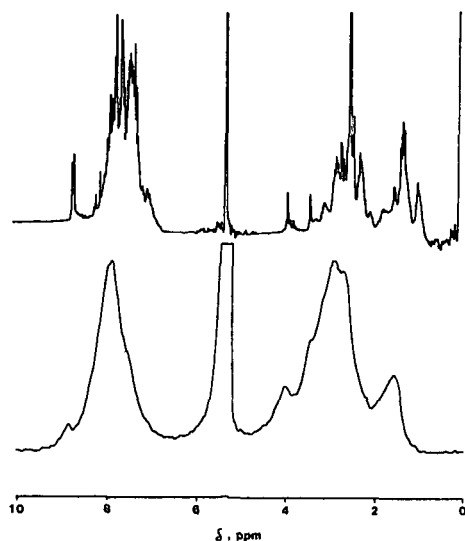


FIGURE 2. ^1H NMR spectrum (top) and ^2H NMR spectrum of the aromatic fraction of autoclave Test 5 with Big Brown Texas lignite and $^2\text{H}_2/\text{CO}$.

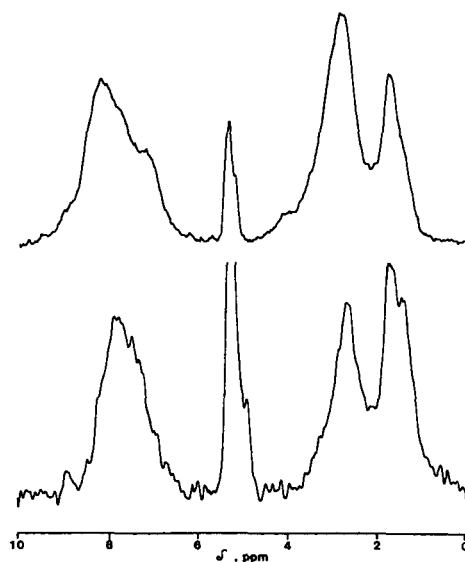


FIGURE 1. ^2H NMR spectra of (top) Run 4 (with added THPen) and (bottom) Run 3 (without THPen). The peak at 5.2 ppm is the NMR solvent, CH_2Cl_2 (top) and CH_2Cl_2 with added $\text{CH}_2\text{Cl}_2\text{-d}_2$ (bottom). The aromatic region is designated as 9.6-5.8 ppm, the α and β region as 5.0 to 1.8 ppm and other region as 1.8 to 0.1 ppm.

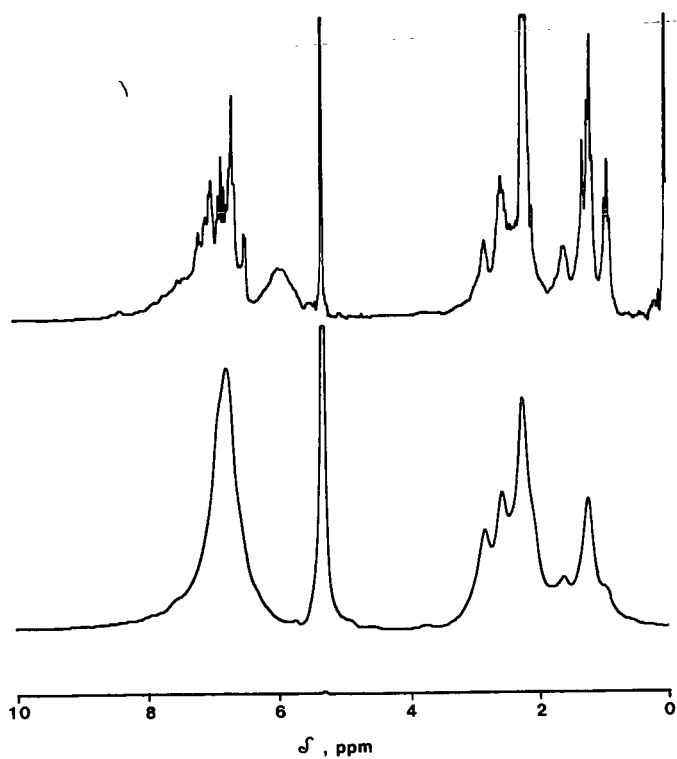


FIGURE 3. ^1H NMR spectrum (top) and ^2H NMR spectrum (bottom) of the polar fraction of autoclave Test 5 with Big Brown Texas lignite and $^2\text{H}_2/\text{CO}$.

INFERENCE OF SUBBITUMINOUS COAL STRUCTURE FROM LIQUEFACTION OF WYODAK COAL IN MODEL SOLVENTS*

Thomas D. Padrick and Steven J. Lockwood
Sandia National Laboratories
Albuquerque, New Mexico 87185

Introduction

Knowledge of the structure of coal is necessary if we are to understand coal liquefaction mechanisms and develop novel process concepts. Two important aspects of coal structure are the detailed structure of coal fragments and the nature of the bonds which hold these fragments together (crosslinks), the latter being the most significant to mechanism studies. The most widely accepted model for coal is that reported by Green, *et al.*¹ Their model consists of a macromolecular three-dimensional network of aromatic "clusters", crosslinked through covalent bonds. In their model, hydrogen bonds play a secondary role, forming only weaker bonds between molecular planes. We shall present evidence in this paper that indicates that hydrogen bonds are the primary bonds holding Wyodak coal fragments together. Evidence also suggest that hydrogen bonds are important in bituminous coal structure,^{2,3} but this will not be discussed here.

Information about the nature of the crosslinks in coal has been obtained by observing the interaction of various solvents with coal. Much of the information for the model of coal presented by Green, *et al.* was obtained from coal swelling experiments.⁴ Pampuch⁵ demonstrated that the specific interaction between polar liquids and coal is the formation of hydrogen bonds. Also, several recent studies have focused on the depolymerization of coal through direct solvent attack. Larsen, *et al.*⁶ observed depolymerization of three coals in pyridine at 350°C. The exact nature of the coal-solvent interaction was not described. Larsen⁷ has also observed depolymerization of Illinois No. 6 coal in aliphatic amine bases at 300°C.

We have studied the interaction behavior of Wyodak subbituminous coal with a variety of model solvents to better understand the nature of the crosslinks in subbituminous coal. We have observed extensive depolymerization of Wyodak coal under low severity conditions, and propose that this depolymerization is the result of disruption of hydrogen bonds in the coal.

Experimental

The data reported below were obtained from batch microreactor runs using Wyodak coal (South Pit Mine) and selected model solvents. The proximate and ultimate analysis of the Wyodak coal are listed in Table 1. The solvents were all used as received from the manufacturer at the stated purity level. The 35 cm³ microreactors were loaded with an 8 gram sample of a 2/1 solvent to coal mixture. They were then pressurized to 1000 psig with either

* This work supported by the U. S. Dept. of Energy at Sandia National Laboratories under Contract No. DE-AC04-76DP00789.

hydrogen or nitrogen. A few solvents were used in experiments at higher solvent to coal ratios to see if solvent volatilization was a problem under our conditions. Negligible differences in conversions indicate that at 375°C and a 1000 psig cold charge, solvent volatilization does not lower the solvent to coal ratio enough to alter our results. The microreactors were heated (~3 minutes to reach reaction temperature) in a fluidized sand bath and held at temperature for the specified time. The microreactors were then cooled (~30 seconds for a 200°C quench) in a second fluidized sand bath held at room temperature. Conversion to THF soluble products was obtained by subsampling the whole liquid product from the microreactor, sonicating the sample in THF and then pressure filtering through a 0.2 micron Milipore filter. The filtrate was then analyzed by gel permeation high performance liquid chromatography (HPLC) to observe differences in product distributions.⁸ This technique separates the filtrate into high, intermediate, and low molecular weight fractions. These fractions are comparable to the classical preasphaltene (mw ~ 1000), asphaltene (mw ~ 450) and oil (mw ~ 250) fractions obtained by Soxhlet analysis.⁸

Capillary GC analysis was performed on an HP 5800 using a crosslinked 5% phenyl methyl silicone column. The oven temperature was programmed from 100°C to 250°C at 2°C/min. The carrier gas flow rate was 0.5 cm³/minute. Separated products were identified by a flame ionization detector. Product molecules as large as four and five member ring compounds have been identified by the above GC analysis technique. However, we cannot be certain all THF soluble material passed through the GC column.

Results and Discussion

We began our investigation of Wyodak coal liquefaction in model solvents by conducting experiments in tetrahydroquinoline (THQ). THQ has been observed to enhance coal conversion³ and also to adduct to coal products.⁹ Thus our initial investigation centered on learning if the same characteristic of THQ was responsible for both adduct formation and enhanced conversion. THQ is both a basic nitrogen compound and a hydrogen donor. While its basic characteristic is probably responsible for adduct formation, it is unknown which property contributes most to the enhanced coal conversions observed in THQ.

Figure 1 tabulates the conversions to THF soluble products and the product distributions for Wyodak coal liquefied at 375°C, 20 minutes and 1000 psig H₂ in 1,2,3,4-THQ, quinoline and 5,6,7,8-THQ. Quinoline is a non-hydrogen donor and shows only 23% conversion compared to 80% conversion for 1,2,3,4-THQ and 58% conversion for 5,6,7,8-THQ. In addition to being a non-hydrogen donor, the nitrogen group in quinoline is a tertiary amine rather than a secondary amine as in 1,2,3,4-THQ. The 5,6,7,8-THQ should have similar hydrogen donor characteristic as the 1,2,3,4-THQ, but the conversion is much lower. The apparent difference between the two hydrogenated quinolines is that 5,6,7,8-THQ has the same base structure as quinoline.

For comparison, we measured the conversion of Wyodak coal in conventional hydrogen donor solvents, such as tetralin, hexahydronaphthalene and dihydrophenanthrene. Figure 2 shows the results for these three solvents. While some slight differences are observed, Wyodak conversion to THF soluble products in a good hydrogen donor solvent is 55-60% at these low severity conditions.

This is the same level of conversion that was observed for 5,6,7,8-THQ. Apparently, in 5,6,7,8-THQ only the hydrogen donor characteristic contributes to the observed conversion, i.e., there is little contribution from the quinoline type nitrogen structure. If 5,6,7,8-THQ and 1,2,3,4-THQ are similar hydrogen donors, this data would suggest that the enhanced conversion observed in 1,2,3,4-THQ is a result of the secondary amine structure.

We next conducted experiments in other basic solvents, which did not possess hydrogen donor characteristics. This was done to clarify the role of the basic functionality. Figure 3 shows the results of three liquefaction runs made in benzofuran, indole and acridine. We measured a 62% conversion for Wyodak coal liquefied in indole. Conversions in acridine and benzofuran were quite low. The high conversion in indole, a non-donor solvent, suggests a strong interaction between the coal and the basic nitrogen functionality.

The HPLC spectra from the experiments with several basic nitrogen solvents showed a new peak in the product distribution. Figure 4 illustrates the appearance of this new molecular weight peak. We see that a small complex observed with 1,2,3,4-THQ has grown to be a predominant peak in the molecular weight distribution of the THF soluble filtrate from Wyodak liquefaction in indole. We propose that this new peak is the result of an association between solvent and coal molecules.

Using preparatory-scale HPLC, we isolated samples corresponding to the new peaks shown in Figure 4. Since the complex peak occurs near the asphaltene peak, we assumed that the molecular weight of the isolated samples was approximately 400 amu. Knowing the elemental composition of indole, Wyodak coal and the isolated samples, and assuming a uniform elemental distribution for the coal, allowed us to conclude that the isolated samples contained approximately 60% indole. This result is consistent with a complex composed of two indole molecules and one coal molecule. The coal molecule would have a molecular weight of approximately 160 amu if the elemental distribution of Wyodak coal is assumed. Such a complex would have a molecular weight of ~ 394 amu, in excellent agreement with the value of ~ 400 amu observed for the isolated samples. Thus, our elemental analyses, in conjunction with the location of the complex peak in the HPLC molecular weight spectrum, are consistent with a complex composed of two indoles to one ~ 160 amu coal molecule.

If the indole-coal complex is held together by hydrogen bonds, a stronger base should displace the indole from the complex. We refluxed a portion of the complex in dibutylamine at $\sim 150^\circ\text{C}$ for 2 hours. Capillary GC of the complex before and after refluxing showed striking differences. Before reaction with dibutylamine, the capillary GC spectrum had only two major peaks at very long retention time. Following the dibutylamine reflux, a large peak for free indole was detected and several new peaks appeared at intermediate retention times. The major peaks previously associated with the complex were nearly eliminated. This indicates that the coal-indole complex was bound together through associative hydrogen bonds.

Indole may participate in a hydrogen bond as either an electron-acceptor or a electron-donor by virtue of the N-H group. However, since the unshared electron pair on the nitrogen participates in the ring resonance, we would expect indole to be a poor electron donor. We tested the hydrogen bonding role of indole by liquifying Wyodak in 1-methylindole. With this solvent, in which the hydrogen on the nitrogen has been replaced by a methyl group,

the solvent cannot act as an electron-acceptor in the formation of hydrogen bonds. Table 2 lists the conversion results and structural differences for indole and methylindole. Besides the dramatic decrease in Wyodak conversion, HPLC spectra indicate very little complex formation for liquefaction in methylindole. These results indicate that indole acts primarily as an electron-acceptor in hydrogen bond formation and that loss of hydrogen bonding ability of the solvent severely reduces the Wyodak conversion.

The initial experiments were performed under 1000 psig hydrogen. If indole is solubilizing coal through disruption of coal-coal hydrogen bonds and formation of coal-indole hydrogen bonds, then there should be no hydrogen consumption. We measured the % conversion to THF soluble products for a poor solvent (quinoline) and indole under both hydrogen and nitrogen pressure. Conversions for quinoline and indole were virtually the same under either reacting atmosphere. This suggests little or no hydrogen consumption from the gas phase, despite the lack of hydrogen available from either solvent.

At 375°C, there is sufficient thermal energy for some bond rupture, both covalent bonds and hydrogen bonds. However, under hydrogen deficient conditions, little conversion can be attributed to covalent bond rupture as indicated by a measured 20% conversion in naphthalene. 375°C should be sufficient to break most hydrogen bonds. Without a strong hydrogen bonding solvent, these bonds would reassociate as the liquefaction product cools to room temperature. With indole or another solvent capable of forming hydrogen bonds as strong or stronger than those present in the coal, these hydrogen bonding sites in the coal molecule are tied up as coal-indole bonds. Now as the product cools, reassociation between coal molecules does not occur and soluble coal-indole complexes are formed. This mechanism is shown in Figure 5. This type of mechanism is consistent with our data and suggest that a large fraction of the Wyodak "clusters" are held together solely by hydrogen bonds.

Conclusions

We have observed a high conversion of Wyodak coal to THF soluble products using indole as the liquefaction vehicle. We observed formation of hydrogen bonded complexes between indole and coal molecules. We determined that the important structural feature of indole is the N-H group which acts primarily as an electron-acceptor in forming hydrogen bonds. Solubilization of Wyodak coal in indole can best be represented by the pathway presented in Figure 5.

These results for Wyodak liquefaction in indole depict a liquefaction mechanism based on stabilization of hydrogen bonding sites in the coal. But more importantly, they indicate that a large fraction of Wyodak coal is crosslinked by hydrogen bonds. The large fraction of product which is produced as a complex with molecular weight near the classical asphaltene molecular weight range suggests that Wyodak coal is composed of clusters with molecular weights ~160. This structural information suggests that a liquefaction procedure designed to attack the oxygen functionality responsible for hydrogen bonding in the coal would result in high conversion to a low molecular weight product.

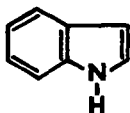
Table 1. Proximate and Ultimate Analysis of Wyodak Coal
(South Pit Mine)

<u>Proximate*</u>		<u>Ultimate*</u>	
% Moisture	8.45	% Moisture	8.45
% Volatile	40.66	% Carbon	60.62
% Fixed Carbon	41.02	% Hydrogen	4.35
% Ash	<u>9.87</u>	% Nitrogen	0.94
	100.00	% Sulfur	0.68
		% Oxygen (diff)	15.09
		% Ash	<u>9.87</u>
			100.00

* Commercial Testing & Engineering Co., Denver, CO 80239

Table 2. Wyodak liquefaction results at 375°C, 20 minutes
and 1000 psig nitrogen.

Indole

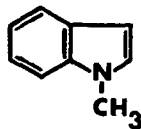


% THF

Conversion

62%

Methylindole



35%

References

1. Tom Green, Jeffrey Kovac, Douglas Brenner, and John W. Larsen in "Coal Structure" (Ed., Robert A. Meyers), Academic Press, New York, 1982, pp. 199-282.
2. T. D. Padrick, M. G. Thomas and D. E. Trudell, presented at Gordon Conference on Fuel Science, Plymouth, NH, July 1981.
3. Dwain Spencer, EPRI Journal, May, p. 31 (1982).
4. John W. Larsen and Jeffrey Kovac in "Organic Chemistry of Coal" (Ed., John W. Larsen), American Chemical Society, Washington, DC, 1978, pp. 36-49.
5. Roman Pampuch, Prace Glownego Instytutu Goinictwa, No. 153, p. 1-16 (1954).
6. John W. Larsen, Yuda Yurum and Terry L. Sams, Fuel 62, 476 (1983).
7. John W. Larsen, Advanced Research & Technology Development Coal Liquefaction Projects Meeting, Pittsburgh, PA, October 1983.
8. Arthur W. Lynch and Michael G. Thomas, Fuel Processing Technology 8, 13 (1983).
9. D. C. Cronauer, R. D. McNeil and D. C. Young, Quarterly Progress Report for October-December 1981, DOE/PC/30080-7, June 1982.

Figure 1. Liquefaction results for Wyodak coal in quinoline type solvents.

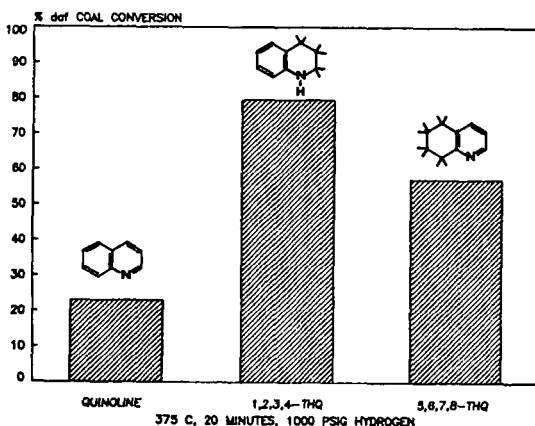


Figure 2. Liquefaction results for Wyodak coal in hydrogen donor solvents.

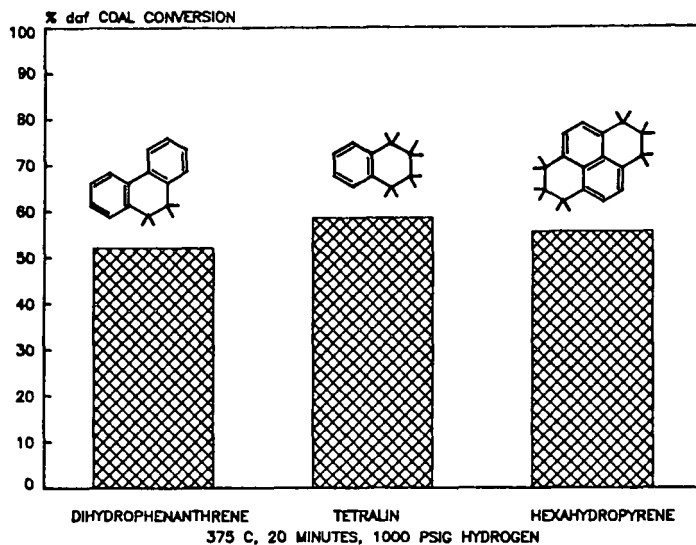


Figure 3. Liquefaction results for Wyodak coal in other basic solvents.

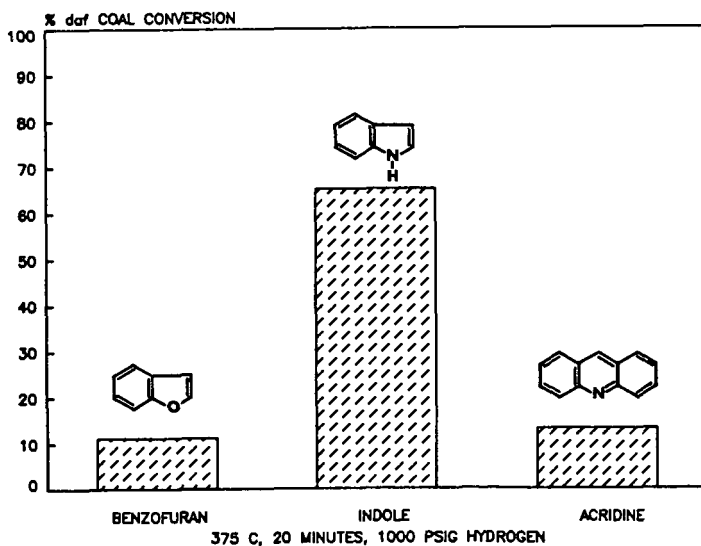


Figure 4. HPLC spectra of the THF soluble filtrate from microreactor runs.

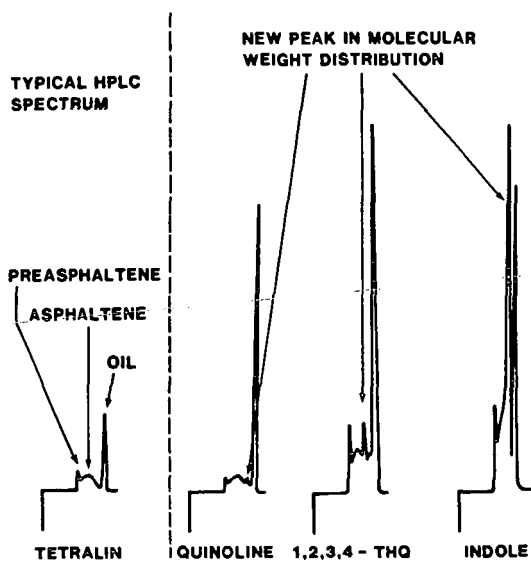
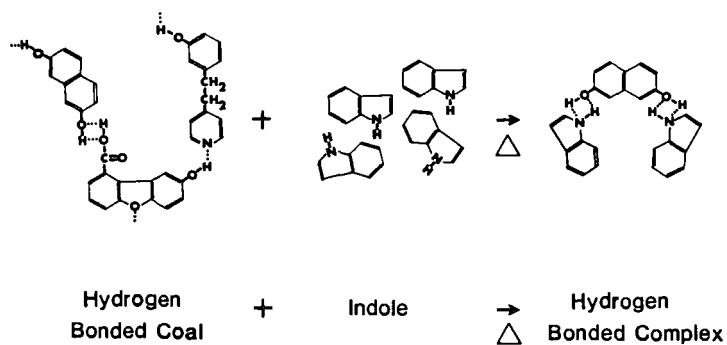


Figure 5. Indole disrupts hydrogen bonded coal matrix to form THF soluble complexes.



THERMAL REACTIVITY STUDIES OF SOLVENT REFINED COAL

R. L. Miller and N. Shankar
Chemical Engineering Department

University of Wyoming, Laramie, Wyoming 82071

ABSTRACT

Four solvent refined coal (SRC) samples obtained from Kentucky 9/14 and Illinois 6 coals have been thermally hydrogenated in a stirred microautoclave reactor at short contact time coal liquefaction reaction conditions. No coal or catalyst was used in any of the runs. Reactivity of each SRC sample was monitored using C_4 -427°C distillate yield, hydrogen consumption, hydrogen-free gas make, and solvent solubility measurements.

Initial results indicated the existence of various interconversion reactions among the oil, asphaltene, preasphaltene, and pyridine insoluble organic matter (IOM) fractions of catalytically unhydrogenated Kentucky SRC at selected reaction conditions. The net result of this reaction sequence was a relatively high C_4 -427°C distillate yield with minimal hydrogen-free gas make and hydrogen consumption. Kentucky and Illinois SRC samples which had been catalytically hydrogenated prior to use in the present study did not undergo the same types of reactions. Hydrogen-free gas make and hydrogen consumption were higher and C_4 -427°C distillate yield was lower in runs using hydrogenated SRC samples.

INTRODUCTION

The primary reaction step in direct coal liquefaction is generally believed to involve thermal rupture of various labile bonds within the coal structure (1, 2, 3). If the reactive free radical coal fragments formed can be quickly capped with available hydrogen from a hydrogen-donor solvent or from portions of the coal itself (autostabilization), a complex mixture of stabilized products is obtained. For convenience, these mixtures have been operationally classified according to a series of solvent solubility tests summarized in Table I (4). Unfortunately, such a classification system does not produce fractions with simple chemical identities.

Preasphaltenes constitute the predominate primary liquefaction product with asphaltenes, oils (distillable and nondistillable), and gases formed in lesser amounts. Secondary reactions involving conversion of preasphaltenes and asphaltenes to produce additional quantities of oil and gas form an important part of coal conversion to distillable liquids. Furthermore, the use of residuum recycle has been shown to have a significant influence on liquefaction process performance. Silver reported that up to 50 wt% of the total distillate obtained in two-stage liquefaction of Wyodak coal could be attributed to conversion of mildly hydrogenated residuum (5). The need for a better understanding of residuum conversion to lighter products is necessary to further improve existing liquefaction processes.

The objective of the research described in this paper was to investigate the thermal conversion of coal-derived residuum in the absence of coal and catalyst at representative coal liquefaction conditions. Particular emphasis was placed on residuum behavior at short contact time reaction conditions similar to those employed in the Lummus ITSL process (6).

EXPERIMENTAL PROCEDURE

Solvent refined coal (SRC) produced from Kentucky 9/14 coal was used as feed residuum in the initial thermal reactivity experiments. This material, designated

F-51, boils above 427°C and was produced in the Pittsburg and Midway SRC-I pilot plant near Tacoma, Washington. To reduce SRC viscosity, blends of approximately 50 wt% F-51 and 50 wt% Kentucky 9/14 coal-derived distillate, designated F-7, were used as reactor feed. The F-7 distillate is a nominal 260-427°C boiling range fraction which was also produced at the Tacoma SRC-I pilot plant. Table II gives a brief description of F-51/F-7 properties.

Three other SRC-distillate mixtures were used in additional reactivity studies. Properties of these mixtures are also included in Table II. Sample F-102A was prepared by mildly hydrogenating a portion of F-51/F-7 at 370°C and 13.9 MPa initial cold hydrogen pressure for one hour over thermally activated Nalco 477 cobalt-molybdate catalyst in a batch reactor. Samples F-128 and F-129 are Illinois 6 coal-derived hydrotreated recycle residuum from Wilsonville, Alabama pilot plant runs 242 and 243, respectively. Run 242 was operated using a short contact time thermal reactor while run 243 utilized a long residence time dissolver. Both of these samples were obtained from essentially steady-state operations and represent residuum which had been recycled through the process many times. The C₉-427°C distillate content of both F-128 and F-129 was only about 30 wt%. Several reactivity runs were performed using F-128 or F-129 diluted with additional Illinois 6 coal-derived distillate to obtain feed mixtures containing about 50 wt% distillate. Results from these runs indicated that within experimental error, there was no effect on yields from the SRC when the feed distillate content was varied between 30 wt% and 50 wt%. Thus, yield data from the four SRC-distillate mixtures listed in Table II can be directly compared.

The thermal reactivity experiments were carried out in a 60 ml stirred microautoclave reactor system designed and constructed at the University of Wyoming. The reactor is similar to larger Autoclave batch reactors except that heating is accomplished with a high temperature sandbath. At the end of each run, the reactor and its contents are quenched with an icewater bath. This reactor system can provide the benefits of small tubing bomb reactors (quick heatup (~2 min.) and cool down (~30 sec.)) while at the same time insuring sufficient mechanical agitation of the reactants with an Autoclave Magnedrive II stirring assembly to minimize hydrogen mass transfer effects. Furthermore, the system is designed so that the reactor pressure is very nearly constant throughout an experiment.

The reactor runs were completed at 454°C and 6.9 MPa initial cold hydrogen pressure for reaction times in the range of 5 - 15 minutes. To simulate the slug flow behavior of commercial small diameter SCT reactors in which significant gas phase hydrogen mass transfer effects exist, the Magnedrive stirrer was turned off during these runs. These conditions are believed to simulate SCT operations reasonably closely.

Portions of the liquid products from each run were distilled to a 427°C endpoint using a microdistillation apparatus. Additional portions of the liquid product were sequentially extracted in a Soxhlet extractor using cyclohexane, toluene, and pyridine. Product gases were analyzed on an HP 5840A gas chromatograph.

RESULTS AND DISCUSSION

Using the experimental methods described, the product composition from each reactor run was measured. This data is summarized in Figures 1-4 in which weight fraction compositional changes as a function of reaction time are shown for each SRC-distillate sample. The weight fraction of hydrogen-free gas produced was always less than about 0.01 and is not shown on these figures. Results shown for F-51/F-7 are average values from duplicate runs, while data for the other three SRC-distillate samples were obtained in single runs. Based on previous experience with the reactor system and product analysis methods used, the weight fraction data presented has an experimental error of approximately ± 10 relative percent.

Several interesting observations can be made from these results. First, a detailed examination of the material balance data indicates that the asphaltene fraction of F-51/F-7 formed both distillate and preasphaltenes particularly at reaction times greater than about 5 minutes. Several authors have previously noted this type of disproportionation behavior (7, 8, 9). In some cases these results have been interpreted as evidence of reaction "reversibility". However, as will be noted shortly, such reversibility does not really exist here, since the preasphaltenes formed by asphaltene disproportionation differ from the coal-derived preasphaltenes found in F-51/F-7. Figure 1 also shows a decline in the nondistillable oil content most likely caused by thermal cracking of oils to form additional distillate and gas. No significant amount of pyridine insoluble organic matter (IOM) was formed during the F-51/F-7 runs.

In contrast, results shown in Figures 2-4 for the hydrogenated SRC-distillate samples indicate somewhat different behavior. In each case, the asphaltene fraction apparently shows no propensity toward disproportionation. Rather, material balance data suggests that preasphaltenes and asphaltenes were slowly converted to nondistillable oils, and eventually cracked to distillate and gas in a series type mechanism. After about ten minutes reaction time, the conversion of nondistillable oils to distillate and gas was the only significant reaction taking place in the F-128 and F-129 samples. Once again, very little IOM was produced in any of the runs. This is not surprising since other researchers have noted the refractory nature of hydrogenated asphaltenes toward thermal or catalytic conversion to lower boiling products (10, 11).

The overall effect of differences in asphaltene and preasphaltene thermal reactivity between the unhydrogenated and hydrogenated SRC-distillate samples is summarized in Figure 5. In this plot, hydrogen utilization efficiency, defined as the mass of $C_{10}-427^{\circ}C$ distillate produced per unit mass of hydrogen consumed is plotted as a function of reaction time for each of the four SRC-distillate samples. The unhydrogenated F-51/F-7 sample obviously produces a significant amount of distillate with minimal hydrogen consumption when compared with yield data from the hydrogenated samples. Furthermore, Figure 6 shows that the hydrogen-free gas make was found to be 2 to 6 times less in the F-51/F-7 runs. It appears that asphaltene disproportionation is a more efficient method of distillate production than thermal cracking of nondistillable oils. However, it is apparent that even mild catalytic hydrotreatment of the SRC results in drastically reduced hydrogen utilization efficiency.

In an attempt to further study differences between the reaction pathways of unhydrogenated and hydrogenated asphaltenes and preasphaltenes, the preasphaltene fractions from the F-51/F-7 and F-102A thermal reactivity experiments were subdivided into chloroform soluble-toluene insoluble and pyridine soluble-chloroform insoluble subfractions, designated preasphaltene-1 and preasphaltene-2, respectively. Boduszynski has reported that preasphaltene-1 samples generally resemble asphaltenes in the number of function groups and degree of aromaticity (12). Preasphaltene-2 samples are more highly functional and are believed to fairly well represent coal-derived preasphaltene material. As shown in Figure 7, the increase in total preasphaltene content for the F-51/F-7 runs was due to an increase in preasphaltenes-1. At least a portion of the preasphaltenes-1 was obtained as a disproportionation product from the asphaltenes. The fact that the total preasphaltene content did not remain constant or decrease precludes the reaction sequence: preasphaltenes-2 to preasphaltenes-1 to asphaltenes as the only pathway involving these fractions. In contrast, as shown in Figure 8, the decrease in F-102A preasphaltenes occurred because of preasphaltenes-2 consumption. No significant buildup of preasphaltenes-1 was noted. Once again, this suggests that F-102A asphaltenes did not undergo disproportionation.

The exact mechanism responsible for the apparent change in asphaltene reactivity is not yet known. Painter (13) and Whitehurst (14) have indicated that retrogressive reactions of SRC fractions to ultimately form char involve the condensation of alkyl and phenolic functional groups rather than direct aromatic ring fusing. It is quite possible that the same functional groups are involved during asphaltene disproportionation. Catalytic hydrotreatment of the SRC would result in fewer available functional groups with which the disproportionation could occur. Efforts are currently underway to test this hypothesis by observing detailed structural changes of the F-51/F-7 and F-102A preasphaltene and asphaltene fractions during thermal hydrogenation.

CONCLUSIONS

The thermal reactivity behavior of one unhydrogenated and three hydrogenated SRC-distillate samples has been studied at simulated short contact time (SCT) reaction conditions. Unhydrogenated coal-derived asphaltenes were found to disproportionate into primarily C₄-427°C distillate and preasphaltene-1 material resulting in high hydrogen utilization efficiency and low hydrogen-free gas make. Asphaltenes from the hydrogenated SRC-distillate samples did not disproportionate. As a result, hydrogen utilization efficiency was significantly lower and hydrogen-free gas make was higher in runs using the hydrogenated samples.

ACKNOWLEDGEMENTS

Financial support for this research was provided by the Electric Power Research Institute under Contract Number RP 1604-04. Mr. Norman Stewart of EPRI provided helpful comments.

LITERATURE CITED

1. Farcasiu, M., ACS Div. Fuel Chem. Preprints, 24, 1, 121, (1979).
2. Han, K.W., and Wen, C.Y., Fuel, 58, 779, (1979).
3. Neavel, R.C., Fuel, 55, 237, (1976).
4. Schweighardt, F.K., Retcofsky, H.L., and Raymond, R., ACS Div. Fuel Chem. Preprints, 21, 7, 27, (1976).
5. Silver, H.F., Corry, R.G., Miller, R.L., and Hurtubise, R.J., Fuel, 61, 111, (1982).
6. Schindler, H.D., Chen, J.M., and Peluso, M., "Liquefaction of Eastern Bituminous Coals by the Integrated Two-Stage Liquefaction (ITSL) Process", Proceedings of the Seventh Annual EPRI Contractors' Conference on Coal Liquefaction, Palo Alto, California, (May, 1982).
7. Thomas, M.G., "Catalyst Behavior in Direct Coal Liquefaction", Proceedings of the Sixth Annual EPRI Contractors' Conference on Coal Liquefaction, Palo Alto, California, (May, 1981).
8. Lee, W.C., Interconversion of Coal-Derived Products, Ph.D. Dissertation, University of Southern California, (1980).
9. Farcasiu, M., Mitchell, T.O., and Whitehurst, D.D., ACS Div. Fuel Chem. Preprints, 21, 7, 11, (1976).
10. Baldwin, R.M., Personal Communication, (1983).

11. Silver, H.F., Corry, R.G., and Miller, R.L., "Coal Liquefaction Studies", Final Report for EPRI Projects 779-23 and 2210-1, (December, 1982).
12. Boduszynski, M.M., Hurtubise, R.J., and Silver, H.F., Anal. Chem., 54, 375, (1982).
13. Painter, P.C., Yamada, Y., Jenkins, R.G., Coleman, M.M., and Walker, P.L., Jr., Fuel, 58, 4, 293, (1979).
14. Whitehurst, D.D., Mitchell, T.O., Farcasiu, M., and Dickert, J.J., Jr., "The Nature and Origin of Asphaltenes in Processed Coal", Final Report for EPRI Project 410, vol. 2, (December, 1979).

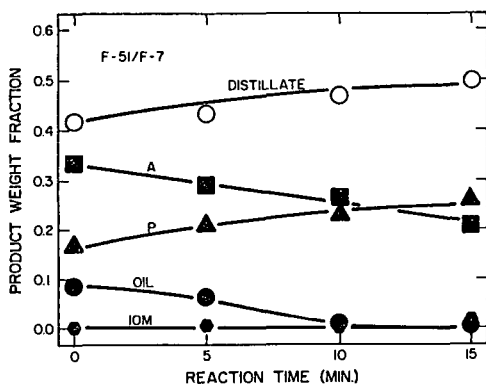


Figure 1 - Product Distribution for F-51/F-7 Runs

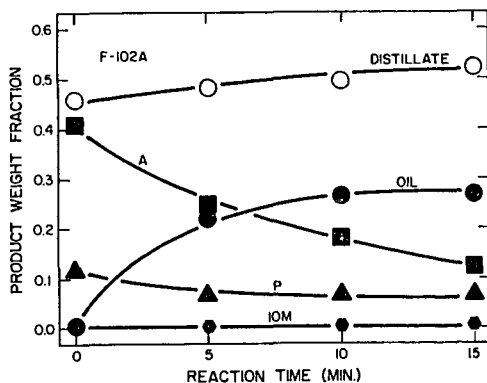


Figure 2 - Product Distribution for F-102A Runs

Table I
Classification of Coal Liquefaction Products

<u>Fraction</u>	<u>Definition</u>
Insoluble Organic Matter	Pyridine or THF insoluble
Preasphaltenes	Pyridine or THF soluble; benzene or toluene insoluble
Asphaltenes	Benzene or toluene soluble; pentane, hexane, or cyclohexane insoluble
Oils	Pentane, hexane, or cyclohexane soluble

Table II
SRC - Distillate Feed Mixture Properties

SAMPLE	F-51/F-7	F-102A	F-128	F-129
SOURCE COAL	KY 9/14	KY 9/14	ILLINOIS 6	ILLINOIS 6
WT.% BOILING ABOVE 427°C	58.0	54.8	68.5	69.2
HYDROGENATION LEVEL	NONE	MILD	SEVERE	SEVERE
ULTIMATE ANALYSIS (WT% DRY BASIS)				
CARBON	86.4	86.9	89.1	89.3
HYDROGEN	7.1	8.0	8.9	8.9
NITROGEN	1.9	1.5	0.4	0.6
SULFUR	0.8	0.6	0.1	0.1
OXYGEN (DIFFERENCE)	3.7	2.9	1.1	0.9
ASH	0.1	0.1	0.4	0.2

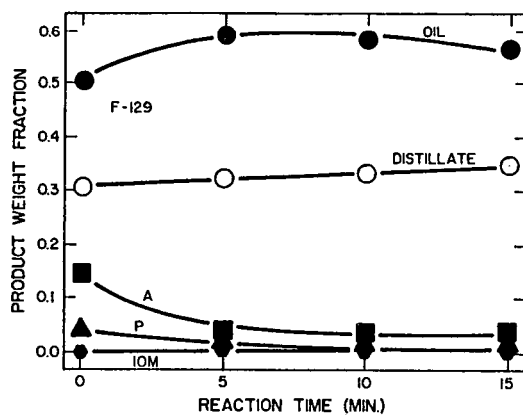


Figure 4 - Product Distribution for F-129 Runs

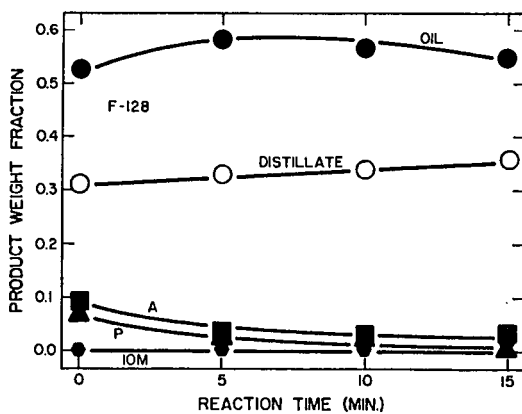


Figure 3 - Product Distribution for F-128 Runs

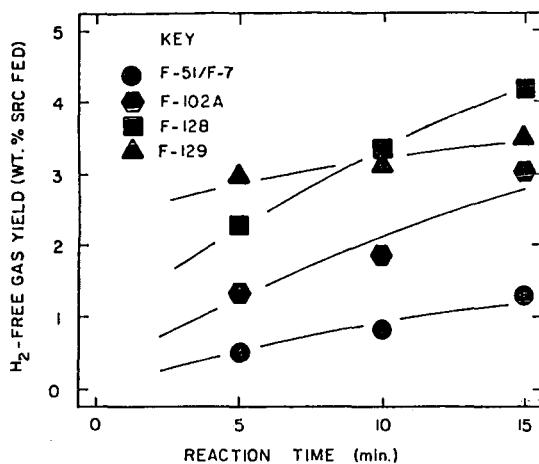


Figure 6 - Hydrogen-free Gas Yield as a Function of SRC Feedstock and Reaction Time

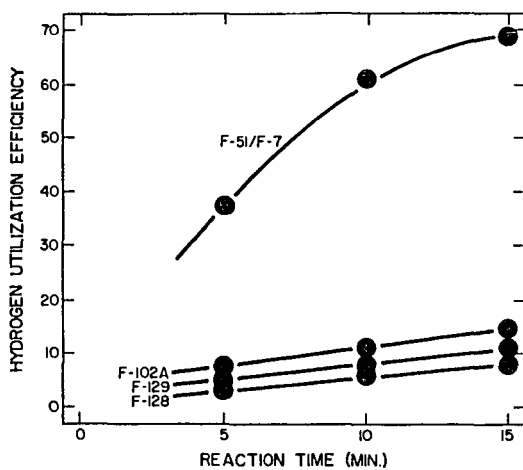


Figure 5 - Hydrogen Utilization Efficiency as a Function of SRC Feedstock and Reaction Time

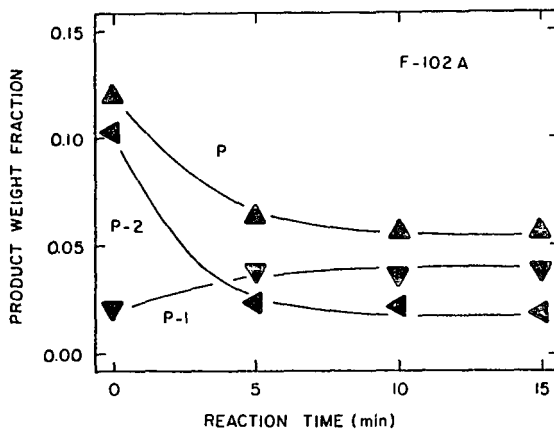


Figure 8 - Preasphaltene Composition for F-102A Runs

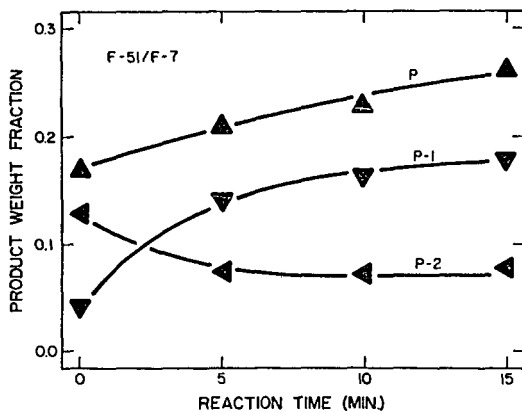


Figure 7 - Preasphaltene Composition for F-51/F-7 Runs

ANALYSIS OF RESINS IN HIGH-ASH COAL-DERIVED PRODUCTS

F. M. Lancas, H. S. Karam and H. M. McNair
Department of Chemistry
Virginia Polytechnic Institute and State University
Blacksburg, VA 24061

INTRODUCTION

The past few years have witnessed extensive efforts to characterize coal-derived liquids. One widely used method to characterize these liquids is the SARA fractionation method by which the fossil fuel is fractionated into saturates, aromatics, resins and asphaltenes. One of these fractions, resins, is believed to play an important role in the conversion process of coal into liquid products. Liquid chromatography and solubility tests are two different approaches to the SARA fractionation. Following precipitation of asphaltenes in non-polar hydrocarbons (such as n-pentane), the deasphaltened solution can be chromatographed on silica or alumina to obtain the resins. The deasphaltened solution can also be applied to a clay column and eluted with pentane to separate resins from oils, or it can be treated with propane gas to precipitate the resins.

In this paper, resins obtained by five different methods are compared gravimetrically and by reverse phase high performance liquid chromatography. These methods are: 1) the Phillips Petroleum procedure; 2) our alternative SARA procedure; 3) fractionation by solubility; 4) fractionation by clay; and 5) our new preparative scale LC method.

Experimental

a) Preparation of resins by the different methods

The five methods investigated are conducted on the same coal, a high ash Brazilian "Mina Do Leao" coal, under the same conditions of sample preparation, extraction, and solvent evaporation. Such experimental conditions are described in detail in our previous work (1).

The Phillips Petroleum Procedure: Method 1

Ten gm coal, 60 mesh, are extracted with 100 ml hexane and the insolubles (asphaltenes) are filtered through a Whatman No. 1 cellulose filter paper. A portion of the hexane extract is applied to the top of a glass column (500 x 11 mm) dry packed with 20 gm alumina, activity I, 80-200 mesh (Fisher Scientific, Pittsburgh, PA). Saturates are eluted with 50 ml of hexane; aromatics with 75 ml of toluene; and resins with 50 ml of methanol (1,2).

The Alternative SARA Method: Method 2

This is an improved method developed in our laboratory at VPI (1). Coal is extracted with tetrahydrofuran (THF) and the unreacted coal is removed by filtration. The coal derived product, after removal of the solvent, is dissolved in 1 ml THF; then it is applied to the top of a glass column (500 x 11 mm) slurry packed with 20 gm of silica gel 60 - 200 mesh (Fisher Scientific, Pittsburg, PA). Saturates are eluted with 50 ml of hexane; aromatics with 75 ml of toluene; resins with 50 ml of methanol; and asphaltenes with 50 ml of THF.

Fractionation by Solubility: Method 3

Following extraction of the coal with tetrahydrofuran (THF) and removal of the solvent; the coal-derived product is dissolved in 2 ml of THF then treated with 80 ml of n-pentane to precipitate the asphaltenes (3). The volume of the deasphaltened solution (maltenes) is reduced to 30 ml by evaporation, then placed in an ice-water bath and an excess of propane gas (99% chemically pure) is added with constant stirring, thus precipitating the resins (3). The solution is then filtered through a Whatman No. 1 cellulose filter, and the precipitate washed with propane-saturated pentane, dried, then weighed.

Fractionation by Attapulgus (florsil) column: Method 4

The deasphaltened solution, as obtained in method 3, is stripped off solvent then dissolved in 1 ml of a 1:1 mixture acetone:methylene chloride. This solution of maltenes is applied to the top of a glass column (500 x 11 mm) slurry packed with 12 gm florisil, 60-100 mesh (Supelco, Bellefonte, PA). Seventy-five ml n-pentane are passed to elute "the oils", while 50 ml of 1:1 acetone:methylene chloride are passed afterwards to elute the retained "resins" in accordance with the literature (4).

New Preparative Scale LC Fractionation: Method 5

Following extraction and solvent evaporation, the THF coal derived product is dissolved in 1 ml THF, then applied to the top of a glass column (500 x 11 mm), slurry packed with 20 gm silica gel, 40-60 mesh Si-60 (EM Science, Gibbstown, NJ). Eight fractions are collected from the preparative scale column in the following order: saturates, monoaromatics, diaromatics, triaromatics, polynuclear aromatics, resins, asphaltenes and asphaltols. Table 1 shows the eluents utilized to give the best separation among the group types; the volumes used; and the fractions eluted. More details about this method can be found in the literature (5). Figures 1 and 2 show the chromatograms obtained for the non-polar and polar fractions.

TABLE 1
Eluents and Fractions Collected in the Preparative
Scale Fractionation Method: Method 5

<u>Fraction Eluted</u>	<u>Eluent</u>	<u>Volume (ml)</u>
1. Saturates	Hexane (C ₆)	40
2. Monoaromatics	Hexane (C ₆)	27
3. Diaromatics	11.5% benzene in C ₆	36
4. Triaromatics	32.0% benzene in C ₆	24
5. Polynuclear aromatics	32.0% benzene in C ₆	25
6. Resins	Benzene/(CH ₃) ₂ CO/MeCl ₂ (3/4/3)	65
7. Asphaltenes	(CH ₃) ₂ CO/THF(2/8)	60
8. Asphaltols	Pyridine	65

b) High Performance Liquid Chromatographic Separation

The analytical instrument used was a Varian Model 5020 High Performance Liquid Chromatograph. Detection was made using a Varian Varichrom Detector at 254 nm. The peaks were recorded on a Varian Model 9176 recorder. A high pressure sixport Valco valve model N-60 was utilized with a sample loop of 10 μ l. The column used was 150 x 4 mm Micropak 5 μ , RP-18. Mobile phase was a 70/30 acetonitrile/water at a flow rate of 1 ml/min. Each resins fraction, after removal of the solvent, was dissolved in THF to a concentration of 10 mg/ml. The solutions were then double filtered through 5.0 μ m Millipore filters (type LS) and finally diluted to a concentration of 0.4 mg/ml with acetonitrile prior to injection on the HPLC system.

Results and Discussion

a) Gravimetric analysis of resins

Table 2 displays a comparison of the relative distribution of resins among the five methods investigated as applied to the Brazilian coal.

TABLE 2

Relative Distribution of Resins in the Brazilian
Coal Extract Using Different Separation Methods

<u>Method</u>	<u>Wt. % Resins*</u>	<u>σ</u>	<u>% σ (RSD)</u>
1. Phillips	29.4	10	35
2. Alternative SARA	51.8	---	---
3. Fractionation by solubility	15.1	0.44	2.9
4. Fractionation by Clay	10.5	0.15	1.4
5. LC Preparative Scale	57.8	0.33	0.57

*Results from 4 repetitive runs

Table 2 shows that method 5 is by far the most reproducible system investigated. In both methods 2 and 5, resins are the major fraction in the coal-derived product. It is important to note that in methods 2 and 5 the whole THF coal extract was applied to the chromatographic column without any previous precipitation of asphaltenes (methods 1, 3, 4) or resins (method 3). The new preparative scale LC method is more complete than method 2, yielding eight discrete and pure chemical classes as has been evidenced by HPLC (see figures 1 and 2). In addition, it has a recovery of more than 94% of the loaded sample (6). The fractionation of the whole coal extract by this method yields purer fractions than those obtained by the traditional solubility fractionation, thus avoiding the contamination by co-precipitation commonly encountered in this method (1). In a different set of experiments, an asphaltenes sample (benzene soluble, pentane insoluble) from the solubility fractionation method was studied by the new method and the result showed that what seemed to be asphaltenes was in fact more than 70% resins (7).

High Performance Liquid Chromatography Analysis

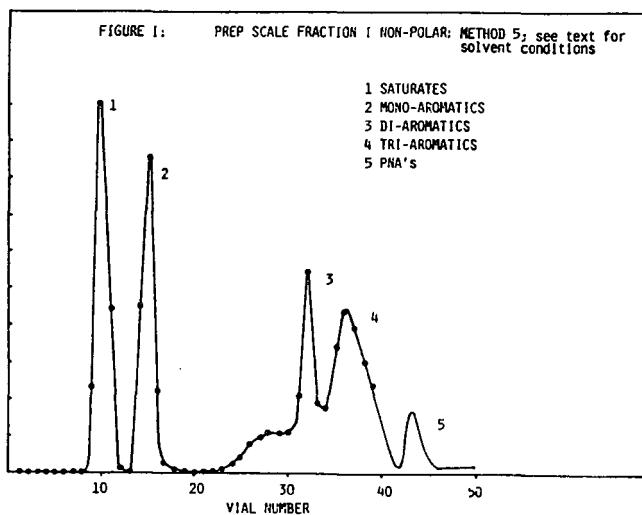
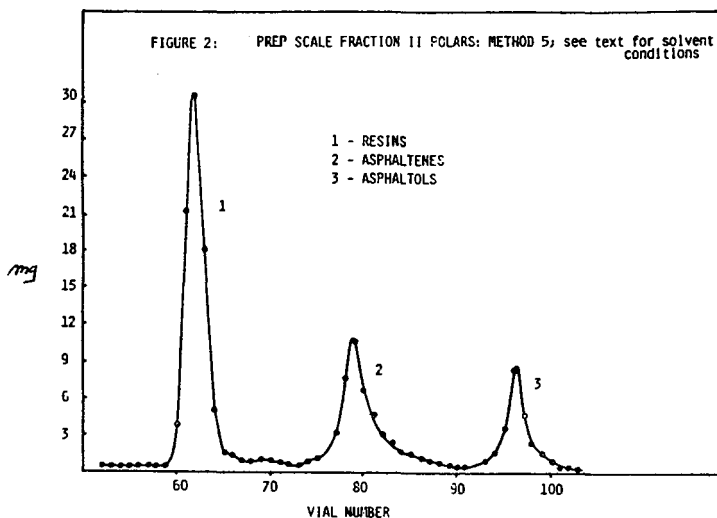
The chromatogram in figure 3 is for a standard mixture of polar compounds found in coal-derived liquids. A range of functional groups was chosen to represent many of the compound classes which could be found in coal. Structures of these compounds are shown in figure 3. Figure 4 shows a chromatogram for resins produced by method 5 while figures 5 and 6 show chromatograms for resins produced by methods 4 and 3. It is important to note that all resin solutions were chromatographed under identical conditions. Figure 3 shows that the column is very efficient. Figures 4, 5 and 6 show that the resin fraction obtained from coal by several separation procedures is still extremely complex and even better sample separation schemes need to be developed. We are continuing efforts along these lines.

Conclusion

Both gravimetric and HPLC results show that depending on the fractionation method of the coal-derived product one gets different distributions of resins. Among the different methods studied, the new preparative LC scale method seems to yield purer fractions; it produces a higher yield of sample (94%); and it is a complete method that fractionates the whole coal derived product in a single step without the inconvenience of precipitating asphaltenes or resins.

REFERENCES

1. Lancas, F. M., Karam, H. S. and McNair, H. M. Preprint Am. Chem. Soc., Div. Fuel Chem., Vol. 28, No. 4, 1983
2. Phillips Petroleum Company, Research and Development Method 8045-AS(1980)
3. Bunger, J. W., and Li, N. C., eds., "Chemistry of Asphaltenes; advances in Chem. Series." No. 195, AMS (1981)
4. Galya, L. G. and Suatoni, J. C. J. Liquid Chrom. 3,229-242(1980)
5. Lancas, F. M., Karam, H. S. and McNair, H. M. Paper submitted to J. Chromatography, Oct. 1983
6. Lancas, F. M., Karam, H. S. and McNair, H. M., in preparation
7. Karam, H. S. Unpublished results



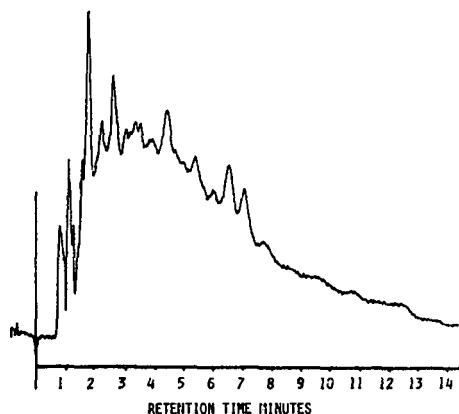


FIGURE 4: RESINS FRACTION PRODUCED BY METHOD 5
ISOCRATIC; 70/30 ACETONITRILE/WATER
2 ml/min. U.V. AT 254 x 0.05 AUFS

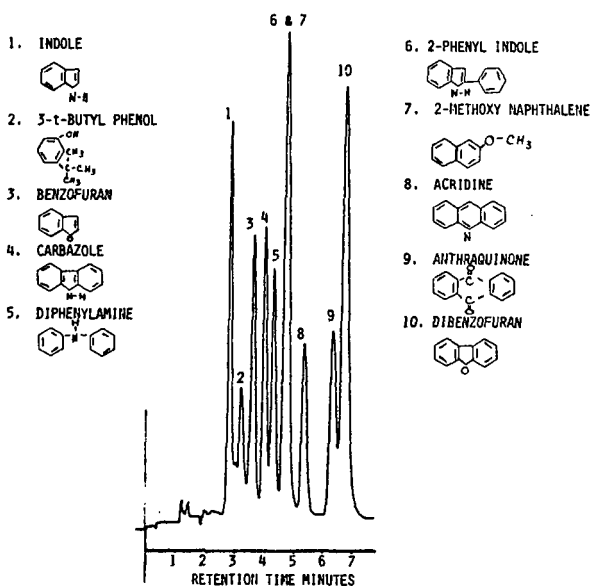


FIGURE 3: REVERSE PHASE SEPARATION OF
STANDARD MIXTURE; TEMPERATURE AMBIENT:
COLUMN 150 x 4 mm RP-18 HICOPAK 5 μ ,
FLOW RATE 1ml/min ISOCRATIC: 70/30
ACETONITRILE/WATER U.V. AT 254 nm,
0.2 AUFS

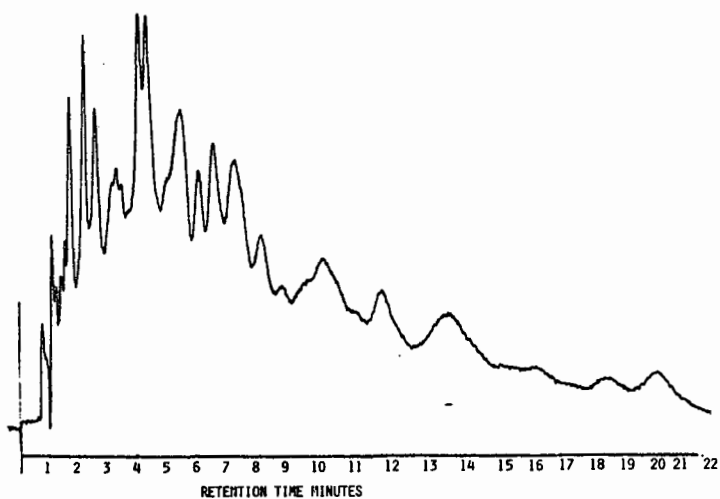


FIGURE 6: RESINS FRACTION PRODUCED BY METHOD 3; conditions same as figure 4

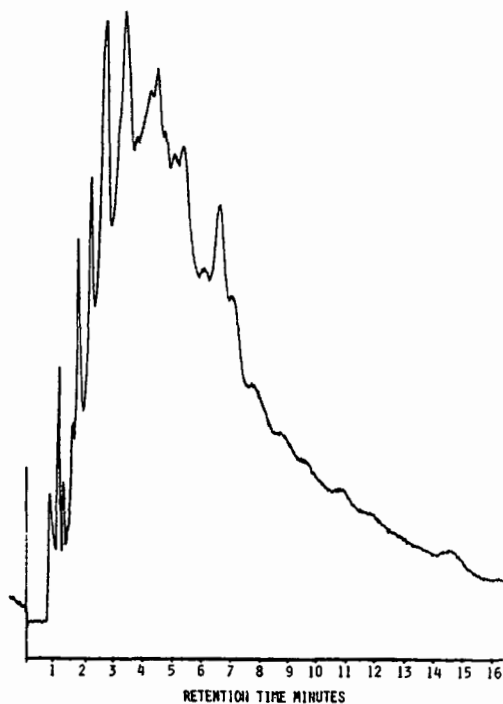


FIGURE 5: RESINS FRACTION PRODUCED BY METHOD 4; conditions same as figure 4

Oxygen Absorption and Light Scattering Studies of the Stability of Liquid Fuels

by N.F. Yaggi,¹ S.H. Lee,¹ J. Ge¹ and N.C. Li^{1, 2}

¹Duquesne University, Department of Chemistry, Pittsburgh, PA 15282 and

²Department of Chemistry, Catholic University of America, Washington, D.C. 20064

INTRODUCTION

Extensive literature (1, 2) have shown that 2,5-dimethylpyrrole (DMP) is particularly deleterious to stability of liquid fuels, in that this alkylated pyrrole promotes very drastically the formation of insoluble sediments and adherent gums. DMP also promotes extensive light scattering and oxygen absorption, so that their measurements are useful in monitoring the instability of liquid fuels. When the methyl group is on the ring nitrogen in pyrrole, as in N-methyl pyrrole (NMP), the ability to promote sediment formation, light scattering and oxygen absorption becomes much less.

Smith and Jensen (3) have given data on consumption of oxygen by pure pyrroles and have shown that at 323K, the oxygen uptake by DMP is much higher and faster than NMP. The purpose of this research is to determine whether results of oxygen absorption, light scattering and deposit formation can be correlated in studying the instability of liquid fuels. The liquid fuels used are SRC-II and H-coal middle distillates and the upgraded liquids prepared by Chevron Research Co. (4), as well as petroleum-derived JP-5 fuels. Synergistic effects between DMP and thiophenol have been found and are reported in this paper also.

EXPERIMENTAL

The apparatus used for determination of oxygen absorption is shown in Figure 1. It is a semi-closed atmospheric pressure unit in which a static atmosphere of oxygen over an aqueous manometric fluid (Krebs' manometer fluid (5)) is allowed to come in contact with a vigorously stirred sample for ageing. The loss of volatile material during ageing is minimized by the use of an efficient water condenser and a cold trap connected in tandem. In a typical experiment the side-arm flask containing a weighed sample is attached to the bottom of the water condenser. With all the stopcocks open and the reservoir R filled with Krebs' manometer fluid, oxygen gas is passed through the entire system for several seconds. Then the side-arm stopcock is closed and the reservoir is filled with oxygen to a point between the 425 and 450 ml marks. The oxygen inlet stopcock A is then closed and the leveling bulb B is adjusted so as to maintain the same liquid levels in R and B. One or more initial readings of atmospheric pressure, ambient temperature and gas volume in R are made. Additional readings are made, usually 3-5 times a day, for several days, until the liquid level in R neared the "0 ml" mark or the oxygen uptake appeared to stop.

Laser light scattering measurements were carried out with a photometer described by Berry (6) modified by introduction of a laser light source (Spectra-Physics Model 155 0.5 mW He-Ne laser, 632.8 nm). Light scattering cells of the design by Dandliker and Kraut (7) were used. The Pyrex cells were in the form of truncated cones, in order to reduce the stray light pickup by the detector. The additives were weighed in volumetric flasks and then filled to the mark with liquid fuel; the time of mixing was taken as zero time. The liquid was then introduced into a light-scattering cell; the cell was mounted on a cell holder, which in turn was mounted in a cell compartment. Care was taken to insure proper alignment of the cell with the very narrow light beam and the detector. The instrument was calibrated periodically by replacing the cell with a turbid standard glass block. The experiments were conducted at 298 \pm 2K.

SRC-II process products were made from Pittsburgh Seam Coal at Pittsburgh and Midway Coal Co. These products were blended in the ratio recommended by the Department of Energy Technical officer to represent a typical net whole liquid product from the SRC-II process. The blend is referred to as SRC-II syncrude. H-coal process products derived from Illinois no. 6 coal were blended in the ratio recommended by Hydrocarbon Research Inc. to represent a net whole liquid product from the H-coal process. This blend is referred to as H-coal syncrude. The syncrudes (or middle distillates) were hydrotreated using Chevron's ICR catalyst (containing nickel, tungsten, silica and alumina) at 672 K and approximately 15.6 MPa H_2 partial pressure. The properties of the syncrudes and their upgraded liquids are listed in Table I of ref. (4). Petroleum-derived JP-5, no. 80-8 and no. 80-12, were obtained from the Naval Research Laboratory.

RESULTS AND DISCUSSION

Figure 2 shows oxygen uptake curves obtained at 323 K for a middle distillate, an upgraded coal liquid, and petroleum JP-5. The coal-derived middle distillate shows much higher oxygen uptake than the upgraded liquid, which in turn is only slightly greater than the petroleum jet fuel. This means that Chevron Research Inc. have upgraded the coal liquid to about the same stability characteristics (as shown by the extent of oxygen uptake) as the petroleum jet fuel. Other characteristics of the upgraded coal liquids have been discussed in ref. (4).

Figure 3 shows oxygen uptake of SRC-II syncrude at 348 K in the absence and presence of 0.1 g copper shavings per 5 g of fuel. Several investigators (8-10) have discussed copper catalysis of the ageing of SRC-II middle distillate by a perenol oxidative coupling mechanism, and Figure 3 shows that the copper catalysis is also manifested by increase in oxygen uptake.

IR spectra of dilute solutions of SRC-II middle distillate (from Illinois no. 6 coal), before and after ageing for 5 days at 335 K, have been published by Jones and Li (9). The unaged coal liquid exhibits a prominent free hydroxyl stretching band at 3600 cm^{-1} . The intensity of this band is not significantly affected by ageing with copper or oxygen alone; but with both the intensity of this band is reduced. This indicates that the hydroxyl group is modified during ageing, and that the presence of copper is necessary. The unaged coal liquid is completely soluble in pentane. However, after ageing for 5 days with $Cu + O_2$ at 335 K, 30% of the aged coal liquid became insoluble in pentane. The insoluble fraction contained 3.5% copper in oxidation state II (10). The fact that copper (II) is present signifies that it acts as a reactant in addition to its role as a catalyst.

Iron (II) phthalocyanine ($PcFe$) also acts as a catalyst in the oxygen uptake by H-coal middle distillate, as shown in Figure 4. In the absence of $PcFe$, a long induction period of 160 hrs. exists. In the presence of 0.025 g $PcFe$ in 5 g of the middle distillate, the induction period disappears, and a significant oxygen uptake occurs. This constitutes an example of the use of $PcFe$ as a catalyst in the oxidation of coal liquids. Kropf (11) has previously proposed that, in the oxidation of cumene below 373 K, copper phthalocyanine activated a molecular oxygen through its coordination with the metal ion to form a phthalocyanine- O_2 complex, which then abstracted the tertiary hydrogen of cumene to initiate the oxidation. Hara et al. (12) found that the addition of a small amount of pyridine to metal- Pc and cumene mixtures induced a drastic shortening of the induction period and a considerable increase in oxidation rate. In our experiment (Figure 4) addition of pyridine is not necessary, since the H-coal middle distillate already contains many nitrogen-containing compounds.

Figure 5 gives plots of moles O_2 absorbed per mole of N-methyl pyrrole (NMP) vs. time at three temperatures. Increase in temperature means increase in accelerated ageing and therefore results in greater oxygen uptake. At a given temperature, longer storage time results in more ageing and greater oxygen uptake. Jones, Hardy, and Hazlett (13) have shown that for petroleum-derived diesel fuel marine, increase in stress temperature results in a shorter time necessary to form equivalent weights of total insolubles. The data of Fig. 5 also show that increase in temperature results in a shorter time necessary to absorb equivalent amount of oxygen per mole of NMP. A plot of $\log t$ vs. $1/T$ can be constructed, where t is the time in hours required at any particular temperature of stressing to absorb 0.01 mole O_2 /mole NMP. The plot is almost linear. Figure 5 also shows that 2,5-dimethylpyrrole (DMP) exhibits much higher oxygen uptake than does NMP. This is in line with the fact (1, 2) that DMP promotes very drastically the formation of insoluble gums and light scattering in fuels, whereas the effect of NMP is very small. Reactions leading to sediment formation may be characterized as free radical, autoxidative reactions. The greater extent of radical formation in DMP may explain in part the greater oxygen uptake by DMP than NMP and the greater ability to promote deposit formation and light scattering, by DMP than by NMP.

Figure 6 shows plots of light scattering intensity at 90° scattering angle for petroleum JP-5 containing 50 ppm (N) DMP and various additives. The presence of 0.2M thiophene, 0.2 M 1,5-hexadiene, or 0.2M thiophenol alone in the petroleum JP-5 results in no change in I_{90} . In the presence of DMP however, thiophenol gives the largest light scattering followed by hexadiene and then thiophene. The implication is that these individual sulfur-containing compounds by themselves are not deleterious to the stability of the liquid fuel. However, in the presence of nitrogen-containing compound like DMP, the instability effect is shown. Therefore, the combined effect of nitrogen and sulfur-containing compounds must be considered. Figure 7 shows similar plots for upgraded H-coal. Here the scattering angle is 45° , because the intensity at 90° is too small to differentiate between the different additives. The order of instability is: thiophenol > 1, 5-hexadiene > 1-hexene, > thiophene.

Figure 8 gives plot of I_{90} vs. time for 2,6-dimethylquinoline (DMQ) and additives vs. time.

In our experiments, positive synergism involving DMP or DMQ is greatest for thiophenol, and the order of other sulfur compounds and unsaturated compound, is the same, whether the fuel is petroleum, upgraded H-coal or upgraded SRC-II liquids. DMQ has less effect on light scattering than DMP, and promotes much less deposit formation than DMP.

CONCLUSIONS

Coal-derived middle distillates have higher oxygen uptake than upgraded coal liquids, which in turn are only slightly higher than the petroleum jet fuel. DMP promotes oxygen absorption, light scattering, and deposit formation, much more than NMP. These three techniques can be correlated in studying the instability of liquid fuels. Synergistic effects between nitrogen and sulfur-containing compounds are apparent.

ACKNOWLEDGEMENT

The support of the U.S. Department of Energy to Duquesne University and the Naval Air Systems Command to Catholic University of America is acknowledged. Thanks are due to G. Berry for use of the light scattering facility at Carnegie-Mellon University, R. Sullivan for generously supplying the upgraded coal liquids, and R.N. Hazlett for helpful discussions.

REFERENCES

- (1) Brinkman, D.W., Frankenfeld, J.W., Taylor, W.F. and Bruncati, R.L., Fundamental Synthetic Fuel Stability Study, DOE/BC/10045-23, 1982; other DOE reports
- (2) Jones, L., Hazlett, R.N., Li, N.C., and Ge, J., ACS Div. Fuel, Chem. Preprints, 28 (1), 196 (1983)
- (3) Smith, E.B. and Jensen, H.B., J. Org. Chem., 1967, 32, 3330
- (4) Young, L-J.S., Li, N.C., Hardy, D., Fuel, 1983, 62, 718
- (5) Krebs, H.A., Biochem. J., 1951, 48, 240
- (6) Berry, G.C., J. Chem. Phys. 1966, 44, 4550
- (7) Dandliker, W.B. and Kraut, K.F. J. Am. Chem. Soc. 1956, 78, 2380
- (8) Hara, T., Jones, L., Li, N.C., and Tewari, K.C., Fuel 1981, 60, 1143
- (9) Jones, L. and Li, N.C. Fuel, 1983, 62, 1156
- (10) White, C.M., Jones, L., and Li, N.C. Fuel, in press
- (11) Kropf, H. Ann. Chem. 1960, 637, 73
- (12) Hara, T., Ohkatsu, Y. and Osa, T. Bull. Chem. Soc. Japan, 1974, 48, 85
- (13) Jones, L., Hardy, D., and Hazlett, R.N. Preprint, ACS Div. Petrol. Chem., 1983, 28(5), 1157

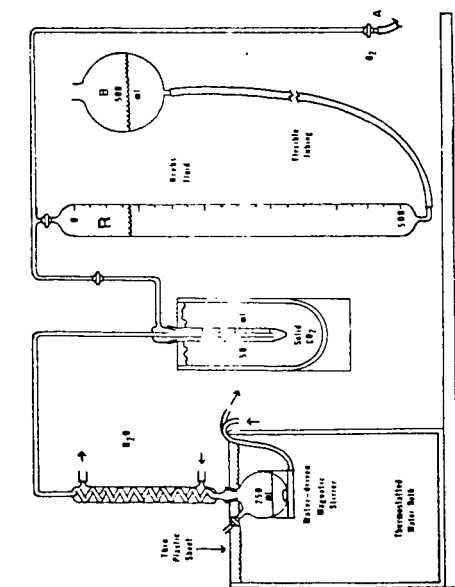


Fig. 1 Apparatus for oxygen-consumption measurement

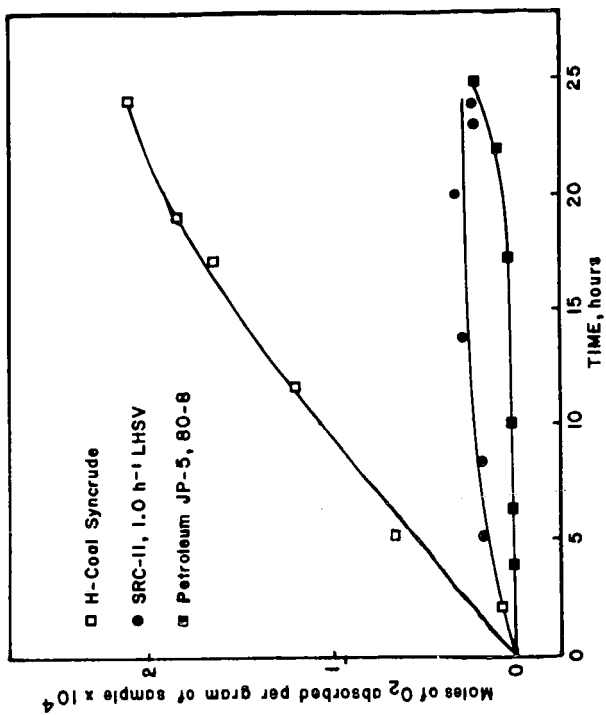


Fig. 2 Oxygen uptake by liquid fuels at 323 K

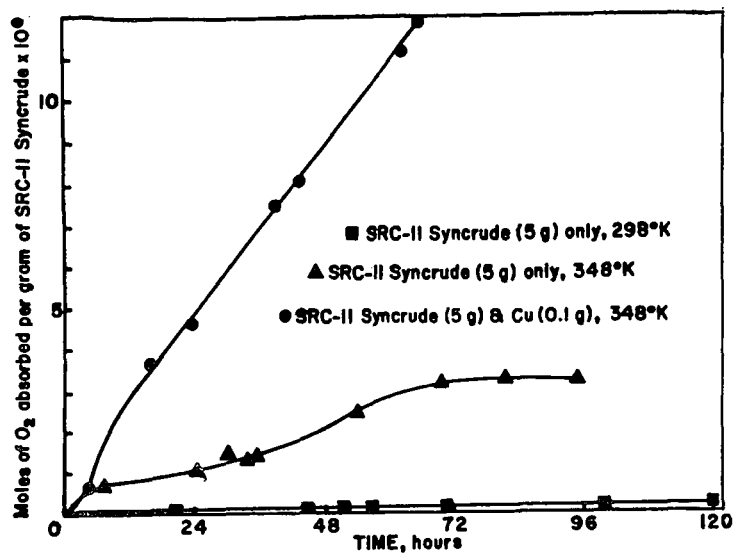


Fig. 3 Oxygen uptake by 5g SRC-II syncrude with and without Cu (0.1g)

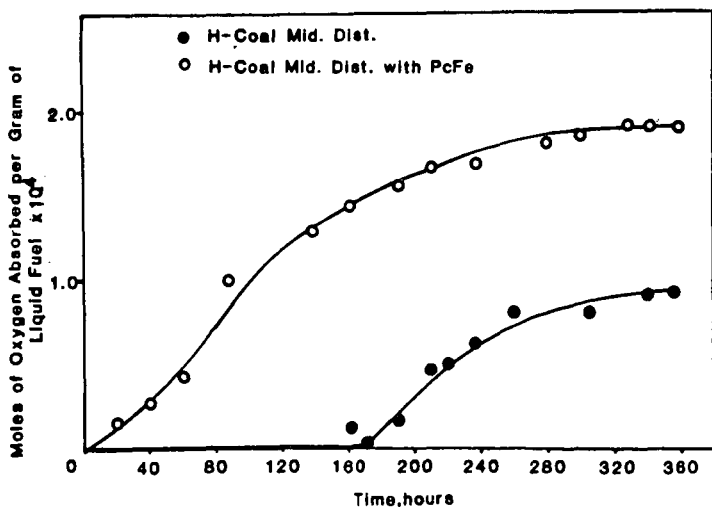


Fig. 4 Oxygen uptake by 5g H-coal middle distillate with and without Pc Fe (0.025g), 296 K

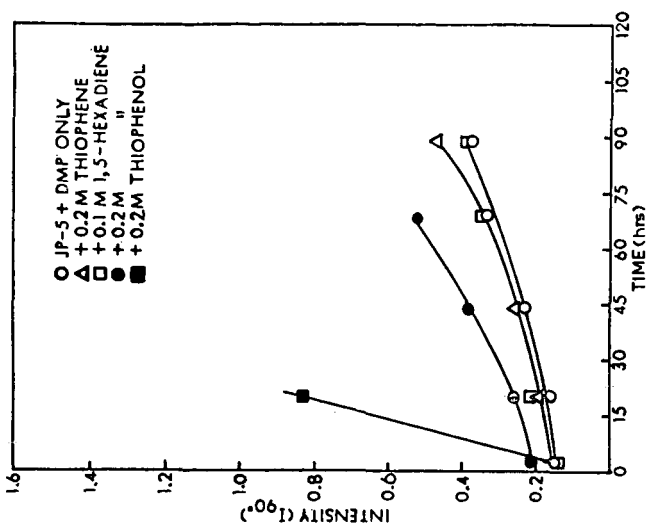


Fig. 6 Light scattering curves for petroleum JP-5, DMP and additives

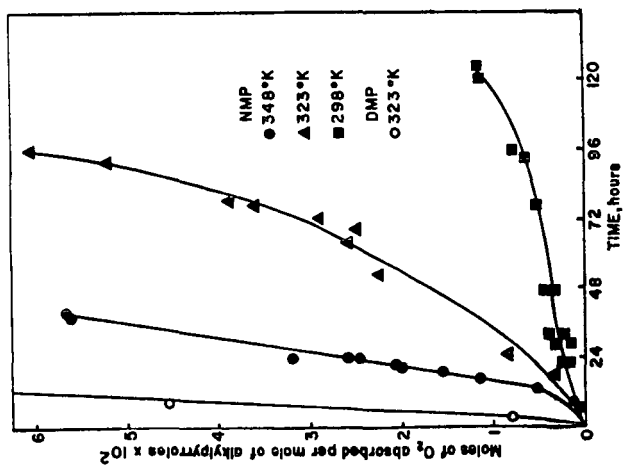


Fig. 5 Oxygen uptake by pure NMP and pure DMP

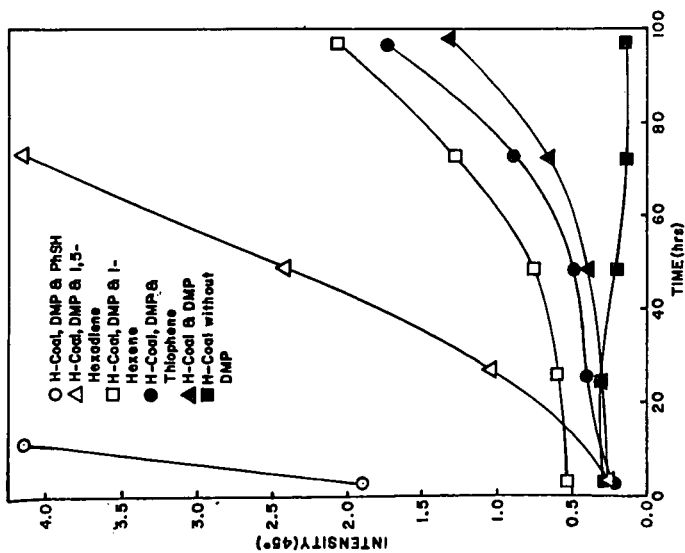


Fig. 7 Light scattering curves for upgraded H-coal (LHSV 0.5) DMP (0.021 M) and additives (each 0.1M)

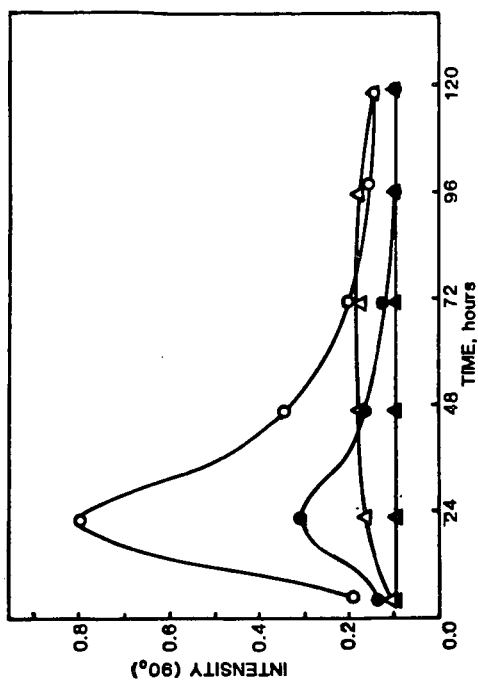


Fig. 8 Light scattering curves for upgraded SRC-II (LHSV 0.5) plus additives:
 ▲ : 0.036M DMQ only; 0.1M thiophenol only
 △ : 3-mercaptopropionic acid (MPA), 0.1M;
 ● : 0.036 M DMQ + 0.1 M MPA
 ○ : 0.036 M DMQ + 0.1 M thiophenol

EVALUATION OF OLIGOMERIC MODELS OF COAL ASPHALTENES AND PREASPHALTENES AS GPC CALIBRATION STANDARDS

Richard J. Baltisberger, S.E. Wagner, S.P. Rao, J.F. Schwan and M.B. Jones

Department of Chemistry, University of North Dakota,
Grand Forks, ND 58202

INTRODUCTION

One important facet of the characterization of coal and coal derived materials is that of molecular weight determination. The initial goal of this study was to synthesize a series of model oligomers that were in agreement with the average structural formulas of some selected coal derived asphaltene and preasphaltene samples as determined by proton nuclear magnetic resonance spectroscopy, elemental analyses and various oxygen derivatization procedures. The second goal was to test these model compounds along with some commercially available polystyrene standards as calibration standards for high pressure gel permeation chromatographic procedures. The retention volumes of these model compounds were compared with those volumes for a group of coal derived asphaltene and preasphaltene samples which had been previously isolated by preparative gel permeation chromatographic techniques.

The application of GPC to the characterization of coal derived materials has been studied by a number of researchers (1-13). Coleman et al. (2-3) demonstrated that three column packings; styrene-divinylbenzene (Bio-Beads S-X4), cross-linked poly(acryloylmorpholine), and modified alkylated dextran (Sephadex LH-20) polymers; could be used for the GPC separation of THF and CHCl_3 solvent refined coal (SRC) fractions. Schwager et al. (1) isolated four SRC asphaltene fractions by preparative techniques using Bio-Beads SX8. A linear relationship between the logarithm of number average molecular weight and retention volume was observed using an analytical μ -styragel HPLC column. The analytical column was calibrated with a series of aromatic hydrocarbons, a porphyrin and propylene glycols of known molecular weight. Curtis et al. (4) studied the characteristics of an SRC (Amax) using GPC techniques. The separation employed three μ -styragel columns using THF as the solvent and was calibrated with a series of polyethylene glycol and various polynuclear aromatic hydrocarbon standards. Sephadex LH-20 has also been used to fractionate the hexane soluble portion of the pyridine extract from a Sorachi coal (5). Khan (6) compared the use of GPC and vapor pressure osmometry (VPO) to obtain molecular weight data for the hexane soluble portion of three H-coal liquids. Two packings, polyvinylacetate (Fractogel PVC 500) and styrene-divinylbenzene copolymer (Toyo Soda, G2000H10) were used as analytical columns. Calibration of the columns was accomplished by VPO measurement of number average molecular weight in toluene of preparative scale fractions obtained from a Fractogel column.

All of this work has demonstrated that the quantitative interpretation of GPC chromatograms raises two problems. First, the response of the detector must remain constant on a per weight basis over the molecular range (i.e., type and distribution of chromophores must be constant). A constancy of uv absorbance per gram for a series of SRL materials has been reported in work by Ruud (9). However, this point needs to be investigated more thoroughly. A second problem, which is the focus of this paper, is the establishment of the response curve with suitable calibration standards.

EXPERIMENTAL

Materials

Polystyrene standards used to obtain the reference GPC curve were obtained from Polysciences, Inc. Other standard compounds were synthesized from starting materials obtained from various commercial sources (14). Solvent refined lignite (SRL) samples produced at 460°C, 27.6 MPa (4000 psig) using synthesis gas were obtained from the Grand Forks Energy Technology Center and solvent fractionated to obtain asphaltene and preasphaltene fractions (15). The lignite used was from a North Dakota seam, Beulah three.

Preparative Scale GPC

The SRL asphaltenes and preasphaltenes were further separated using a 50 mm id x 120 cm glass column packed with Bio-Beads S-X3 (200-400 mesh) styrene-divinyl benzene. Prior to GPC separation all the SRL samples were acetylated in order to convert the hydroxyl sites to their acetate forms. Freshly distilled toluene or pyridine was used as the solvent. Typical analytical GPC chromatograms of an asphaltene sample obtained from the preparative column are presented in Figure 1. Elemental analyses of the fractions were performed by Spang Microanalytical Laboratory and number average molecular weights were determined in our laboratory using a Wescan Model 117 Vapor Pressure Osmometer. In normal runs, 2-3 concentrations over the range 1 to 50 g/kg of pyridine were employed for extrapolation to infinite dilution.

Analytical Scale GPC

Analytical scale GPC analyses (HPLC) were carried out using three 10 nm and one 50 nm μ -styragel columns in series, with THF (UV grade, Burdick and Jackson) as the mobile phase. A Laboratory Data Control Model 1205 UV Monitor was used as the detector (254 nm) and a Waters Model UK6 injector was used to inject samples of about 10 μ l at 10 mg/ml. Samples were filtered across a 0.5 μ m millipore filter prior to injection. The flow rate was usually maintained at 1.0 mL/min to prevent pressures in excess of 1000 psig.

RESULTS AND DISCUSSION

The determination of the number average molecular weights of the asphaltene and preasphaltene SRL fractions by vapor pressure osmometry (VPO) makes it possible to establish the experimental relationships between elution volume in the analytical GPC and molecular weight. Band broadening of the peaks as shown in Figure 1 is a function of the number of theoretical plates of the column and the polydispersity of the sample. The column system was found to have 7,500 plates when using pyrene in THF. The polydispersity ratios (M_w/M_n) of the SRL samples were measured using commercial polystyrene for calibration of the molecular weight and retention volumes assuming a linear response. The polydispersity ratio for each of the polystyrene standards was 1.3. The range of polydispersity values of the SRL fractions was found to be 1.05 to 1.3.

Figure 2 shows a plot of the logarithm of molecular weight versus retention volume for the polystyrene standards, the acetylated SRL asphaltenes and preasphaltenes and a series of oligo(aryl ethers) and oligo(aryl methylenes) from 170-570 g/mole. A nearly linear relationship was found provided the aryl moieties were benzenoid. However, deviations from linearity were observed for both model compounds and SRL samples containing more

condensed aromatic nuclei (i.e., naphthalene, phenanthrene and pyrene). Substances containing larger aromatic nuclei were found to elute too late for their molecular weight. The length per molecular weight of these compounds is less than a benzenoid molecule of the same weight. Because of the smaller size these compounds elute at a later time. The fraction of aromatic carbons present as edge carbons ($H_{\text{aru}}/C_{\text{ar}}$) was measured by proton nmr to be 0.63 to 0.90 for the asphaltenes and preasphaltenes. Calculated values of $H_{\text{aru}}/C_{\text{ar}}$ for the model compounds ranged from 0.67 to 1.0 and for the polystyrene standards were 1.0. Those SRL samples with $H_{\text{aru}}/C_{\text{ar}}$ ratios greater than 0.70 gave nearly a coincident linear plot with the polystyrene standards as shown in Figure 2.

Philip and Anthony (12) have shown that when THF is used as a mobile phase species capable of hydrogen bonding result in elutions corresponding to larger molecular size and smaller retention volumes. We observed this effect particularly for 200-300 g/mole model compounds containing a phenolic hydroxyl group. Philip and Anthony (12) also observed that rigid molecules such as polynuclear aromatics have smaller molecular sizes and thus larger retention volumes. The present direction of our research is to prepare a series of condensed aromatic oligomers so we can better match the $H_{\text{aru}}/C_{\text{ar}}$ values of the calibration standards and the coal derived liquids.

CONCLUSIONS

Polystyrene, oligo(phenyl ethers) and/or oligo(phenyl methylenes) are suitable GPC calibration standards for most derivatized SRL asphaltenes and preasphaltenes. More condensed aromatic oligomers (i.e., containing phenanthryl and pyrenyl moieties) may be required for accurate GPC determination of the molecular weights of SRL samples with low $H_{\text{aru}}/C_{\text{ar}}$ (highly condensed aromatics). The SRL samples must be derivatized to block free -OH groups and prevent interaction with the GPC solvent, THF.

ACKNOWLEDGEMENT

The research was supported by DOE through contract number DE-FG22-81PC40810.

REFERENCES

1. Schwager, I.; Kwan, J.T.; Lee, W.C.; Meng, S.; Yen, T.F. *Anal. Chem.*, **1979**, *51*, 1803-1806.
2. Coleman, W.M.; Wooton, D.L.; Dorn, H.C.; Taylor, L.T. *J. of Chromatography*, **1976**, *123*, 419-428.
3. Coleman, W.M.; Wooton, D.L.; Dorn, H.C.; Taylor, L.T. *Anal. Chem.*, **1977**, *49*, 533-537.
4. Curtis, C.W.; Hathaway, C.D.; Guin, J.A.; Tarrer, A.R. *Fuel*, **1980**, *59*, 575-582.
5. Yoshii, T.; Sato, Y. *Fuel*, **1979**, *58*, 534-538.
6. Khan, M.M. *Fuel*, **1982**, *61*, 553-556.
7. Nomura, M.; Kurosaki, T.; Miyake, M. *Chem. Letters*, **1983**, 329-332.
8. Knudson, C.L.; Schiller, J.E.; Ruud, A.L. In "Organic Chemistry of Coal"; Larsen, L.W., Ed.; A.C.S. Symposium Series, *71*; American Chemical Society: Washington, **1978**; Chapter 22.
9. Ruud, A.L. M.S. Thesis, The University of North Dakota, Grand Forks, ND, **1979**.

10. Wagner, S.E. M.S. Thesis, The University of North Dakota, Grand Forks, ND, 1983.
11. Beilina, N.Y.; Zhidkova, A.F.; Fedotov, M.V. Khimiya Tv. Topliva (Solid Fuel Chemistry), 1983, 17, 93-96 (English Translation).
12. Philip, C.V.; Anthony, R.G. Am. Chem. Soc., Div. Fuel Prepr., 1979, 24(3), 204-214.
13. Wong, J.L.; Gladstone, C.M. Fuel, 1983, 62, 870-872.
14. Baltisberger, R.J.; Jones, M.B. April, 1983, DOE Report DOE/PC/40810-5. Baltisberger, R.J.; Jones, M.B. Sept., 1982, DOE Report DOE/PC/40810-3.
15. Steffgen, F.W.; Schroeder, K.T.; Bockrath, B.C. Anal. Chem., 1979, 51, 1164-1168.

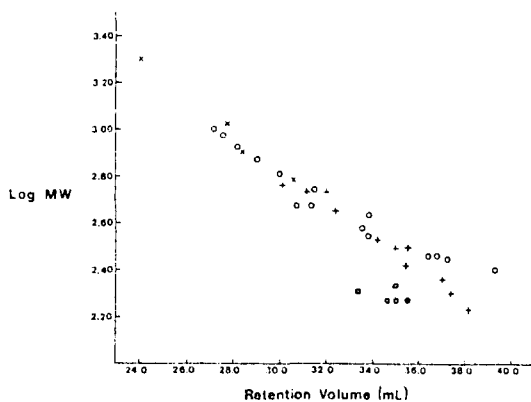


Figure 2. GPC calibration plot. X = polystyrene standards; O = SRL samples with $H_{\text{aru}}/C_{\text{ar}} \geq 0.70$; + = model compounds with $H_{\text{aru}}/C_{\text{ar}} \geq 0.89$ and without phenolic -OH; ● = model compounds with $H_{\text{aru}}/C_{\text{ar}} \geq 0.89$ and with phenolic -OH.

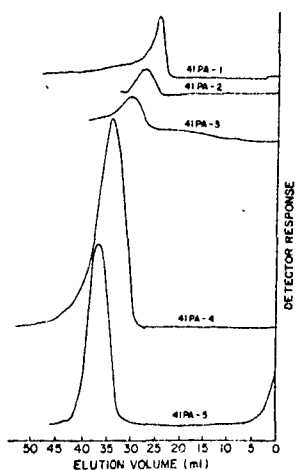


Figure 1. HPLC GPC chromatograms of acetylated SRL preasphaltenes separated by preparative GPC.

The Uses of Isothermal Plastometry

William G. Lloyd,* John W. Reasoner,* James C. Hower** and Linda P. Yates**

*Department of Chemistry, Western Kentucky University, Bowling Green, KY 42101

**Institute for Mining and Minerals Research, University of Kentucky,
Lexington, KY 40506

The most widely used characterization of coal fluidity is the plastometric method developed by Gieseler (1). In a modified form, with a torque clutch replacing the original pulleys and weights, this has become a standard American procedure (2). Its relationship to dilatometry is well established (3-6).

The standard 3 deg/min Gieseler analysis provides a fixed-angle 'slice' across the fluidity-temperature surface, and in a single determination may provide plasticity information across a span of 50-100 deg C. It often reveals fluidity differences of more than a thousandfold among coals of similar rank and chemical composition.

There are, however, several advantages to be gained by conducting Gieseler analyses under isothermal conditions. The resulting data permit the estimation of 'melting' and 'coking' rates and hence (from several runs at different temperatures) the determination of temperature dependencies of these rates. Isothermal data generally provide better simulation of the fluidity characteristics of coal in an actual continuous process such as extrusion feeding (7-9). Isothermal data clearly distinguish among coals of differing temperatures of maximum fluidity.

Fitzgerald has shown that when $\ln(\text{fluidity})$ is plotted against time under isothermal conditions the coking slope is substantially linear. The coking slopes of a group of English coals in his study exhibit Arrhenius temperature dependencies, with activation energies in the vicinity of 50 kcal (10,11).

We have confirmed these observations for a group of 29 hvb coals from the eastern mid-continent beds. For most of these coals the isothermal melting curve is also found to be substantially linear (12,13). Figure 1 illustrates a typical isothermal run. The data provide not only classical information (softening point, time of maximum fluidity, solidification point and maximum observed fluidity) but also estimates of the melting and coking slopes and an additional measure, intersection maximum fluidity. This last is obtained by extrapolation of the two slopes to their point of intersection.

Intersection maximum fluidity has several advantages over observed maximum fluidity. Some coals have a flattish and poorly defined region of maximum fluidity. Coals which outgas vigorously are likely to produce irregular and irreproducible readings in the vicinity of maximum fluidity. Highly plastic coals may develop fluidity in excess of 30,000 ddpm, greater than can be measured by the Gieseler plastometer. In all such cases the intersection maximum fluidity is accessible and in our experience is a more consistent and reproducible measure, even for the case of ASTM temperature-gradient runs (Figure 2).

In the present study a number of freshly sampled coals from active mines and coal cleaning plants have been obtained and reduced, stored under inert gas at -40° , and then analyzed using a research model Gieseler plastometer (Standard Instrumentation), sensitive to 0.1 ddpm (roughly 100 megapoise for a Newtonian fluid). Three of these coals are characterized in Table 1.

When a coal is examined in a series of isothermal runs, both melting and coking slopes are steeper at higher temperatures. These trends are illustrated in Figure 3. For this moderately plastic coal, maximum fluidity is increased over tenfold by raising temperature from 412 to 431°C.

Figure 4 is an Arrhenius plot based upon 20 isothermal runs at 412-438°C with Coal #41. The top slope shows the variation of $\ln \ln(\text{intersection maximum fluidity})$ with reciprocal temperature. The middle and lower slopes show the corresponding variations of $\ln(\text{melting slope})$ and $\ln(\text{coking slope})$. Each of these is essentially linear over the experimental range.

During an isothermal Gieseler run the solder-pot furnace maintains a nearly constant temperature (standard deviation less than 1.0°C). The linearity of the Arrhenius slopes permits the determination of activation energies with fairly good precision (Table 2). The Arrhenius relationship also permits the interpolation of data so that slopes and fluidities of a number of coals can be determined at precisely the same temperature.

Overall isothermal fluidity characteristics of these and other coals which we are studying (14) are summarized in Table 3. These data suggest some general trends among hvb coals. Activation energies of the coking slopes are all in the vicinity of 50 kcal, as Fitzgerald found with English coals (11). Coking slope values are slightly higher for the sparingly plastic coals. Activation energies of the melting slopes tend to increase with increasing plasticity, from 25-30 kcal for sparingly plastic coals to 50-55 kcal for highly plastic coals. Activation energies of $\ln(\text{maximum fluidity})$ decrease with increasing plasticity, from 30-35 kcal for sparingly plastic coals to 10-20 kcal for highly plastic coals. The ratio (melting slope) / (coking slope) is notably higher for the highly plastic coals.

Maximum fluidities measured under isothermal conditions, at or near the ASTM temperature of maximum fluidity, are substantially greater than the corresponding ASTM maximum fluidities. For sparingly fluid coals the maximum isothermal fluidity is typically two- to three-fold that observed in an ASTM run. This ratio increases with coal fluidity, with values typically in the range 5-8 for moderately plastic (30-300 ddpn) coals. Table 4 summarizes this trend for 17 coals for which isothermal data have been obtained at or very near the ASTM temperature of maximum fluidity. For highly fluid coals the isothermal data was obtained at temperatures appreciably below $T(\text{max flu})$. The maximum fluidity obtained in an ASTM run can be matched in an isothermal run conducted at 10-15 deg C below the ASTM temperature of maximum fluidity.

Discussion.

Since a very large number of parallel reactions is involved in both the melting and coking regions of an isothermal run, it is reasonable to ask why - for a semilogarithmic plot or any other plot - the change in fluidity with time has domains of substantial linearity. The condition necessary to find linearity under some conditions is that the major contributing reactions be of the same kinetic order:

$$-d[B]/dt = w_1 k_1 [B]^{n_1} + w_2 k_2 [B]^{n_2} + \dots \quad (1)$$

where the w_i 's and k_i 's denote weighting factors and empirical rate constants.

The right-hand terms are then easily collected into a single term. The observation that plots of $\ln(\text{fluidity})$ vs. time yield melting and coking slopes which are essentially linear suggests that Equation 1 is in fact followed.

This does not mean, as some have suggested, that isothermal coking is a set of first-order processes. Since slurry fluidity is not a linear function of fluid fraction, the coking process is not kinetically first-order. Further work is needed before kinetic dependencies can be inferred from these curves.

Since melting and coking slopes and $\ln(\text{maximum fluidity})$ all follow Arrhenius dependencies, the fluidity span (the time interval during which fluidity exceeds a specified value) can also be calculated at any interpolated temperature. This can be seen analytically. If f is $\ln(\text{intersection maximum fluidity})$, t_m the time interval from initial softening to maximum fluidity and t_c the time interval from maximum fluidity to coking point, then the melting slope m is equal to f/t_m and the coking slope c is equal to f/t_c . The total time span ($t_m + t_c$) is then:

$$t = f \cdot (1/m + 1/c) \quad (2)$$

If a process requires a minimum fluidity F' which is any value less than the maximum fluidity, then:

$$t' = (f - f') \cdot (1/m + 1/c) \quad (3)$$

where $f' = \ln(F')$.

This study is part of an investigation into the predictability of plastic behavior in bituminous coals (14). We acknowledge with thanks the support of this work by the U.S. Department of Energy.

References

1. K. Gieseler, *Gluckauf*, 70, 178 (1934).
2. ASTM Method D2639, Amer. Soc. for Testing and Materials, Phila., PA, 1982.
3. D. W. van Krevelen, E. J. Huntjens and H. N. M. Dormans, *Fuel*, 35, 462 (1956).
4. R. Loison, A. Peytavy, A. F. Boyer and R. Grillot, in H. H. Lowry, ed., "Chemistry of Coal Utilization - Supplementary Volume", John Wiley & Sons, NY, 1963.
5. A. V. Khimichenko, et al., *Khim. Tverd. Topl.*, 1971, 48.
6. W. R. K. Wu and W. H. Frederic, *USBM Bulletin* 661 (1971).
7. V. Kevorkian and F. J. Cumings, U.S. Patent 4,106,997 (1978).
8. P. R. Ryason and C. England, *Fuel*, 57, 241 (1978).
9. C. England, *Proc. 17th Intersoc. Energy Conversion Conf.*, 2, 864 (1982).
10. D. Fitzgerald, *Fuel*, 35, 178 (1956).
11. D. Fitzgerald, *Trans. Faraday Soc.*, 52, 362 (1956).
12. W. G. Lloyd, "Development of Methods of Characterizing Coal in its Plastic State", final rept., Caltech contract #954, 920 (1978).
13. W. G. Lloyd, H. E. Francis, M. R. Yewell, Jr., R. D. Kushida and V. D. Sankur, *Amer. Chem. Soc. Divn. Fuel Chem. Preprints*, 25 (2), 128 (1980).
14. W. G. Lloyd, J. W. Reasoner, J. C. Hower and L. P. Yates, "Predictors of Plasticity in Bituminous Coals", USDOE Contract DE-FG22-81PC40793.
15. Idem, ref. 14, *Techn. Progr. Rept.* 7, June 1983.

Table 1
Coal Characterization Data*

	<u>Coal #18</u>	<u>Coal #22</u>	<u>Coal #41</u>
County	Muhlenberg	Union	Butler
Seam and rank	KY #9, hvBb	KY #6, hvAb	Amos, hvBb
Moisture	7.09%	2.40%	7.78%
Ash	8.36	9.60	2.77
Volatile matter	40.6	39.4	42.1
% Carbon	74.1	76.0	80.7
% Hydrogen	5.11	5.42	5.74
% Nitrogen	1.50	1.44	1.61
% Sulfur	3.59	2.91	1.06
Heating value, Btu/lb	13,020	13,490	14,280
Free swelling index	4.5	8.	3.
% Vitrinite	76.1%	70.7%	79.0%
% Pseudovitrinite	1.2	5.3	6.7
% Exinite	3.5	3.2	6.3
% Resinite	0.4	0.5	0.9
% Fusinite	3.3	3.5	0.4
% Semifusinite	3.6	2.8	0.7
% Micrinite	1.7	1.9	2.7
% Macrinite	0.2	0.1	0.0
Mineral matter (Parr)	11.0	12.0	3.3
Vitrinite max reflect	0.54	0.73	0.67
ASTM Gieseler data:			
T(softening)**	388	376	398
T(max fluidity)	428	422-435	436
T(solidification)**	447	467	459
Max fluidity (observed)	26.8	>30,000	217
Max fluidity (intersctn)	44.5	2.61E+6	590

* Moisture is as determined, other values on a dry ash-included basis.

** Temperature at which fluidity value is 1.0 ddpm.

Table 2
Precision of Arrhenius Temperature Dependencies*

<u>Coal</u>	<u>n</u>	<u>Melting slope</u>	<u>Coking slope</u>	<u>ln(Intersection max flu)</u>
#18	20	31.0 \pm 2.5	48.5 \pm 3.2	35.9 \pm 2.5
#22	19	56.5 \pm 1.8	48.7 \pm 2.0	20.0 \pm 1.5
#41	20	43.8 \pm 1.8	51.4 \pm 2.0	19.7 \pm 0.8

* Least-squares values in kcal and standard deviations.

Table 3

Fluidity Characteristics of Selected Coals*

Coals	Intersection max flu			Melting slope ¹			Coking slope ¹		
	400°C	420°C	E(a)	400°C	420°C	E(a)	400°C	420°C	E(a)
#22	2540	1.8E5	20.0	0.70	2.38	56.5	0.13	0.37	48.7
average of 5 other highly plastic coals	14300	2.5E5	12.3	0.99	3.0	51.	0.16	0.43	44.5
#41	40	277	19.7	0.24	0.62	43.8	0.14	0.43	51.4
average of 5 other medium plastic coals	40	366	21.4	0.34	0.82	42.1	0.19	0.53	48.7
#18	8	88	35.9	0.40	0.77	31.0	0.27	0.77	48.5
average of 5 other slightly plastic coals	5	24	33.2	0.35	0.62	26.9	0.20	0.60	50.8

* Fluidity averages are logarithmic. Properties averaged from coals 21, 25, 27, 32 and 34 (highly plastic); 15, 26, 36, 37 and 39 (medium plastic); and 02, 03, 09, 24 and 40 (slightly plastic), ref. 15.

¹ Slopes are in reciprocal minutes.

Table 4

Maximum Observed Fluidities under ASTM and Isothermal Conditions

no. of coals	Maximum fluidity (MF) range, ddpm	ASTM Conditions		Isothermal Conditions		Ratio*
		Avg MF	Avg T	Avg MF	Avg T	
5	2 < MF < 8	3.8	422°	10.2	421°	2.7
6	8 < MF < 32	12.8	426°	51.2	426°	4.0
6	32 < MF < 256	136.	430°	829.	430°	6.1

* Ratio of (maximum isothermal fluidity) / (maximum ASTM fluidity)

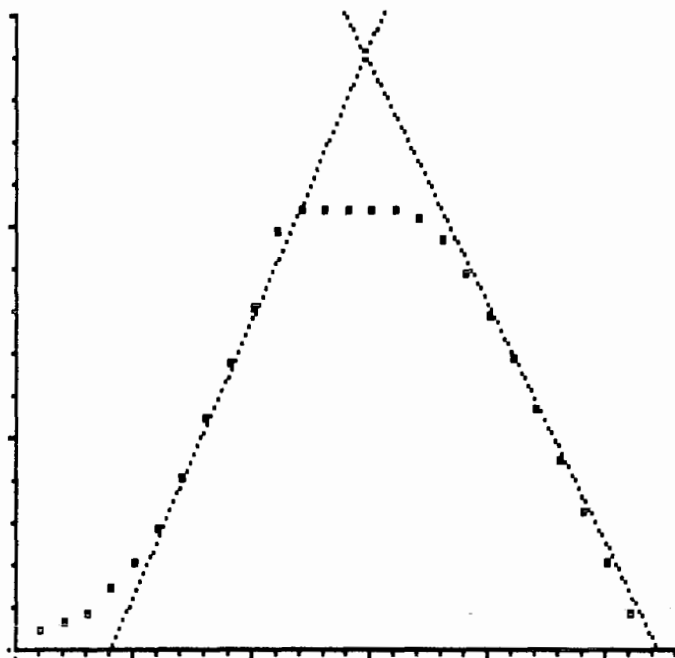


FIGURE 2. ASTM PLASTOMETRY OF A hvAb COAL. Horizontal: time in minutes, scale 0 to 28. Vertical: $\ln(\text{fluidity in ddpm})$, scale 0 to 15. The flat top of the experimental curve marks the instrument limit of 30,000 ddpm.

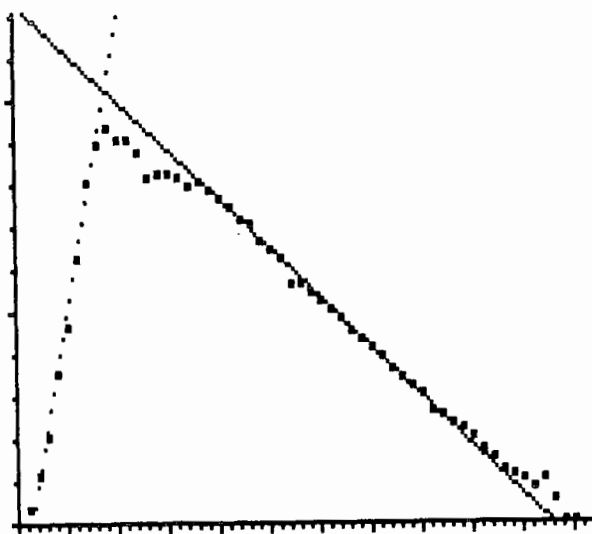


FIGURE 1. ISOTHERMAL PLASTOMETRY OF A hvAb COAL AT 405°C. Horizontal: time in minutes, scale 0 to 56. Vertical: $\ln(\text{fluidity in ddpm})$, scale 0 to 12. Slope calculations use fluidities above 10 ddpm and below one quarter of the observed maximum fluidity.

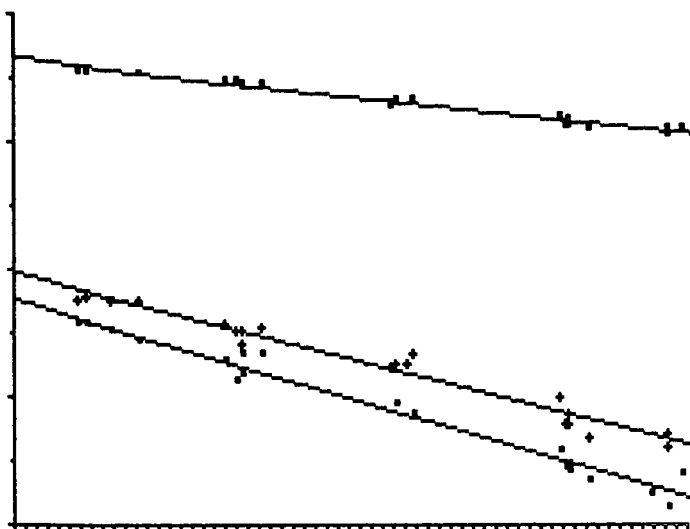


FIGURE 4. ARRHENIUS PLOT OF FLUIDITY CHARACTERISTICS OF COAL #41. Horizontal: $1000/K$, scale 1.40 to 1.46 ($441-412^{\circ}\text{C}$). Vertical: $\ln(\text{function})$, scale -1.5 to $+2.5$. From top to bottom: $\ln(\text{maximum fluidity})$, melting slope, coking slope.

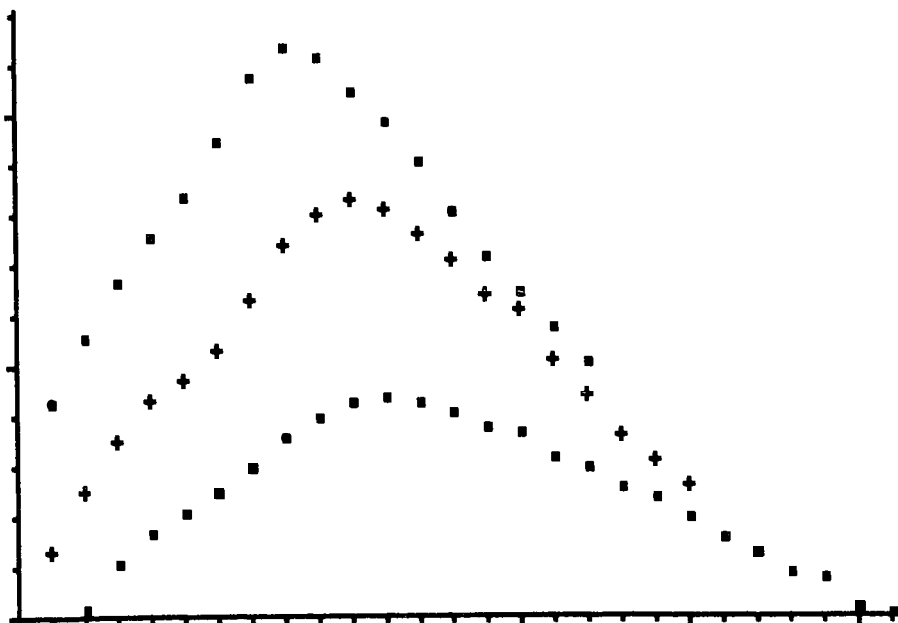


FIGURE 3. ISOTHERMAL PLASTOMETRY OF COAL #41 AT 431 , 424 AND 412°C . Horizontal: time in minutes, scale 0 to 26 . Vertical: $\ln(\text{fluidity in ddpm})$, curves offset.

Predictors of Isothermal Fluid Properties of Coals

William G. Lloyd,* John W. Reasoner,* Carol L. Reagles,**
Carol P. Clark,* Jana M. Whitt,* James C. Hower,***
Linda P. Yates,*** and Eileen Davis***

*Department of Chemistry, Western Kentucky University, Bowling Green, KY 42101

**Department of Mathematics, Western Kentucky University, Bowling Green, KY 42101

***Institute for Mining and Minerals Research, University of Kentucky,
Lexington, KY 40506

Fluidity, which typically develops in the range 380-420°C, is a unique property of mid-ranked coals. Coals of similar rank and composition, however, often exhibit Gieseler fluidities differing by several orders of magnitude. The objective of this study is to seek to identify predictively useful correlations between other well-defined parameters and the fluid properties of hvb coals.

In the standard Gieseler plastometer analysis (1) the coal is heated at a constant 3 deg C/min throughout the run. There are, however, several advantages to be gained by operating the plastometer in an isothermal mode, among them the more accurate determination of melting and coking slopes and the determination of the activation energies associated with these slopes and with maximum fluidities (2). In this study we use the isothermal fluid characteristics of a group of hvb coals as the dependent variables. We will examine a number of standard and nonstandard characterizations of coals for their predictive power with regard to these fluid properties.

Twenty-nine coal samples were collected from eastern mid-continent seams (mostly from western Kentucky), from active mines and from coal cleaning plants using freshly mined coal of known local origin. To minimize adventitious weathering of the samples, all coals were reduced, split and stored in sealed heavy plastic under inert gas at freezer temperatures prior to testing. The proximate, ultimate and short petrographic characterizations are given in Table 1. More detailed source information is available elsewhere (3).

For each of these coals a number of isothermal Gieseler determinations (at least 18) has been made. Both melting and coking slopes follow Arrhenius dependencies (2,4), as do $\ln(\text{maximum observed fluidity})$ and $\ln(\text{intersection maximum fluidity})$ (2). For direct coal-to-coal comparison it is convenient to make an interpolation or short extrapolation of temperature to a benchmark value such as 400°C. Table 2 summarizes the fluidity characteristics of these coals, with slope and fluidity data estimated for 380, 400 and 420°C. The maximum Gieseler fluidities (by slope intersection) of these coals cover a wide range, ranging at 400°C from 62,300 ddpm (coal 25) to 1.8 ddpm (coal 28).

In addition to the characterization data summarized in Table 1, several nonstandard measurements have been made. These are described below.

When small portions (3-5 mg) of coal are pyrolyzed at a high ramp (500 deg C/sec) and low ceiling temperature (450°C) onto a nonpolar chromatographic column, the resulting chromatogram provides information in two distinct regions, a gaseous product mixture which quickly elutes from a 50 cm silicone (OV 101) column at 60°C, and a larger vapor product mixture eluting at 200-250°C. A standard pyrolysis/GC procedure has been developed (5), wherein the integrator signals in several one-minute windows are found to correlate significantly with observed fluid properties. This is a reasonably reproducible procedure, with standard deviations

(quadruplicate analyses) averaging 6.5% of the total integrator signal per microgram coal.

Total organic material extractable by refluxing tetrahydrofuran (THF) and refluxing N,N-dimethylformamide (DMF) has been determined for all coals by Soxhlet extraction in triplicate. The average amount extracted by THF (dry ash-included basis) is 14.3%, average standard deviation 0.29%. The average amount extracted by DMF (same basis) is 25.1%, average standard deviation 0.85%. It is necessary to heat residues to 150°C under 1 torr in order to obtain complete desorption of the nitrogen base (6).

Two other kinds of data were obtained and found to have no predictive value with regard to plasticity. If fluid properties were related to low covalent crosslink densities, then the swelling (7,8) of DMF extraction residues by cold DMF might be expected to correlate with fluidities. Residues from four coals were swelled to equilibrium by direct contact with liquid solvent in a simple apparatus adapted from Larsen (7). The four coals had ASTM maximum fluidities ranging from 35 to over 30,000 ddpn. The swelling ratios were all between 2.1 and 2.5, with the most fluid coal having one of the lower swelling ratios. This observation seems to rule out the possibility that fluidity differences among hvb coals arise from differences in covalent crosslink densities.

The second experiment productive of negative results was that of FTIR examination of selected coals and their THF extracts, using the procedure described by Painter (9,10) and the H(aromatic)/H(aliphatic) ratio technique of Solomon (11). Two low-fluidity coals, 03 and 24, and two highly fluid coals, 22 and 34, were compared. The aromatic/aliphatic ratios are slightly different for the raw coals (0.43 and 0.45 for the low-fluidity coals and 0.47 and 0.49 for the high-fluidity coals), and are identical for the THF extracts (0.33 for all four coal extracts). This appears to rule out the view that variations in fluid behavior reflect substantial variations in the chemical characteristics of the sol fractions.

The following 'independent' variables were collected for first-round prediction testing:

- 16 classical characterizations, including seven petrographic measurements;

- 6 semistandard characterizations (ash sulfate, organic and pyritic sulfur, aliphatic/aromatic ratio, and DMF and THF extractables);

- 25 measures (with considerable redundancy) of the pyrolysis/GC chromatograms; and

- 9 sets of values derived from the above (five estimates of reactive macerals, 2 estimates of H/C ratio, an empirical formula for estimating liquefaction reactivity from % hydrogen and organic sulfur, and an estimate of extractable 'preasphaltenes' as [DMF-THF]).

These parameters were examined separately by simple linear regression, using the SAS (12) R-square test, to reduce the candidate independent variables to a manageable number. The number of variables was reduced to 13, using two criteria. A candidate variable is rejected if the fraction of the total sums of squares accounted for by a simple linear regression using the candidate variable is less than 0.1, and/or the variable is redundant with another variable which has stronger predictive power. (For example, pyritic sulfur is less predictive than total sulfur, and with total sulfur present in the analysis pyritic sulfur does not

provide sufficient additional predictivity.) The variables surviving this screening are shown in Table 3.

The best single predictor of fluidity at 400-420°C is the 4-5 min pyrolysis/GC signal (the gas signal from fast pyrolysis to 450°C), which affords correlation coefficients of .850 at 420 and .867 at 400°C. In the absence of pyrolysis/GC data the next best predictor is total DMF-extractables, affording correlation coefficients of .851 at 420 and .812 at 400°C.

The expansion of the regression equation to include additional independent variables always increases the goodness of fit. After the third variable is added, however, improvement in the correlation coefficient R becomes quite small. In predicting ln(maximum intersection fluidity) at 400°C, for instance, the values of R with the successive addition of the 4-5 min pyrolysis/GC signal, vitrinite reflectance, THF-extractables and total sulfur are .867, .895, .920 and .935. When pyrolysis data are excluded, the successive inclusion of DMF-extractables, vitrinite reflectance, THF-extractables and % resinite yields R values of .812, .856, .890 and .901. In these and other cases the improvement obtained by adding the fourth predictive variable is of marginal statistical significance. The following observations are based upon the most consistent three-variable regressions provided by this database.

When only classical and petrographic data are available the best three-term linear regressions provide fits with R in the vicinity of 0.7-0.8 (Table 4). This is illustrated by the regression plot for ln(maximum intersection fluidity) at 400°C (Figure 1). The variables used here are heating value, total sulfur, and maximum vitrinite reflectance.

With the addition of quantitative Soxhlet extraction data, a regression on the same fluidity data using vitrinite reflectance, THF-extractables and DMF-extractables provides a reasonably good fit (Figure 2), with R = .890.

With the further addition of the pyrolysis/GC data, inclusion of the 4-5 min pyrolysis signal, along with vitrinite reflectance and THF-extractables, provides a still better fit (Figure 3), with R = .920. The predictions at 420°C are comparably good (Table 4).

An important test for the adequacy of any predictive model is the examination of residuals for possible patterning. A plot of the residuals from the regression of Figure 3 is shown in Figure 4. The substantially random distribution of these residuals suggests that most of the data scatter of Figure 3 represents random error (sample inhomogeneity and errors of sampling, analysis, and possibly adventitious sample ageing during the various analyses).

Discussion.

It has not proven to be possible to predict fluid properties of coals on the basis of a single chemical or petrographic characterization. Even solvent extraction with pyridine or quinoline (13) appears to be little more than roughly indicative. In the present study DMF-extractables constitute an approximate predictor ($R > 0.8$), and a part of the 450° pyrolysis gas signal is a slightly better predictor.

The above data (Table 4) show reasonably good prediction (R 's > 0.9) of maximum fluidity and melting and coking slopes by multiple linear regression equations using three predictive variables. The data fits are not quite as good when pyrolysis or extraction data are excluded. The correlation coefficient falls to 0.85 when both pyrolysis and extraction data are excluded (Figure 1).

The measurements with the greatest significance for our data are the 4-min. pyrolysis/GC signal (or other nearly equivalent pyrolysis data), THF-extractables, DMF-extractables, heating value and vitrinite reflectance. Increases in the values of any of the first four correlate with increasing the melting slope; increasing reflectance makes little change in melting slope but diminishes the coking slope. Increases in any of these variables correlate with increased maximum fluidity.

The relative importance of predictive variables varies with the situation. DMF-extractables is a considerably better single predictor than THF-extractables; yet in most multivariate cases THF-extractables make a larger Type IV contribution to regression sums of squares than do the DMF data. It is tentatively suggested that the DMF data are partially redundant with the pyrolysis data. We are not yet able to offer a specific mechanistic interpretation of these observations.

After examination of a number of expressions containing predictors raised to other than the first power, and a number of expressions with cross-terms containing products of two predictors, the simple first-order linear equations of Table 4 seem to be as good as any. We are continuing to apply factor analysis to these data, with the objective of characterizing more clearly the underlying physicochemical features controlling fluid behavior in coals.

This work is part of a larger study of coal plasticity, for which we acknowledge with thanks the support of the U.S. Department of Energy (3).

References

1. ASTM Method D 2639, Amer. Soc. for Testing and Materials, Phila., PA, 1982.
2. W. G. Lloyd, J. W. Reasoner, J. C. Hower and L. P. Yates, Amer. Chem. Soc., Divn. Fuel Chem., preceding paper.
3. W. G. Lloyd, J. W. Reasoner, J. C. Hower, L. P. Yates, C. P. Clark, E. Davis, A. Fitzpatrick, S. Irefin, A. Jimenez, T. McC. Jones, C. L. Reagles, L. P. Sturgeon, J. M. Whitt and G. Wild, 'Predictors of Plasticity in Bituminous Coals', Final Techn. Rept., U. S. Dept. of Energy Contract DE-FG22-81PC40793, January 1984.
4. W. G. Lloyd, H. E. Francis, M. R. Yewell, Jr., R. O. Kushida and V. D. Sankur, Amer. Chem. Soc., Divn. Fuel Chem. Preprints, 25, no. 2, 128 (1980).
5. J. W. Reasoner, J. C. Hower, L. P. Yates and W. G. Lloyd, submitted to Fuel.
6. A. W. Fort (Univ. of Kentucky), private communication.
7. J. W. Larsen, 'Coal Structure and Reactivity', USDOE Contractors' Conf., Pittsburgh, PA, Oct. 1982.
8. N. A. Peppas, L. M. Lucht, M. E. Hill-Lievense and D. T. Hooker, II, 'Macromolecular Structural Changes in Bituminous Coals during Extraction and Solubilization', Final Techn. Rept., U. S. Dept. of Energy Contract DE-FG22-80PC30222, August 1983.
9. P. C. Painter, R. W. Snyder, M. Starsinic, M. M. Coleman, D. W. Kuehn and A. A. Davis, Appl. Spectroscopy, 35, 475 (1981).
10. P. C. Painter, R. W. Snyder, M. Starsinic, M. M. Coleman, D. W. Kuehn and A. A. Davis, 'Coal and Coal Products: Analytical Characterization Techniques', in E. L. Fuller, ed., ACS Symp. Ser. 205, Amer. Chem. Soc., Washington, DC, 1982.
11. P. R. Solomon, Amer. Chem. Soc., Divn. Fuel Chem. Preprints, 24, no. 3, 184 (1979).
12. Statistical Analysis System, SAS Institute, Inc., Cary, NC.
13. K. Ouchi, K. Tanimoto, M. Makube and H. Itoh, Fuel, 62, 1227 (1983).

Table 1¹

coal	rank	moist.	ash	VM	%C	%H	%N	%S	pyrS	orgS	Btu	FSI	vit ²	lip ³	min ⁴	refl ⁵
02	hvBb	7.86	10.77	42.6	71.67	5.05	1.62	3.41	1.43	1.96	12620	4.5	66.4	7.2	13.5	0.42
03	hvBb	6.75	5.40	41.6	77.60	5.38	1.60	2.02	0.98	1.02	13720	4.5	85.2	5.0	7.0	0.70
04	hvBb	5.33	6.44	46.8	76.48	5.37	1.60	3.29	2.22	0.92	13650	3.5	74.4	7.6	8.8	0.59
06	hvBb	5.02	7.86	44.5	72.19	5.09	1.11	3.68	1.38	2.27	13300	6	78.4	4.2	10.5	0.57
07	hvBb	5.21	6.48	44.8	76.46	4.78	1.04	3.20	1.08	2.08	13590	3.5	81.9	2.7	8.8	0.60
09	hvBb	7.76	8.79	41.4	73.16	5.43	1.52	3.13	1.25	1.99	13050	4.5	75.4	4.2	11.6	0.58
10	hvBb	6.32	8.49	41.7	75.08	4.30	1.13	3.14	1.18	1.85	13330	4	75.5	2.8	10.9	0.57
11	hvBb	5.94	17.71	38.4	63.32	4.61	1.25	3.40	1.61	1.63	11770	2.5	69.7	3.2	21.0	0.56
14	hvBb	6.70	7.60	41.1	74.12	5.21	1.35	2.75	0.93	1.76	13410	4	79.1	3.1	9.7	0.54
15	hvBb	6.31	10.38	41.3	73.18	5.47	1.54	3.77	1.62	2.10	12850	4.5	71.7	3.7	13.3	0.61
18	hvBb	7.09	8.36	40.6	74.08	5.11	1.50	3.59	1.47	1.86	13020	4.5	77.3	3.9	11.0	0.54
20	hvBb	7.77	9.70	43.5	74.06	5.28	1.22	2.92	0.92	1.71	12910	5	79.9	2.9	11.8	0.53
21	hvAb	2.57	8.68	40.3	75.41	5.27	1.07	3.35	1.33	1.93	13540	8.5	75.5	4.3	11.2	0.71
22	hvAb	2.45	9.60	39.4	75.98	5.42	1.44	2.91	1.45	1.35	13490	8	76.0	3.7	12.0	0.73
24	hvBb	7.87	7.15	42.8	75.68	5.55	1.51	3.56	1.22	2.27	13300	4	80.2	3.2	9.7	0.60
25	hvAb	1.68	6.79	40.2	77.79	5.33	2.04	1.38	0.19	1.17	14250	7	75.7	5.7	8.1	0.87
26	hvAb	2.12	14.20	32.2	69.87	4.43	1.50	2.76	0.48	2.20	12610	7	72.2	2.7	17.3	0.87
27	hvAb	2.86	8.12	40.0	76.18	5.17	1.54	3.53	0.48	2.97	13650	7	71.1	3.6	10.7	0.76
28	hvcB	10.96	8.26	42.2	76.65	5.78	1.58	1.42	0.80	0.59	13240	2.5	69.0	7.8	9.7	0.64
30	hvBb	6.44	8.95	48.7	74.67	5.41	1.54	4.01	1.46	2.23	13010	4.5	68.4	9.6	11.9	0.58
32	hvAb	2.94	7.23	42.8	76.05	5.37	1.65	3.00	0.92	2.05	13730	5	78.5	3.1	9.5	0.65
34	hvAb	2.28	8.03	41.0	74.36	5.25	1.45	2.77	1.08	1.67	13670	6.5	80.5	3.9	10.2	0.69
35	hvBb	6.59	10.61	39.3	73.77	5.10	1.25	4.06	2.05	1.91	12775	6	77.5	2.7	13.7	0.58
36	hvBb	7.00	12.58	38.2	70.38	4.91	1.29	4.06	2.22	1.72	12470	4.5	76.2	2.5	15.8	0.58
37	hvAb	3.30	12.48	37.2	72.88	4.91	1.53	2.90	1.70	1.16	12740	4.5	75.3	2.4	15.1	0.66
38	hvBb	9.89	3.41	40.5	81.75	5.64	1.65	0.83	--	--	14170	3	76.7	8.4	3.9	0.67
39	hvBb	7.63	13.41	38.5	70.57	5.12	1.56	1.91	--	--	12530	3	72.2	7.6	15.6	0.65
40	hvBb	9.29	3.75	39.6	81.33	5.68	1.73	0.80	--	--	14150	2.5	80.1	7.9	4.6	0.70
41	hvBb	7.78	2.77	42.1	80.73	5.74	1.61	1.06	--	--	14280	3	85.7	7.2	3.3	0.67

¹ Moisture is as determined; other analyses are on a dry ash-included basis. ² Vitrinite and pseudovitrinite.

³ Exinite and resinite. ⁴ Mineral matter content by Parr procedure. ⁵ Vitrinite maximum reflectance in oil at 546 nm.

Table 2

coal	exptl T range, °C	melting slope, min ⁻¹		coking slope, min ⁻¹		ln(max observed fluidity) ¹		ln(max intersection flu) ¹	
		@380°	@400°	@380°	@400°	@380°	@400°	@380°	@400°
25	404-420°	0.246	0.631	1.535	0.379	1.05	2.76	9.52	9.93
34	390-409	0.371	1.232	3.823	0.653	1.74	4.36	8.24	9.74
32	389-411	0.392	1.187	3.373	0.797	2.06	5.06	5.56	8.40
27	379-404	0.197	0.875	3.564	0.565	1.53	3.91	4.37	8.43
21	387-410	0.340	1.023	2.885	0.567	1.79	5.26	4.84	8.11
22	389-413	0.193	0.702	2.375	0.429	1.31	3.74	4.05	6.71
35	400-419	0.263	0.656	1.551	0.912	2.45	6.24	3.63	5.87
06	393-418	0.156	0.518	1.606	0.620	2.05	6.34	2.96	5.67
07	404-426	0.219	0.505	1.109	0.614	2.06	6.45	2.58	4.43
37	406-432	0.179	0.431	0.986	0.648	1.95	5.49	1.98	3.40
36	404-425	0.140	0.382	0.982	0.829	2.40	6.56	2.00	3.46
14	398-422	0.215	0.466	0.966	0.942	2.73	7.45	1.61	3.03
15	400-427	0.137	0.350	0.844	1.02	2.76	7.06	2.10	3.47
41	412-438	0.088	0.240	0.616	0.435	1.41	4.29	1.95	3.20
04	406-431	0.070	0.252	0.842	0.475	1.68	5.54	1.33	2.84
39	410-435	0.101	0.267	0.667	0.565	1.67	4.60	1.74	3.03
26	412-436	0.113	0.280	0.661	0.363	1.09	3.04	1.18	2.23
38	411-436	0.044	0.155	0.505	0.341	1.19	3.85	1.49	2.70
40	417-443	0.278	0.424	0.631	0.587	1.61	4.18	0.476	1.09
20	401-428	0.221	0.420	0.769	0.993	2.72	7.04	0.616	1.61
10	403-429	0.222	0.442	0.846	0.588	2.14	7.23	0.651	1.57
30	399-426	0.191	0.400	0.803	0.965	2.67	6.94	0.287	0.967
18	398-424	0.195	0.396	0.773	0.889	2.70	7.67	0.428	1.26
24	403-431	0.282	0.435	0.653	1.09	2.84	7.01	0.394	0.916
11	412-432	0.286	0.493	0.824	0.486	1.79	6.11	0.631	1.28
09	403-427	0.174	0.352	0.683	0.592	2.07	6.71	0.252	0.813
03	408-433	0.092	0.235	0.569	0.368	1.36	4.67	0.273	0.704
02	406-423	0.176	0.316	0.546	0.611	2.21	7.39	0.380	0.852
28	413-437	0.201	0.394	0.743	0.123	0.670	3.29	0.160	0.339

¹ Activation energy in kcal. The average standard deviation of E(a) of 1.9 kcal.

Table 3
Variables Retained for Multiple Linear Regression Analysis

<u>Class:</u>		<u>R² in simple regression*</u>
Classical	FSI	.260
	BTU	.122
	% Sulfur	.031 ¹
Petrographic	Exinite	.128
	Resinite	.105
	Pseudovitrinite	.290
	Max Vitrinite Reflectance	.246
Extraction	DMF-extractables	.554
	THF-extractables	.199
Pyrolysis/GC	4-5 min signal % ²	.595
	2-5 min signal counts ²	.572
	14-16 min signal counts ³	.572
	13-17 min window counts ³	.565

* Averages for six estimates: max observed fluidity at 400° and 420°, and E(act), and max intersection fluidity at 400° and 420°, and E(act).

¹ Retained owing to good predictive power for coking slopes.

² The 4-5 min signal % and 2-5 min signal counts are substantially redundant.

³ The 14-16 min and 13-17 min signal counts are substantially redundant.

Table 4
Best-fit Three-value Multiple Linear Regression Equations

<u>Equation¹</u>	<u>Corr. coeff.</u>
<u>CLASSICAL AND PETROGRAPHIC DATA ONLY:</u>	
MELT400 = -1.128 +1.309E-4 * BTU -8.857E-2 * EXIN +2.531E-1 * RESI	.785
MELT420 = -5.986 +5.793E-4 * BTU -2.758E-1 * EXIN +6.919E-1 * RESI	.692
COKE400 = +0.078 +1.582E-5 * BTU +3.356E-2 * SULF -3.018E-1 * REFL	.806 ²
COKE420 = +0.757 +2.401E-5 * BTU +6.273E-2 * SULF -1.103E0 * REFL	.913 ²
FCAL400 = -44.32 +2.419E-3 * BTU +1.815E0 * SULF +1.789E+1 * REFL	.721
FCAL420 = -54.54 +3.101E-3 * BTU +2.643E0 * SULF +1.962E+1 * REFL	.723
<u>WITH EXTRACTION AND PYROLYSIS/GC DATA AVAILABLE:</u>	
MELT400 = -0.311 +1.224E-1 * RESI +3.168E-2 * THF +3.287E-1 * PYR4	.906
MELT420 = -1.369 +2.388E-1 * RESI +1.025E-1 * THF +1.285E0 * PYR4	.904
FCAL400 = -9.998 +1.102E+1 * REFL +3.374E-1 * THF +3.369E0 * PYR4	.920
FCAL420 = -11.59 +1.134E+1 * REFL +5.767E-1 * THF +3.731E0 * PYR4	.912

¹ Abbreviations: MELT400 and MELT420 - melting slopes at 400° and 420°C; COKE400 and COKE420 - coking slopes at 400° and 420°C; FCAL400 and FCAL420 - ln(intersection maximum fluidity) at 400° and 420°C; BTU - heating value; EXI - % exinite; REFL - % maximum vitrinite reflectance; RESI - % resinite; SULF - % sulfur; THF - % extractable by THF. ² Best three-variable fit.

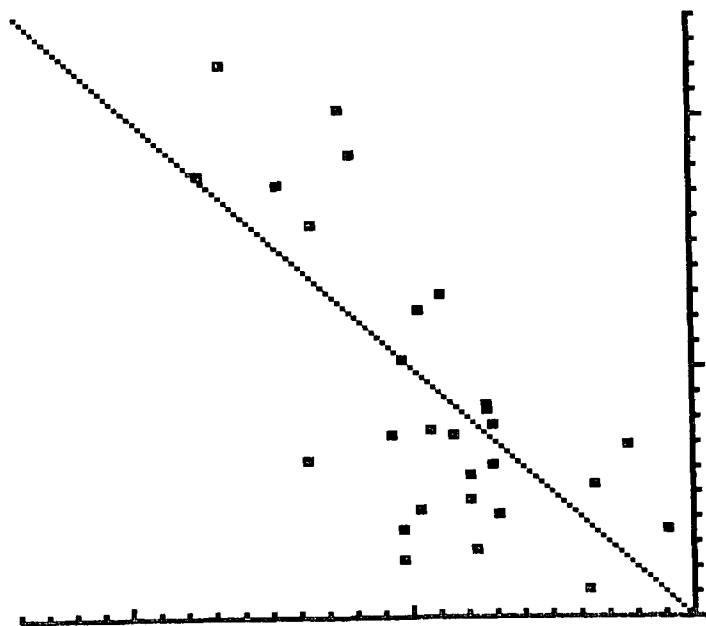


FIGURE 1. PREDICTION OF LN(MAXIMUM FLUIDITY) AT 400°C, EXCLUDING EXTRACTION AND PYROLYSIS DATA. Horizontal: $\ln(\text{observed dpm})$. Vertical: $\ln(\text{predicted dpm})$. Both scales 0 to 12. Independent variables: heating value, total sulfur, maximum vitrinite reflectance. $R^2 = .320$ (29 coals).

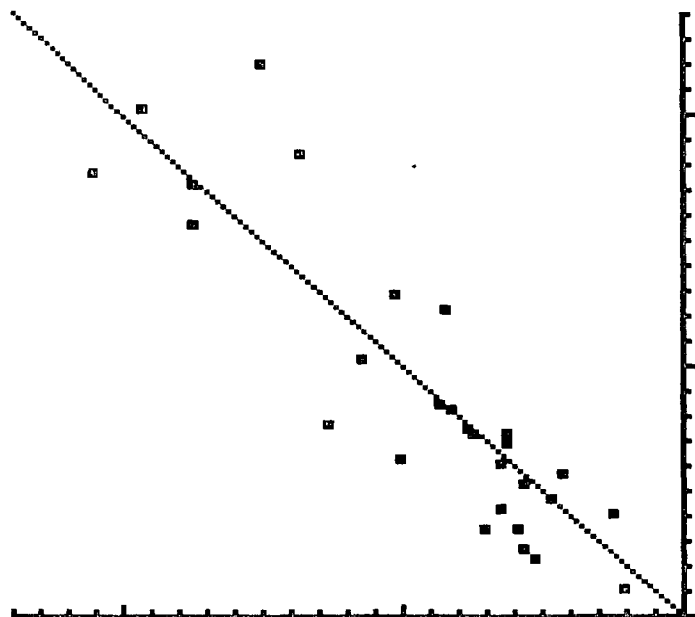


FIGURE 2. PREDICTION OF LN(MAXIMUM FLUIDITY) AT 400°C, INCLUDING EXTRACTION DATA. Horizontal: $\ln(\text{observed dpm})$. Vertical: $\ln(\text{predicted dpm})$. Both scales 0 to 12. Independent variables: maximum vitrinite reflectance, DMF-extractables, THF-extractables. $R^2 = .792$ (29 coals).

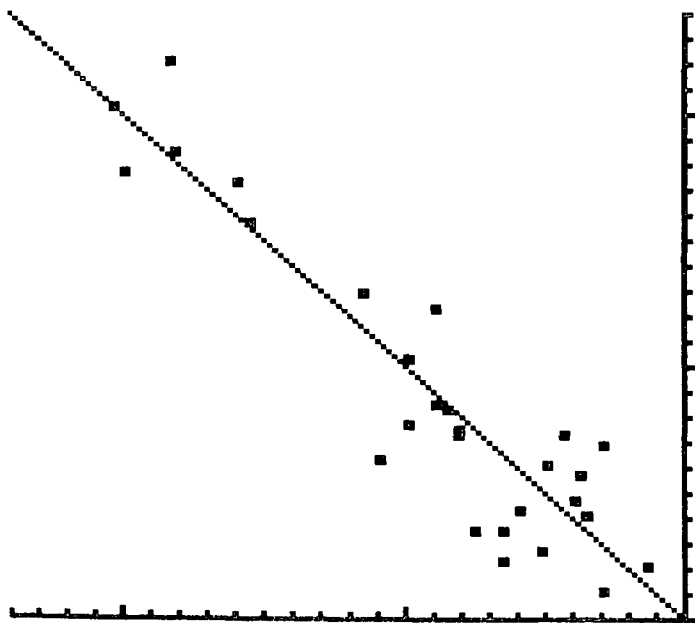


FIGURE 3. PREDICTION OF LN(MAXIMUM FLUIDITY) AT 400°C, INCLUDING PYROLYSIS DATA. Horizontal: $\ln(\text{observed ddpm})$. Vertical: $\ln(\text{predicted ddpm})$. Both scales 0 to 12. Independent variables: maximum vitrinite reflectance, THF-extractables, 4-5 min pyrolysis/GC signal. $R^2 = .847$ (29 coals).

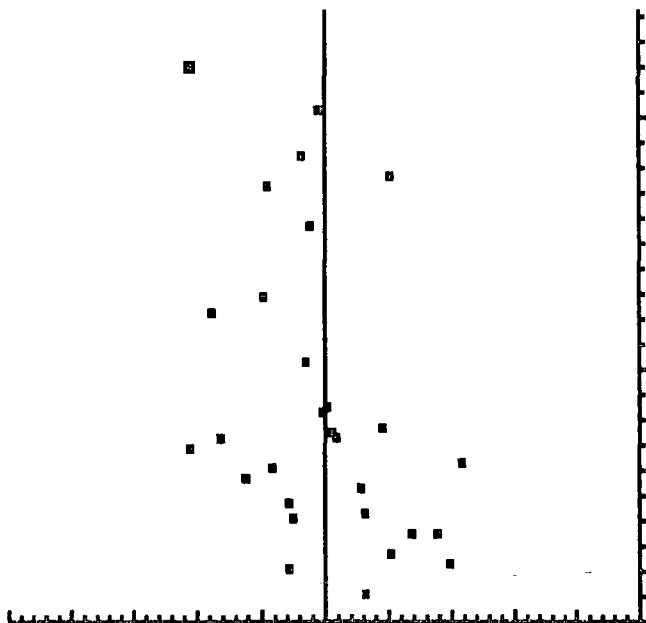


FIGURE 4. ANALYSIS OF RESIDUALS IN THE REGRESSION OF FIGURE 3. Horizontal: $\ln(\text{observed fluidity, ddpm})$, scale 0 to 12. Vertical: residuals from regression [observed - predicted], scale -5 to +5.

VISCOELASTIC PROPERTIES OF BITUMINOUS COALS

John M. Howell and Nikolaos A. Peppas¹

School of Chemical Engineering
Purdue University
West Lafayette, Indiana 47907

INTRODUCTION

The study of the swelling and thermal behavior of coals and the implications these have on possible coal structures are of increasing interest as industrial processes are developed for coal utilization (liquifaction and gasification). Developing accurate structural models and appropriate relations to predict the swelling and thermal behavior of coals would greatly aid plant design by enabling engineers to estimate reaction kinetics and mechanisms for reactions.

It is useful to consider coal as a crosslinked macromolecular network when explaining its swelling and thermal behavior. A crosslinked structure such as that illustrated in Figure 1 has been proposed by Lucht and Peppas [1]. This type of model is in agreement with current experimental findings and is applied in the analysis of experimental results.

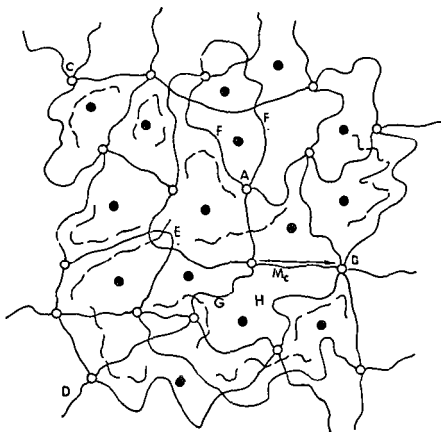


Figure 1. Simplified representation of the crosslinked structure of coal including possible defects. —: Chains participating in network structure; - - - - -: extractable (unreacted or degraded) chains; O : crosslinks (junctions); ● : molecules of swelling agent; M_c : molecular weight between crosslinks; A: tetra-functional crosslink; B: multifunctional crosslink; C: unreacted functionalities; D: chain end; E: entanglement; F: chain loop; G: effective network chain; H: mesh size.

Chemical and Physical Structure of Coal

Interpreting the physical structure of macromolecular chains in coal with cross-linked macromolecular network models and theories has become increasingly common in the recent past, although such models have existed for over twenty years [2]. If mineral matter, ash and other impurities naturally occurring in coal are excluded,

1. Corresponding author

coal structures can be described by two distinct phases. The first phase consists of small and large molecules which are uncrosslinked and occupy a substantial portion of the whole coal sample. These macromolecular chains can be intact uncrosslinked molecules formed during diagenesis [3], or somewhat degraded chains formed by depolymerization reactions during the metamorphic stage of coal development. The primary phase of the coal structure consists of a highly crosslinked macromolecular phase forming a crosslinked three-dimensional network (coal matrix) [1]. This is the structure shown in Figure 1, which depicts several forms of macromolecular chains and possible chain defects.

The crosslinked structure cannot be extracted or dissolved at low temperatures (unless the solvent acts by combined diffusion and reaction, as in depolymerization), and is characterized by both physical and chemical crosslinks. Physical crosslinks are found in highly entangled macromolecular chains that, because of inherent rigidity, have restricted mobility. In this case, disentanglement is not likely. Chemical crosslinks are formed by chemical reactions between two or more coal chains, which lead to multifunctional crosslinks.

Coal researchers have considered models of various "reconstructed" chemical structures of coal as a means to support their theories [3]. But model networks such as those proposed by Wiser and Given are only indicative of the type of chemical crosslinks one would expect in coal, and are not proof of the physical structure of coal or the size of macromolecular chains between crosslinks. Chain ends, unreacted functionalities, chain loops and multifunctional crosslinks are types of defects which make an accurate analysis of the coal network unlikely.

The nature of the crosslinks in coal is a point of scientific dispute. Most of the work on identifying coal crosslinks relies on analysis of the products of depolymerization and degradation reactions. Because the system is complex and strong intermolecular interactions occur, analyzing the results is difficult, often leading only to speculations about chemical structure [3,4].

A promising analytical technique for degradation products (coal liquids) is based on mass-analyzed ion kinetic energy spectrometry. Other techniques have been used including elemental analysis and identification of decomposition and extraction products from coal, IR spectroscopy, high resolution NMR, and GC/mass spectroscopy. These results have given us a clearer understanding of the types of chemical bonds involved in crosslinking.

Viscoelastic Properties of Coal

One aspect of the macromolecular coal structure which has been given very little attention upto now is its viscoelastic behavior. It is in general known that coal at high temperatures, close to the liquefaction temperature of 300-350°C, softens and behaves as a highly viscous material. Its viscosity becomes dependent on the conditions of application of stress or strain. For example, Nazem [5] studied the non-Newtonian behavior of carbonaceous mesophase pitch at high temperatures using a Haake viscometer and established the non-Newtonian behavior in terms of the viscosity as a function of the shear rate. Briggs [6] investigated the viscosity of coal tar pitch as a function of temperature. Covey and Stanmore [7] attempted to present a constitutive equation for the rheological behavior of Victorian brown coals of Australia.

An alternative approach of investigation of the viscoelastic behavior of coals is through thermal analysis at high temperatures. The early work of Bangham and Franklin [8] established characteristics of the change and expansion of the coal structure at high temperatures. More recently Sanada and Honda [9] used creep deformation experiments of various Japanese coals to establish their mechanical behavior at high temperatures. Finally, Rovenskii and Melnik [10] were the first and probably the only investigators upto now to investigate the use of thermomechanical analysis as a method of characterization of coals.

Here we present new and important information on the results of thermomechanical analysis of some American bituminous coals.

EXPERIMENTAL PART

Previously stored in nitrogen, flat coal samples of the following coals were used in the present studies: PSOC-418 (69.95% C, dmmf basis), PSOC-791 (72.75% C), PSOC-312 (78.33% C), PSOC-853 (80.15% C), PSOC-402 (82.48% C) and PSOC-989 (88.81% C); all obtained from the coal bank of the Pennsylvania State University. All samples had an initial surface area of approximately 2.5 mm^2 . They were tested in a thermo-mechanical analyzer (model TMS-2, Perkin Elmer, Norwalk, Conn.) using the penetration mode of the device, under continuous purging of nitrogen and starting from an initial temperature of 35°C . The tip of the probe was round with a surface area of 0.6207 mm^2 . All samples were tested under the application of loads of 10, 20, 30 and 40 g corresponding to stresses of 0.158, 0.316, 0.474 and 0.632 MPa, respectively. Unless otherwise noted, all studies were performed at a scanning speed of $10^\circ\text{C}/\text{min}$ and upto 350°C . The deformation was determined as a function of time and transform to strain by dividing by the original thickness of the flat samples.

RESULTS AND DISCUSSION

Figures 2 and 3 present the strain versus time curves for two of the samples tested, a PSOC-791 sample with 72.75% C on a dmmf basis and a PSOC-312 sample with 78.33% C. It must be remembered that, since the scanning speed is $10^\circ\text{C}/\text{min}$, the same plots represent the deformation, as designated by the strain, as a function of temperature.

All curves show an early induction period which lasts for approximately 5-10 minutes or $50-100^\circ\text{C}$ and is characteristic of the very slow compressive creep of highly glassy polymeric materials. Indeed for these coals we have determined [11] values of T_g in the range of $300-350^\circ\text{C}$, much higher than the temperatures at the beginning of these experiments. After about 18 to 25 minutes from the beginning of the experiment, corresponding to temperatures of 215°C to 285°C , a plateau is observed in the strain versus time behavior. Further temperature increase leads to considerable increase of the strain probably due, either to yielding of the macromolecular coal structure at temperatures where enough mobility of the macromolecular chains has been attained, or to thermal degradation at these temperatures. However, the second explanation is probably not valid since thermogravimetric

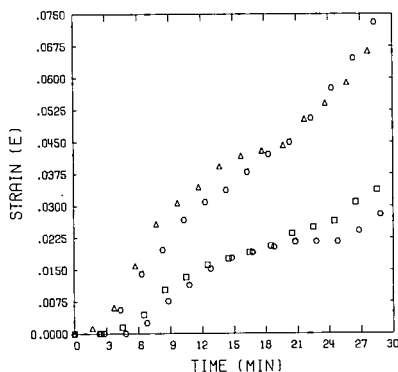


Figure 2: Compressive strain as a function of time for flat coal samples of PSOC-791 (72.75% C, dmmf basis). The results are for applied stresses of 0.158 (○), 0.316 (□), 0.47 (Δ) and 0.632 (◇) MPa.

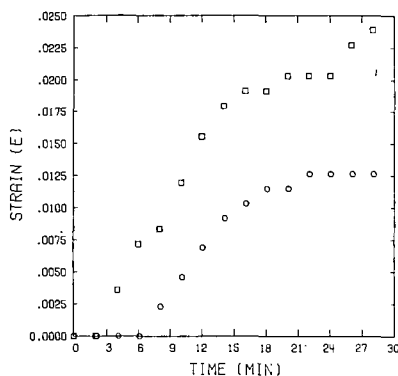


Figure 3: Compressive strain as a function of time for flat coal samples of PSOC-312 (78.33% C). The results are for applied stresses of 0.474 (o) and 0.632 (□) MPa.

analysis experiments under the same scanning speed using a thermogravimetric analyzer (TGS-2, Perkin Elmer, Norwalk, Conn.) showed little measurable weight change of the coal samples up to 250°C.

Figure 2 shows also the general dependence of the strain on stress. Indeed, as the stress increases, the strain is higher and the point of deviation from the original plateau is at lower temperatures (or times), which is characteristic and typical of similar behavior in polymer networks.

Finally, comparison of the data of Figures 2 and 3 at the same stress shows that for the coal samples with the lower carbon content, at the same scanning time the strain is much higher than that of the samples with higher carbon content. This is a clear indication that PSOC-791 is less crosslinked than PSOC-312, a notion which is clearly supported by our recent data on the determination of M_c of these and other coals [12]. Samples PSOC-402 (with 82.48% C) and PSOC-989 (with 88.81% C) were tested not only at these stresses but also at 0.790 and 0.948 MPa. In no cases was any deformation observed, an observation characteristic of very highly crosslinked structures.

Further analysis of these data was achieved by using the Nutting theory, which when applied to creep data, suggests that the creep compliance is logarithmically dependent on time according to equation (1).

$$J = \psi t^n \quad (1)$$

Here J is the coal structure compliance, which is calculated from the previous graphs by dividing the strain by the applied stress, t is the creep time and ψ and n are two constants characteristic of the coal structure.

Figure 4 shows a plot of $\ln J$ versus $\ln t$ for the samples of PSOC-791 plotted earlier. Although one would expect a linear relationship between these two parameters there are some important deviations. For example, the initial portion of the graph, characteristic of the slowly changing induction period could not be represented by the Nutting equation, because of the highly "frozen" structure of the macromolecular network of coal. The region between $\ln t$ of 2 and 3.2 can be reasonably represented by straight lines, which in accordance with Nutting's equation, are parallel for different stresses.

An interesting aspect of these studies is also shown in Figure 5 which presents the insignificant effect of the scanning speed rate on the strain-time behavior. The same figure shows that a continuous increase of the strain is observed even

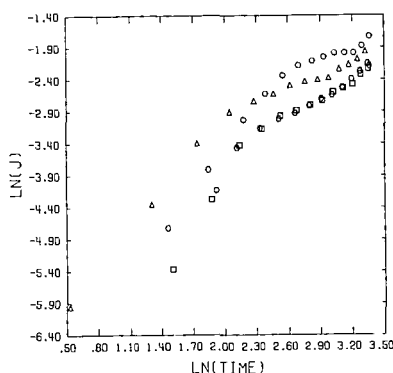


Figure 4: Nutting plot of the compliance of coal structures as a function of time for PSOC-791 (72.75% C). The data are for the same stresses as in Figure 2.

after 60 minutes (at 5°C/min), corresponding to a temperature of 335°C, where the coal "flows" since it is above its T_g.

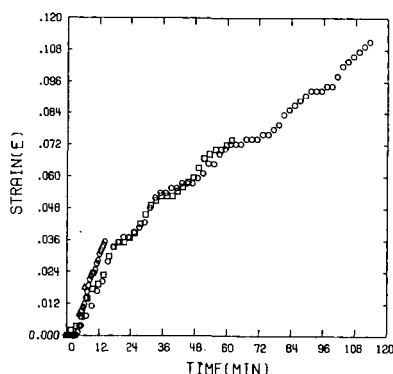


Figure 5: Effect of scanning speed on the strain-time curve. Results for coal PSOC-418 (69.95% C) with 2.5 (○), 5(□), 10 (Δ) and 20 (◇) °C/min.

CONCLUSIONS

These results further support the idea of a highly crosslinked, macromolecular coal network [1], and are indicative of the difficulty by which the thermal degradation occurs.

Aknowledgements

This work was supported by research grant DOE-F6-22-83PC60792 of the Department of Energy, Pittsburgh Energy Technology Center. Helpful discussions with Dr. L.M. Lucht are kindly acknowledged.

REFERENCES

1. L.M. Lucht and N.A. Peppas, in B.R. Cooper and L. Petrakis, eds., "Chemistry

- and Physics of Coal Utilization," 28, American Institute of Physics, New York, N.Y. 1981.
2. L. Lazarov and G. Angelova, Khim. Tverd. Topl., 10(3), 15 (1976).
 3. N. Berkowitz, "An Introduction to Coal Technology," Academic Press, New York, Y.Y., 1979.
 4. J.W. Larsen and E.W. Keummerle, Fuel, 55, 162 (1976).
 5. F.F. Nazem, Fuel, 59, 851 (1980).
 6. D.K.H. Briggs, Fuel, 59, 201 (1980).
 7. G.H. Covey and B.R. Stanmore, Fuel, 59, 124 (1980).
 8. D.H. Bangham and R.E. Franklin, Trans. Faraday Soc., 42B, 289 (1946).
 9. Y. Sanada and H. Honda, Fuel, 42, 479 (1963).
 10. V.I. Rovenskii and N.P. Mel'nik, Khim. Tverd. Topl., 9(4), 36 (1975).
 11. L.M. Lucht, J.M. Larson and N.A. Peppas, Bull. Amer. Phys. Soc., 28, 566 (1983).
 12. L.M. Lucht, Ph.D. Thesis, School of Chemical Engineering, Purdue University, 1983.

THE MOLECULAR WEIGHT BETWEEN CROSSLINKS OF SELECTED AMERICAN COALS

Lucy M. Lucht¹ and Nikolaos A. Peppas²

School of Chemical Engineering
Purdue University
West Lafayette, Indiana 47907

INTRODUCTION

Van Krevelen (1961) and Sanada and Honda (1966, 1967) were the first to propose that the organic portion of bituminous coals can be considered as a "crosslinked polymer" (sic). Since then, Larsen and Kovac (1978), and Lucht and Peppas (1981a) have developed mathematical, topological, and physicochemical models which describe network structure of coals by accurate and physically complete theories.

Lucht and Peppas (1981a) proposed that the organic phase of coal consists of a crosslinked macromolecular structure which does not dissolve at low temperatures unless reaction and degradation occur; and of a portion of uncrosslinked macromolecular chains of predominately aliphatic character, which can be extracted at low or moderate temperatures if an appropriate solvent is used. These uncrosslinked molecules may be material from the original matter formed during diagenesis, or partially degraded chains that were formed through depolymerization reactions during the development of coal. Figure 1 shows a simplified description of the organic phase according to Lucht and Peppas. The same scheme includes not only ideal chemical crosslinks (A,B) but also unreacted functionalities (C), chain ends (D), and various defects of the macromolecular structure such as loops (F) and physical crosslinks (E), known as entanglements. Physical crosslinks occur because the system is highly entangled, that is the chains are rigid and have limited mobility. Hence, they are unlikely to disentangle when stressed or swelled. Chemical crosslinks are formed by chemical reaction of two or more chains to yield a multifunctional crosslink.

The chemical nature of the crosslinks found in coal has not been adequately determined. In the development of mathematical models to describe the behavior of the network, crosslinks are assumed to be points or short bridges with a molecular weight much smaller than M_c . Here M_c refers to the statistical number average molecular weight between crosslinks of the coal structure. Obviously, as M_c increases the degree of crosslinking decreases.

To further simplify the macromolecular structure in order to make it tractable for statistical analysis, Lucht and Peppas (1981b) proposed a crosslinked coal structure, where the crosslinks are bonding regions similar to groups proposed by Wiser (1977) (see Figure 2). Each chain consists of groups of aromatic clusters and connecting bonds. The cluster may be a structure of two or more aromatic or heterocyclic rings fused together, whereas the connecting bonds are simple groups such as -O-, -S-S- and -CH₂-. In addition, the macromolecular chains which constitute a large portion of the coal do not exhibit a repeating unit, as defined in conventional polymers. Thus, coal does not have a "polymer structure" but a macromolecular structure.

The unfortunate use of the term "polymeric structure" by Van Krevelen (1961), has created some confusion, not only among coal scientists, who try to analyze the crosslinked structure, but also among polymer scientists, who try to apply statistical mechanical theories. A hypothetical repeating unit may be defined, solely for purposes of application of topological, statistical mechanical, and swelling theories, for the determination of M_c .

Experimental techniques which support the existence of a crosslinked structure are based on extraction and swelling of the coal sample or coal matrix with thermodynamically "good" solvents such as pyridine and ethylene diamine, and thermodynamically

1. Present address: Lawrence Livermore Laboratory, P.O. Box 808, Livermore, CA 94550.

2. Corresponding author.

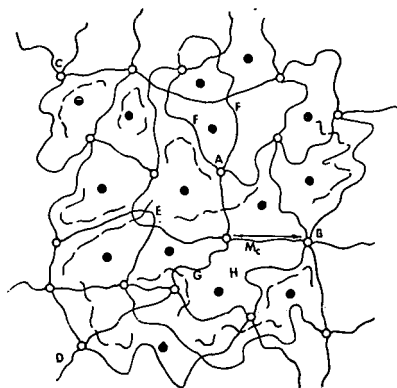
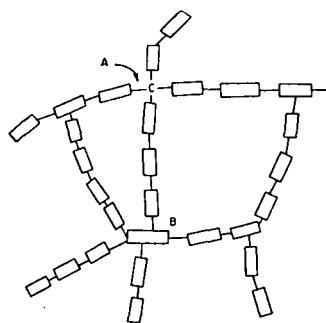


Figure 1. Simplified Representation of the Crosslinked Structure of Coal Including Possible Defects. —: Chains participating in network structure; ----: extractable (unreacted or degraded) chains; o: crosslinks (junctions); •: molecules of swelling agent; \bar{M}_c : molecular weight between crosslinks; A: tetrafunctional crosslink; B: multifunctional crosslink; C: unreacted functionalites; D: chain end; E: entanglement; F: chain loop; G: effective network chain; H: mesh size.



Proposed Crosslinked Structure in Coals.

- Aromatic ring cluster
- Connecting band
- A Tetrafunctional crosslink
- B Multifunctional crosslink

Figure 2. Proposed Crosslinked Structure in Coals According to Lucht and Peppas (1981).

"poor" solvents such as methanol, benzene, ethanol, etc. Most of the studies have been performed using either Soxhlet extraction, or simple or sophisticated dynamic swelling experiments. The term "solvent" is used here interchangeably to describe liquids which dissolve coal, and also liquids which swell it or react with it.

Here we present recent experimental results which characterize the organic phase of coal in terms of parameters of the crosslinked structure.

EXPERIMENTAL PART

Coal samples which had been ground to an average particle size of 20-30 mesh (600-850 μm) and packed under nitrogen were furnished by the coal bank of Pennsylvania State University.

Extraction was used to separate the coal matrix from material which is free or loosely held in the interstices. In a typical extraction, a coal sample of 20-30 mesh particle size and approximately 3 g. was weighed to ± 0.0001 g, and extracted in a Soxhlet apparatus using pyridine (Aldrich) under nitrogen at 115.5°C . The extract solution was replaced every one to four days with fresh pyridine until the extract solution appeared to be pure pyridine (usually one to eight weeks). The extracted residue was dried to constant weight under vacuum at $\text{ca } 60^\circ\text{C}$ and $\text{ca } 0.93$ MPa under flowing nitrogen.

Equilibrium swelling studies were conducted to provide the final values of the equilibrium volume fraction of coal in a solvent-swelled system at a specified swelling temperature. Data were collected via gravimetric sorption studies. Samples were dried at 60° to 80°C under flowing nitrogen at slightly greater than atmospheric pressure for at least 24 hours to remove free surface water. Prewedged samples were exposed to an environment saturated with vapors of pyridine in dessicators at specified temperatures, maintained constant either with a water bath or with a convection oven. The time required for swelling equilibrium was between 5-12 weeks. At the end of the swelling period, the samples were removed and reweighed.

RESULTS AND DISCUSSION

Equilibrium swelling studies provide the final values of the equilibrium volume fraction of coal in a solvent-swelled system, v_2 , at a specified swelling temperature. The degree of swelling, $Q = 1/v_2$, is an indicator of both solvent/coal thermodynamic interactions and of the physicochemical structures of coal. It can be used in any Gaussian or modified Gaussian network equation such as equation (1) to determine \bar{M}_c and other crosslinking parameters. In addition, results can be used to quantify favorable thermodynamic interactions with a solvent for liquefaction purposes.

$$\frac{1}{\bar{M}_c} = \frac{\frac{v}{V_1} [\ln(1 - v_2) + v_2 + \chi v_2^2] [1 - \frac{1}{N} v_2^{2/3}]^3}{[\frac{1}{2} v_2 - v_2^{1/3}] [1 + \frac{1}{N} v_2^{1/3}]^2} \quad (1)$$

Here, \bar{M}_c is the number average molecular weight between crosslinks; v is the specific volume of the macromolecule; V_1 is the molar volume of the swelling agent; v_2 is the volume fraction of the macromolecule in the swollen system; χ is the Flory-Huggins thermodynamic interaction parameter; and N is the number of bond vectors in a single chain, given by equation (2) where M_r is the molecular weight of the characteristic repeating unit.

$$N = \frac{\bar{M}_c}{M_r} \quad (2)$$

Equation (1) was developed specifically for application to the equilibrium solvent swelling of coals. This approach accounts for the finite expansion of solvent-swelled coals by limiting the extensibility of the individual chain. It is therefore more appropriate for determination of the molecular weight between crosslinks, \bar{M}_c , via solvent-swelling studies, than the Flory-Rehner equation, which assumes that the end-to-end distance between chain ends is much less than the contour length of the chain and thus allows a chain to be infinitely extensible.

It must be noted that in our proposed model (Figure 2), a repeating unit consists

of a cluster and a connecting bond. This is a reasonable assumption in view of the comparatively small size of the connecting bond (usually $-\text{CH}_2-$, $-\text{S}-$, or $-\text{O}-$) with respect to the cluster size. The molecular weight of a repeating unit is about 130 for lignites, 170 for bituminous coals up to 86% C (dmmf), and 370 for coals with a higher carbon content.

Pyridine was used as the probe for most experiments because it is one of the few solvents which causes significant swelling in all but the highest rank coals; some researchers (e.g., Marzec *et al.*, 1979) believe that pyridine has a stronger interaction with coal than the extractables and that pyridine may be able to destroy hydrogen-bonding in the coal structure.

Figure 3 is a typical graph of results showing the dependence of the degree of swelling, Q , corrected for mineral matter on carbon content (on a dmmf basis). It was assumed that the organic vapor does not swell clays or metals to a significant degree, so their weight was subtracted from the total. Pyridine vapor swelling was conducted at $35.0 \pm 0.5^\circ\text{C}$ for 60 days to swelling equilibrium and compared with the data obtained, as described above, over 51 days at $60 \pm 0.5^\circ\text{C}$. The degree of swelling is significantly greater at 60°C than at 35°C , although the shapes of the curves are similar. At 35°C , the degree of swelling is constant at $Q = 1.8$ - 2.0 from ca 70% C and up to approximately 86% C, dropping as in the higher temperature case to $Q = 1.1$ at 91% C.

Experimental data were also obtained which show the effect of pyridine pretreatments on the solvent vapor swelling of coals. Equilibrium swelling of these samples was performed at $60 \pm 0.5^\circ\text{C}$ for 51 days and these data are shown in Figure 4. The shape of the curve is similar to that of the unextracted coals swelled by pyridine as shown in Figure 3, although the magnitude of the degree of swelling in the pyridine extracted coals over the carbon content range of 69.94 to 82.48% C (dmmf) is somewhat lower than for the unextracted coals, ranging from $Q = 2.2$ to 2.5 for the pyridine extracted coal samples as compared to $Q = 2.5$ to 2.8 for the untreated coal samples.

ANALYSIS

The modified Gaussian network equation (1) can be applied only to the results of swelling of coal networks which are free of uncrosslinked material, i.e., extractable material. Thus, only the results from the equilibrium swelling of pyridine-extracted coal samples were used in the determination of the molecular weight between crosslinks.

In the determination of the molecular weight between crosslinks, the volume fraction of coal in the pyridine swollen system, $v_2 = 1/Q$, was calculated on a mineral matter free basis, assuming that pores with diameter of greater than 50 Å contained condensed solvent only which did not contribute to swelling. The values of these pore volumes were determined by mercury porosimetry.

The average values of the molecular weight of a hypothetical repeating unit of coal were taken to be 130 for lignite or sub-bituminous coal samples, 170 for bituminous coal samples with carbon contents up to ca 86% C (dmmf), and 370 for all coal samples of rank greater than medium volatile bituminous up to semi-anthracite samples. These values were determined from the present view of the size of the aromatic/hydroaromatic clusters and their crosslinks.

The values of the thermodynamic interaction parameter, χ , for coals with carbon contents of 75.9, 82.4, and 88.2% C (dmmf) were determined by the Hildebrand-Skatchard regular solution theory from the solubility parameters determined by Kirov *et al.*, (1967). The values of the solubility parameter reported in that study were determined at 25°C , while the equilibrium swelling experiments of our work were carried out at 35, 60 and 80°C . Therefore, corrections in the solubility parameter values were made for different temperatures in the following way.

The dependence of the effective number of repeating units between crosslinks, N , on carbon content is shown in Figure 5 while the dependence of the effective molecular weight between crosslinks, \bar{M}_c , on carbon content is shown in Figure 6. Results from equilibrium swelling by pyridine vapor at 35°C of pyridine extracted coals were used in the application of equation (1).

The number of repeating units between crosslinks is relatively constant, ranging from $N = 7.0$ to 8.5 , over the carbon content range of 69.96 to 82.48% C (dmmf). At a carbon content of 86.01% C (dmmf), the value of N drops to 4.6 and continues to decline

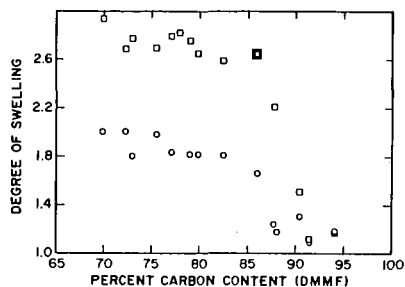


Figure 3. Equilibrium Swelling by Pyridine Vapor of 20-30 mesh, Untreated Coal Particles. (\square) 60°C; (\circ) 35°C.

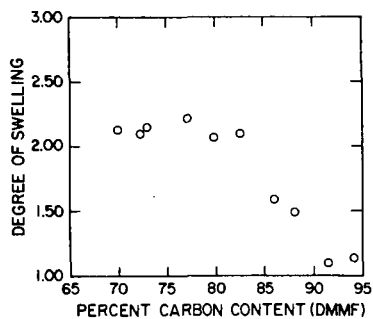


Figure 4. Equilibrium Swelling by Pyridine Vapor of 20-30 mesh, Pyridine-Extracted Coal Particles at 60°C.

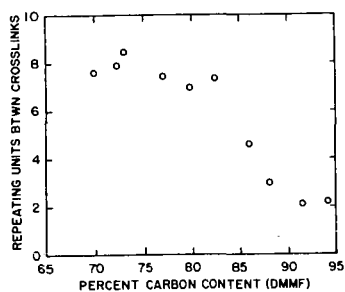


Figure 5. Dependence of Number of Repeating Units Between Crosslinks on Carbon Content of Coal Sample.

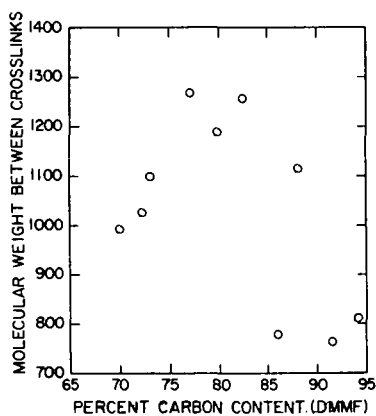


Figure 6. Dependence of Molecular Weight Between Crosslinks on Carbon Content of Coal Sample.

to a value of 2.2 at a carbon content of 91.54%C (dmf).

Nelson (1983) obtained solvent uptake data for methanol vapor into coal over a range of activities of methanol and then applied modification and rearrangements of the Flory-Rehner network swelling equation and of the modified Gaussian network equation (1) to these results. The modification he made was to assume that the swollen coal system was infinitely dilute in coal, and thus the volume fraction of solvent could be approximated as the activity of the solvent. This is obviously an invalid approximation as the volume fraction of coal in a methanol swelled coal system is on the order of 0.7. He also assumed in his determination of the molecular weight between crosslinks that the number of repeating units between crosslinks was about 7. This defeats the purpose of the modified Gaussian equation, which is to elucidate the effective flexibility or number of repeating units between crosslinks. It is the size of the repeating unit which must be known or estimated. The values of the molecular weight between crosslinks determined by Nelson for swelling by methanol were ca 70 and ca 120, using the Flory-Rehner and modified Gaussian equations, respectively.

Equilibrium swelling results of pyridine extracted coals in pyridine liquid at room temperature were obtained by Kirov *et al.* (1967). The research group of Sanada and Honda (1966) performed equilibrium swelling of pyridine extracted coals with pyridine vapor at room temperature. Both groups used their data in the Flory-Rehner Gaussian equation. The results have been recalculated (Larsen and Kovac, 1978; Lucht and Peppas, 1981a) to correct some errors in the initial work of Sanada and Honda and to convert the values of volume between crosslinks determined by Kirov *et al.* to the more commonly used molecular weight between crosslinks.

The values of M_c determined by us from the data of Kirov *et al.* are 2595, 2100 and 940 for coals with carbon content of 75.9, 82.4 and 88.2%C (daf). The magnitude of the values M_c are approximately twice those of our values, which could result from an apparent high degree of swelling due to solvent between particles in the liquid equilibrium swelling procedure used. Our corrected results of the data of Sanada and Honda range from M_c equal to zero (a large negative number) to about 15,000, although many of their values of M_c range from 700 to 2000. The unreasonable values of M_c result from the values they used of the thermodynamic interaction parameter, χ , obtained from the results of osmotic pressure data for pyridine extractables of Wynne-Jones *et al.* (1952). When the value of χ increases for a given set of conditions, the value of M_c will also increase until χ reaches a certain critical value, beyond which the Gaussian and the modified Gaussian equations predict a negative molecular weight between crosslinks. Rephrased, it is impossible to have simultaneously a high degree of swelling and unfavorable interaction between a solvent and the macromolecule being swelled.

REFERENCES

- Kirov, N.Y., J.M. O'Shea and G.D. Sergent, *Fuel*, 46, 415 (1967).
Larsen, J.W. and J. Kovac, in "Organic Chemistry of Coal," J.W. Larsen, ed., p. 36, ACS Symposium Series No. 71, American Chemical Society, Washington, D.C., 1978.
Lucht, L.M. and N.A. Peppas, in "New Approaches in Coal Chemistry," B. Blaustein, B.C. Bocrath and S. Friedman, eds., ACS Symposium Series, American Chemical Society, Washington, D.C., 43, 1981a.
Lucht, L.M., and N.A. Peppas in "Chemistry and Physics of Coal Utilization," B.R. Cooper and L. Petrakis, eds., AIP Conference Proceedings, No. 70, p. 28, American Institute of Physics, New York, N.Y., 1981b.
Marzec, A., M. Juzwa, K. Betlej and M. Sobkowiak, *Fuel Process. Tech.*, 2, 35 (1979).
Nelson, J.R., *Fuel*, 62, 112 (1983).
Sanada, Y. and H. Honda, *Fuel*, 45, 295 (1966).
Sanada, Y. and H. Honda, *Fuel*, 46, 451 (1967).
Van Krevelen, D.W., "Coal", Elsevier Publishing Co., New York, N.Y., 1961.
Wiser, W.H., Proceed. Conf. Scient. Probl. Coal Utiliz., DOE Symp. Series, Morgantown, West Virginia, (1977).

Supported by DOE grants Nos. DE-FG22-80PC30222 and DE-F622-78ET13379, and by the Exxon Education Foundation.

REACTIONS OF THE COAL CLEAVING REAGENT, PYRIDINE HYDRIODIDE,
WITH ETHERS AND ESTERS

David H. Buchanan, A. Mei-Ying Chen and James N. O. Sy

Department of Chemistry, Eastern Illinois University,
Charleston, IL 61920, U.S.A.

INTRODUCTION

Mayo reported(1,2,3) efforts to break cross-links in coal under mild conditions, by treating a toluene insoluble, pyridine soluble (TIPS) fraction of Illinois No.6 coal with pyridine hydriodide (Py-HI) in pyridine, at room temperature, for six days. The hydroxyl content of the product increased, the molecular weight (VPO, GPC) decreased and iodine was incorporated. Lithium iodide in pyridine showed a similar effect. Treatment of TIPS with sodium in liquid ammonia quenched by NH_4Cl also increased the hydroxyl content but the decrease in molecular weight was less than with Py-HI. Treatment of the sodium/ammonia products with Py-HI further reduced the molecular weight. The suggestion is that these reagents are cleaving similar, if not identical, functional groups in coal.

Sodium in liquid ammonia cleaves ethers in coal(4,5), most likely diaryl or aryl-benzyl but not alkyl-aryl or dialkyl ethers, by a radical anion mechanism.(6)

This study was undertaken to determine if ether or ester groups of types which may be present in coal are cleaved by Py-HI or LiI in pyridine, at moderate temperatures, to produce phenols. Py-HBr(7) cleaves alkyl-naphthyl ethers above 230°, but low temperature cleavage reactions with Py-HI have not been reported. Lithium iodide demethylates 2-methoxynaphthalene in refluxing collidine (172°).(8)

Mono-functional ethers or esters treated with Py-HI or LiI in the presence and absence of coal fractions, solvents, sulfides and radical sources are unreactive at low temperatures but alkoxy groups ortho to an aromatic carboxyl group are cleaved.

EXPERIMENTAL

Pyridine hydriodide was prepared in 78% yield by passing HI gas into a dry toluene solution of pyridine and recrystallizing the solid product from methanol. The following compounds were synthesized by standard methods and have physical constants in agreement with literature values: Benzyl phenyl ether (I), 2-naphthyl-methyl-2-naphthyl ether (II), 1-naphthylmethyl-1-naphthyl ether (III), cyclohexyl phenyl ether (IV), phenyl phenethyl ether (V), and 1-naphthyl benzoate (VI). Other model compounds were reagent grade commercial products, checked for purity by HPLC and NMR, and used without further purification.

Pyridine was distilled from barium oxide under nitrogen before use. Reactions were usually conducted on a .1-10 mmole scale (.02-.3M), under nitrogen. Products were isolated from pyridine solutions by quenching with aqueous acid followed by extraction and quantitative analysis using either gas chromatography (12% FFAP column) or HPLC (C₁₈ reverse phase column). The reported yields (or recoveries) are reproducible within ±3% absolute. Fractions of an Illinois No. 5 coal (PSOC-252) from the Penn State Coal Data Bank were isolated by the methods of Mayo. For experiments in which ethers and Py-HI were mixed with coal fractions, an aspirator vacuum was applied and broken with nitrogen several times to speed up the swelling or dissolution of the fraction and diffusion of reagents into the coal network.

REACTIONS WITHOUT SOLVENT

As expected from Royer's work(7), the following compounds were cleaved by excess Py-HI in an evacuated, sealed tube at 210° for 45 hrs: Anisole, (I), (IV), (V) and

methyl benzoate. From the ether reactions, phenol was isolated; from the ester, benzoic acid. Only trace amounts of alkyl iodides were found since they react with HI at 210° to yield the observed hydrocarbons. These results show the ethers to behave normally and also indicate that the reactivity of Py-HI is slightly greater than that of Py-HBr, as expected for cleavage by nucleophilic substitution. At 196° and 25 hours, Py-HI converted 2-methoxy benzoic acid to a complex mixture of products including several ring iodinated species (mass spec).

REACTIONS IN SOLUTION

As expected, 2-naphthylmethyl-2-naphthyl ether (II) is cleaved by refluxing 57% aqueous HI to yield 2-naphthol. However, at temperatures of 50 to 115°, for up to seven days, Py-HI did not cleave the monofunctional aromatic ethers or esters listed in Table 1 in either wet or dry pyridine, acetonitrile or ethanol. The addition of radical initiators, AIBN or benzoyl peroxide, did not produce cleavage, nor did FeS, FeS₂ or FeCl₂ added to mimic mineral matter in coal. Added diphenyl sulfide also had no effect.

Ethers (I) and (II) were mixed with Py-HI and TIPS or extracted coal, in pyridine, under nitrogen for up to seven days at 55 or 115°. No cleavage products were detected by HPLC (2% detection limit) and ether (II) was recovered from the coal in high yield.

HYDROGEN BONDED ETHERS

Recent data from Larsen(9) and Gethner(10) indicate that ether oxygen in coal may already be protonated and perhaps activated toward iodide attack. Larsen showed that all hydroxyl groups in coal can be derivatized with bis(tri-n-butyltin)oxide and that each introduced tin atom is within hydrogen bonding distance of another heteroatom. Elemental composition requires that this atom be oxygen. Gethner's FTIR study of D₂O exchanged coal shows that all phenolic hydroxyl groups in Illinois No.6 coal are hydrogen bonded, suggesting that the geometry seen in Larsen's tin derivative is also present in coal itself.

We propose that these results can be explained by structure (VII) in which ether oxygen within a coal cross-link is hydrogen bonded to a phenolic hydroxyl group which is also covalently linked to part of the network. Such ethers may be activated toward iodide attack in pyridine solution where simple ethers would not react.

If a structure such as (VII) were present in TIPS, would it activate the ether toward cleavage by iodide? To answer this, we used 2-methoxy phenol, 2-phenylmethoxy phenol and several alkoxy substituted benzoic acids as model ethers for reactions with Py-HI, LiI and KI in pyridine, acetonitrile and DMSO and found that both 2-methoxy and 2-ethoxy benzoic acid are cleaved by sources of iodide ion in pyridine at 85-115° to produce salicylic acid. The two phenols and the 4-methoxy and 2-phenoxy benzoic acids are inert under these conditions. Results are summarized in Table 2.

The substituted benzoic acids were chosen as compounds in which the effect of internal hydrogen bonding on ether cleavage could be conveniently tested and these results do not imply that ethers cleaved in coal are ortho to carboxylic acids. These results do show that Py-HI and LiI can cleave alkyl-aryl ethers in pyridine if the ether oxygen can be protonated by intramolecular hydrogen bonding. Intramolecular hydrogen bonding in 2-methoxy benzoic acid has been demonstrated in the concentration range of our experiments, conditions where benzoic and 2-methyl benzoic acids are largely dimeric.(11)

Based on fluorescence studies, Ware and co-workers(12) concluded that the carboxyl proton of 3-hydroxy-2-naphthoic acid hydrogen bonds to added pyridine, in toluene solution, without complete ionization of the O-H bond. This implies that the acid proton is available for activating an adjacent ether, possibly as in structure (VIII).

If structures such as (VIII) are present in pyridine solution, and provide conditions sufficient for cleavage, then the reactions with KI and LiI are rationalized. The failure of 4-methoxy benzoic acid to react suggests that electronic effects through the ring are not responsible for the reactions of the ortho isomers. Although kinetics have not been determined, the reaction order methyl>ethyl>>phenyl is consistent with cleavage via nucleophilic substitution on carbon.

The failure of 2-methoxy phenol and 2-phenylmethoxy phenol to react is a problem, since the hydrogen bond in structures such as (VII) must come from hydroxyl rather than carboxyl to be consistent with Larsen's and Gethner's data. Perhaps the geometry for strong internal hydrogen bonding in the model phenols is not appropriate (five versus six membered ring) or the electronic effect of one oxygen inhibits activation of the adjacent oxygen-carbon bond. Studies of other substituted phenols are currently in progress.

SUMMARY

Pyridine hydriodide and lithium iodide, in pyridine, dealkylate 2-methoxy and 2-ethoxy, but not 4-methoxy benzoic acids at 115°. These results plus the reports of Mayo *et al* (1,2,3) allow, but do not require, the conclusion that iodide reagents cleave ethers in coal. Based upon the behavior of these and other model compounds, we believe that any ethers in coal cleaved by LiI or Py-HI in pyridine must have structures which provide intramolecular hydrogen bonding to the ether oxygen to activate the oxygen-carbon bond toward attack by iodide ion. Gethner's and Larsen's recent results indicate that ethers in coal may meet this requirement.

ACKNOWLEDGEMENTS

Financial support from the Illinois Coal Research Board and the Faculty Research Council of Eastern Illinois University, plus laboratory assistance from Ken Osborne and Alan Wilcox, is gratefully acknowledged.

REFERENCES

1. Mayo, F.R., Buchanan, D.H. and Pavelka, L.A., Fuel Division, Am. Chem. Soc., Preprints, 1980, 25, No. 2, 182
2. Mayo, F.R., Buchanan, D.H., Pavelka, L.A. and Hirschon, A.S., Manuscript submitted to Fuel
3. Mayo, F.R., Hirschon, A.S., Zevely, J.S., Sundback, K., Fuel Division, Am. Chem. Soc., Preprints, 1983, 28, No. 5, 253
4. Lazarov, L. and Angelova, G., Fuel, 1968, 47, 333
5. Alemany, L.B. and Stock, L.M., Fuel, 1981, 60, 1002
6. Burwell, R.L., Chem. Rev., 1954, 54, 615
7. Royer, R., Buisson, J.P. and Demerseman, P., Bull. Soc. Chim. Fr., 1971, 4362
8. Harrison, I.T., Chem Comm., 1969, 616
9. Larsen, J.W., Nadar, P.A., Mohammadi, M. and Montano, P.A., Fuel, 1982, 61, 889
10. Gethner, J.S., Fuel, 1982, 61, 1273
11. Miller, K.J., J. Chem. and Eng. Data, 1976, 21, 308
12. Ware, W.R., Shukla, P.R., Sullivan, P.J. and Bremphis, R.V., J. Chem. Phys., 1971, 55, 4048

Table 1 Starting material recovery from reactions of Py-HI with model ethers or esters

Compound ^a	Solvent	Catalyst	Time	Temp (°C)	% Recovery ^b
I	Py	None, Ext Coal TIPS	5hr-7d	55-80	89-93
I	Py, CH ₃ CN	AIBN, (PhCOO) ₂	1-2d	70-95	87-94
II	Py	FeS, FeS ₂ , Ph ₂ S Ext Coal, H ₂ O, FeCl ₂	3-7d	90-115	94-100
II ^c	Py	None	5d	90	98
II	CH ₃ CN	None	5d	78	94
III	Py	None	3d	115	100
IV, V	CH ₃ CN	None	1, 3d	81	93, 94
VI	Py	None	3d	115	96
Anisole	Py, EtOH	None	5-6hr	Reflux	92-93
Methyl Benzoate	CH ₃ CN	None	10hr	81	93

a Identified in Experimental Section

b No cleavage products detected (<2%)

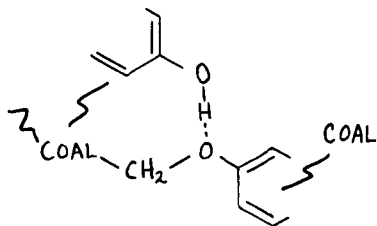
c LiI-H₂O in place of Py-HI

Table 2 Reaction of substituted benzoic acids or phenols with iodide salts

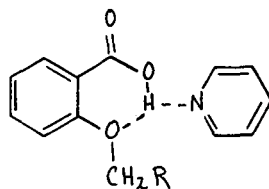
Substituent	Reagent	Solvent	Temp ^a (°C)	% Acid Product	% Ether Recovered
Benzoic Acids					
2-methoxy	Py-HI	Py	85	10	80
2-methoxy	Py-HI	Py	115	81	14
2-methoxy	LiI-H ₂ O	Py	85	54	44
2-methoxy	KI	Py	115	58	33
2-methoxy	Py-HI	CH ₃ CN	75	-- ^b	99
2-methoxy	Py-HI	DMSO	75	--	94
2-ethoxy	Py-HI	Py	115	18	84
2-phenoxy	Py-HI	Py	115	--	100
2-phenoxy	LiI-H ₂ O	Py	90	--	94
4-methoxy	Py-HI	Py	115	--	96
Phenols					
2-methoxy phenol	Py-HI	Py	115	--	100
2-phenylmethoxy phenol	Py-HI	Py	115	--	100

a Reaction time 3 days

b No cleavage products detected (<2%)



Structure (VII)



Structure (VIII)

EXPERIMENTAL AND MODELING STUDIES IN FIXED-BED COAL GASIFICATION

B. Joseph, A. Bhattacharya, L. Salam and M. P. Duduković

Chemical Engineering Department
Washington University
Campus Box 1198
St. Louis, MO 63130

ABSTRACT

A laboratory scale fixed-bed coal gasification reactor was built with the objective of obtaining detailed temperature profiles inside the bed during the gasification process. Such data are needed in validating proposed models for fixed-bed gasification and in the estimation of suitable parameters for use with proposed models. This article describes the experimental setup and presents the results of a run using Wyoming coal. The experimental data are compared with simulation results obtained using a detailed two-dimensional model of the gasifier.

1. INTRODUCTION

Fixed-bed coal gasification is a commercially used technology for reacting coal with steam and oxygen to produce useful gases such as CH_4 , CO , and H_2 . Considerable work has been done lately on modeling of the fixed-bed gasifier. A rather detailed model was presented by Yoon et al. (1). Further improvements on this model have been made by Cho and Joseph (2) and Kim and Joseph (3). It has been difficult to establish the validity of these models fully because of the lack of sufficient operational data on commercial scale gasifiers. The research presented here was undertaken to remedy this situation by developing an experimental procedure for generating data which can be used directly in the verification of proposed models and to determine parameters that are required in the model. The paper contains a detailed description of the apparatus used, the experimental procedure and selected results on gasification of Wyoming coal. The paper also includes a brief sketch of the modeling effort and a comparison between the experimental data and model predictions.

2. DESCRIPTION OF EXPERIMENTAL SETUP

In a commercial scale fixed-bed gasifier, coal is fed continuously at the top at a slow rate while steam and oxygen (or air) is fed at the bottom. The coal undergoes drying and devolatilization at the top of the gasifier and char descends slowly through the reactor. Because the char-bed is moving slowly it is termed as a fixed-bed reactor. For the purposes of this research it was decided that the runs will be conducted on a bed of char which is stationary. Hence it approximates the commercial process with the coal feed cut off. The resulting transient data (since we will have a reaction front moving through the char bed) is then used for validating models of gasifiers.

Figure 1 shows the schematic of the experimental setup. The major pieces of equipment are a steam generator, feed preheater, the tubular reactor, a condenser for removing tars and water, gas chromatograph for product gas analysis and a data acquisition system for monitoring the temperature.

The gasification vessel is a 4 in. diameter, 4 ft. long cylindrical stainless steel tube insulated with refractory and surrounded by a 6 inch diameter stainless steel tube. The vessel can be operated at temperatures as high as 1200°C . This reactor is packed with devolatilized coal. The

devolatilization is carried out separately in another furnace in a nitrogen atmosphere at a temperature of approximately 800°C until no further weight loss occurs. The coal used is in the size range 8 - 20 mesh (2.3 - .833 mm). Each run requires approximately 4 kg of coal. A superficial gas velocity of approximately 1 ft/sec is used in the gasifier.

Figure 2 shows a detail of the gasification reactor. The reactor is designed to operate close to atmospheric pressure. Heat losses are minimized by a refractory lining around the reactor tube and by ceramic beads at both ends of the tube. An ignition coil at the top of the bed is used to start the combustion reaction. Initially the inside liner of the gasifier was constructed with ceramic but it cracked repeatedly due to thermal shock.

The product gases are sent through a condenser and liquid separator to remove water, tar and ash. The remaining gases are flared. A sample is sent through the GC for analysis every 15 minutes.

Temperature profiles in the bed are measured by means of two thermowells inserted axially at $r = 0$ and $r = .36$ cm. Type K (chromel/alumel) thermocouples were used. The thermocouple locations are shown in Figure 2. The data from the thermocouples was collected by means of an LSI/11 microcomputer and stored on tape. This data was then transmitted to a DEC-20 mainframe where the data is analyzed further.

3. EXPERIMENTAL RESULTS

Two successful runs were made using char generated from Wyoming coal. The results of the second run are reported here. The coal analysis is given in Table 1. The operating conditions of the gasifier are reported in Table 2. Note that the air flow had to be decreased after 45 minutes to maintain the maximum temperatures below 1200°C. The run was terminated after 50 minutes. An analysis of the material remaining in the gasifier indicated some unconverted carbon (see Table 2). The bed length was only 12 cm indicating that the ash collapsed.

The results of the run are shown in Figures 3, 4 and 5. Figure 3 shows the temperature profiles of the inner thermocouples. Note that after the temperature has reached a peak, the thermocouple is sitting in a bed of ash and the drop in temperature is caused by heat loss from the bed to the walls and the gases. The peak temperatures are around 1200°C and the peak value decreases as the bed is reacted. Also there is a considerable spreading of the profile in the axial direction towards the end of the run.

Figure 4 shows the temperature profiles of the outer thermocouples. These temperatures are notably lower than the inner ones. This is not surprising since the wall acts as a heat sink lowering the temperatures close to the wall. Also the spreading of the temperatures in the axial direction is seen in this set of profiles also.

Figure 5 shows the product gas composition as a function of time. After the initial transient the composition attains nearly constant values. There is some oxygen bypassing in the gasifier. The fluctuations are probably caused by errors in analysis. Due to the use of helium as the carrier gas in the gas chromatograph, hydrogen analysis had a large correction factor and hence has greater error than the other gases. Attempts on closing a hydrogen mass balance around the system confirmed this.

Whether or not the oxygen bypassing occurred through the bed or the insulated wall is difficult to determine. As the reaction progresses, the bed length decreases and hence the associated pressure drop through the bed also decreases. This might have contributed to decreased bypassing of the oxygen.

4. COMPARISON WITH SIMULATION RESULTS

In parallel with this experimental investigation, a modeling study was conducted with two objectives. The first was to be able to study the behavior of large scale fixed-bed gasifiers such as the Lurgi-type. The second was to be able to validate the model using the results from the laboratory scale gasifier. The details of the model was published elsewhere (Joseph, et al., 1983). A brief summary is given here.

In a typical commercial scale gasifier the coal is moving at a much smaller velocity than the gases. As a result, the gasifier can be divided into two zones, one for drying and devolatilization and another for combustion and gasification. The first zone is relatively narrow and can be assumed to take place instantaneously for practical purposes. It is the second zone that determines the operating characteristics of the gasifier. In this zone, char descends slowly reaching with the gases rising from the combustion zone. This was the reason for using char instead of coal in the experimental studies. The main reactions in this zone are char-oxygen, char-steam, char-carbon dioxide and the water-gas shift reaction. In addition to these reaction kinetics, the heat and mass transfer in both axial and radial directions play a significant role.

A number of assumptions are required to develop a model that is both mathematically and computationally tractable. Some major assumptions include a shrinking-core model for gas-solid kinetics, no axial dispersion of heat and a homogeneous gas-solid temperature in the bed. The equations resulting from the mass and energy balances are solved numerically using suitable integration methods. The interested reader is referred to Joseph et al. (4).

Figures 6 and 7 show a comparison of temperatures predicted by the model and those experimentally observed. The agreement between the two during the early part of the run is good. However the temperature profiles predicted by the model tend to be rather uniform with respect to time whereas the experimental profiles exhibit a marked decrease in the peak value and a spreading of the profile in the axial direction.

Similar trends were observed in another run as reported in Salam (5). This spreading of the temperature profile could have been caused by a number of reasons. Sources of modeling errors include (i) axial dispersion of heat (ii) thermal storage and conductivity of the thermowells (iii) reduction in bed length caused by collapsing ash layer (iv) effect of heat transfer by radiation to the walls and (v) effect of channeling and bypassing of oxygen through the bed.

5. CONCLUSIONS

This paper presented the results of a char gasification run using Wyoming coal in a fixed-bed laboratory gasifier. The temperature profiles in the bed at various axial and radial positions are presented as a function of time. The results are useful in validating proposed models for fixed-bed gasifiers. Comparison with one such model indicates that the model is capable of predicting

the initial temperature profiles reasonably well, but requires further refinement to be able to explain some flattening trends in the temperatures. Current research is focused on trying to update the model in order to explain the experimental observations.

6. REFERENCES

1. Yoon, H., J. Wei and M. M. Denn, "Model for Moving-Bed Coal Gasification Reactors", *AIChE Journal* 24, p. 885 (1978).
2. Cho, Y. S. and B. Joseph, "A Heterogeneous Model for Moving-Bed Coal Gasifiers", *Industrial and Engineering Chemistry, Process Design and Development*, Vol. 20, 318 (1981).
3. Kim, M. and B. Joseph, "Dynamic Modeling of Moving-Bed Coal Gasifiers", *Industrial and Engineering Chemistry, Process Design and Development*, Vol. 22, 212 (1983).
4. Joseph, B. A. Bhattacharya, L. Salam and M. P. Duduković, "Modeling and Simulation of Fixed-bed Coal Gasification Reactors, Systems Simulation of Fossil Energy Processes", Symposium organized by Morgantown Energy Technology Center, Department of Energy, Morgantown, West Virginia (Dec., 1983). Proceedings to appear.
5. Salam, L., "An Experimental Investigation of Fixed-Bed Coal Gasification", M.S. Thesis, Washington University, St. Louis (August, 1983).

Coal Analysis

Mine. Wyodak
Town. Campbell
County. Campbell
State. Wyoming
Abbreviated ID. Wyo 1
Sample Date 7-15-78
Bin # 3500

Proximate Analysis:

As Received

Moisture 31.87
Volatile Matter. 32.46
Fixed Carbon 30.16
Ash. 5.51
Heating Value (Btu/lb) 7978

Ultimate Analysis:

Moisture-free

Ash. 8.09

Moisture- and Ash-free

Hydrogen 5.75
Carbon 74.05
Nitrogen 1.39
Sulfur 0.53
Oxygen (by diff) 18.28
Heating Value MAF (Btu/lb) 12,742
H/C Ratio. 0.93

Table 1. Analysis of Coal Used in the Gasification Runs

Char Loaded:	3645.7 gms devolatilized Wyodak char	
Char Composition:	83.56% Carbon	
	11.97% Ash	
	2.33% Oxygen	> Moisture included
	1.02% Hydrogen	
	0.62% Nitrogen	
	0.50% Sulfur	
<u>Time 0-45 min.</u>		
INLET	Air Flowrate:	1.478 m ³ /hr*
	Water Flowrate:	3.48 gm/min
	O ₂ /H ₂ O:	2.12 gm/gm (1.192 mol/mol)
OUTLET	Product Gas Flowrate:	2.055 m ³ /hr*
	Total Condensate:	0 gm
<u>Time 45-580</u>		
INLET	Air Flowrate:	1.206 m ³ /hr*
	Water Flowrate:	3.48 gm/min
	O ₂ /H ₂ O:	1.73 gm/gm (0.975 mol/mol)
OUTLET	Product Gas Flowrate:	2.022 m ³ /hr*
	Total Condensate:	382.2 gms
Unreacted Carbon:	697.8 gms	
Reactor Pressure:	0.1910 MPa	* at 25°C, 0.1013 MPa
Original Bed Length:	85.7 cm	
Final Bed Length:	approximately 12.0 cm	

Table 2. Summary of Operating Conditions for Gasification Run #072483

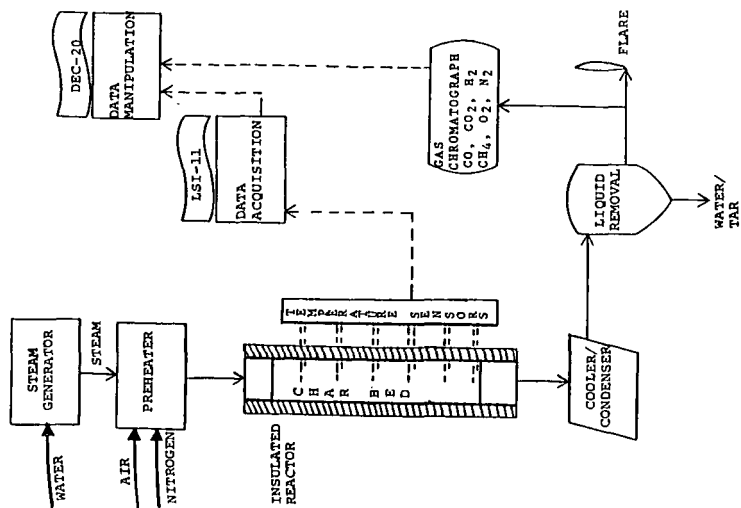


Figure 1. Schematic of Experimental Setup

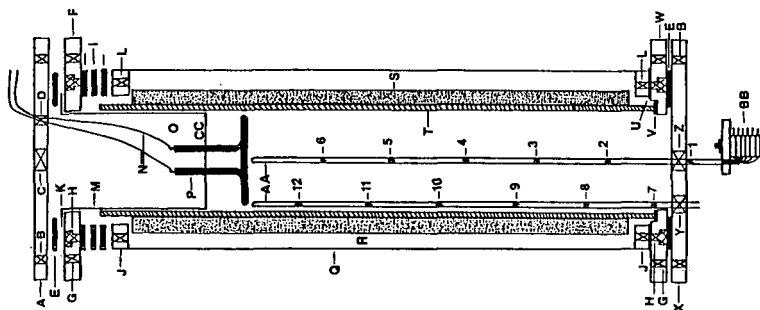
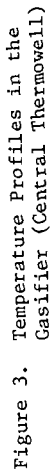


Figure 2. Detail of Gasification Vessel.
See next page for Legend.



Legend for Figure 2

[illegible]

Thermocouple Locations From Top of Well (Ft)

1.	113.0 cm	7.	105.1 cm
2.	91.8 cm	8.	85.7 cm
3.	71.1 cm	9.	65.7 cm
4.	51.1 cm	10.	44.4 cm
5.	29.8 cm	11.	24.3 cm
6.	11.0 cm	12.	4.8 cm

Note all thermocouples are 0.02" (0.508 cm) diameter Inconel sheathed Chromel/Alumel rated at 1150°C.

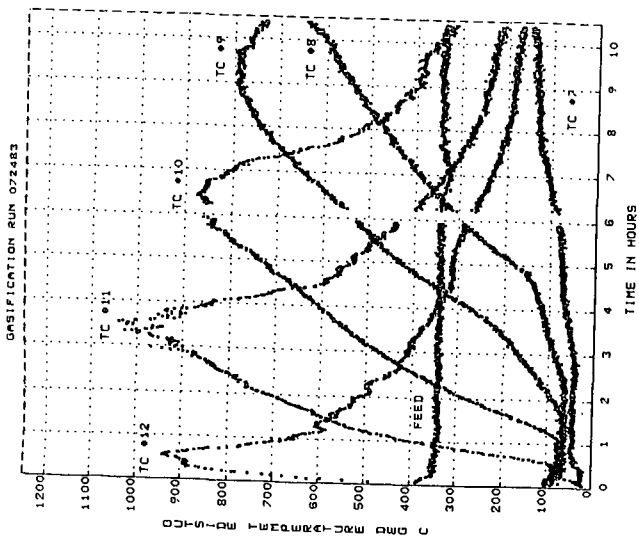


Figure 4. Temperature Profiles in the Gasifier (Thermowell near the Wall)

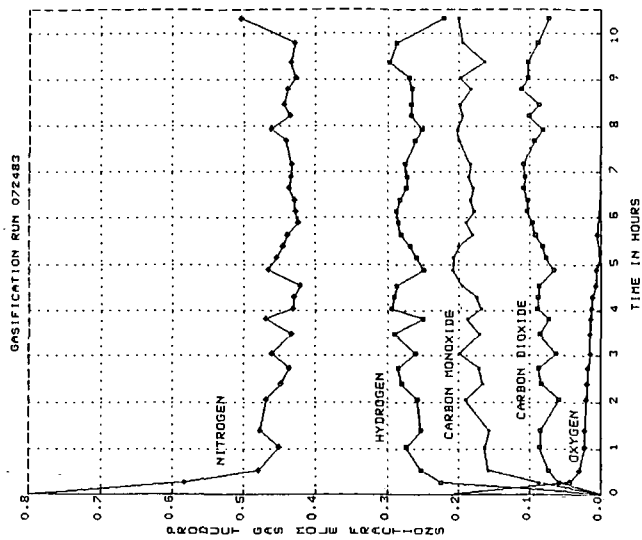


Figure 5. Product Gas Composition as a Function of Time

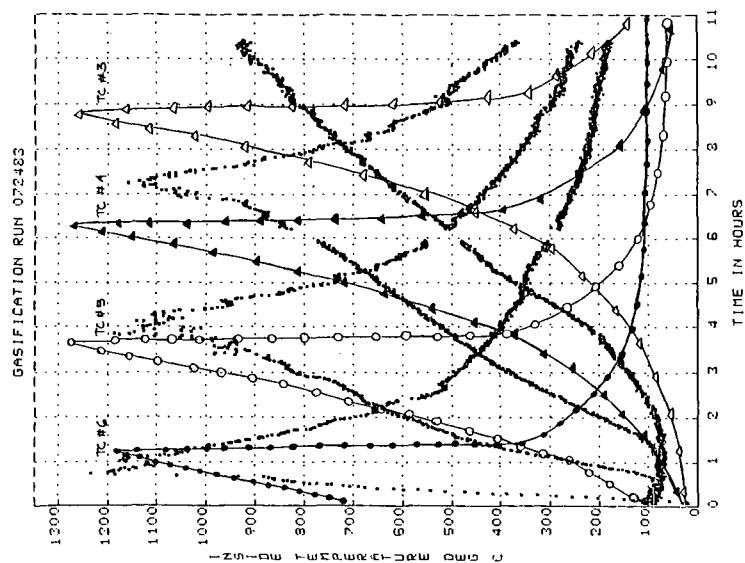


Figure 6. Comparison of Temperature Histories at Thermocouple Locations, Inner Thermowell. Straight Lines are Model Predictions.

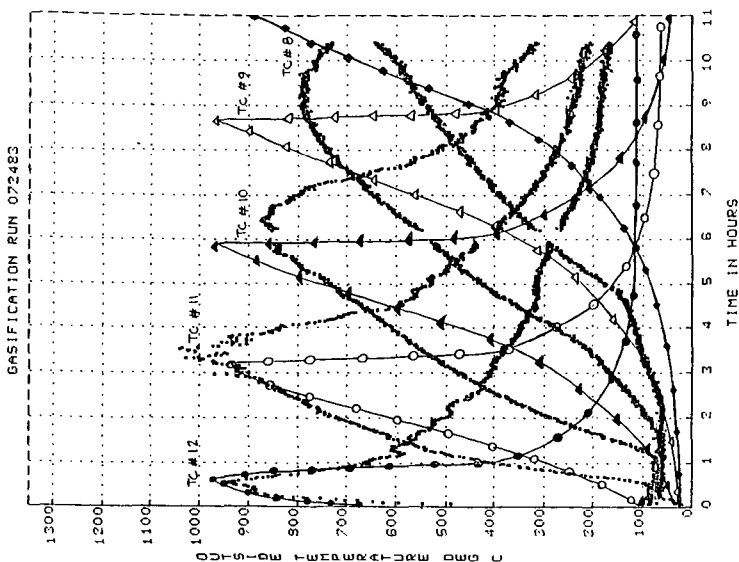


Figure 7. Comparison of Temperature Profiles for the Thermocouples near the Wall. Straight Lines are Model Predictions.